Processing and Characterization of Mg Matrix Composites Reinforced with TiC and TiB$_2$ Phases using an *In-situ* Reactive Infiltration Technique

Mohammed E. Shamekh

A Thesis

In the Department

of

Mechanical and Industrial Engineering

Presented in Partial Fulfillment of the Requirements

For the Degree of Doctor in Philosophy (Mechanical Engineering) at

Concordia University

Montreal, Quebec, Canada

July 2011

CONCORDIA UNIVERSITY

SCHOOL OF GRADUATE STUDIES

This is to certify that the thesis prepared

Entitled: **Processing and Characterization of Mg Matrix Composites Reinforced with TiC and TiB₂ Phases using an *In-Situ* Reactive Infiltration Technique**

and submitted in partial fulfillment of the requirements for the degree of

DOCTOR OF PHILOSOPHY (Mechanical Engineering)

complies with the regulations of the University and meets the accepted standards with respect to originality and quality.

Signed by the final examining committee:

_____ Chair
Dr. M. Kahrizi

_____ External Examiner
Dr. V. Krstic

_____ External to Program
Dr. Z. Tian

_____ Examiner
Dr. R. Drew

_____ Examiner
Dr. P. Wood-Adams

_____ Thesis Co-Supervisor
Dr. M. Medraj

_____ Thesis Co-Supervisor
Dr. M. Pugh

Approved by
                Dr. W-F. Xie, Graduate Program Director

July 4, 2011   _____
                Dr. Robin A.L. Drew, Dean
                Faculty of Engineering & Computer Science

ABSTRACT

Processing and Characterization of Mg Matrix Composites Reinforced with TiC and TiB$_2$ Phases using an *In-situ* Reactive Infiltration Technique

Mohammed Shamekh, Ph.D.
Concordia University, 2011

Magnesium matrix composites are attractive for different applications especially in automotive and aerospace industries due to their superior specific properties. The main purpose of this work is to produce a new magnesium matrix composite reinforced with a network of TiC and TiB$_2$ compounds via an *in-situ* reactive infiltration technique. In this process, the ceramic reinforcement phases, TiC and TiB$_2$, were synthesized *in-situ* from the starting powders of Ti and B$_4$C without any addition of a third metal powder such as Al. The molten magnesium infiltrates the preform of 3Ti-B$_4$C by capillary forces. Furthermore, adding Mg or MgH$_2$ powder with different weight percentages to the 3Ti-B$_4$C preforms was used in an attempt to increase the Mg content in the fabricated composites. The results of the *in-situ* reaction mechanism investigation of the Ti-B$_4$C and Mg-B$_4$C systems show that the infiltrated magnesium not only infiltrates through the 3Ti-B$_4$C preform and thus densifies the fabricated composite as a matrix metal, but also acts as an intermediary making the reaction possible at a lower temperature than that required for solid-state reaction between Ti and B$_4$C and accelerates the reaction rate. The investigation of the *in-situ* reaction mechanism after adding Mg or MgH$_2$ powder to the 3Ti-B$_4$C preforms show that the reaction mechanisms are similar. However, the presence of the Mg or MgH$_2$ in the preform accelerates the reaction rate making the reaction take place and finish in a shorter time.

Also, the results of the parametric study show that the processing conditions such as temperature, holding time and green compact relative density have a significant influence on the reaction mechanism and the fabrication of the composite. Based on this work, it is recommended to fabricate the composite samples at 900°C for 1.5 h and using a green compact of 70% relative density. The required equilibrium phases, TiC_x and TiB_2, formed in the composites with very small amounts of the residual Ti, boron carbide and intermediate phases such as TiB, Ti_3B_4 and MgB_2. The fabrication of composites at these processing conditions avoids significant oxidation of Mg and formation of the ternary compound (Ti_2AlC) in the cases of AZ91D or AM60B alloys composites, which can adversely affect the mechanical properties of the composites.

Furthermore, the results reveal that the percentage of reinforcing phases, when the optimal processing parameters are used, can be tailored by controlling either the green compact relative density or the weight percentages of Mg or MgH_2 powder added to the $3Ti-B_4C$ preform.

Microstructural characterization reveals a relatively uniform distribution of the reinforcing phases TiC_x and TiB_2 in the magnesium matrix. Mechanical properties of these composites such as elastic modulus, flexural and compressive strengths are greatly improved compared with those of the unreinforced Mg or Mg alloys. In contrast, the ductility of TiC_x-TiB_2/Mg composites is lower than that of the unreinforced Mg or Mg alloys. However, this lower ductility was improved by the addition of Mg or MgH_2 powder in the preform. Secondary scanning electron microscopy was used to investigate the fracture surfaces after the flexural strength test. The composites show signs of mixed fracture; cleavage regions and some dimpling. In addition, microcracks observed in the

matrix show that the failure might have initiated in the matrix rather than from the reinforcing particulates. Also, the results show that the hardness and the wear resistance of the composites are improved, compared with those of the unreinforced Mg alloy.

DEDICATION

I dedicate this thesis to my late father, my mother, and my wife.

ACKNOWLEDGEMENTS

Table of Contents

List of Figures

xiv

xvi

xxiii

xxv

List of Tables

xxviii

List of Acronyms

Abbreviations

AM60B	Magnesium alloy with about 6 wt.% Al and less than 1 wt.% Mn
AZ91D	Magnesium alloy with about 9 wt.% Al and about 1 wt.% Zn
AE42	Magnesium alloy with about 4 wt.% Al and about 2 wt.% mischmetal
BHN	Brinell hardness number
BSE	Backscatter electron
EDS	Energy Dispersive X-Ray spectroscopy
EPMA	Electron probe micro-analyzer
FAS	Flux-assisted synthesis
IMCs	Intermetallic matrix composites
PRMMCs	Particulate reinforced metal matrix composites
QE22	Magnesium alloy with 2.5% Ag, 2% RE and 0.7% Zr
RD	Remelting and dilution
RD	Relative density
ROM	Rule of Mixtures
RSI	Reactive spontaneous infiltration
RSI	Reactive spontaneous infiltration
SEI	Secondary electron imaging
SEM	Scanning electron microscope
SHS	Self-propagating high temperature synthesis
UTS	Ultimate tensile strength
VH	Vickers hardness
XRD	X-ray diffraction
YS	Yield strength
YCS	Yield compressive strength

Symbols

ΔG	Change in Gibbs free energy
ΔH	Change in the reaction enthalpy
ε_{th}	Thermal mismatch strain
E_{T160}	Tangent elastic modulus at 160 MPa stress level
HV_{10}	Vickers hardness using a load of 10 kg
$HV_{1.0}$	Vickers microhardness using a load of 1 kg
$\rho_{p,c}$	Density of the preform or composite
ρ_{B4C}	Density of boron carbide
ρ_{Ti}	Density of titanium
$\rho_{theo.}$	Theoretical density
ρ_{Mg}	Density of magnesium
ρ_{TiC}	Density of titanium carbide
ρ_{TiB2}	Density of titanium diboride
ρ_B	Bulk density
P_{closed}	Closed porosity
P_{open}	Open porosity
P_{total}	Total porosity
σ_{fs}	Flexural strength
σ_t	Tensile strength
σ_y	Yield strength

Chapter 1

Introduction

1.1 Background

The need for materials having superior mechanical properties and low density led to the development of metal matrix composites (MMCs) in early 1960s [1]. Composites were developed because it was very difficult to find a structural material satisfying all the desired attributes for a given application [1, 2]. By developing MMCs, the attractive properties of metals such as ductility, toughness, thermal and electrical conductivity can be combined with those of ceramics such as high strength and modulus to obtain light and strong materials.

Metal matrix composites reinforced with suitable ceramic reinforcements possess high strength and modulus as well as good high-temperature properties when compared to unreinforced matrix alloys. Discontinuously reinforced MMCs including particulates (PRMMCs), short fibers, or whiskers are more preferred for automotive applications than continuously reinforced MMCs because of their relative ease in fabrication, cost and nearly isotropic properties [1, 3].

Recently, among numerous PRMMCs, magnesium (Mg) matrix composites reinforced with ceramic particles have received attention in the automotive and aerospace applications because of their high *specific* modulus and tensile strength, high wear resistance and excellent thermal and electrical conductivities [4-7]. Mg represents a natural candidate since it is 35% lighter than aluminum and over four times lighter than

steel [8]. Magnesium has comparable density to polymers but much better mechanical and physical properties. Hence, magnesium has been selected as a matrix because of the great demand for low density composites especially in the automotive industry since these composites have advantages over monolithic metals and alloys.

Although costly magnesium alloys, such as those containing rare earth elements, can achieve high strength even at elevated temperatures, other properties such as a lower coefficient of thermal expansion, a higher elastic modulus and wear resistance can only be obtained by the addition of strong and stiff second phases to the magnesium. So, Mg matrix composites reinforced with suitable ceramic particles can compensate for some of the major limitations of monolithic magnesium such as low elastic modulus, rapid loss of strength with temperature and poor creep resistance at elevated temperature [2, 9].

There are several methods to fabricate particulate reinforced Mg MMCs by ex-situ routes including powder metallurgy, preform infiltration, spray deposition, mechanical alloying and different casting technologies such as squeeze casting, rheocasting and compocasting [10]. However, *in-situ* MMCs can exhibit excellent mechanical properties due to the formation of ultra fine, homogeneously dispersed and thermodynamically stable ceramic reinforcements with clean reinforcement-matrix interfaces. Also, near-net-shape composites can be fabricated with a high volume percentage of the reinforcing ceramic phase at an effective cost [3, 11].

TiC and TiB_2 ceramic particles are considered good potential reinforcing candidates in magnesium matrices due to their desirable characteristics such as low densities, high melting points, good thermal and chemical stability, high hardness and

2

excellent wear resistance [12, 13]. Moreover, TiB_2 is a suitable reinforcement because it has a crystal lattice coherent with that of the magnesium matrix [14].

Mg matrix composites reinforced with *in-situ* TiC and TiB_2 particles have been fabricated using various techniques such as self-propagating high temperature synthesis (SHS) and remelting and dilution (RD). For example, Ma *et al.* [15] fabricated TiB_2-TiC/Mg matrix composites using the SHS technique via a master alloy route using a low cost Al-Ti-B_4C system. They were the first to use B_4C instead of B and/or C in the starting materials. On the other hand, Zhang *et al.* [16] successfully fabricated TiB_2-TiC/Mg matrix composites using the RD technique and a preform of a sintered block of a mixture of Al-Ti-B_4C.

It is important to note that all these techniques used to fabricate *in-situ* TiC-TiB_2/Mg matrix composites depend on the addition of aluminum powder to the starting materials where in the Ti-B_4C system, this aluminum acts as a reactive intermediary to facilitate the reaction between Ti and B_4C. However, this aluminum also diffuses into the magnesium melt and forms $Mg_{17}Al_{12}$ (γ-phase) during solidification resulting in limited ductility of the matrix [17]. Also, poor strength at elevated temperatures and low creep resistance of magnesium alloys are caused by the weak $Mg/Mg_{17}Al_{12}$ interface [18].

An innovative process called *in-situ* reactive infiltration technique can be used to fabricate magnesium matrix composites reinforced with in-*situ* TiC and TiB_2 particles. In this technique, there are two processes that take place simultaneously. First is the infiltration of the molten metal through the preform by capillary forces. Second is the *in-*

situ reaction between the starting powders and the molten metal to synthesize the reinforcement phases. Magnesium matrix composites reinforced with ceramic particles have been successfully manufactured via this technique with great reduction in cost [11]. Thus, this technique can overcome the high cost problem of other MMCs.

To date, papers on the production of (TiC-TiB$_2$)/Mg matrix composites starting with Ti and B$_4$C **without Al** could not be found in the literature. Also, the *in-situ* reactive infiltration technique has not been used before to fabricate magnesium matrix composites using the Ti-B$_4$C system however, a few researchers [11, 19-24] used this technique with Ti and C to produce TiC/Mg matrix composites.

1.2 Motivation

On the basis of the above information, fabrication of magnesium matrix composites reinforced with *in-situ* TiC and TiB$_2$ particles using a mixture of Ti and B$_4$C particle powders without adding a third metal powder such as Al is an attractive prospect to overcome the poor mechanical properties specially at elevated temperatures caused by the addition of Al. This research is focused on the fabrication of these composites using an *in-situ* reactive infiltration technique which is a practical and cost-effective process, understanding the reaction mechanism behind it and finally studying the properties of these composites.

1.3 Thesis Layout

The thesis consists of eight chapters. This chapter provides the background to particulate reinforced metal matrix composites and presents the motivation of the present work and finally the thesis layout. Chapter Two outlines the particulate reinforced metal matrix

4

composites (PRMMCs), reviews the previous studies on the methods used to fabricate these composites focusing on magnesium matrix composites and their fabrication with *in-situ* TiC and TiB_2 particles. Chapter Three gives the objectives of this work. The raw materials, the experimental procedure for fabrication of the composite samples and the experimental test facilities for the characterization of the composites are presented in detail in Chapter Four. Understanding the *in-situ* reaction mechanism behind the fabrication of these composites is presented in Chapter Five. Chapter Six presents the effect of the processing parameters on the fabrication of the composites. All theoretical and experimental results and discussions of the compression, 4-point bending, hardness and wear resistance tests are given in Chapter Seven. Finally, the conclusions of the current investigations are presented in Chapter Eight in addition to the recommendation for future works.

Chapter 2

Literature Review

2.1 Metal Matrix Composites (MMCs)

In recent years, metal matrix composites have been getting considerable attention particularly in the area of processing techniques. Metal matrix composite (MMC) refers to a kind of material that consists of at least two chemically and physically distinct phases; a fibrous or particulate phase distributed in a metallic matrix. Metal matrix composites (MMCs) are attractive for several applications especially in automotive and aerospace industries where they have a combination of the properties of the matrix (metallic phase) such as ductility, toughness and thermal and electrical conductivity with the properties of the reinforcement (ceramic material) such as high strength, modulus and wear resistance [3]. Therefore, MMCs can improve the wear resistance, elastic modulus and tensile strength of the unreinforced metals and alloys [25].

In general, based on the type of reinforcement point of view, the metal matrix composites can be categorized into three kinds:

(i) particle reinforced MMCs (PRMMCs),

(ii) short fiber or whisker reinforced MMCs, and

(iii) continuous fiber or sheet reinforced MMCs.

The aspect ratio is used to distinguish between these different forms of reinforcements. The aspect ratio is the ratio of length to diameter (or thickness) of the reinforcement. In the case of equiaxed particles, this ratio is around unity [26].

2.2 Particulate-Reinforced Metal Matrix Composites (PRMMCs)

The family of discontinuously reinforced MMCs includes both particulates and short whiskers or fibers. PRMMCs are more preferable for automotive applications than fiber-reinforced MMCs due to their ease of fabrication, lower cost, and isotropic properties [3, 27]. Moreover, discontinuous or particulate reinforcements can solve the problems associated with fabrication of continuously reinforced MMCs, such as: fiber damage, microstructural nonuniformity, fiber to fiber contact and extensive interfacial reactions [28].

PRMMCs can be classified into two groups according to the volume fraction of reinforcement; high volume fraction and low volume fraction materials. High volume fraction materials with reinforcement concentration greater than about 40 vol.% can achieve a network of contacting particles. These materials are typically produced by infiltrating a molten metal into a powder preform. In the 1990's, these materials appeared in electronic packaging applications where high concentrations of the reinforcement are desired. On the other hand, most ceramic particles are completely surrounded by matrix in low volume particulate reinforced metals with less than about 30 vol.% ceramic to maintain the ductility and toughness at levels comparable to engineering alloys [29].

In general, ceramic particulate reinforced metal matrix composites have better properties compared to the matrix material. Properties, such as wear resistance, stiffness, damping capacity and thermal expansion, can be tailored by adjusting the ceramic volume fraction in the composites [29].

Recently, there are numerous PRMMCs systems being developed. Magnesium matrix composites reinforced with ceramic particles have received considerable attention

in the automotive, aerospace and electronics applications because of their high *specific* modulus and tensile strength, high wear resistance and excellent thermal and electrical conductivities [4-6].

2.2.1 Matrix Definition and Selection

The matrix is the monolithic material into which the reinforcement is embedded, and is completely continuous. This means that there is a path through the matrix to any point in the material, unlike two materials sandwiched together. In structural applications, the matrix is usually a lighter metal such as aluminum, magnesium, or titanium, and provides an amenable support for the reinforcement. The purpose of the matrix in composites is to combine the reinforcing particles into a monolithic material to enable shaping it into the required geometrical form and dimensions, as well as to take up and distribute external loads within the material bulk. In addition, the matrices protect the reinforcing phase against external effects: mechanical damage, erosion and corrosion caused by the surrounding medium or reinforcement-reinforcement contact.

Structural alloy systems such as Al, Mg, Si, Ti, Cu, Ni, Fe and Pb have been used as matrix materials for PRMMCs. However, aluminum, magnesium and titanium alloys are considered the most commonly used matrices especially for the applications which require low density with reasonably high thermal conductivity [30].

2.2.2 Reinforcement Selection

One of the most important factors influencing the mechanical properties of composites is the reinforcement: type, size, and distribution. Reinforcement materials used with MMCs include carbides (e.g., SiC, B_4C and TiC), nitrides (e.g., Si_3N_4, AlN), oxides (e.g., Al_2O_3,

SiO_2) and elemental materials (e.g., C, Si). These reinforcements may be in the form of continuous fibers, chopped fibers, whiskers, platelets, or particulates. SiC, for example, has been used in aluminum and magnesium MMCs in all of the above mentioned forms while carbon and silicon fibers have been used in aluminum, magnesium and copper-matrix composites [31].

The ceramic reinforcement of the PRMMCs can be selected based on several criteria such as elastic modulus, tensile strength, density, melting temperature, thermal stability, coefficient of thermal expansion, size and shape, compatibility with matrix material, and cost. The density, elastic modulus, and tensile strength of the reinforcing phases affect the structural efficiency of discontinuously reinforced MMCs. On the other hand, the chemical stability and compatibility of the reinforcements with the matrix material are essential during material production and also for end applications. In addition, for the composites exposed to thermal cycling, the thermal mismatch strain, ε_{th}, between reinforcement and matrix is very important and has to be taken into consideration [30]. So, in general, the choice of the reinforcement is dictated by several factors such as particle shape, method of composite manufacture, cost and application of the composite [32]. The purpose of the reinforcement of magnesium alloys is to improve critical properties of the unreinforced matrix such as elastic modulus, high temperature strength, wear resistance and thermal expansion [33].

2.2.3 Processing of Particulate Reinforced MMCs

Several processing techniques have been used over the years to optimize the microstructure and mechanical properties of PRMMCs. These processing techniques can be divided into two groups: primary material production and secondary consolidation or

forming operations [34, 35]. The most common techniques used to fabricate particulate ceramic reinforced metal matrix composites include powder metallurgy, slurry casting, spray deposition, melt infiltration and reactive processing (*in-situ* particulate formation) [36].

These methods will be briefly discussed in the following subsections in relation to particulate reinforced magnesium matrix composites. Because of the peculiarity of the present work, special subdivisions of the review have focused on the fabricating techniques of PRMMCs by reactive processing (*in-situ*) and melt infiltration processes.

2.2.3.1 Powder Metallurgy

In the powder metallurgical process, matrix and reinforcement powders are mixed, pressed, degassed and then sintered at a certain temperature under a controlled atmosphere or in a vacuum.

The main advantages of this processing method can be summarized in its capability for incorporating a relatively high volume fraction of reinforcement and fabrication of composites with matrix alloy and reinforcement systems that are immiscible by liquid casting. However, due to the cost of the required alloy powders and the complexity of the process during the material fabrication, this process is not ideal for mass production [27].

Various magnesium matrix composites have been fabricated using powder metallurgy such as $SiC_P/AZ91$ [37], $(B_4C_p)/Mg$ [38], TiC_p/Mg [39] and TiB_{2p}/Mg [40].

2.2.3.2 Stir Casting

In general, the stir casting process involves the incorporation of particulates or loose fibers into a mechanically stirred molten matrix alloy. After solidification, a desired distribution of the dispersed phase in the cast matrix can be obtained [32, 41].

Stir casting can be considered a promising route for manufacturing discontinuous metal matrix composites. This processing method has several advantages summarized by its simplicity, flexibility and applicability to large quantity production. It is attractive because it represents the simplest and the most cost-effective method of all solidification processes used for producing metal matrix composites [42].

According to Skibo *et al.* [43], using a casting method for preparing composites costs around one-third to half that of competitive methods and falls to one-tenth for high volume production making it the most popular commercial method of producing aluminum-based composites. However, poor wettability between the particles and the liquid metal, and floating of the particles depending on their density relative to the liquid, represent major problems for this method [44]. Also, shrinkage resulting from metal contraction during solidification results in gas porosity which represents a quality-related problem in cast composites [32].

So, the factors that have to be considered when this process is used to produce metal matrix composites are summarized in the difficulty of achieving a uniform distribution of the reinforcement material, the poor wettability between the two particles and the liquid metal, porosity in the cast metal matrix composites and chemical reactions between the reinforcement material and the matrix alloy. Thus, metal matrix composite with optimum properties can be achieved by uniform distribution of the reinforcement

11

material in the matrix alloy, optimizing wettability or bonding between these substances, minimizing the porosity levels and avoiding the chemical reactions between the reinforcement materials and the matrix alloy [41].

Magnesium composites with different matrix compositions such as for example CP-Mg (chemically pure magnesium) [45] and AZ91 [46] reinforced with SiC particulates have been produced using this method.

2.2.3.3 Spray Deposition

Spray forming or spray deposition is a process during which an atomized stream of molten material droplets impacts a substrate at high velocity to build up bulk metallic materials. For a metal matrix composite, discontinuous reinforcing particulates are co-injected with the metal spray allowing particulate engulfment in molten or partially molten metal droplets to form a composite. The deposition rate is in the range of about 6-10 kg/min while the droplet velocities are about 20–40 m/s, and ceramic particles are often distributed inhomogeneously in the spray-formed metal matrix composite [47-49].

The Osprey process which was developed commercially in the late 1970s and during the 1980s by Osprey Ltd (Neath, UK) [50] is a suitable process for illustrating this kind of fabrication. Osprey MMC material has good microstructural features such as a strong interfacial bond and porosity of about 5% which can be eliminated by secondary processing [1, 50].

There are a number of studies [51-53] on the fabrication of magnesium matrix composites using the spray forming method in which the relationships between the spray processing parameters, the microstructure, and the mechanical properties of the composites have been examined. It was found that the process has a considerable

influence on the microstructure and properties of QE22 alloy reinforced with SiC particles [51]. But, the sprayed composite usually shows microstructural features such as fine grains, porosity, and absence of brittle phases at the SiC/matrix interface due to the high cooling rate [53].

2.2.3.4 Reactive Processing (*in-situ* composites)

During the past three decades, considerable research effort has been directed to the development of *in-situ* metal matrix composites (MMCs). Unlike other composite fabrication methods of the composites, *in-situ* synthesis is a process wherein the reinforcements are synthesized in the metallic melt by chemical reactions among elements or between an element and a compound during the composite fabrication [3, 54, 55]. Hence, homogeneously dispersed reinforcement in the matrix alloy is one of the final reaction products.

Compared to conventional MMCs produced by *ex-situ* methods, *in-situ* MMCs exhibit the following advantages: (a) the formed reinforcements are finer in size, homogeneously dispersed and thermodynamically stable yielding better mechanical properties and less degradation at elevated temperatures, (b) high bonding strength due to the clean interface between reinforcement and matrix, (c) near-net-shape composites can be easily fabricated with a high volume percentage of the reinforcing ceramic phase and effective cost [3, 11]. The anticipated reaction has to be thermodynamically favorable. The reaction kinetics are also required to be reasonably fast to make the fabrication process practical [27].

Several processing techniques have evolved over the last decades to optimize the structure and properties of metal matrix composites (MMCs) reinforced with *in-situ*

13

ceramic phase(s). However, the terminology in the literature for this processing route is inconsistent and confused. Koczak and Premkumar [56] have tried to formalize the terminology for the processing routes when they suggested that the *in-situ* reactions can be categorized in terms of the starting phases, such as gas-liquid, liquid-solid, liquid-liquid etc. Based on this, the processing methods utilized to manufacture the *in-situ* MMCs can be categorized according to the processing temperature.

Accordingly, the processing methods can be classified into four categories as follows: (a) solid-liquid reaction process; (b) vapor-liquid-solid reaction process; (c) solid-solid reaction process, and (d) liquid-liquid reaction process [3]. Reactive processing (*in-situ*) technique has been used to fabricate aluminum and magnesium matrix composites.

In early experiments, Labotz and Mason [57] were the first to produce magnesium matrix composite by *in-situ* synthesis when they fabricated Mg-Mg$_2$Si composites. The high melting point, high elastic modulus, low density and the ease of formation of Mg$_2$Si were the reasons for its choice as a reinforcement. The coarse needle-shaped Mg$_2$Si phase was obtained through conventional casting with a high Si concentration and as a result the composite had poor mechanical properties. Afterwards, various efforts have been made to modify the microstructure and to improve the mechanical properties of the Mg-Mg$_2$Si *in-situ* system [58-63]

A number of other *in-situ* systems have also been explored such as Mg-MgO composite formed by the reaction between Mg and B$_2$O$_3$ [64]. Further advancement took place when Yamada *et al.* [65] fabricated Mg-TiC composite via mechanical alloying where the composite material was formed through the reaction between Mg, C and Ti

powders. Several researchers worked on this system and some examples will be discussed here [4, 5, 11, 19-24, 39, 54, 65, 66]. A recent study [67] was published in 2001, where through the reaction of Mg with KBF_4 and K_2TiF_6, Mg-TiB_2-TiB composite was formed and this can be considered the first attempt on this system. This work will be discussed in more detail later. The progress of *in-situ* fabricated magnesium matrix composites reinforced with TiC, TiB_2, and TiC + TiB_2 particles is also discussed in this chapter.

2.2.3.5 Melt Infiltration Methods

Liquid-metal infiltration is a common process utilized for the fabrication of metal matrix composites. In this method, the gases within a porous body are gradually replaced by a liquid metal of low viscosity eliminating the solid/vapor interface in the system. Hence, metal infiltration refers to a process whereby molten metal penetrates the pore channels of a porous ceramic compact. Liquid-metal infiltration methods are suitable for fabricating composite materials because of their simplicity and possibility of introducing small particles into the matrix [68, 69]. Furthermore, producing materials with a high ceramic content and near-net-shape fabrication represent the main advantages of this method [70].

The motive force for an infiltration process may be either by an external force (pressure or vacuum) applied to the liquid matrix phase as in the case of squeeze casting or by a capillary force which develops when the liquid metal wets the ceramic particles (spontaneous or pressureless infiltration). These techniques are discussed in the following sections.

Squeeze Casting Infiltration

Squeeze casting infiltration is one of the forced infiltration methods for liquid phase fabrication of metal matrix composites. In this process, a movable mold part (ram) is used to apply pressure on the molten metal forcing it to penetrate into a porous preform of the reinforcing phase, placed into the lower fixed mold part [71].

Although, the concept of squeeze casting was first introduced in the 1800s, the first actual squeeze casting experiment was conducted after 1931 [27]. Figure 1.2 illustrates the process of the squeeze casting of a metal matrix composite [71]. By forcing the molten metal through the small pores of a particle preform during this process, the requirement of good wettability of the reinforcement by the molten metal can be obviated where the external pressure overcomes the increased interfacial energy of the system.

Upper movable mold half

Molten metal

Lower fixed mold half

Ejector Pin

Preform

Metal Matrix Composite
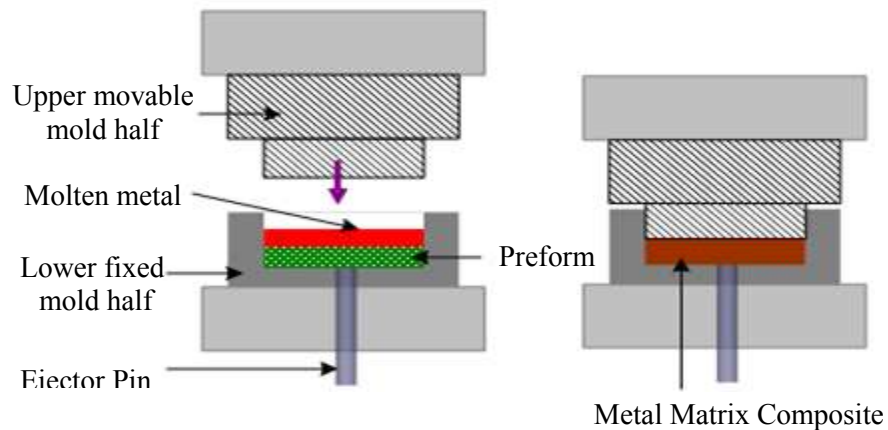
Figure 2.1 Schematic representation of Squeeze Casting [71]

Such pressure is required during infiltration to avoid solidification especially when the temperature of the preform is lower than the melting point of the metal [72]. At the same time, the high pressure makes the inherent castability of the alloy less important. In

addition, there is little or no need for subsequent machining since squeeze casting is considered a near-shape process [73].

By squeeze casting, higher volume fractions (up to 40–50%) of reinforcement can be incorporated into the magnesium alloys which is difficult by stir casting [74]. Minimal reaction between the reinforcement and molten metal takes place due to short contact time at high temperature. Also, composites fabricated by this process are free from common casting defects such as porosity and shrinkage cavities yielding improved material properties [34, 50].

Several magnesium matrix composites have been produced using this technique such as SiC_w/Mg [75], $SiC_w/AZ91$ [76], Mg_2Si/Mg [77].

Gas Pressure Casting Infiltration

Infiltration of the liquid metal into a porous preform using a pressurized inert gas is another method of liquid phase fabrication of MMCs. Figure 2.2 illustrates this process.

Molten metal   Pressurized gas (N_2)

Preform   Metal Matrix
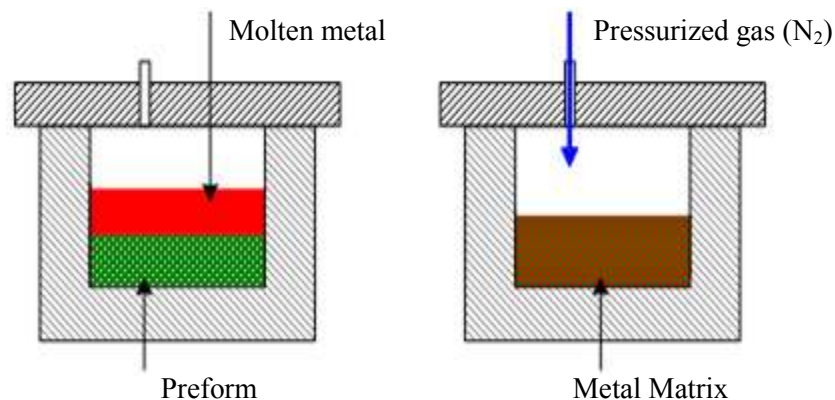
Figure 2.2 Schematic representation of Gas Pressure Casting [71]

This method is used for producing large composite parts. There is no need to enhance the wettability by coating the reinforcing fibers or particles due to the short

contact time with the hot metal. By using gas pressure infiltration, there is no damage to the fibers which may happen when mechanical force is used [71] such as in squeeze casting.

In 2000, this method was used to fabricate an *in-situ* Mg_2Si-reinforced magnesium matrix composite using a hybrid preform (7 vol.% C-fibers and 4 vol.% of Si particles bonded with SiO_2) gas infiltrated with AZ31, AZ91, and AE42 magnesium alloys [78].

Pressureless Infiltration

During the infiltration process, liquid metal or alloy can be driven into a porous preform simply by the capillary action. This preform is a compact of the reinforcement in the form of particles, whiskers or fibers with the same shape as the final MMC component. Pressureless infiltration refers to the molten metal infiltration through the preform without an applied load.

This process is attractive because it is simple. Besides, high ceramic content and near-net-shape can be obtained. Highly homogeneously distributed particles can be obtained by this method because they are not distributed by the liquid. This method can be used to manufacture the parts that require high reproducibility [79]. Importantly, this process is faster than the powder metallurgical route depending on the composite system [34, 68, 80]. However, compared with pressurized infiltration, pressureless infiltration takes more time [79]. In pressureless infiltration, to promote spontaneous infiltration, wetting of the solid by the liquid phase is required. In metallic systems, wetting can be enhanced through mutual solubilities or by the formation of intermetallic compounds at

18

the interface. However, in the case of fabricating metal/ceramic composites, molten alloys do not normally wet ceramic reinforcements [81].

A TiC/Mg composite has been obtained using this method [66]. The experimental set-up of the spontaneous infiltration is shown schematically in Figure 2.3.
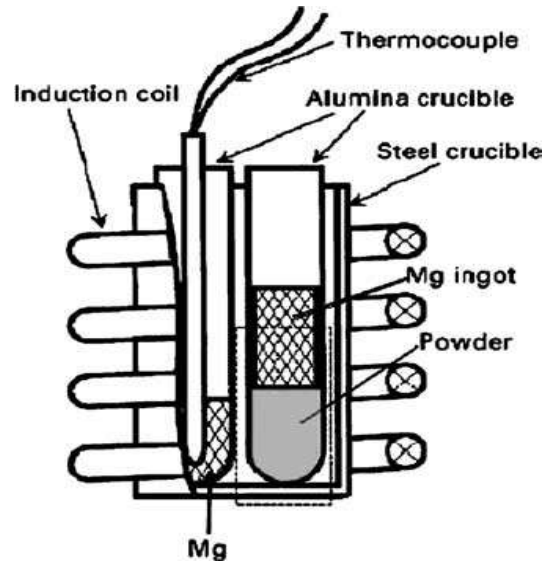
Figure 2.3 Mg infiltration in mixed SiC and SiO_2 powders [82]

2.3 (TiC-TiB$_2$) reinforced Magnesium Matrix Composites

2.3.1 Advantages and Limitations of Magnesium and its Alloys

In recent years, the demand for magnesium and magnesium alloys is increasing due to their light weight especially in automotive applications. Weight reduction is considered the best cost-effective option for significant reduction in fuel consumption and CO_2 emission [83]. By comparing the *specific* strength and stiffness of Mg with those of Al and Fe, it was found that Mg has a higher specific strength than both while the difference in specific stiffness is very small as shown in Figure 2.4 [8]. In addition, magnesium alloys possess good damping capacity, excellent castability and superior machinability [27].

19

The application of magnesium alloys in automotive and aerospace applications has been limited because of its rapid loss of strength with increasing temperature, low elastic modulus, low wear resistance at elevated temperatures, poor creep resistance, high coefficient of thermal expansion, and poor corrosion resistance [6, 16].
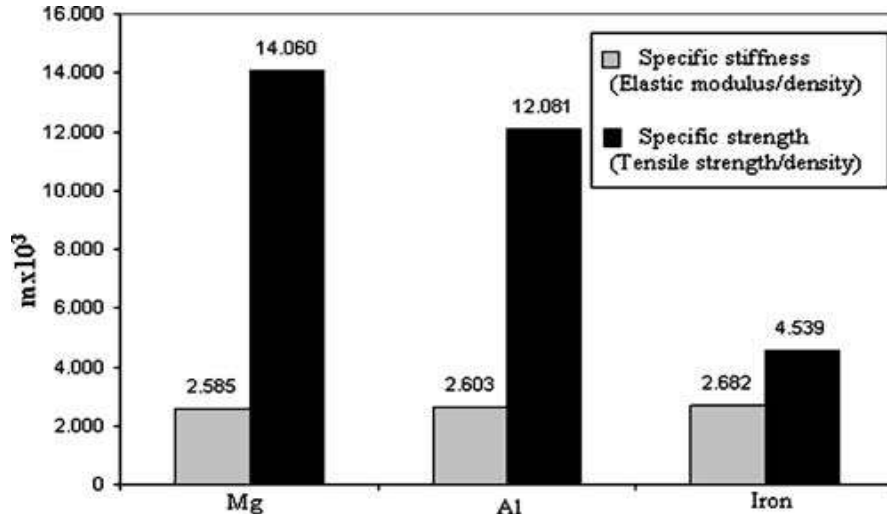
Figure 2.4 Comparison of basic structural properties of magnesium with Al and iron [8]

Some of the magnesium properties such as elastic constants cannot be improved using conventional alloying techniques. The limited solubility of alloying elements in magnesium restricts the possibility of improving the mechanical properties and chemical behavior. In addition, the hexagonal crystal structure of magnesium limits its inherent ductility. Lithium can be considered as the only alloying element that can cause a phase change to BCC. This can increase the ductility but decreases the strength as well [6]. However, the use of Li is very complex and therefore not desired by industry.

Magnesium matrix composites reinforced with suitable ceramic particles can compensate for some of the limitations of the magnesium and magnesium alloys and improve their properties [10]. Moreover, since composites are flexible in constituent

20

selection, their properties can be tailored more than what can be achieved by alloying elements [6, 27].

Compared to magnesium alloys, magnesium matrix composites can be considered as an excellent alternative because of their higher specific stiffness, higher specific strength, high wear resistance and good elevated temperature creep properties [84]. Hence, the demand for magnesium matrix composites for the automotive and aerospace components is increasing such as automotive pulleys, cog-tooth sprockets, oil-pump covers, cylinder liners, and aircraft engine casings [4].

Mg-Al alloys such as AM60 and AZ91 can be considered the most prevalent magnesium alloys used in the automotive industry. Most Mg matrix composites studies are based on these alloys. Pure magnesium and other magnesium alloys such as Mg-Li alloy and Mg-Ag-Re (QE22) alloys have also been employed as a matrix material but less frequently [27]. The composition and mechanical properties of some of the Mg alloys presently used as matrix material are listed in Table 2.1 [50, 85-87].

Table 2.1 Chemical composition and mechanical properties of pure Mg and some Mg alloys used to fabricate MMCs [50, 85-87]

Matrix in MMC		Mechanical Properties					
Code name	Composition	UTS MPa	YS MPa	Modulus GPa	YCS MPa	Elongation %	BHN
Pure Mg		180	80	45	---	12	30
AM60B (F Temper)	Mg 6% Al 0.13% Mn	240	130	45	130	6	63
AZ91D (F Temper)	Mg 9% Al 0.13% Mn 0.7% Zn	250	160	45	165	3	63

2.3.2 Reinforcements for Magnesium Matrix Composites

For magnesium matrix composites, the reinforcement can be either ceramic, which is mostly used, or metallic/intermetallic. Ceramic reinforcements are more common because of their low density, high hardness, strength, and stiffness. However, they have some limitations such as low ductility and low wettability with the magnesium matrix [27].

Carbide and boride ceramics possess many desirable properties as reinforcements. Among these carbides and borides, TiC and TiB_2 are good potential reinforcing candidates in magnesium matrices. This is due to their low densities, high melting points, good thermal and chemical stability, high hardness and excellent wear resistance [12, 13]. It is very important to mention that TiB_2 is a suitable reinforcement because it is coherent with the magnesium matrix due to their having the same crystal lattice [14]. In particular, the use of TiB_2 and TiC in composites offers more advantages over the unreinforced magnesium alloy such as high stiffness, high hardness, wear resistance and low thermal expansion making them suitable advanced structural materials.

2.3.2.1 Titanium carbide (TiC) Properties and Crystal Structure

TiC is one of the hardest materials known. It has attracted much attention because of its excellent characteristics such as low density, high melting point, good thermal and chemical stability, high hardness and excellent wear resistance [12, 13]. Therefore, TiC is used in different applications such as protective coatings for cutting and molding tools, ball-bearings spray gun nozzles and for fusion-reactor applications, high-temperature heat exchangers, turbine engine seals etc. [88].

22

Some of physical and mechanical properties of TiC are presented in Table 2.2. Also, TiC has been employed in different composite materials systems such as Al-TiC, Mg-TiC, SiC-TiC and TiB_2-TiC. Titanium carbide based composites with nickel alloys and steels are now used in high performance applications where wear and corrosion represent the main sources of material failure [89].

Table 2.2 Typical properties of TiC [90-93]

Property	
Elastic Modulus, GPa	439.43 at RT
Shear Modulus, GPa	110 - 193
Compressive Strength, MPa	2500
Hardness, Rockwell A	93
Flexural Strength, 4-point bending MPa	560
Microhardness (VH), 50g Ceramic , kg/mm^2	2900 - 3200
Density, g/cm^3	4.938
Melting Point (ºC)	3070
CTE, $10^{-6}/K$	7.7
Specific Heat, J/Kg. K	564.33
Thermal Conductivity, W/m. K	17.14 – 30.93 at RT 5.64 at 1000ºC
Poisson' Ratio	0.187-0.189

Crystal Structure of TiC

TiC is a mainly covalently-bonded ceramic with partly ionic bonding. TiC crystallizes in the rock salt structure (NaCl) which is a face-centered cubic close-packed crystal structure (FCC) as shown in Figure 2.5. TiC belongs to the group of *interstitial carbides* where carbon atoms occupy the (interstitial) octahedral sites between the close packed Ti atoms [94, 95].

TiC exists over a wide range of substoichiometry (i.e. TiC_x, x=0.6-0.98) with the carbon content varying between 32 and 49 at.%. Due to this variation, a large amount of carbon vacancies may be present [96] causing a variation in cell parameters and consequently variations in properties.
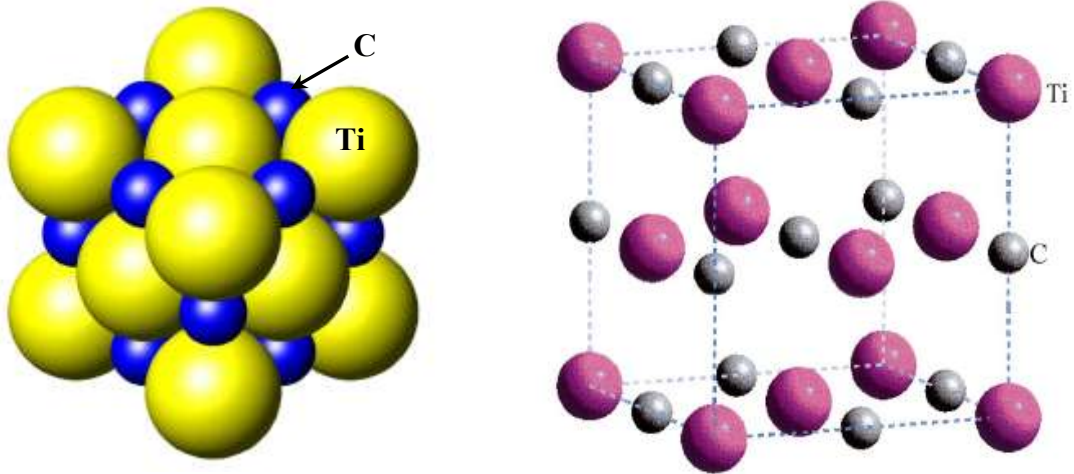
Figure 2.5 NaCl crystal structure of TiC with interstitial C at the octahedral sites [94, 95]

It has been observed that if the C vacancies in the TiC structure are ordered, this can help Al to fill the spaces forming a ternary compound: Ti_2AlC or Ti_3AlC_2 [97, 98]. The crystal structure of Ti_2AlC and Ti_3AlC_2 is hexagonal and the stacking sequence depends on the stoichiometry where Ti_3AlC_2 has one Al layer for every third TiC layer while Ti_2AlC has one Al layer for every second TiC layer as shown in Figure 2.6.

The atomic bonding in these ternary compounds is a combination of metallic, ionic, and covalent [99]. The covalent-ionic Ti-C bonds are comparable to bonds in the binary TiC but they are stronger than the metallic Ti-Al bonds in the ternary structure [100]. Because of the relatively weak bonds between the TiC and Al layers in the basal planes, these materials have an anisotropic character [101].

24
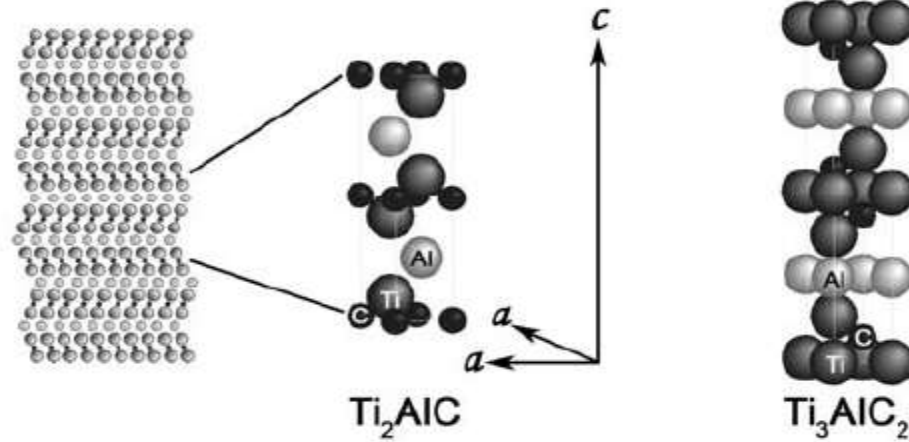
Figure 2.6 Crystal structures of Ti_2AlC and Ti_3AlC_2 [97, 98]

Ti_2AlC exhibits a combination of properties of both ceramics and metals such as low density, high modulus, good thermal and electrical conductivity, excellent thermal shock and high-temperature-oxidation resistance, and machinability. This attractive combination of properties makes Ti_2AlC a highly promising candidate for different applications. However, its low hardness and lower strength limit the applications of Ti_2AlC especially at elevated temperatures [102]. Some of the mechanical properties of Ti_2AlC are presented in Table 2.3.

Table 2.3 Mechanical properties of Ti_2AlC [103]

Compressive strength (MPa)	Flexural strength (MPa)	Vickers hardness (GPa)
670	384	4.2-5.7

2.3.2.2 Titanium diboride (TiB₂) Properties and Crystal Structure

TiB_2 is one of transition metal–metalloid compounds. TiB_2 is characterized by attractive physical and mechanical properties such as high melting point, low density, high hardness, high specific strength, good wear resistance and excellent thermal and chemical

stability up to 1700ºC [104]. There are several applications of TiB_2 such as impact resistant armor, cutting tools, wear resistant coatings and crucibles [105]. Some of the physical and mechanical properties of titanium diboride are presented in Table 2.4. TiB_2 particles are used in steel [106], Al [107], Mg matrix composites [108] or ceramic composites with titanium and boron carbides [109]. TiB_2, as all diborides, is essentially stoichiometric which represents an important advantage over carbides and nitrides. Thus, they have much lower defect-controlled resistivity making them promising for industrial application in electronic devices [110].

Table 2.4 Typical properties of TiB_2 [90-93]

Property	
Elastic Modulus, GPa	565 at RT
Shear Modulus, GPa	255
Compressive Strength, MPa	1800
Flexural Strength, 4-point bending MPa	500
Microhardness (VH), 50g Ceramic , kg/mm^2	3400
Density, g/cm^3	4.5
Melting Point (ºC)	3225
CTE, 10^{-6}/K	6.4
Specific Heat, J/Kg. K	617
Thermal Conductivity, W/m. K	96 at RT and 78.1 at 1000ºC
Poisson' Ratio	0.108

Crystal Structure of TiB_2

Titanium diboride crystallizes in the hexagonal structure as AlB_2 with the space group *P6/mmm* and lattice parameters: *a* = 3.0236 Å, *c* = 3.2204 Å as shown in Figure 2.7.

Ti atom exists at the origin of the unit cell while the two boron atoms are at the (1/3, 2/3, 1/2) and (2/3, 1/3, 1/2) sites.

The structure is simple and defined by two lattice parameters, *a* and *c,* and has a very small unit cell [105].
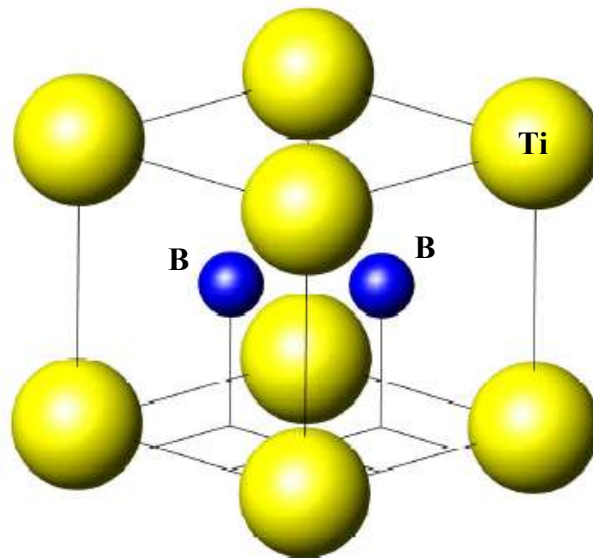
Figure 2.7 The hexagonal unit cell of single crystal TiB_2 [91]

2.3.3 Fabrication of (TiC-TiB₂)/Mg matrix composites

There are several methods to fabricate particulate reinforced Mg MMCs as discussed previously (section 2.2.3). In these techniques, the combination of the reinforcing particle phase (borides, carbides nitrides, and oxides) and the matrix material takes place by *ex-situ* methods. However, in this section, the fabrication of magnesium matrix composites reinforced with *in-situ* TiC, TiB_2 or $TiC-TiB_2$ particles based on solid-liquid reaction process is discussed. This process can be considered a solvent-assisted reaction wherein the reinforcing particles are created in the solvent medium (the matrix) through diffusion

of the components. Based on the parameters, this process can be categorized into the following routes [3].

2.3.3.1 Self-propagating high-temperature synthesis (SHS)

SHS was developed in the late 1960s by Merzhanov and coworkers [111-114]. In this process, materials with a sufficiently high heat of formation are synthesized in a combustion wave, which after ignition, spontaneously propagates throughout the reactants converting them into the products. The self-sustaining reaction front is a very important feature of these reactions. SHS reactions have to satisfy three basic requirements in order to be self-sustaining. The first is that the reaction has to be highly exothermic to maintain the propagation front by heating the unreacted portion of the sample [115]. The second is that one of the reactants should form a liquid or vapor phase to facilitate the diffusion of the fluid phase reactant to the reaction front. Also, the rate of heat dissipation (via conduction or radiation) must be less than the rate of heat generation otherwise the reaction will be extinguished [3].

SHS, also known as combustion synthesis, is gaining much attention as an important technique for synthesis of refractory materials because of its many attractive advantages, such as high purity of product, low processing cost, and efficient in energy and time [5].

In the 1980s and 1990s, the SHS process was extensively utilized for the production of ceramics, intermetallic and intermetallic matrix composites (IMCs). However, its use for MMCs was limited [3]. This is because for MMCs, the `inert' matrix acts as a diluent which can cause damping of the combustion wave while the reactions for the reinforcement formation and matrix formation are exothermic in the case of IMCs.

Therefore, only ceramic reinforcements with a high heat of formation are suitable for SHS processing of MMCs. Furthermore, a high fraction of ceramic reinforcement should be maintained which is another basic requirement. For Mg-based MMCs, TiC and TiB_2 seem to be feasible reinforcements, both from the point of view of the exothermicity of the formation reactions and their stability in the Mg matrix.

TiC Reinforced Magnesium Matrix Composites using SHS

Many researchers [4, 5, 25, 54] have worked on the TiC-Mg system using SHS technique. Wang *et al.* [54] fabricated TiC/Mg composites using the SHS reaction of molten magnesium and a preform consisting of (Al-Ti-C) powders. In the process, a blend of Al, Ti and graphite powders was pressed at 70-75 MPa by a hydrostatic press. The resulting compact was preheated in a vacuum oven at 300, 450 and 600ºC before putting it in a liquid AZ91D magnesium alloy under a SF_6/CO_2 protective atmosphere. They [54] only focused on understanding the SHS reaction mechanism without testing the material. They found that the effect of preheating of the preform plays an important role in the SHS reaction in the molten magnesium. However, the interpretation of the effect of the preheating temperature and the optimum value were not reported. Microstructural examination reveals a relatively uniform rather than highly uniform distribution of TiC particulates in the magnesium matrix and this is because it is difficult to control the stirring parameters. The effect of Al in the preform was predominant in the SHS reaction besides serving as a diluent to lower the combustion temperature.

In the same framework, Jiang *et al.* [5] prepared magnesium matrix composites reinforced with TiC particles via SHS. In this study, a TiC–Al master alloy was processed via SHS reaction of (Al-Ti-C) powders through the ignition of the compact bottom

29

surface by applying a current of 12A through a resistance wire. The master alloy was preheated to 200ºC and then added into molten magnesium to avoid a large temperature decrease during this process. After that, by using the semi-solid slurry stirring technique and casting, TiC PRMMCs were obtained. They suggested an SHS reaction mechanism similar to that suggested by Wang *et al.* [54].

In the combustion reaction of the Al-Ti-C system, titanium reacts with aluminum to form titanium aluminides ($TiAl_x$) followed by $TiAl_x$-C reaction to form TiC. The TiC was used as a reinforcement for the magnesium matrix while Al was used as an alloying element. Homogenously clean, fine TiC particles embedded in a magnesium alloy matrix were obtained by stirring. The UTS, hardness, and wear resistance of the fabricated composites were tested and found higher than those of the unreinforced magnesium alloys. It was observed that the presence of aluminum surrounding the TiC particles enhanced the wetting of TiC particulates by the magnesium alloy.

Using the same technique (SHS), Guan *et al.* [4] studied the effect of the compact density on the fabrication of *in-situ* Mg-TiC composites. In this process, a blend of (Al-Ti-C) was pressed under a hydraulic press at pressures of 60-100 MPa to give different relative densities from 65 to 85%. Then the compact was added into liquid magnesium. To reach the initiation temperature of the SHS of the Ti-C-Al system, the combustion reaction was ignited by heating the bottom surface of the compact through a tungsten filament. They found that the ignition temperature of various compact densities are about 835-965 K and they suggested that the combustion reaction can be ignited as the compacts were put in liquid magnesium at temperature over 1023 K to form *in-situ* TiC particles in the liquid magnesium resulting in *in-situ* Mg-TiC composites. They supported

the reaction mechanism of the thermal explosion synthesis in Ti-C-Al suggested by Wang *et al.* [54]. They found that the density of the green compact plays a crucial role in the SHS reaction in the liquid magnesium but this factor was not completely discussed and needs more investigation. The tensile strength, hardness, and abrasive wear resistance were studied for the successfully fabricated composites and they were higher than those of unreinforced AZ91 magnesium alloy.

Chaubey *et al.* [25] also studied the effect of the compact density and preheating temperature of the compact on the SHS reaction and then on the fabrication of i*n-situ* Mg-TiC composites. For this purpose, compacts of Al-Ti-C with different densities and preheat temperatures were added to the magnesium melt under a protective gas of Ar. Then processing of the magnesium matrix composites was carried out by melt stirring and composite casting. Also, the results support the mechanism of the thermal explosion synthesis in Ti-C-Al reported by Wang *et al.* [54]. Chaubey *et al.* [25] interpreted the effect of the compact density very well on the capillary spreading and particle rearrangement while it couldn't interpret the role of the preheating temperature of the compact on the SHS reaction. The results revealed that no SHS reaction occurs in the magnesium melt when the preform temperature is below 450ºC and the compact density is less than 68% of the theoretical density. Compact density of 75% was found optimum for SHS reaction and TiC particle distribution.

TiB$_2$ Reinforced Magnesium Matrix Composites using SHS

Wang *et al.* [36] fabricated *in-situ* TiB$_2$/Mg matrix composites using SHS technique through the reaction between the molten magnesium and green preform consisting of Al, Ti and B powders. They found a relatively uniform distribution of TiB$_2$ particulates in the

matrix but the unfavorable brittle Al_3Ti phase with large size was also formed in the Mg composites, which may degrade the plasticity of the composite. Afterwards, Wang *et al.* [116] succeeded in eliminating Al_3Ti from the TiB_2-Al master alloy by controlling the molar ratio of Ti to B in the starting mixture (Al-Ti-B). They found that the transient Al_3Ti was almost eliminated in the master alloy and then in the TiB_2/AZ91 composite fabricated using a master alloy with $n_{Ti}:n_B = 1:2.5$ in the starting mixture. Also, the distribution of TiB_2 through the Mg composite appeared to be more homogeneous.

(TiC-TiB_2) Reinforced Magnesium Matrix Composites using SHS

Wang *et al.* [117] also attempted to fabricate magnesium matrix composites reinforced with TiB_2 and TiC-TiB_2 particles. First, they fabricated TiB_2/Mg MMC by adding a TiB_2-Al master alloy processed via SHS reaction in the Al-Ti-B system into molten magnesium. They again found large brittle Al_3Ti flakes in the composite microstructure. Secondly, they incorporated the Al-Ti-B system with an appropriate amount of carbon to form the (TiB_2-TiC)-Al master alloy by SHS. Carbon was used to eliminate the brittle flakes. Finally this master alloy was used to fabricate the (TiC-TiB_2)/Mg composite. However, the reaction mechanism was not completely investigated.

Using the same technique (SHS), Ma *et al.* [15] fabricated magnesium matrix composites reinforced with TiB_2 and TiC particles but in this case via a master alloy route using a low cost Al-Ti-B_4C system. They are the first to use B_4C instead of B or C in the starting materials. Reaction mechanism, hardness and wear resistance of the composites were investigated. They found that the hardness and the wear resistance of the (TiB_2-TiC)$_p$/AZ91 composites were significantly improved compared to the alloy.

32

2.3.3.2 Flux-assisted Synthesis (FAS)

This patented process which is also known as mixed-salt reaction was developed by the London Scandinavian Metallurgical Company (LSM) to fabricate *in-situ* aluminum matrix composites as shown in Fig. 2.8 [118].
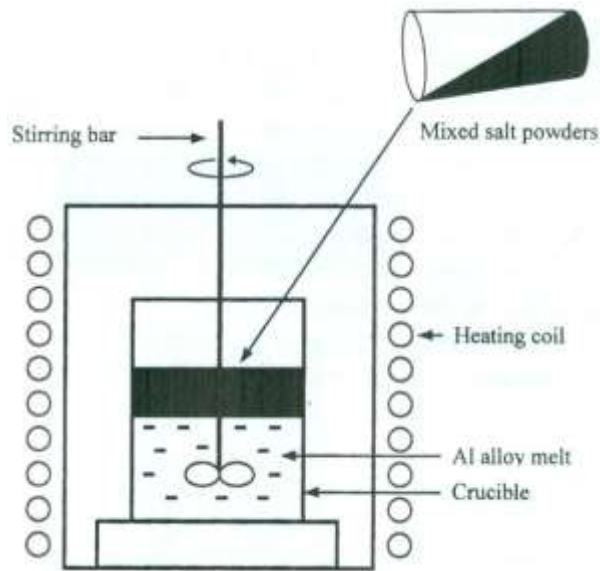
Figure 2.8 Schematic diagram of an apparatus for fabricating *in-situ* MMCs by FAS [118]

During the synthesis, salts of potassium hexafluorotitanate (K_2TiF_6) and potassium tetrafluororate (KBF_4) are mixed with each other and then introduced into a stirred aluminum melt with an atomic ratio corresponding to Ti/2B. The salts and the molten aluminum, during stirring, react exothermally to form *in-situ* TiB_2 according the following sequences [119]:

$$3K_2TiF_6 + 13Al = 3TiAl_3 + 3KAlF_4 + K_3AlF_6 \tag{2.1}$$

$$2KBF_4 + 3Al = AlB_2 + 2KAlF_4 \tag{2.2}$$

$$AlB_2 + TiAl_3 = TiB_2 + 4Al \tag{2.3}$$
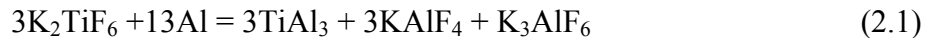
After that, the mixture is cast into a mold to remove the slag containing $KAlF_4$ and K_3AlF_6 [119].

Many works were dictated on *in-situ* Al metal matrix composites utilizing the FAS process [120-124] while the works on *in-situ* magnesium matrix composites are still limited.

Matin and Lu [67] are probably the first researchers to fabricate Mg MMCs reinforced with *in-situ* $TiB+TiB_2$ particulates using the FAS process via reacting magnesium melt with KBF_4 and K_2TiF_6 compounds. It was observed that both thermodynamics and kinetics played an important role in the formation of the Mg *in-situ* composite. It was found that the formation of various phases depends on both temperature and duration of reaction holding time. Magnesium plays an important role in the reaction when the reaction between the compounds, KBF_4 and K_2TiF_6, is chemically and thermodynamically unfavorable. Finally the *in-situ* formed compounds were not only TiB_2 but also, TiB and MgB_6.

Going one step further, Cao *et al.* [125] fabricated a TiB_2/Mg matrix composite by adding a TiB_2-Al master alloy into molten magnesium. However, this master alloy was processed via a FAS reaction where the same two salts (KBF_4 and K_2TiF_6) were mixed and introduced into a stirred aluminum melt to react with liquid Al to form the TiB_2-Al master alloy.

2.3.3.3 Remelting and Dilution (RD)

This technique is one of the *in-situ* synthesis methods combining two processes. The first one is the preparation of the master alloy that contains the reinforcements. The second one is dilution of the master alloy into the metal matrix melt. By using the RD technique,

Zhang *et al* [126] fabricated a TiC/AZ91D matrix composite starting with a mixture of Al, Ti and C powders and after the sintering of the compact of this mixture, the block was diluted in a molten Mg alloy. The matrix and fabricated samples were age hardened. It was found that adding TiC particle to the AZ91D matrix gave a fine grain size, more interfaces between TiC and magnesium and a high dislocation density in the magnesium matrix accelerating the precipitation of $Mg_{17}Al_{12}$ phase. Also, it was found that age hardening time and temperature play a very important role in the hardening of the AZ91D alloy and composites.

By using the same technique, Wang *et al.* [16] successfully fabricated (TiB_2-TiC)/Mg matrix composites. The preform was a sintered block of a mixture of Al-Ti-B_4C as in their previous work [15]. Microstructure and tensile characterizations were performed on the fabricated composites. The results revealed that (TiB_2-TiC)/Mg composites had higher modulus, 0.2% YS, and UTS than heat-treated AZ91 alloys, while ductility was lower.

Also, Zhang *et al.* [14] have successfully fabricated Mg-MMCs reinforced with TiB_2 and TiC ceramic particulates using the same technique (RD). They observed that the particulates are uniformly distributed in the matrix due to the fine size of the reinforcements, the good wettability between magnesium and reinforcement, and the accurate selection of stirring parameters. Also, the results revealed that the fabricated composites have improved mechanical properties compared to the unreinforced matrix alloy. On the other hand, brittle fracture was observed and this can be attributed to the HCP crystal lattice of magnesium matrix and the presence of brittle reinforcement particulates.

2.3.3.4 Reactive Spontaneous Infiltration (RSI)

Reactive Spontaneous Infiltration or *in-situ* reactive infiltration technique is an innovative process which is used for the production of MMCs. In this technique, there are two processes that take place simultaneously. First is the infiltration of the molten metal through the preform by the capillary effect without externally applied pressure. Second is the *in-situ* reaction between the starting powders and the molten metal to synthesize the reinforcement phases. Finally, MMCs reinforced with a very fine and thermodynamically stable reinforcing ceramic phase can be produced.

Magnesium matrix composites reinforced with ceramic particles have been successfully manufactured via this technique with great reduction in cost [11]. Thus, this technique can overcome the high cost problem of other MMCs. Besides, it is a simple process.

The spontaneous infiltration of the molten metal into the preform depends on the ability of the liquid to wet or spread on the solid surface which is called wettability or wetting. In general, this wetting behavior has to be considered in the composites fabrication since the bond between the reinforcing particles and the matrix strongly depends on it [127].

Dong *et al.* [20] utilized the *in-situ* reactive infiltration technique, a combined processing route of *in-situ* reaction of elemental Ti and C powders and spontaneous infiltration of molten magnesium into the ($Ti_p + C_p$) preform to fabricate TiC particulate reinforced magnesium matrix composites. No third metal powder, such as Al, was added to the preform and no reactive gas was used unlike the (Ti + C)/Al system [7]. It was observed that smaller elemental particle size and an elevated temperature up to 1073 K

36

were necessary to synthesize TiC_p reinforced magnesium matrix composites. However, still not all the Ti and C in the preform reacted to form TiC as noted from SEM and XRD analyses.

Chen *et al.* [11] using the same technique fabricated TiC/AZ91D magnesium matrix composites with interpenetrating networks based on the results of Dong *et al.* [20]. They used a preform consisting of coarse Ti powder but very fine C powder to enhance the reaction between Ti and C. The volume percentage of the ceramic reinforcement formed *in-situ* could be controlled by the relative density of the preform ($Ti_p + C_p$) and considering the intrinsic shrinkage of the reaction products resulting from the *in-situ* reaction. Hence, tailoring the mechanical and physical behaviors of the composite is possible. The TiC_x formed in this process has a variable stoichiometry, where x depends on both the processing conditions and initial particle sizes of the elemental powders utilized. However, they also observed residual carbon in the as-fabricated TiC/Mg composites. Thus, to eliminate this residual carbon in the as–fabricated composites, the recommended C/Ti molar ratio has to be lower than 1. The effects of Ti and C particle size, the processing parameters (temperature and time), and the magnesium melt were studied. These results were supported by the work of Qun *et al.* [21].

Chen *et al.* [22] fabricated 47.5 vol.% TiC/AZ91D magnesium matrix composites using the RSI technique. They studied the tensile strength of the composites at elevated and room temperature and compared them with results from AZ91D magnesium alloy. The results showed that the fabricated composites have higher ultimate strength at room and elevated temperatures. On the other hand, the observation of the fracture surface of the composites revealed brittle characteristics at room and elevated temperatures, while in

the case of unreinforced AZ91D, transition from brittleness to ductility was observed at elevated temperatures.

Similar to the work of Chen *et al.*, Wang *et al.* [23] produced 42.1 vol.% TiC/AZ91D magnesium matrix composites with interpenetrating networks by the same technique and also studied the tensile properties of the composite and the alloy.

For further advancement in this area, Chen *et al.* [19] fabricated exactly the same 42.1 vol.% TiC/AZ91D magnesium matrix composites in order to study the compressive creep behavior of the AZ91D alloy and the composite material. The results revealed that the TiC/AZ91D composite has higher creep resistance than that of the AZ91D alloy. As expected by increasing the deformation temperature or applied stress, the creep rates increases.

To improve the compression properties of magnesium matrix composites, Cao *et al.* [24] produced TiC/Mg matrix composites via *in-situ* reactive infiltration process and tested the alloy and the fabricated composite through compression testing at different temperatures and strain rates. The preform is a mixture of Ti and C powders without the Al additions that are responsible for poor mechanical properties especially at elevated temperatures. The results revealed that the TiC/Mg composites have improved compressive properties at room and elevated temperature compared with the AZ91 alloy. But these improvements are limited by higher temperature and lower strain rate. They also studied the fracture mechanism where a typical brittle fracture was observed. The results revealed a low ductility for the TiC/AZ91D at room temperature while an adequate elongation to fracture was observed at elevated temperature.

After that Cao *et al.* [128] fabricated magnesium matrix composite reinforced TiC particles by the spontaneous infiltration of molten magnesium alloy into preforms consisting of Al-Ti-C powders. In this process they added Al again to the Ti-C preform to enhance the reaction between Ti and C in the liquid of magnesium alloy. They studied the damping capacity of the AZ91D alloy and TiC/AZ91D matrix composite with different reinforcement percentages. They found an increase in the damping capacity of the composites compared to that of AZ91D alloy and that the damping capacity increases with increasing the reinforcement volume percentage.

To date, the *in-situ* reactive infiltration technique has not been used to fabricate magnesium matrix composites using the Ti-B$_4$C system.

It can be concluded that all the techniques used to fabricate *in-situ* (TiC-TiB$_2$)/Mg matrix composites depend on the addition of aluminum powder to the starting materials, either Ti-B or Ti-B$_4$C system, because aluminum acts as a reaction intermediary to facilitate the reaction between Ti and B or Ti and B$_4$C. Aluminum diffuses into the magnesium melt and forms Mg$_{17}$Al$_{12}$ (γ-phase) during solidification. As known, aluminum is the most important alloying element in magnesium alloys where it improves the tensile strength of the alloy by the formation of Mg$_{17}$Al$_{12}$ intermetallic phase. However, high aluminum content leads to the formation of the interdentritic grain boundary phase Mg$_{17}$Al$_{12}$ leading to limited ductility of the alloy [17]. The BCC structure of Mg$_{17}$Al$_{12}$ is not coherent with the HCP structure of magnesium leading to a weak Mg/Mg$_{17}$Al$_{12}$ interface. Also, at elevated temperatures, grain boundary sliding can take place due to the poor thermal stability and the discontinuous precipitation of the γ-phase

inside the magnesium alloy [24]. As a result, poor strength at elevated temperatures and low creep resistance of magnesium alloys are obtained [18]. From this point of view, the contribution of this work is to fabricate (TiC-TiB$_2$)/Mg MMCs using *in-situ* reactive infiltration technique using a preform consisting of a mixture of titanium and boron carbide powders without the addition of aluminum.

To date, papers on the production of (TiC-TiB$_2$)/Mg matrix composites starting with either Ti and B or Ti and B$_4$C without Al could not be found in the literature. Also, the *in-situ* reactive infiltration technique has not been used before to fabricate magnesium matrix composites using the Ti-B$_4$C system. However, a few researchers [11, 19-24] used this technique with Ti and C to produce TiC/Mg matrix composites.

2.4 Mechanical Properties of Mg MMCs

As mentioned earlier, the mechanical properties of magnesium or magnesium alloys such as tensile strength and Young's modulus can be improved by introducing suitable ceramic reinforcing particles into the matrix material such as TiC and TiB$_2$ particles. But at the same time, this improvement has to be weighed against reduction in other properties such as ductility and the additional cost.

2.4.1 Tensile Strength

In general, the stiffness, hardness, tensile strength and wear resistance of magnesium matrix composites increase with increasing the volume percentage of the reinforcing particles or short fibers while the ductility decreases. Greater strengthening effect can be achieved by hybrid reinforcements which involve more than one kind of particles or whiskers than a single reinforcement [129]. The strengthening mechsanisms in

40

magnesium matrix composites are achieved due to particle strengthening, work hardening, load transfer and grain refinement of the matrix alloy. The dispersion of fine and hard particles in the matrix significantly blocks dislocation motion and hence strengthens the material. When the composite is strained, work hardening takes place by generating a high density of dislocations due to the strain mismatch between the matrix and the reinforcement. Also, it can be said that magnesium strength is highly susceptible to grain size. Hence, higher strength at room temperature for both Mg alloys and their composites can be obtained by grain refinement [27]. Table 2.5 [16, 130] shows a comparison of the typical properties of commercially available magnesium matrix reinforced with TiC or TiC-TiB$_2$ particles with unreinforced alloy.

Table 2.5 Mechanical Properties of some *in-situ* magnesium matrix composites at room temperature [16, 130]

Material	E (GPa)	YS (MPa)	UTS (MPa)	Elongation (%)
AZ91	45	97	165	2.5
AZ91-5 vol.% TiC	47.5	106	197	1.9
AZ91-8 vol.% TiC	49.1	113	225	1.2
AZ91-10 vol.% TiC	50.7	114	232	1.1
AZ91-8 wt.% (TiC-TiB$_2$)[*]	53	95	298	2.4

* AZ91 matrix alloy used with this composite has 6.0% elongation.

It is clear that all of these composites have higher strength than that of the unreinforced alloy by introducing the ceramic hard particles into the matrix alloy. Also as shown in Table 2.6, compared to the AZ91 alloy, the mechanical properties of 8 wt.% TiC/AZ91 improve due to the grain refinement and high dislocation density in the composites [131].

Table 2.6 Mechanical Properties of 8 wt.% TiC/AZ91D matrix composite and the AZ91D alloy [131]

Material	E (GPa)	Grain size (μm)	YS (MPa)	UTS (MPa)	Elongation (%)
AZ91	45±0.5	62±2	95±0.5	198±0.5	2.5±0.5
AZ91-8 wt.% TiC	49.1±0.5	12±2	115±0.5	235±0.5	1.0±0.5

2.4.2 Ductility

Generally, hard ceramic particles reduce the ductility of magnesium matrix composites due to the resistance to the dislocation motion of the hard particles. In contrast to ceramic reinforced magnesium matrix composites, magnesium matrix composites reinforced with elemental metallic powders have a much better ductility because of the reduced possibility of the breaking of the particles and interface [27]. As shown in Tables 2.5 and 2.6, the elongation decreases with the addition of hard ceramic reinforcing particles.

2.4.3 Hardness

Jiang *et al.* [5] indicated that the hardness of 10 vol.% TiC reinforced AZ91 matrix composite increased by ~ 40% compared with the unreinforced matrix alloy. Also, Ma *et al.* [15] showed that the hardness of AZ91 reinforced with 5.5 wt.% TiC-TiB$_2$ particles is increased by about 42% compared with the unreinforced AZ91D matrix. Moreover, Zhang *et al.* [131] found that the hardness of Mg MMCs reinforced with 8 wt.% TiC-TiB$_2$ particles is improved by about 60% compared with that of the unreinforced AZ91D.

It can be concluded that the increase in hardness is attributed to (a) the presence of TiC or TiC-TiB$_2$ particles in the matrix and (b) a higher resistance to localized plastic deformation of the matrix due to the presence of these particles.

2.4.4 Young's Modulus

Zhang *et al.* [130] found that a wide range of mechanical properties such as strength, ductility and Young's modulus can be achieved by controlling the volume percentage of the reinforcing particles in the matrix. The results revealed that Young's modulus increased to 50.7 GPa when 10 vol.% TiC reinforced the AZ91D alloy. Also, Zhang *et al.* [131] found that Young's modulus increased to 49.1 GPa when 8 wt.% TiC reinforced AZ91 alloy. Furthermore, Zhang *et al.* [16] reported a significant increase in Young's modulus from 45 GPa for the unreinforced AZ91 alloy to 53 GPa for the composite reinforced with 8 wt.% TiC-TiB$_2$ particles.

2.4.5 Wear Resistance

Different engineering materials such as MMCs have been employed for applications in which wear resistance is required. This type of material is attractive in tribological applications due to the combination of the toughness of the matrix together with the hardness of the reinforcement particles which enables optimal wear resistance [132].

The dependence of the wear resistance on the hardness and strength of the material was predicted by Archard's Equation [133] as follows:

$$Q = \frac{KWL}{H} \qquad (2.4)$$

Where, Q is the total volume of wear debris produced, W is the total normal load, H is the hardness of the softest contacting surfaces, K is a dimensionless constant and L is the sliding speed. This equation can be used in both sliding adhesive or abrasive wear.

The competitive advantages of MMCs as tribomaterials include their unique ability to fabricate a composite with required specific engineering strength and stiffness

[134].The wear resistance of MMCs depends on the selection of suitable reinforcement particles. Also, it is important for wear resistance to be combined with other properties such as high thermal conductivity to dissipate friction heat.

Many works on magnesium matrix composites reinforced with TiC particles were done to investigate the wear resistance of these composites as attempts to improve the wear resistance of the magnesium matrix [4, 5]. For more investigation, Xiu *et al.* [135] studied the sliding wear behavior of AZ91 alloy and the *in-situ* fabricated TiC/AZ91 matrix composites. They found that the wear volume loss and the friction coefficient increase with increasing the load and time in both materials. However, the wear resistance of the composite is higher than that of the AZ91 alloy and increases with the TiC content.

Afterwards, Yao *et al.* [136] also investigated the wear behavior of AZ91D and the TiC/AZ91 composites fabricated by spray deposition. They found the same trend as Xiu *et al.* [135]. Besides, they studied the wear mechanism at different applied loads where they found the dominant wear mechanism was an oxidative mechanism at low load (10N) while at higher load (50N), delamination was the dominant one. However, the authors reported unrealistic values for Young's modulus of the matrix and the composite which puts doubt on this work.

It can be observed in all studies on the wear behavior of the composite and the unreinforced matrix that the wear resistance strongly depends on the hardness of the material where the wear resistance increases with increasing the hardness. On the other hand, works on the investigation of the wear resistance of (TiC-TiB$_2$)/Mg matrix composites are still limited. As mentioned before, Ma *et al.* [15] investigated the wear

44

resistance of fabricated magnesium matrix composites reinforced with TiB_2 and TiC particles and found an improvement in wear resistance in composite which has higher hardness than the alloy.

Chapter 3

Objectives

Based on the literature review in the previous chapter, it is apparent that researchers have succeeded to produce magnesium matrix composites reinforced with *in-situ* TiC and TiB_2 particles using for example self-propagating high temperature synthesis (SHS) and remelting and dilution (RD) technique. In all these works, they added Al powder to the starting raw material in order to facilitate the reaction between titanium and boron carbide where Al acts as a reactive intermediary. However, the free Al remaining after the reaction diffuses into the magnesium melt forming more $Mg_{17}Al_{12}$ causing poor mechanical properties especially at elevated temperatures.

The main purpose of this work is to fabricate Mg MMCs reinforced with a network of TiC and TiB_2 phases using an *in-situ* reactive infiltration technique without Al addition. The mechanical and physical properties of these composites have been studied. The matrix is pure magnesium, AM60B or AZ91D alloy and the preform consists of a mixture of titanium and boron carbide powders. More emphasis will be directed towards AZ91D alloy in the current research. The preform material in this work is a mixture of Ti and B_4C powders. Hence, fabricating these composites without adding a third metal powder such as Al to the preform will be a major contribution of this work.

The specific objectives are:

- Understanding the *in-situ* reaction mechanism,

- Studying the effect of the processing parameters such as temperature, holding time and the green compact relative density (*RD*) to obtain the optimal processing parameters for producing magnesium matrix composites reinforced with a network of TiC-TiB$_2$,

- Tailoring the volume percentage of the *in-situ* formed reinforcement by controlling the preform relative density taking into consideration the shrinkage of the reaction products,

- Controlling the volume percentage of the *in-situ* formed reinforcements by a second method through mixing of Mg or magnesium hydride (MgH$_2$) powder to the starting powders of Ti and B$_4$C, and

- Characterizing the physical and mechanical properties of the produced Mg matrix composites.

Chapter 4

Materials and Experimental Methods

The present work involves the development of an infiltration technique for fabricating TiC-TiB$_2$ reinforced magnesium alloys composites. Not only has composite fabrication been achieved, but also an important contribution is made in investigating the *in-situ* reaction mechanism. The MMCs have been fabricated without adding aluminum to the preform through a cost-effective infiltration technique. A schematic of the experimental procedure established for the whole study is shown in Figure 4.1. Each of the main steps will be discussed in the following sections.
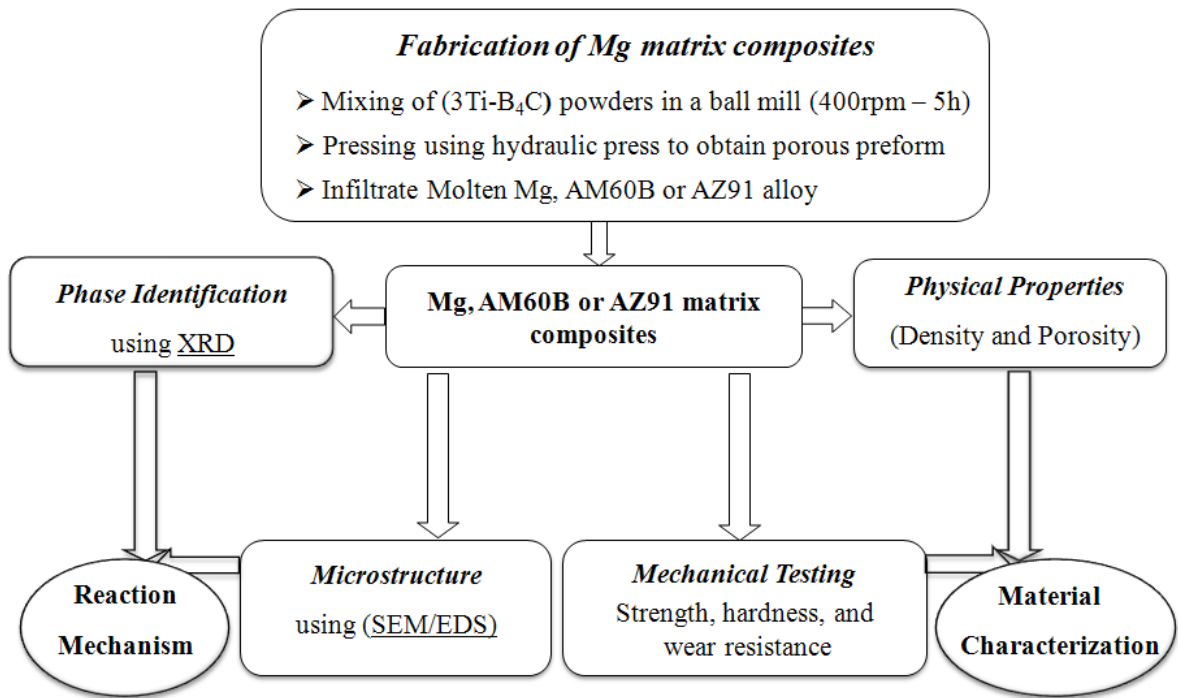
Figure 4.1 Experimental procedure flow chart

In this work, three systems of starting powders have been used to synthesize the ceramic reinforcing phases. The first system is using Ti and B$_4$C powders, the second and

third system are using Ti, B_4C with pure magnesium and Ti, B_4C with magnesium hydride (MgH_2) powders, respectively.

The experimental work is divided into three stages: the first stage is involved with studying the *in-situ* reaction mechanism of the Ti-B_4C system infiltrated with Mg and the role of magnesium to enhance this reaction. This stage also includes studying the reaction mechanism of the Mg-Ti-B_4C and MgH_2-Ti-B_4C systems infiltrated with Mg to investigate the role of Mg or MgH_2 powder on the reaction.

The second stage corresponds to studying the effect of processing parameters on the fabrication of the particulate reinforced MMCs by infiltration of the 3Ti-B_4C preform with molten magnesium or magnesium alloys.

Finally, microstructural and mechanical characterization of the composites has been performed. Throughout this work, different characterization and testing techniques have been utilized. The experimental details associated with these techniques are explained in this chapter.

4.1 Raw Materials

4.1.1 Matrix Materials

Commercial grade pure magnesium and magnesium alloys, AM60B and AZ91D, were used to fabricate the composites. The chemical compositions of the magnesium alloys from the manufacturer (Beijing Guangling Jinghua Science & Technology CO., China) are as shown in Tables 4.1 and 4.2. Some physical properties of pure Mg, AZ91 and AM60B castings are presented in Table 4.3.

Table 4.1 Composition limits of AZ91D from the manufacturer, wt.%

Al	Mn	Zn	Si	Fe	Cu	Ni	Mg
8.94	0.221	0.7	0.0208	0.001	0.0014	0.0003	balance

Table 4.2 Composition limits of AM60B from the manufacturer, wt.%

Al	Mn	Zn	Si	Fe	Cu	Ni	Mg
6	0.25	0.22	0.10	0.005	0.010	0.002	balance

Table 4.3 Some physical properties of Pure Mg, AZ91 and AM60B castings [87]

Property	Pure Mg	AZ91D	AM60B
		F Temper	F Temper
Density (ρ), g/cm^3	1.738	1.81	1.8
Melting Range (T),$^\circ$C	650	468-598	565-615

4.1.2 Reinforcement raw materials

The starting powders for system I (Ti-B$_4$C) used for synthesizing TiC-TiB$_2$/Mg composites are 72.2 wt. % Ti (-325 mesh, 99.61% purity, Alfa Aesar Co.) and 27.8 wt. % B$_4$C (99% purity, <10 μm particle size, Alfa Aesar Co.) powders. Titanium and boron carbide powders are at a molar ratio (3:1) corresponding to that of stoichiometric TiC and TiB$_2$.

For system II (Ti-B$_4$C with pure Mg powder), pure Mg powder (-325 mesh, 99.8% purity, Alfa Aesar Co.) was added to the 3Ti-B$_4$C mixture at different weight percentages while for system III (Ti-B$_4$C with MgH$_2$ powder), MgH$_2$ powder (98 % purity, Alfa Aesar Co.) was added to the 3Ti-B$_4$C mixture at different weight percentages

50

as well. Pure magnesium or MgH_2 powder is added to the $3Ti$-B_4C preform to increase the magnesium content in the composite. The following sections will show the specifications of these powders.

4.1.2.1 Titanium (Ti)

Pure titanium (-325 mesh, 99.5%, Alfa Aesar Co.) powder is used in this work. The chemical composition, as reported by the manufacturer, is listed in Table 4.4. The mean particle size of this powder is about 29 μm. The as-received particle size distributions are obtained using a laser scattering particle size analyzer (Model LA-950) as shown in Figure 4.2.

Table 4.4 Typical chemical analysis for Ti powder

Titanium	(Ti)	99.61 %
Oxygen	O	0.235 %
Hydrogen	H	237 ppm
phosphorus	P	< 0.002 %
Sulfur	S	< 0.001 %
Carbon	C	0.009 %
Manganese	Mn	0.01 %
Chlorine	Cl	0.01 %
Nitrogen	N	0.018 %
Iron	Fe	0.03 %
Aluminum	Al	< 0.01 %
Silicon	Si	0.01 %
Magnesium	Mg	0.01 %
Sodium	Na	< 0.01 %
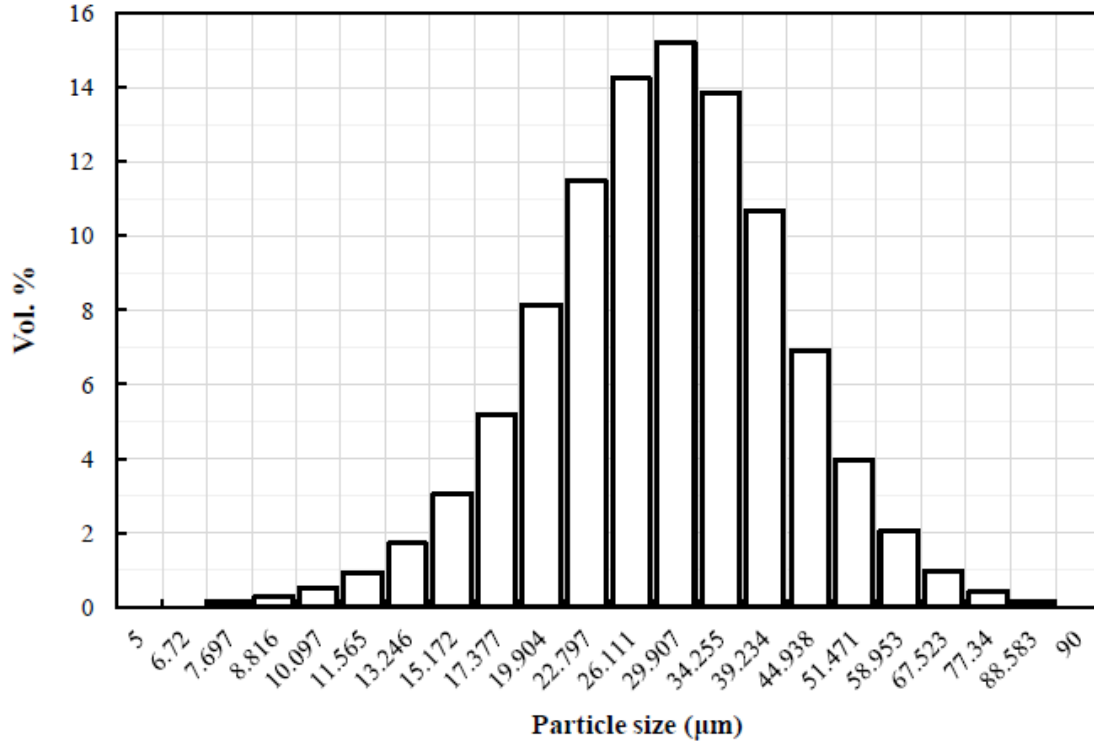
Figure 4.2 Particle distributions of as-received Ti powder

4.1.2.2 Boron Carbide (B₄C)

Pure B₄C (99% purity, Alfa Aesar Co.) is employed in this work. The chemical composition, as reported by the manufacturer, is listed in Table 4.5. The particle size of used B₄C is <10 μm. The as-received particle size distribution is shown in Figure 4.3.

Table 4.5 Typical chemical analysis for B₄C powder

Boron	77.28 %
Carbon	21.72 %
B-10 content	19 % min
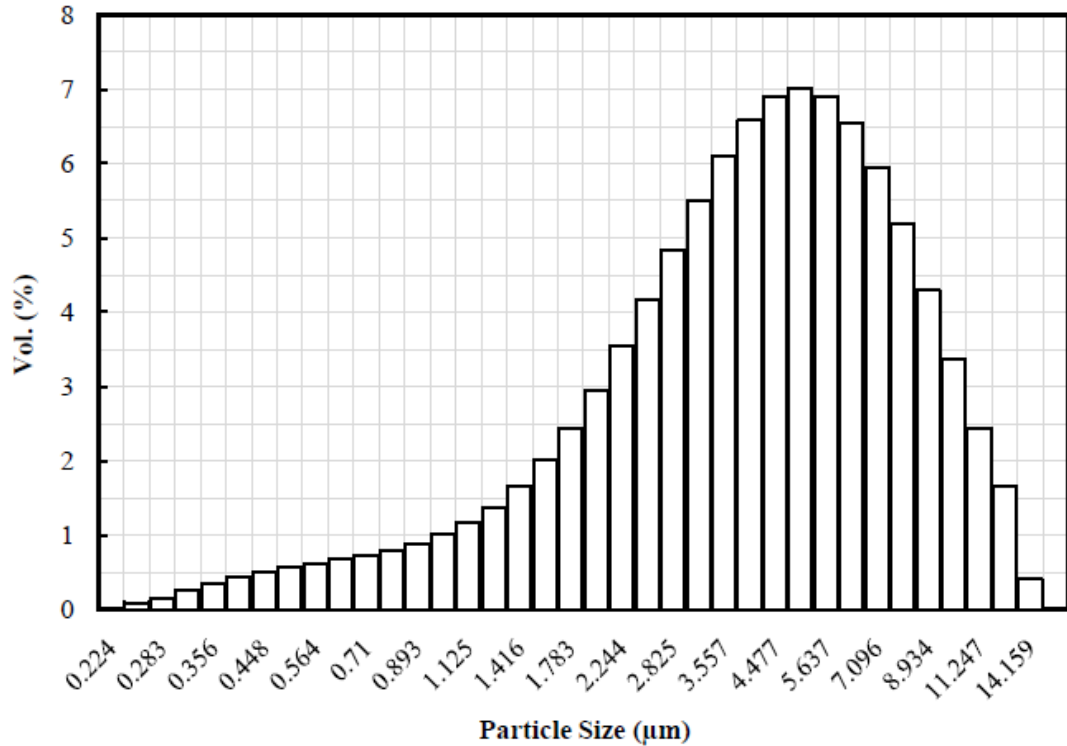
Figure 4.3 Particle distributions of as-received boron carbide (B$_4$C) powder

4.1.2.3 Pure Mg Powder

Pure Magnesium (-325 mesh, 99.8 % purity, Alfa Aesar Co.) powder was used with the 3Ti-B$_4$C preform. The mean particle size of pure Mg powder is < 35 µm. The as-received particle size distribution is shown in Figure 4.4.

4.1.2.4 Magnesium Hydride (MgH$_2$) Powder

MgH$_2$ (98 % purity, Alfa Aesar Co.) powder used with the 3Ti-B$_4$C preform has a mean particle size < 59 µm. The as-received particle size distribution is shown in Figure 4.5. Some physical properties of pure Mg and MgH$_2$ powders from the supplier (Alfa Aesar Co.) are presented in Table 4.6.
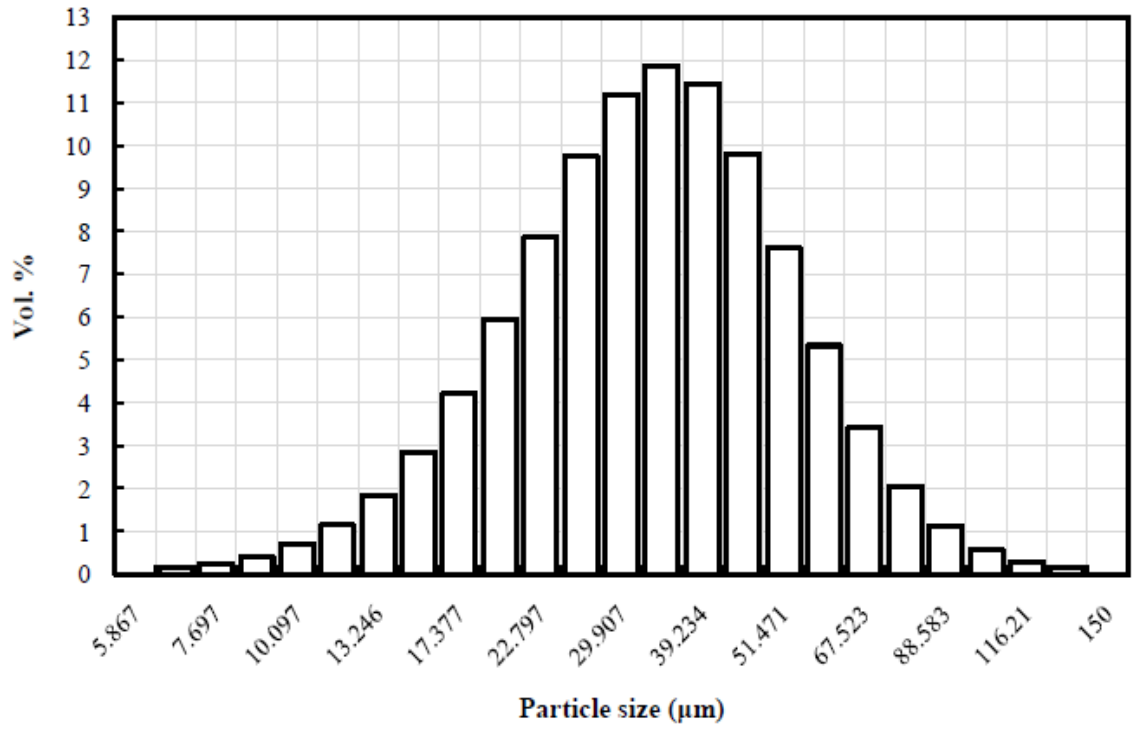
Figure 4.4 Particle distributions of as-received pure Mg powder
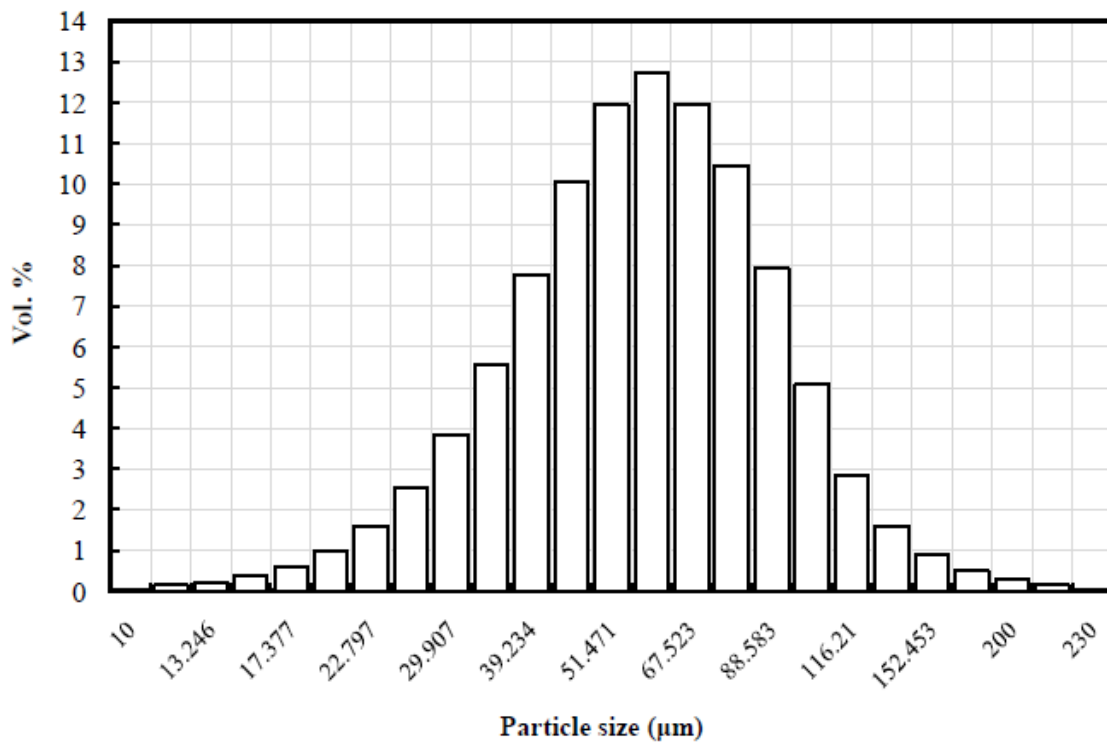
Figure 4.5 Particle distributions of as-received MgH₂ powder

Table 4.6 Some physical properties of pure Mg and MgH$_2$ powders from the supplier
(Alfa Aesar Co.)

Property	Pure Mg powder	MgH$_2$ powder
Density (ρ), g/cm^3	1.738	1.45
Melting Point (T),°C	650	327

4.2 Preparation of the green Compact

For system I, Ti and B$_4$C powders with a molar ratio of 3:1 were mixed under Ar in a

stainless steel jar with stainless steel balls inside a planetary ball mill, in which the ratio

of the balls to the powder was 7:1 and the milling speed and time were 400 rpm and 5 h

respectively. In order to prevent oxidation, the mixtures were prepared in a glove box

filled with Ar gas. The particle size distribution of the mixture is shown in Figure 4.6.

The mean particle size of the mixture was found to be ~ 17.4 μm.
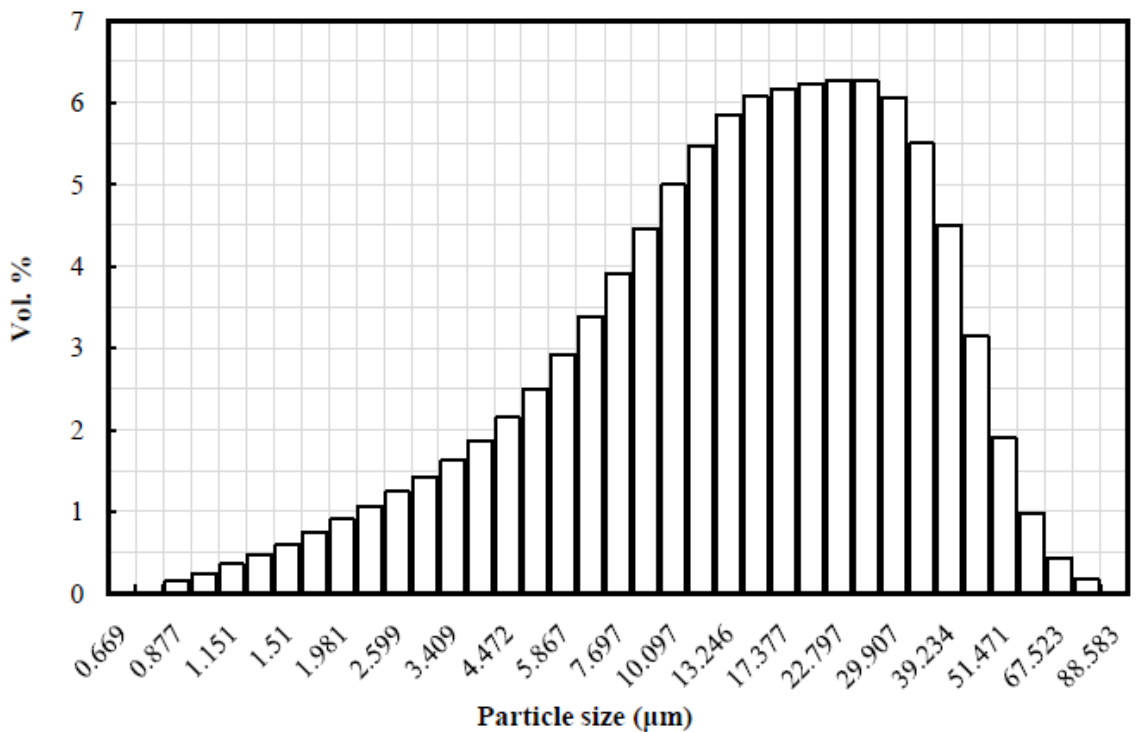
Figure 4.6 Particle distributions of the starting 3Ti-B$_4$C powder mixture

After full mechanical blending, the resulting mixture of Ti and B$_4$C powders were compacted at pressures from 80 to 120 MPa into green compacts of cylindrical shape of 25 mm in diameter and variable heights with various relative densities of approximately 55, 60, 65, and 70% ± 2% using a hardened steel die with two plungers.

These green compacts have been used to study the effect of the processing parameters on the fabrication of the Mg matrix composites and to understand the *in-situ* reaction mechanism responsible for the formation of the reinforcement phases in the Mg matrix. As shown in Figure 4.7, the particles were fragmented and the particle size was decreased for both, Ti and B$_4$C, after the ball milling.
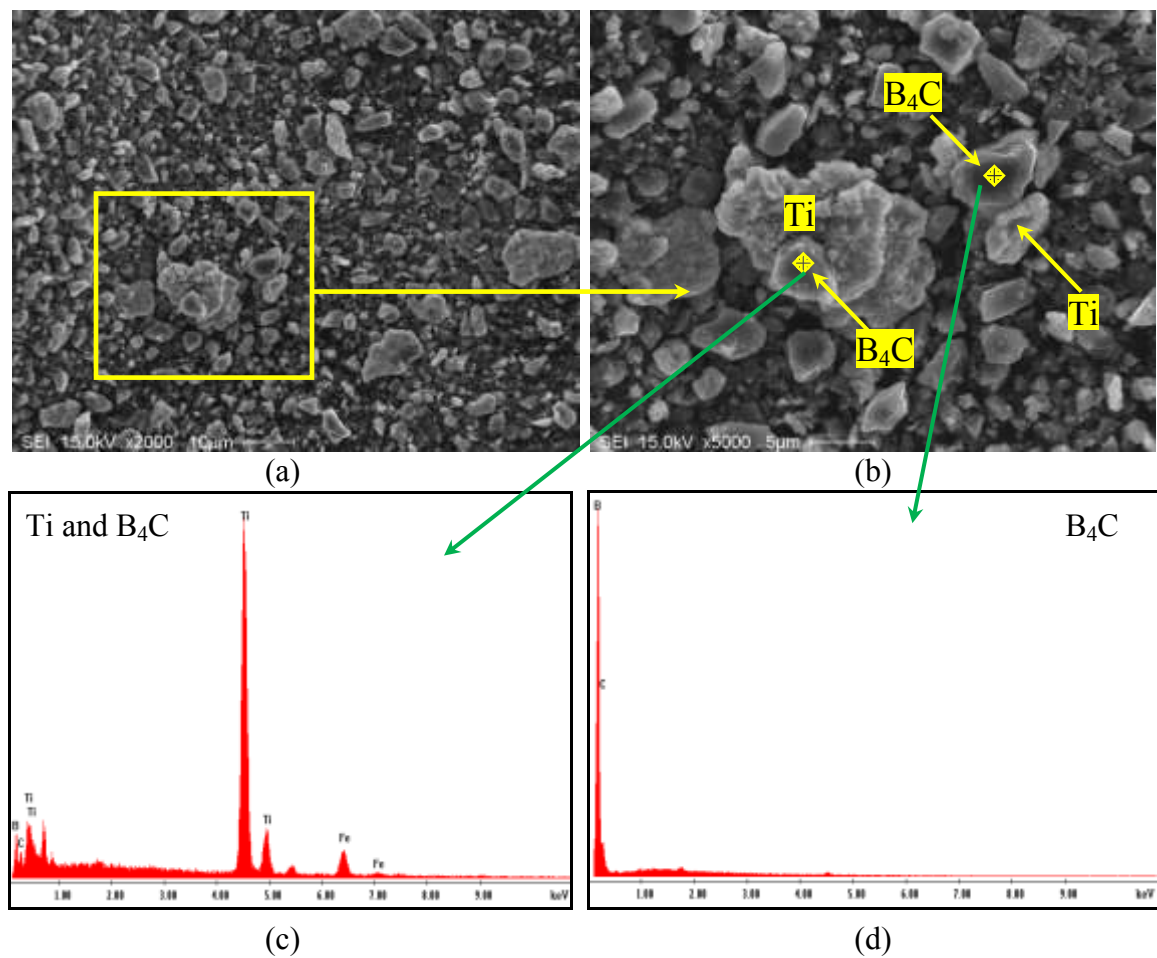
Figure 4.7 SEM-EDS of the 3Ti-B$_4$C Mixture

56

The green compacts Mg-(3Ti-B_4C) and MgH$_2$-(3Ti-B_4C) for systems II and III were prepared in the same fashion.

EDS elemental mapping shows a relatively uniform distribution of Ti and B_4C particles in the mixture as shown in Figure 4.8.

SEI Image	Ti-Kα image

B-Kα image	C-Kα image
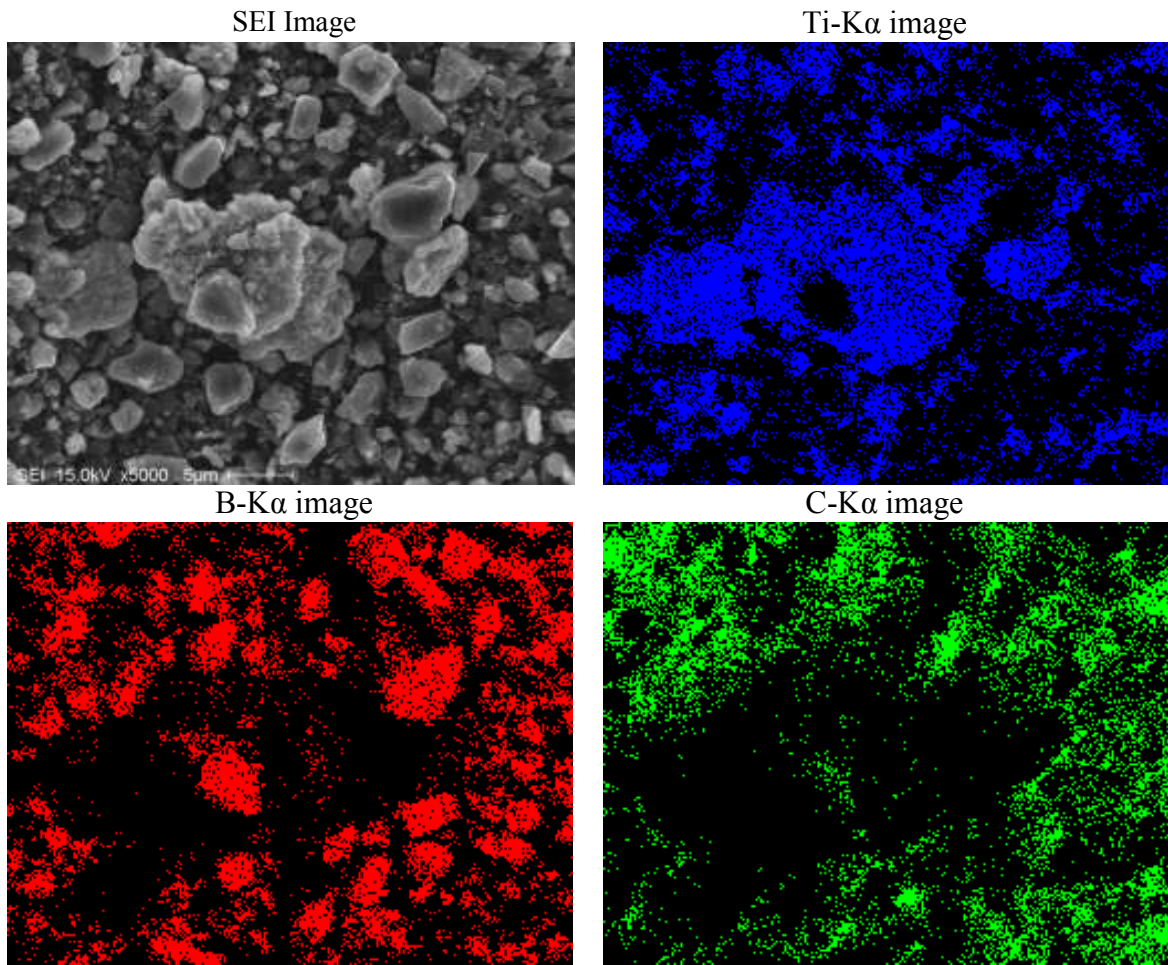
Figure 4.8 SEM microstructure and EDS elemental mapping of the 3Ti-B_4C Mixture

Ti and B_4C powders were mixed in the ball mill at different speeds (400, 450 and 500 rpm) for different holding times (5, 10 and 15 h). These powder mixtures were characterized using X-ray diffraction (XRD) analysis. Figure 4.9 shows the XRD pattern of these mixtures of Ti and B_4C. It is observed that only the diffraction peaks

corresponding to Ti and B$_4$C are present in all cases without any significant contamination. This means that there is no reaction between Ti and B$_4$C particles during the ball milling process. Also, it was found that the change in the mean particle size of the mixture due to varying milling speed and time is insignificant as shown in Table 4.7.
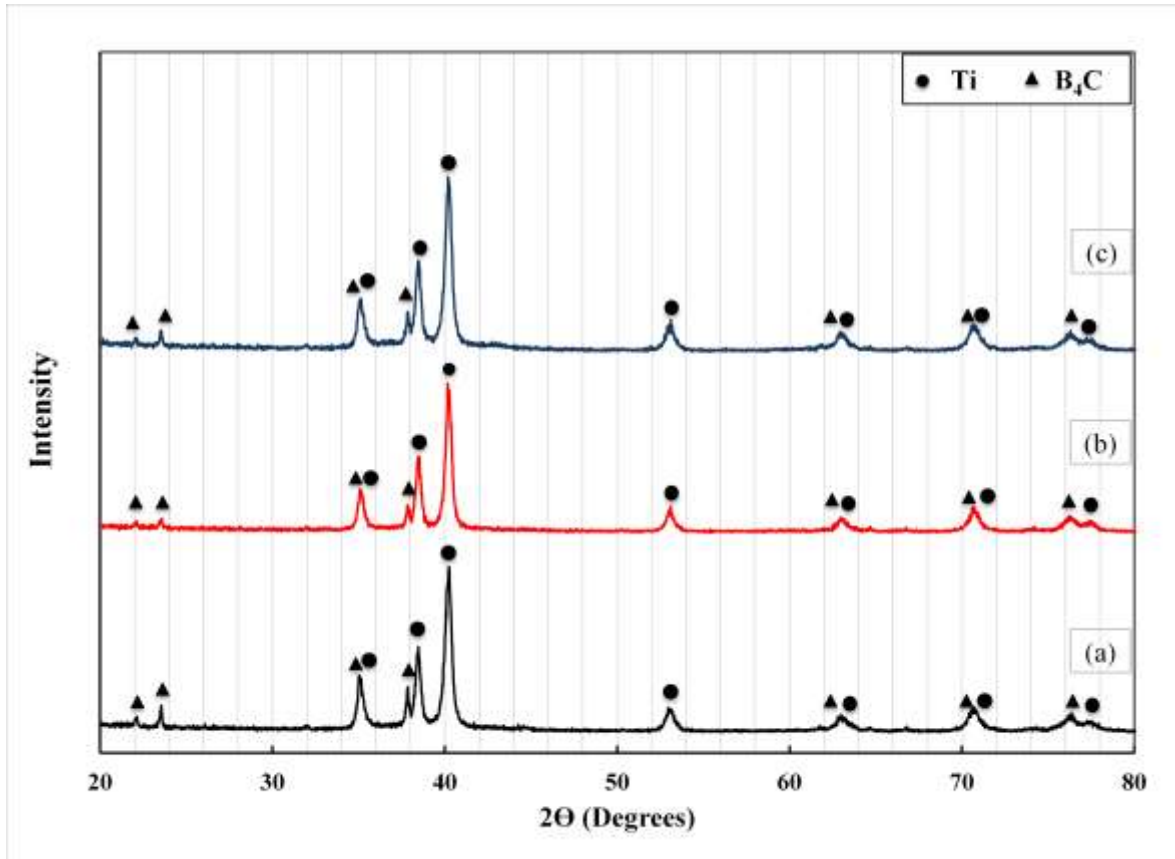
Figure 4.9 XRD pattern of the 3Ti-B$_4$C mixture at 400 rpm and different milling times
(a) 5, (b) 10 and (c) 15 h

Table 4.7 The mean particle sizes of the 3Ti-B$_4$C mixture at different milling speeds and holding times

Milling Speed (rpm)	Milling Time (h)	Particle Size (μm)
400	5	17.43
	10	17.20
	15	16.70
450	5	16.39
500	5	15.84

4.3 Experimental Setup

Figure 4.10 shows the schematic experimental setup for the fabrication of a network of TiC and TiB_2 reinforced magnesium matrix composites. The composite was fabricated by infiltrating molten pure Mg, AM60B or AZ91D alloys into the $3Ti–B_4C$, $Mg-(3Ti–B_4C)$ or $MgH_2-(3Ti–B_4C)$ preforms. The volume percentage of the reinforcement was tailored by controlling the relative density (RD) of the preform and by adding Mg or MgH_2 powder to the preform.
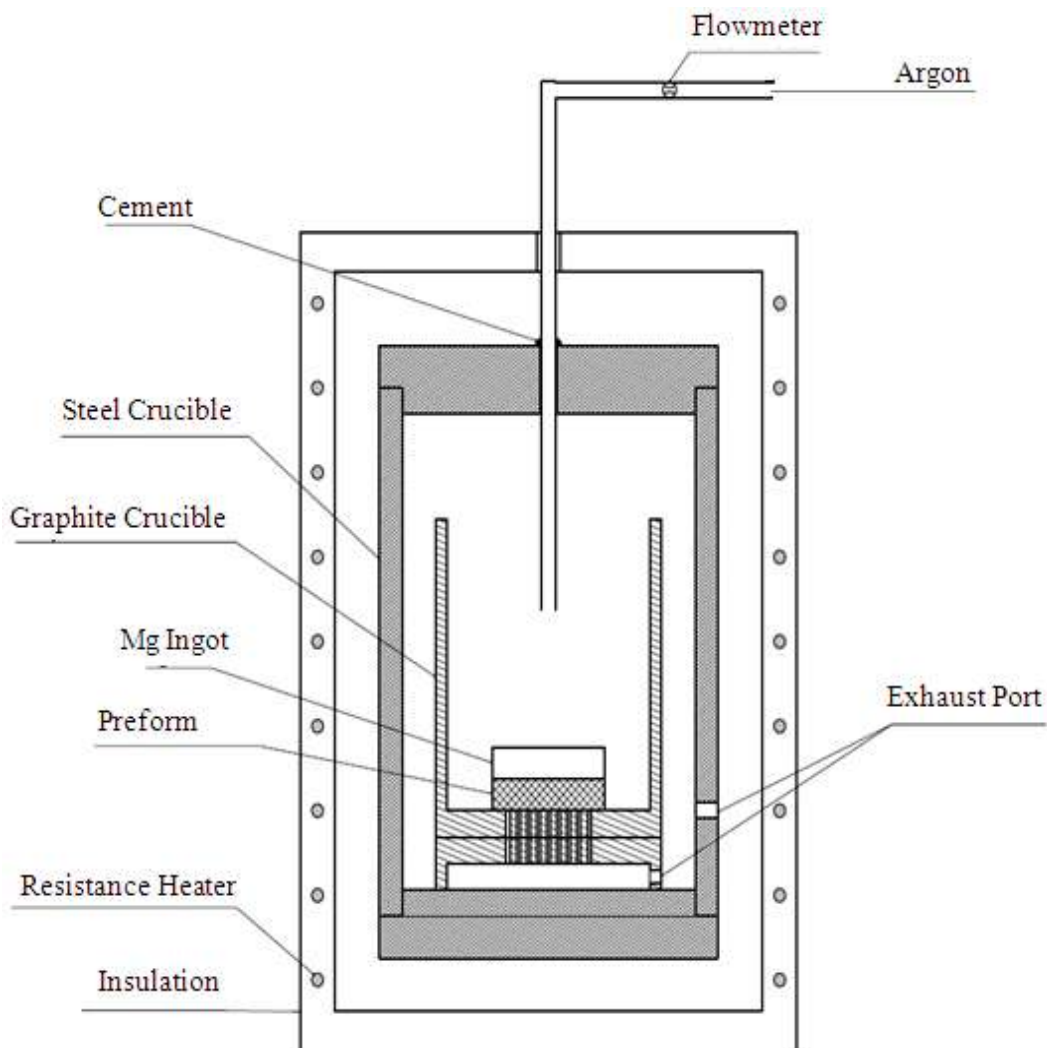
Figure 4.10 Schematic experimental setup for the fabrication of composite samples

As shown in the experimental setup (Figure 4.10), the compacted preform was placed at the bottom of graphite crucible (inner diameter: 45 mm) with a magnesium or magnesium alloy (AM60B or AZ91D) ingot placed on it. The mini ingots of pure Mg or Mg alloy are enough to infiltrate into the preform and also to compensate for the shrinkage of magnesium upon solidification. Several small holes were drilled at the bottom of the graphite crucible in order to release air during the infiltration of the molten alloy into the preform. This graphite crucible was placed inside a steel crucible having two holes, one on the top for inflow of the inert gas and the other on the side for the exhaust. The *in-situ* reactive infiltration experiments were carried out in an electric furnace under the presence of flowing argon gas (purity $\geq$ 99.999%) at a flow rate of 1.5 *l*/min.

The reaction chamber (steel crucible) was degassed prior to heating and then backfilled with Ar. The heating cycle for fabricating the composites is as shown in Figure 4.11.
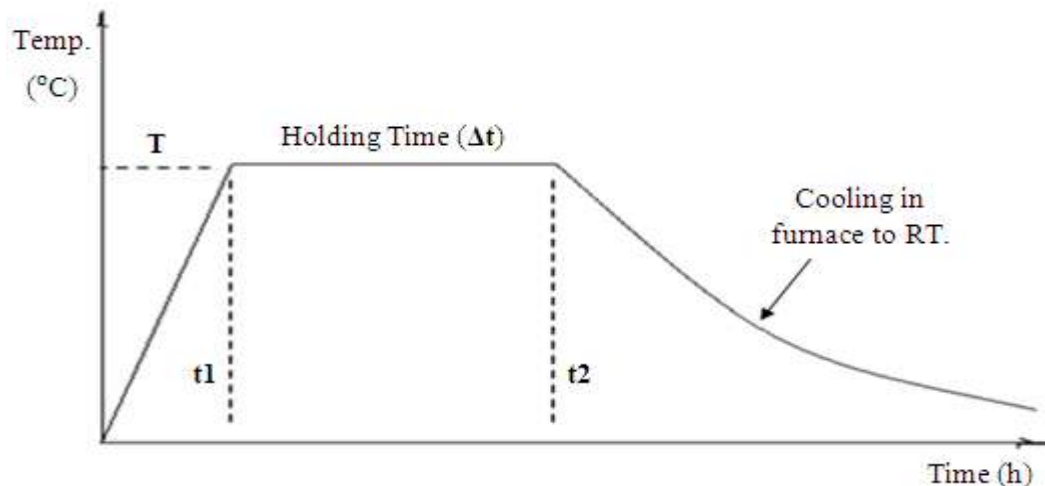
Figure 4.11 Experimental heating cycle with 10ºC/min heating rate for fabricating composite samples

60

The heating temperature was set in the range from 700ºC to 950ºC ± 10ºC with 50ºC intervals and for holding time from 15 min to 6 h, and the heating rate was 10ºC/min. After that the samples were naturally cooled down to room temperature in the furnace.

4.4 Microstructural Characterization

4.4.1 Density and Porosity Measurement

The theoretical density of the preform or magnesium composite samples was calculated using the rule of mixtures as [137]:

$$\rho_{p,c} = \Sigma(f_i \times \rho_i) = f_1 \times \rho_1 + f_2 \times \rho_2 + \,.....+f_n \times \rho_n \qquad (4.1)$$

Where $\rho_{p,c}$ is the density of the preform or composite, ρ_i and f_i are the density and the volume fraction of each constituent in the preform or composite, respectively. For example, the theoretical density for the 3Ti-B$_4$C preform of system I and the composite, if there are only three phases present, is as follows:

$$\rho_{theo.(Preform)} = \rho_{Ti}V_{Ti} + \rho_{B4C}V_{B4C} \qquad (4.2)$$

$$\rho_{theo.(composite)} = \rho_{Mg}V_{Mg} + \rho_{TiC}V_{TiC} + \rho_{TiB2}V_{TiB2} \qquad (4.3)$$

On the other hand, the bulk density and porosity of fabricated pure Mg and Mg alloy composites are measured using the water absorption method based on Archimedes's principle (ASTM C20-00) [138]. The dry samples were weighed in air (*D*), then placed in water and boiled for 2 hours. During boiling, the samples were covered by water without contact with the heated bottom of the container. After boiling, the test specimens were cooled to room temperature while still completely immersed in water for 12 h. Each specimen was measured while being suspended in distilled water (S). The specimen was

61

blotted lightly with a cotton cloth and then weighed in air giving the saturated weight (W). The following equation is used to calculate the bulk density (ρ_B):

$$\rho_B = \frac{D}{V} = \frac{D}{W-S} \tag{4.4}$$

V is called the exterior volume in cubic centimeter by knowing that 1 cm^3 of water weighs 1 g.

Porosity is a measure of the void spaces in the material and can be defined as a fraction of the volume of voids over the total volume. Porosity of the composites is measured for two reasons: the first is that the mechanical properties of the final product of the material are affected by whether this material is porous or solid. The second reason is that the amounts or percentages of matrix and reinforcement of the final composites are affected by the porosity of the preform.

The water absorption method based on Archimedes's principle (ASTM C20-00) [138], was used to determine the open porosity (P_{open}) according to Equation 4.5. The water saturation liquid filling method just measures the open porosity of the samples while the closed porosity (P_{closed}) is calculated by the difference between the total and open porosity using Equation 4.6. The total porosity (P_{total}) was calculated based on the relative density of the composite, Equation 4.7. The relative density represents the ratio of the bulk density (ρ_{bulk}) of a substance to the theoretical density $(\rho_{theo.})$ of solid material calculated using Equation 4.8. The theoretical and bulk densities of the composite samples were calculated using Equations 4.3 and 4.4 respectively.

$$P_{open}(\%) = \frac{W-D}{V} = \frac{W-D}{W-S} \times 100 \tag{4.5}$$

$$P_{total} = P_{open} + P_{closed} \tag{4.6}$$

$$P_{total} = (1 - Relative\ Density) * 100\ \% \qquad (4.7)$$

$$Relative\ Density\ (RD) = (\rho_{bulk}/\rho_{theo.}) \qquad (4.8)$$

4.4.2 Sample preparation for microanalysis

For the samples required for microanalysis, the sample sections were cut from the composite using a diamond blade, mounted in conductive epoxy or bakelite and then manually ground using 60, 120, 240, 320, 400, 600, 800 and 1200 grit SiC emery paper using ethanol as lubricant. Then the mounted and ground samples were polished on soft, synthetic, short-napped fiber cloth using 6, 3 and 1 micron diamond paste with alcohol as lubricant and coolant.

4.4.3 Microscopy and Energy Dispersive Examination (EDS)

The microstructure and the phase analysis of the reacted preforms and fabricated composite samples were investigated using scanning electron microscope (SEM) (Model, Philips XL30 FEG) equipped with Energy Dispersive X-ray spectroscopy (EDS).

The SEM was used either in the secondary electron (SEI) or backscatter electron (BSE) modes at 15 keV. Due to the poor conductivity of TiC and TiB_2 particulates, a thin gold-palladium coating was applied to the polished surfaces using an Anatech-Hummer VI sputtering coater for imaging purposes in case of surface charging. Secondary electron imaging (SEI) was used on samples to determine the distribution of TiC and TiB_2, porosity, crack and fracture surface. Backscattered electron imaging (BSE) provides contrast between chemically different phases in composites due to differences in effective atomic number.

Qualitative EDS analysis is performed on specific features within a sample on both polished and fractured samples. The X-ray mapping technique is performed to analyze the distribution of elements within the polished samples.

4.4.4 X-ray diffraction (XRD)

To determine the crystalline phases in the composites and to investigate the *in-situ* reaction mechanism through the interaction between each component in the reacted mixtures such as $3Ti-B_4C$, $Mg-B_4C$ and $Mg-(3Ti-B_4C)$, X-Ray Diffraction (XRD) was performed.

The XRD pattern was recorded using an X-ray diffractometer, (X'Pert PRO, manufactured by PANalytical Inc.), with a Cu-Kα_1 ($\lambda=1.5418$ Å) radiation produced at an applied voltage and a beam current of 45 kV and 40 mA, respectively. The XRD spectrum was acquired from 10 to 120º 2θ at a 0.02º step size.

For preparation of the samples, powders were ground in a mortar to a uniform particle size distribution and the diffraction patterns were obtained at room temperature. Silicon powder (-325 mesh) is added to all powder samples as an internal standard to correct for any systematic error. To use the peak intensities for comparison between different samples, identical sample preparation technique, amount of the sample, and data collection conditions were used.

X-ray diffraction analysis of the samples is carried out using X'Pert HighScore Plus Rietveld analysis software in combination with Pearson's crystal database [139].

The relative weight fractions of phases in a multiphase material can be calculated directly from scale factors as described by Hill and Howard [140]. Based on that, the weight fraction of phase p can then be derived as:

$$W_P = \frac{S_P(Z.M.V_{u.c})}{\sum_{i=1}^{n} S_i(Z.M.V_{u.c})} \cdot 100\% \tag{4.9}$$

Where: S is the Rietveld scale factor, Z is the number of formula units per unit cell, M is the molecular weight of the formula unit, $V_{u.c}$ is the unit cell volume and i is an index running over all phases. So, using the X'Pert HighScore Plus Rietveld analysis software, the weight percentage of each phase in the system can be calculated and by knowing the density of each phase from the software, the volume percentage of each phase can be calculated.

4.5 Mechanical Testing Experiments

The networks of reinforcing phases are anticipated to be more efficient load bearing structures than single isolated solid particles, whiskers or short fibers. It is expected that this composite may have higher mechanical properties than magnesium alloys. Mechanical characterization of the composites was evaluated through different mechanical tests such as compression, four point bending, hardness and wear resistance tests.

4.5.1 Compression Test

Compression properties of magnesium matrix composites are very important for the structural parts used in the automotive industry because the automotive parts are often loaded under compression at room or elevated temperatures both in present and future applications [24].

The compression tests were conducted on as-received pure Mg, AM60B and AZ91D alloys and TiC-TiB$_2$/Mg composites according to ASTM E9-89a [141]. Specimens were machined to a round cross-section of 12.7 mm (1/2 inch.) in diameter and 25 mm (1 inch.) in height. TiC-TiB$_2$/Mg matrix composites specimens were machined from the *in-situ* reactive infiltrated material.

Testing was performed on MTS 809 equipment, with a 250 kN load capacity at room temperature with a cross-head speed of 0.5 mm/min (equivalent to a strain rate of 0.0003 s^{-1}) and no barreling was observed. To obtain strain measurements, two strain gauges (CEA-06-125UW-350, Vishay Micro-Measurements) were installed longitudinally parallel to the load direction on the side of each test sample with 180º between them. Three samples were tested to guarantee reliable results.

Because the elastic portion of the stress-strain curve was not always linear, tangent elastic modulus was determined from the slope of the stress-strain curve at a fixed level of stress (160 MPa). This slope line is represented in the stress-strain curve by dotted line.

Upon cooling of MMCs, residual stress is created due to the different coefficients of thermal expansion of the matrix and reinforcement causing dislocations to form at the ceramic/metal interface. In the present work, since the compression testing of the composite initially revealed non-linear elastic behavior, a cycling procedure was carried out to stabilize the dislocations in the matrix according to Prangnell *et al.* [142]. By low load cycling, these dislocations were redistributed (or moved) from a high density location (matrix/reinforcement interface) to a lower one without damaging the composite material.

For the low cycle compression test, the TiC-TiB$_2$/Mg composites were initially pre-strained to low level of stress, 25 MPa. On reaching 25 MPa, the stress was reduced to 5 MPa, followed by ten load cycles from 5 MPa to 25 MPa at 0.1 Hz. After cycling, it was ramped down to 0 MPa. Young's modulus was determined from the slope of the linear, stress-strain region, where the cycling was performed as given in Figure 7.5.

This load cycling was also performed to ensure the integrity of the measurement procedure as in some cases; the strain gauges gave spurious outputs on initial load application to the compression samples. This was probably due to the lack of complete parallarity between sample and crosshead platens. The cycling action has allowed some "bedding-in" and produces consistent readings. In some cases, the stress-strain curve has been extrapolated back to zero loads using this cycled behavior to replace the erratic strain data on initial loading.

The Young's modulus obtained by the slope of the stress-strain curve at a fixed level of stress (160 MPa) was verified with the value of the slope of the stress-strain curve of the low cycle compression test done in the range from 5 to 25 MPa.

4.5.2 Flexural Test

Flexural strength is the maximum tensile stress of a beam in bending and is a suitable alternate for the tensile test for not only brittle ceramic materials but also brittle filled composites. Testing was done on a screw-driven Instron model 3382 (Instron Corp.), with a load cell of 100 kN at a cross-head speed of 0.5 mm/min. In the present study, the flexural strength behavior of fabricated Mg matrix composites has been assessed at room temperature.

The four-point bending tests were conducted on the TiC-TiB$_2$/Mg composites according to ASTM 1161-02C [143]. The four-point loading configuration is shown in Figure 4.12, where the load and support span are 20 mm and 40 mm, respectively. The samples were ground using 240, 320, 400, 600, 800 and 1200 grit silicon carbide papers to achieve a mirror finish and to eliminate any residual stresses generated during cutting of these samples. The dimensions of the rectangular specimens are 4 mm x 6 mm x 50 mm, as shown in Figure 4.13.
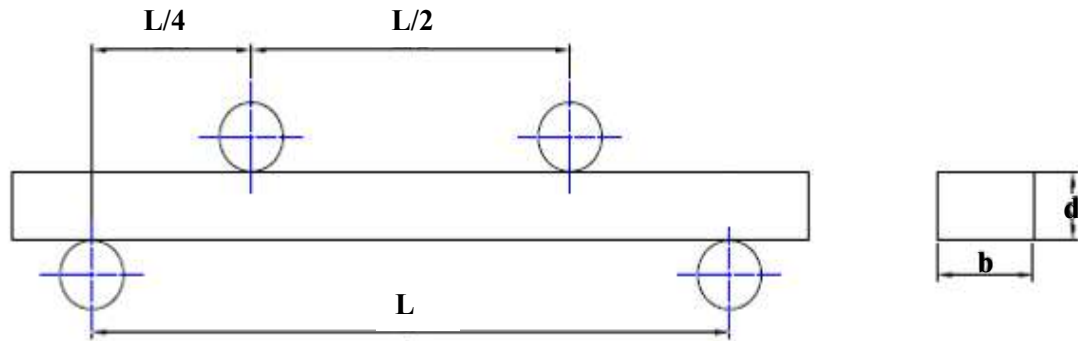
Figure 4.12 Schematic drawing for the four-point bending configuration
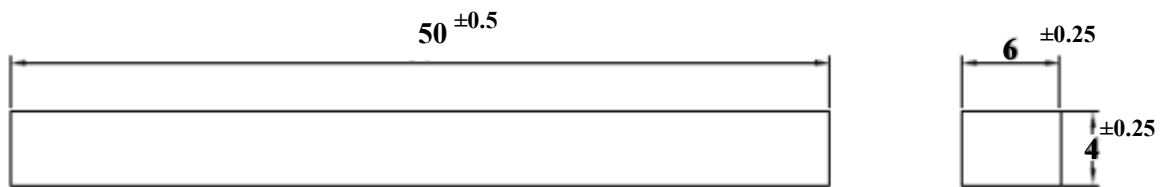
Figure 4.13 Schematic drawing for the rectangular specimen for flexural test

(Dimensions in mm)

The theoretical bending strength for the rectangular specimens is derived from beam theory [144]:

$$\sigma = Mc/I \qquad (4.9)$$

Where M is the maximum bending moment, I is the moment of inertia and c is the distance from the neutral axis to the outer surface of the specimen.

For a rectangular cross section, the expressions used for a four-point loading configuration are presented in Equations 4.10-4.12;

$$M = (P/2)a \qquad\qquad (4.10)$$

$$c = d/2 \qquad\qquad (4.11)$$

$$I = bd^3/12 \qquad\qquad (4.12)$$

Where P is the fracture load, a is the distance between the inner and outer supports (a=L/4), L is the outer support span, d is the thickness and b is the width of the specimen.

Substituting the above equations leads to the following flexural strength formula:

$$\boldsymbol{\sigma_{fs} = 3PL/4bd^2} \qquad\qquad (4.13)$$

4.5.3 Bulk and Microhardness Tests

Microhardness measurements were carried out on polished, pure Mg, AM60B, AZ91D alloy and the composite samples using a MVK–H1 digital microhardness tester with a 136° Vickers diamond pyramid indentor under direct loads of 0.2, 0.5, and 1 kg applied for 15 seconds. It is very important to note that it is very difficult to measure the hardness in the particle–free regions of the matrix because of the fine microstructure. The hardness value was calculated based on the average length of the diagonals of the ensuing pyramid which were measured using a focal scale on the microscope of the testing machine. Each hardness value was the average of at least ten measurements. Hardness assessment of the bulk material was carried out under a 10 kg load using a standard Vickers Hardness Tester. Each hardness value in this case was the average of at least three measurements.

4.5.4 Wear Resistance Test

Fabricated Mg matrix composite materials in this work are supposed to offer some potential benefits for tribological applications where materials with lower density are required.

The abrasive wear testing was performed using pin-on-disk type wear test equipment for the evaluation of dry tribological properties as shown in Figure 4.14. Pins of AZ91D alloy and its respective composites with 12 mm diameter and 15 mm height were cut, ground and polished for these wear tests. In the wear tests, 120 grit SiC abrasive papers (corresponding to 115 µm abrasive particles) were used as the counterface. Sliding speeds of 0.5, 1 and 1.5 m/s and 10, 22.5 and 45 N loads were used. Each time, a fresh SiC paper was used.
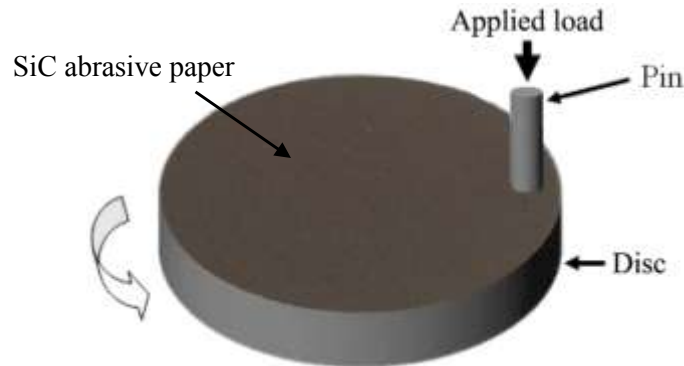
Figure 4.14 Pin-on-disc wear test

The specimens were weighed before and after the test using a balance having an accuracy of 0.1 mg to measure the weight loss. The wear rate was calculated from the mass loss divided by sliding distance. The data for the wear tests were taken from the average of the three measurements. The worn surfaces were observed using the scanning electron microscopy (SEM) and before that the worn surfaces were cleaned thoroughly to remove the loose wear debris.

Chapter 5

In-situ Reaction Mechanism

5.1 Thermodynamic Analysis

For understanding the *in-situ* reaction mechanism, reaction thermodynamics are used to obtain the reaction direction and the expected stable phases and their compositions at elevated temperatures. The potential reactions that can take place in the Mg-Ti–B_4C system and between the reactants and some intermediate phases are as follows:

$$\frac{2}{3} Mg + \frac{1}{3} B_4C = \frac{2}{3} MgB_2 + \frac{1}{3} C \tag{5.1}$$

$$\frac{1}{2} Ti + \frac{1}{2} C = \frac{1}{2} TiC \tag{5.2}$$

$$\frac{5}{6} Ti + \frac{1}{6} B_4C = \frac{2}{3} TiB + \frac{1}{6} TiC \tag{5.3}$$

$$\frac{16}{17} TiB + \frac{1}{17} B_4C = \frac{5}{17} Ti_3B_4 + \frac{1}{17} TiC \tag{5.4}$$

$$\frac{3}{4} Ti_3B_4 + \frac{1}{4} B_4C = 2 TiB_2 + \frac{1}{4} TiC \tag{5.5}$$

$$\frac{2}{3} TiB + \frac{1}{3} MgB_2 = \frac{2}{3} TiB_2 + \frac{1}{3} Mg \tag{5.6}$$

$$\frac{1}{2} Ti + \frac{1}{2} MgB_2 = \frac{1}{2} TiB_2 + \frac{1}{2} Mg \tag{5.7}$$

$$\frac{2}{3} Ti + \frac{1}{3} MgB_4 = \frac{2}{3} TiB_2 + \frac{1}{3} Mg \tag{5.8}$$

$$\frac{3}{4}Ti + \frac{1}{4} B_4C = \frac{1}{2} TiB_2 + \frac{1}{4} TiC \tag{5.9}$$
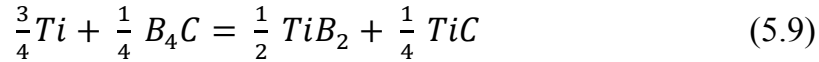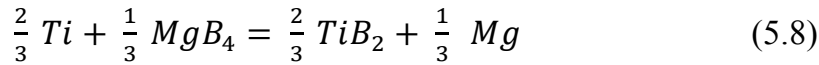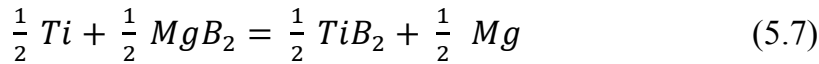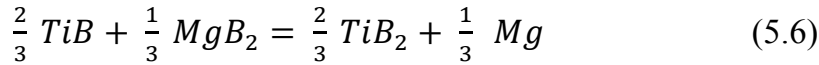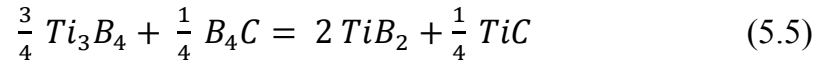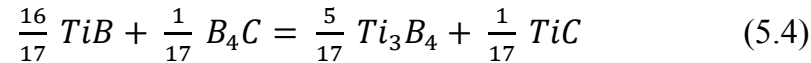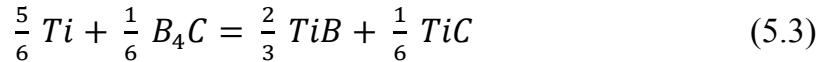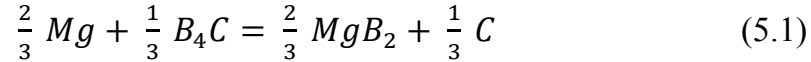
To compare the feasibility and favorability of these reactions, the changes in the Gibbs free energy, *ΔG*, and the reaction enthalpy, *ΔH*, for one mole of the reactants were calculated as shown in Figure 5.1. It can be observed from Figure 5.1 (b) that all reactions are exothermic (*-ve* Δ*H*) and have negative standard Gibbs free energy. Thus, all reactions are thermodynamically favorable as shown in Figure 5.1 (a).
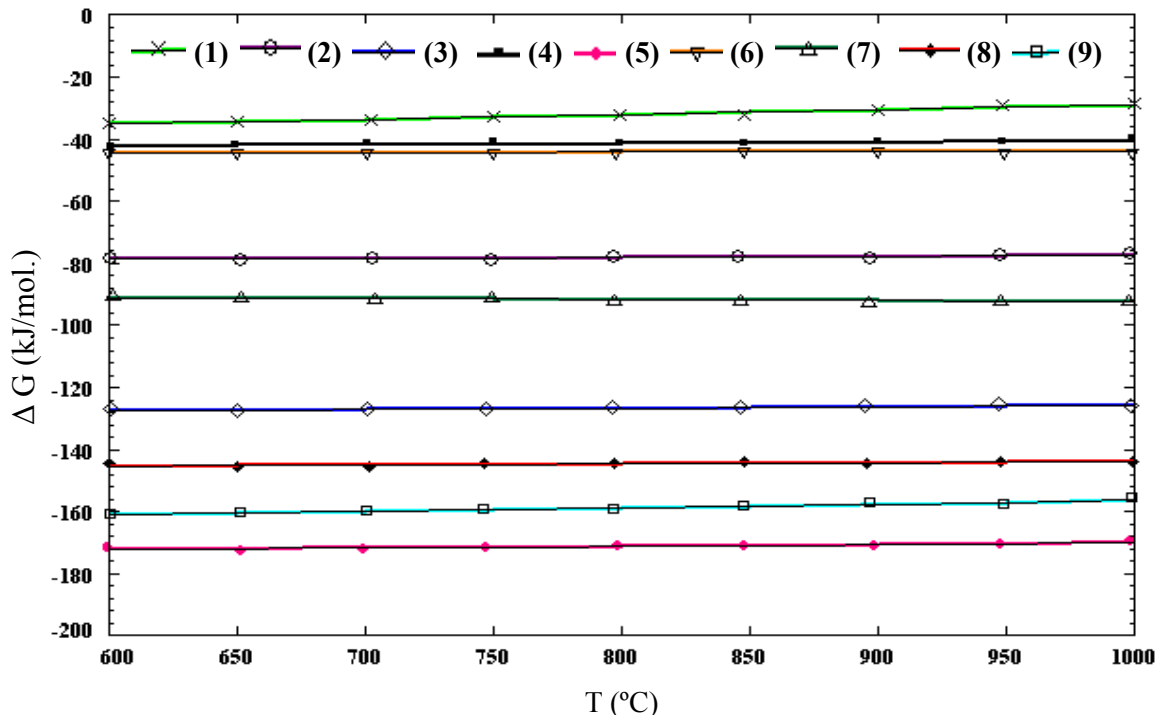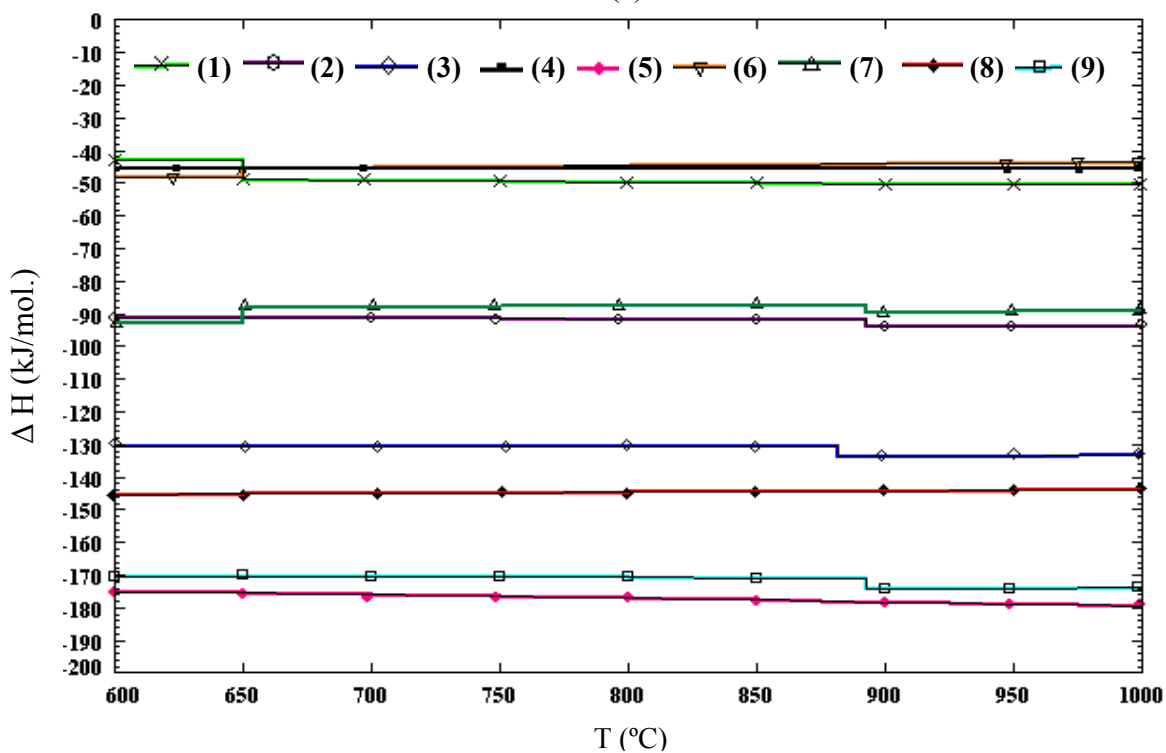
Figure 5.1 Changes in (a) Gibbs free energy, ΔG, and (b) reaction enthalpy, ΔH, for reactions (5.1)-(5.9)

It is worth noting that ΔG_5 and ΔG_9 are more negative for the formation of TiC-TiB$_2$ in the temperature range of interest and thus reactions (5.5) and (5.9) have a higher tendency for the formation of TiC-TiB$_2$ than the other reactions. However, reaction (5.5) is considered an intermediate reaction to form TiC-TiB$_2$. Therefore, from a thermodynamics point of view, it can be deduced that the finial equilibrium phases should be TiB$_2$, TiC and Mg in the composite.

5.2 Reaction Mechanism of Infiltrated Mg-(Ti-B$_4$C) System

The *in-situ* reactive infiltration technique used for fabricating the metal matrix composites generally consists of two steps which cannot be distinguished because they are overlapping and interacting with each other during the fabrication process. One is the *in-situ* reaction between the starting powders and the infiltrated metal liquid and the other is the infiltration of the magnesium melt through the preform. At the initial stage of the infiltration process, Mg melt infiltrates the preform along the pores around Ti particles where they are physically wettable. No intermetallic compounds form between Mg and Ti according to the Ti-Mg binary phase diagram [145]. Because the Ti particles are surrounded by B$_4$C particles, an Mg-Ti-B$_4$C interface is created. Hence, to understand the in-*situ* reaction mechanism for synthesizing TiC-TiB$_2$/AZ91D composites, the reaction mechanisms of the Ti-B$_4$C and Mg-B$_4$C systems have been investigated separately.

5.2.1 The Ti–B$_4$C System

Based on the thermodynamic consideration discussed earlier, the solid-state reaction between Ti and B$_4$C to form TiC and TiB$_2$ is the most favorable reaction but kinetically this reaction it is very slow [146]. To investigate the phases formed from the reaction

between Ti and B_4C without Mg, $3Ti-B_4C$ green compacts with 70% relative density (*RD*) were heated to 900°C and kept in the furnace at this temperature for different holding times (Δt) from 1 to 10 h according to the heating cycle shown in Figure 4.11. It is important to note that all Ti and B_4C compacts employed in this work are with a molar ratio of 3:1. The XRD patterns of the two preforms heated to 900°C for 1 h and 10 h compared with the starting powder mixture of $3Ti-B_4C$ are shown in Figure 5.2.
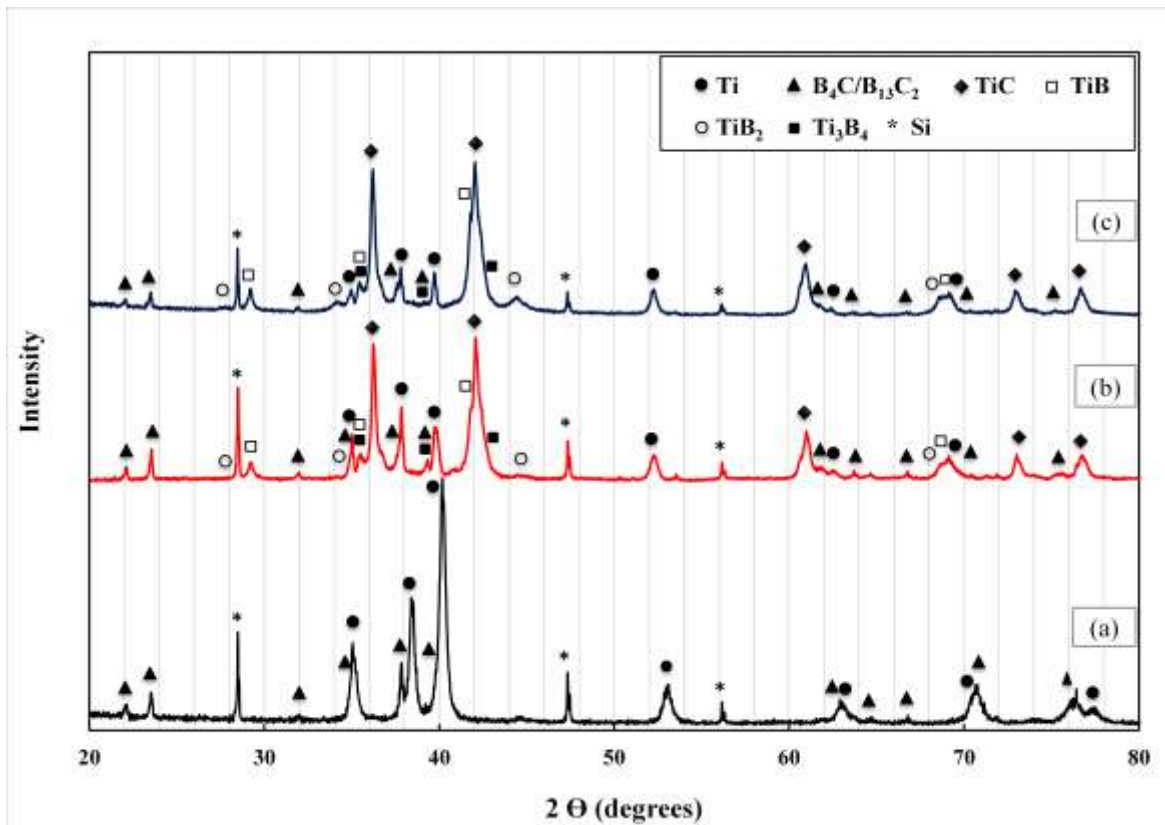
Figure 5.2 XRD pattern of (a) the starting $3Ti-B_4C$ powder mixture and $3Ti-B_4C$ preforms: (b) after heat treatment at 900°C for 1 h and (c) after heat treatment at 900°C for 10 h

The results reveal the formation of substoichiometric TiC_x prior to titanium borides with retained titanium and boron carbide ($B_{13}C_2$) after heat treatment for 1 h and 10 h. Also, it can be observed that TiB and Ti_3B_4 formed before TiB_2. At 1 h, the area

74

under the peak of TiB_2 phase is very small and increases with increasing the holding time to 10 h as shown in Figure 5.2. There is still retained titanium and boron carbide indicating that the reaction is still incomplete even after 10 h holding time.

In the XRD analysis, as the intensities of the different phases agree with the theoretical values, the increase in the area under the peaks provides information about the kinetics of the reaction mechanism. It is also observed that the lattice constant of substoichiometric TiC_x increases with time due to the diffusion of C into TiC_x as shown in Table 5.1. As the lattice parameter of TiC_x increases, the stoichiometry (x) increases. Hence, based on the values of the lattice constant of TiC_x mentioned in Table 5.1, the stoichiometry (x) in TiC_x at 10 h is consistent with that of $TiC_{0.67}$ according to Pearson's Handbook [139].

Table 5.1 Lattice constant of the formed TiC_x after heat treatment of $3Ti-B_4C$ preforms at 900ºC for different holding times

Holding Time (h)	Lattice constant, a, $(\mathring{A})$
1 h	4.29627
10 h	4.305

To investigate the reaction sequence in the $Ti-B_4C$ system experimentally, thin $3Ti-B_4C$ green compacts (to ensure the homogeneity through the thickness) were prepared with 70% *RD* and placed in a quartz tube under Ar as shown in Figure 5.3. The encapsulated samples were heat-treated at different temperatures from 600ºC to 900ºC for 1 h holding time and then quenched in water according to the heating cycle shown in Figure 5.4.
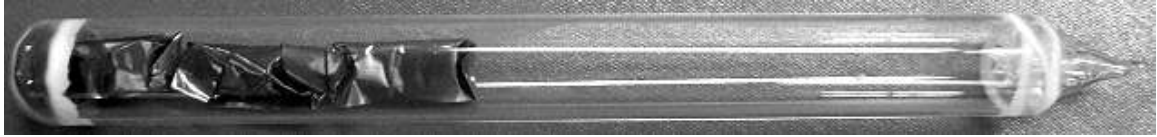
Figure 5.3 Samples in a Quartz Tube
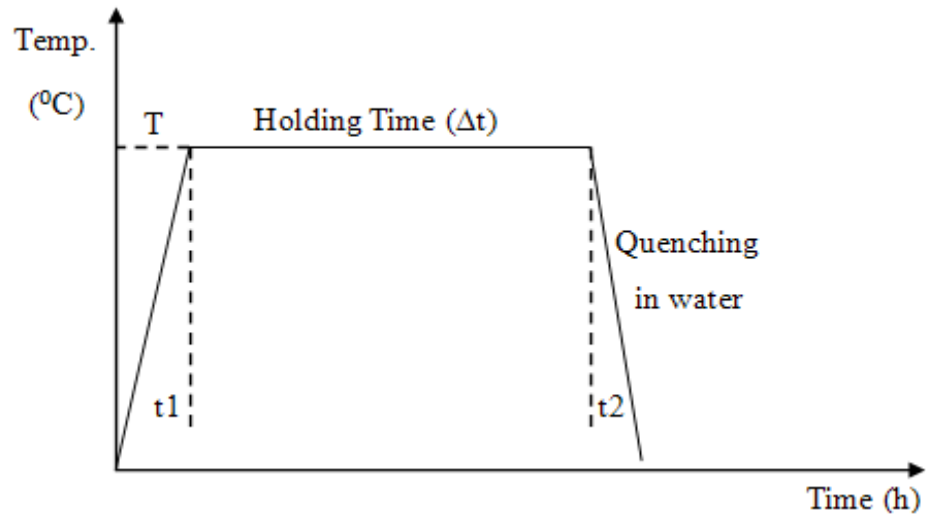
Figure 5.4 The heating cycle for quenched 3Ti-B_4C preforms

Figure 5.5 shows the XRD spectra of heat-treated 3Ti-B_4C compacts for 1 h but at different temperatures. The results revealed that no reaction took place at 600°C where only Ti and B_4C peaks are observed, whereas, at 700°C, Ti, boron carbide ($B_{13}C_2$) and TiC_x peaks are the main peaks in the XRD pattern. However, very low TiB and Ti_3B_4 peaks intensities can also be observed. This shows that the substoichiometric TiC_x formed prior to titanium borides. At 800°C, it was found that the area under the peaks of TiB, Ti_3B_4 and TiC_x increased while those of Ti and boron carbide decreased with very low TiB_2 peaks starting to appear. This shows that TiB and Ti_3B_4 phases formed prior to TiB_2 phase.

Monitoring the change of the area under the peaks of the phases reveals that the amounts of TiB_2, TiC_x increased with increasing temperature to 900°C while those of Ti,

boron carbide, TiB and Ti_3B_4 decreased and it can be said that the retained Ti is very small and can be neglected at 900ºC. These results indicate that the reaction is still incomplete even at 900ºC for 1 h.
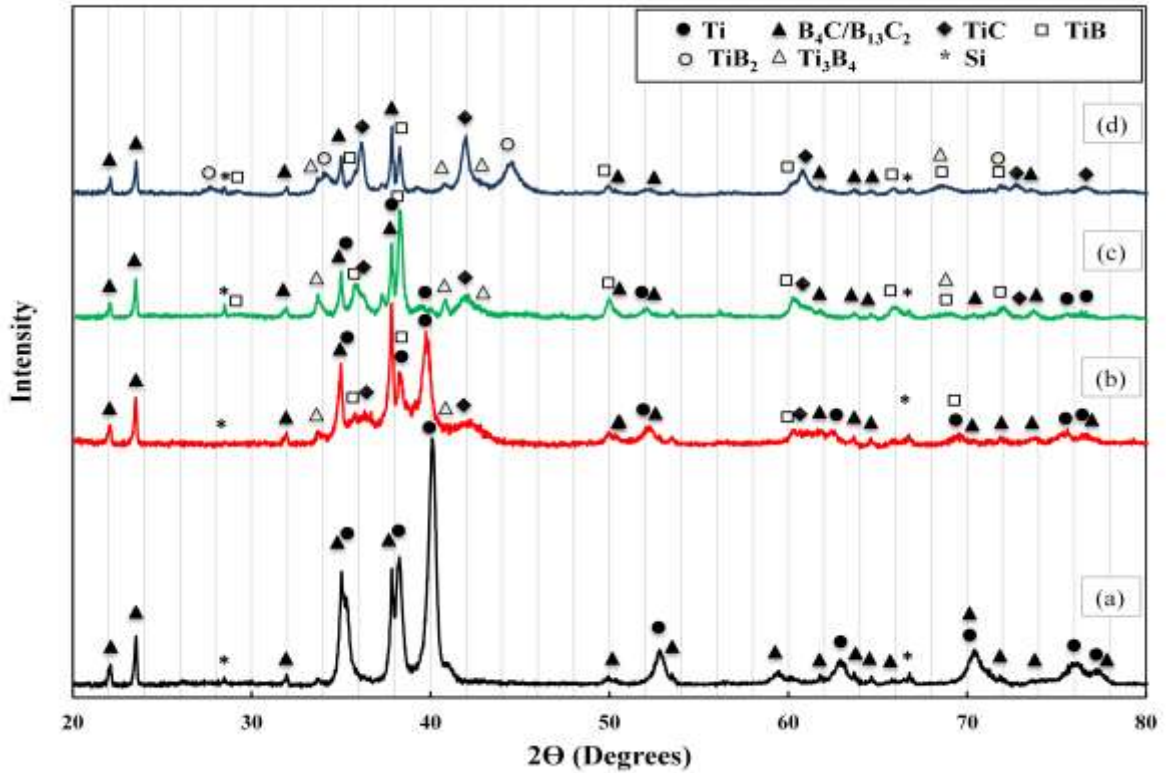
Figure 5.5 XRD patterns of heat-treated $3Ti-B_4C$ samples quenched from different temperatures: (a) 600ºC, (b) 700ºC, (c) 800ºC, and (d) 900ºC after 1 h holding time

The variations of the lattice parameters of Ti and B_4C formed after heat treatment of $3Ti-B_4C$ samples at different temperatures after 1 h holding time are presented in Table 5.2. It can be observed that the lattice parameters of Ti increase with increasing temperature till 700ºC. This means that C-saturated Ti, Ti_{C-sat}, formed prior to titanium carbide due to the diffusion of C from B_4C into Ti. With increasing temperature, the substoichiometric TiC_x forms while the lattice parameters of the retained Ti decreased

77

again. However, this amount of Ti is very small and can be neglected after 700°C. A schematic representation presented in Figure 5.6 shows how the substoichiometric TiC_x forms. The range of the lattice parameters of the boron carbide is found to be consistent with that of the standard lattice constants of $B_{13}C_2$ according to Pearson's Handbook [139].
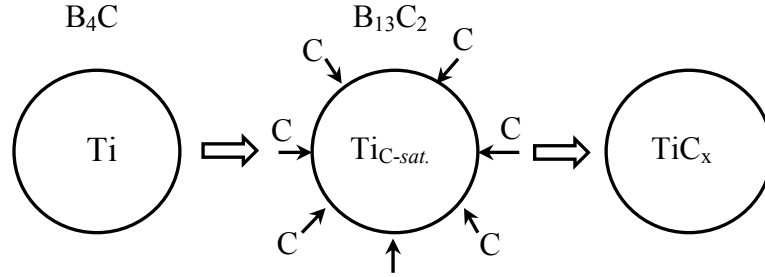
Figure 5.6 Schematic representation of the formation of the substoichiometric TiC_x from the solid-state reaction between Ti and B_4C

Table 5.2 Lattice parameters of Ti and boron carbide for heat treated 3Ti-B_4C compact samples at different temperatures for 1 h

Sample	Processing parameters	Ti		Boron carbide	
		a (Å)	c (Å)	a (Å)	c (Å)
3Ti-B_4C	600°C/1 h	2.9565	4.7108	5.6029	12.0934
	700°C/1 h	2.9767	4.7786	5.6074	12.1045
	800°C/1 h	2.95037	4.6953	5.6047	12.0884
	900°C/1 h	2.900	4.703	5.6039	12.09

Thus, based on these results and the crystallographic data of phases from Pearson's handbook [139], the reaction sequence of the Ti-B_4C system can be presented as follows:

$$3\,Ti + B_4C = Ti_{C-sat.} + B_{13}C_2 \rightarrow Ti_{C-sat.} + B_{13}C_2 + TiC_x \qquad (5.10)$$

$$\rightarrow Ti + B_{13}C_2 + TiC_x + TiB \qquad (5.11)$$

$$\rightarrow Ti + B_{13}C_2 + TiC_x + TiB + Ti_3B_4 \qquad (5.12)$$

$$\rightarrow B_{13}C_2 + TiC_x + TiB + Ti_3B_4 + TiB_2 \rightarrow TiC_x + TiB_2 \qquad (5.13)$$
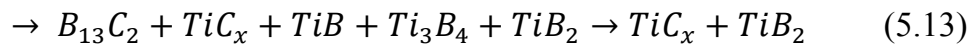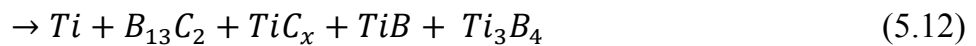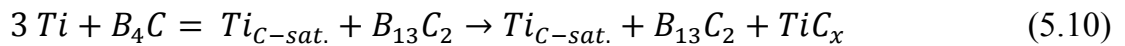
However, the complete formation of TiC_x and TiB_2 requires a very long time if the 3Ti-B_4C preform is heat-treated according to the heating cycle used for the fabrication of the composite (Figure 4.11). This reaction sequence is based on different partial reactions that involve Ti and B_4C and/or the intermediate phases as follows:

$$5/6\,Ti + 1/6\,B_4C = 2/3\,TiB + 1/6\,TiC \qquad (5.14)$$

$$16/17\,TiB + 1/17\,B_4C = 5/17\,Ti_3B_4 + 1/17\,TiC \qquad (5.15)$$

$$3/4\,Ti_3B_4 + 1/4\,B_4C = 2TiB_2 + 1/4\,TiC \qquad (5.16)$$
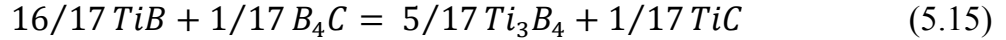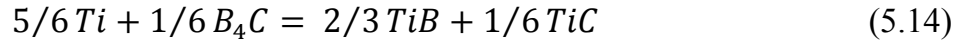
Zhao and Cheng [147] suggested that these reactions take place at relatively low temperatures (T≤1300ºC) when they investigated the formation of TiC-TiB_2 composites by reactive sintering of 3Ti-B_4C compacts at temperatures between 950 and 1650ºC. The formation of substoichiometric TiC_x prior to the titanium borides was also proposed by Zhao and Cheng [147]. This is attributed to the diffusivity of carbon in Ti being much greater than that of boron [148]. Despite the strong covalent bonds between the atoms in the boron carbide structure, carbon diffuses away from boron carbide faster than boron. Therefore, due to the reaction of Ti and B_4C, TiC_x phase formed prior to titanium borides leaving a B-rich boron carbide core in the center of the particles as Shen *et al.* observed [148].

The conversion of B_4C to $B_{13}C_2$ is consistent with Emin's suggestion [149]. According to this suggestion, with decreasing carbon concentration in B_4C, boron substitutes for carbon in the intericosahedral chains converting the C-B-C chains to C-B-B chains (i.e., B_4C changes to $B_{13}C_2$). This also agrees with the work of Shen *et al.* [148].

5.2.2 The Mg-B₄C System

It appears that without magnesium, the solid-state reaction between Ti and B₄C to form

TiC$_x$ and TiB$_2$ is kinetically very slow during the heating cycle used for the fabrication of

composites especially in the temperature range used here. To investigate the effect of Mg

melt during and after the spontaneous infiltration, two pure B₄C preforms were

compacted at 70% *RD*. One of them was heated to 900ºC for 1 h and then naturally

cooled down to room temperature and molten Mg infiltrated through the other preform at

900ºC for 1 h using the setup presented in Figure 4.10. At 800ºC and below, it was found

that no spontaneous infiltration was attained without adding wetting agent such as Ti to

the B₄C powder. Figure 5.7 shows the XRD patterns of these samples.
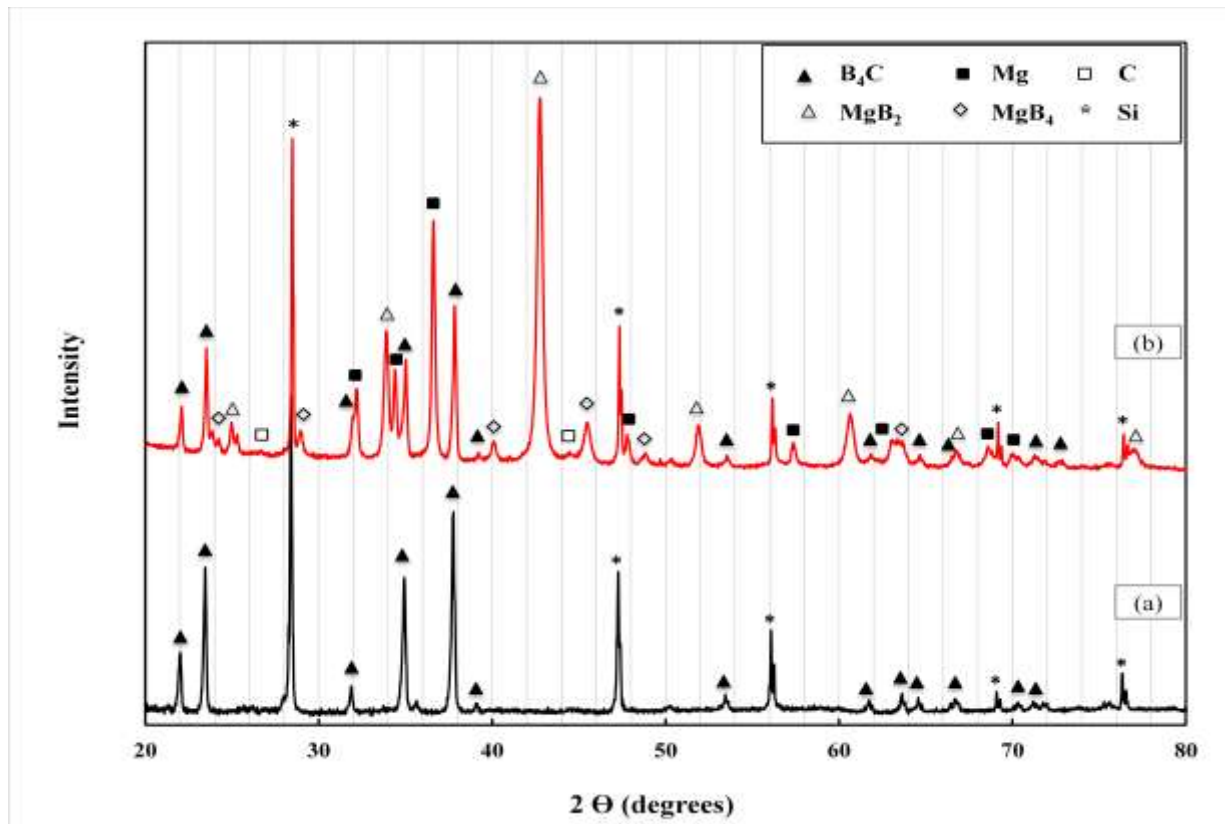
Figure 5.7 XRD pattern of (a) heat-treated B₄C preform and (b) after infiltration of
molten Mg into B₄C preform at 900ºC for 1 h

The results revealed that magnesium infiltrated the preform and the main diffraction peaks corresponding to Mg and MgB_2 were detected but at the same time, there are MgB_4 and retained boron carbide (B_4C) phases in the sample as shown in the figure. This means that magnesium wets B_4C at 900ºC through an interfacial reaction even without adding wetting agent as Ti. This is because the surface tension of liquid decreases with increasing temperature and this agrees with the results of Palmer [150].

To investigate the reaction sequence in the Mg-B_4C system experimentally, thin Mg-B_4C green compacts were prepared with 70% *RD* and placed in a quartz tube under Ar as shown in Figure 5.3. The encapsulated samples were heat-treated at different temperatures from 600ºC to 900ºC for 1 h holding time and then quenched in water according to the heating cycle shown in Figure 5.4. The molar ratio of Mg to B_4C in these preforms is (2.7:1) which matches with 25 wt.% Mg powder in the preform and higher than that required to complete the reaction between Mg and B_4C to form MgB_2. Figure 5.8 shows the XRD spectra of heat-treated Mg-B_4C samples for 1 h at different temperatures.

The results revealed that the peaks of Mg and B_4C are the main peaks after heat-treatment at 600ºC. However, very small MgO particles formed due to the partial reaction of Mg with oxygen. At 700ºC, the peaks of MgB_2, MgB_4 and MgC_2 appeared beside those of Mg and retained B_4C. MgC_2 formed due to the reaction of the liberated carbon with Mg in the system but this phase is unstable and rapidly decomposes. With increasing temperature, the area under the peaks of MgB_2 increased while those of Mg and retained B_4C decreased till those of Mg disappeared at 900ºC.

Figure 5.8 XRD patterns of heat-treated Mg-B$_4$C samples quenched from different temperatures (a) 600, (b) 700, (c) 800 and (d) 900°C after 1 h holding time

It is worth noting that despite the fact that the molar ratio of Mg to B$_4$C is higher than that required to complete the reaction between Mg and B$_4$C to form MgB$_2$, it was found that Mg disappeared while there was still retained B$_4$C in the system. The reason is the partial reaction of Mg with oxygen as mentioned earlier.

Based on the XRD results, it can be suggested that molten magnesium reacts with B$_4$C to form magnesium diboride liberating elemental carbon. This reaction is an exothermic reaction providing heat for further reaction to occur in the system. Hence, the reaction mechanism is as follows:

$$2Mg + B_4C = 2\,MgB_2 + C \tag{5.17}$$
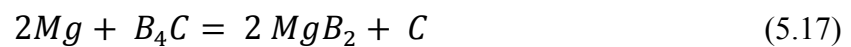
This result agrees with what is suggested by Kevorkijan and Skapin [151]. Also, the presence of MgB_4 peaks in the XRD pattern proves that MgB_2 partially decomposes forming MgB_4 and Mg gas that diffuses through the thin film of MgB_4 as follows:

$$MgB_2 = \frac{1}{2}MgB_4 + \frac{1}{2}Mg\ (g) \tag{5.18}$$

This agrees with the results obtained by Brutti *et al.* [152].

5.2.3 The whole Infiltrated Mg-(Ti-B$_4$C) System

Figure 5.9 shows the XRD patterns of the 3Ti-B$_4$C preform (no Mg) compacted at 70% *RD* after heat-treatment at 900ºC for 1 h in relation to the Mg matrix composite sample fabricated at the same temperature and holding time using a 3Ti-B$_4$C preform of the same relative density (*RD*).
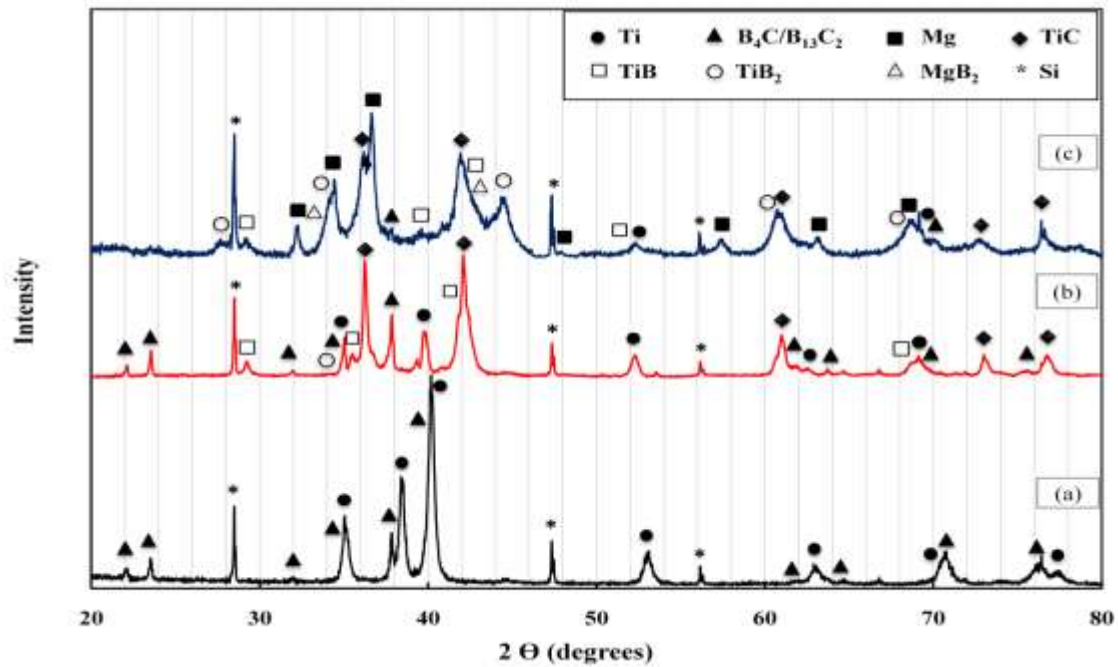
Figure 5.9 XRD pattern of (a) the starting 3Ti-B$_4$C powder mixture, (b) heat-treated 3Ti-B$_4$C preform at 900ºC for 1 h and (c) Mg composite fabricated at 900ºC for 1 h

It can be observed that substoichiometric TiC_x formed in both cases while TiB_2 significantly formed after infiltration of Mg even at this short time. This revealed the role of infiltrated molten Mg or Mg alloy in the reaction which was very important especially because no metal powder such as Al was added to the $Ti-B_4C$ system.

Based on the reaction sequences of the individual systems; $Ti-B_4C$ and $Mg-B_4C$, the reaction mechanism of the whole infiltrated $Mg-(Ti-B_4C)$ system after the infiltration of molten Mg or Mg alloy through the $3Ti-B_4C$ preform can be presented as follows:

$$3\,Ti + B_4C + Mg \;=\; Ti + B_{13}C_2 + TiC_x + TiB + MgB_2 \qquad (5.19)$$
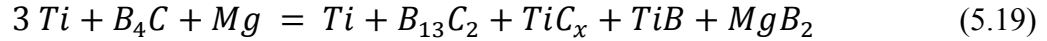
TiC_x formed due to the reaction between Ti and B_4C (Eq. 5.10) and also the diffusion of atomic C liberated by the reaction between Mg and B_4C (Eq. 5.13) into Ti according to the following equation:

$$Ti + C \;=\; TiC_x \qquad (5.20)$$

MgB_2 partially decomposes forming MgB_4 and Mg gas that diffuses through the thin film of MgB_4 according to Eq. 5.18. On the other hand, TiB reacts with B_4C forming Ti_3B_4 and TiC according to Eq. 5.15 then:

$$3\,Ti + B_4C + Mg = Ti + B_{13}C_2 + TiC_x + TiB + Ti_3B_4 + MgB_2 + MgB_4 \quad (5.21)$$
$$\rightarrow B_{13}C_2 + TiC_x + TiB + Ti_3B_4 + TiB_2 + MgB_2 \qquad (5.22)$$

Where:
$$Ti + \tfrac{1}{2}MgB_4 \;=\; 2TiB_2 + \tfrac{3}{2}Mg \qquad (5.23)$$
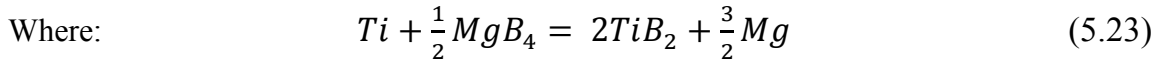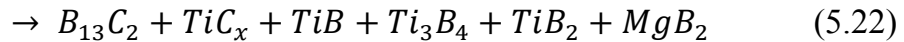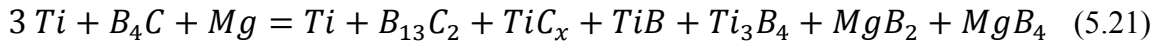
Since MgB_2 reacts with TiB forming TiB_2 and titanium borides, TiB and Ti_3B_4, react with the retained boron carbide as presented earlier in the reaction mechanism of $Ti-B_4C$ system, the reaction between Ti, B_4C and infiltrated molten Mg alloy is finally obtained as follows:

$$\boldsymbol{Ti + B_4C + Mg \rightarrow TiC_x + 2TiB_2 + Mg} \qquad (5.24)$$

84
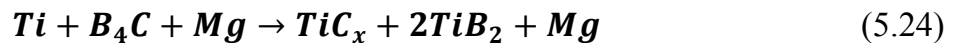
Based on these observations, it can be concluded that Mg melt not only infiltrates through the 3Ti-B$_4$C preform and thus densifies the fabricated composite as a matrix metal but also acts as an intermediary that makes the reaction possible at a lower temperature than that required for solid-state reaction between Ti and B$_4$C.

Finally, the study of the *in-situ* reaction mechanism is very important to understand and analyze the microstructure of the produced composites and their properties. The infiltration of Mg melt through the preform of (3Ti-B$_4$C) basically depends on its viscosity and wettability to Ti and B$_4$C and/or the *in-situ* formed TiC. Mg infiltrated the preform through the pores by the capillary force to get dense microstructure of magnesium matrix composites.

5.3 Reaction Mechanism of Infiltrated Mg-(Mg-Ti-B$_4$C) System

Although, the fabricated Mg matrix composites using a 3Ti-B$_4$C preform are attractive in different applications demanding high volume fraction of the reinforcing phases and hence high strength, hardness and wear resistance, they are not suitable for other applications because of their brittleness. So, this work tried to increase the percentage of magnesium in the composites to improve their ductility. To achieve that, pure Mg, AM60B and AZ91D matrix composites reinforced with TiC and TiB$_2$ compounds have been fabricated using a preform containing Mg or MgH$_2$ powder in addition to the 3Ti-B$_4$C mixture.

5.3.1 The Mg-Ti-B$_4$C System

In this section, the reaction mechanism of the infiltrated Mg-(Mg-Ti-B$_4$C) system is divided into two systems: one is the Mg-Ti-B$_4$C system where Mg powder was added

to the 3Ti-B$_4$C preform and the other is the system after infiltration of the molten Mg into the Mg-(3Ti-B$_4$C) preform. To investigate the reaction sequence in the Mg-Ti-B$_4$C system before and during the infiltration of the molten Mg or Mg alloy experimentally beside those derived from the Mg-B$_4$C and Ti-B$_4$C systems, 25 wt% Mg-(3Ti-B$_4$C) green compacts were prepared with 70% *RD* and placed in a quartz tube under Ar as shown in Figure 5.3. The encapsulated samples were heat-treated at different temperatures from 600°C to 900°C for 1 h holding time and then quenched in water according to the heating cycle shown in Figure 5.4.

Figure 5.10 shows the XRD patterns of the heat-treated 25 wt.% Mg-(3Ti-B$_4$C) samples for 1 h but at different temperatures.
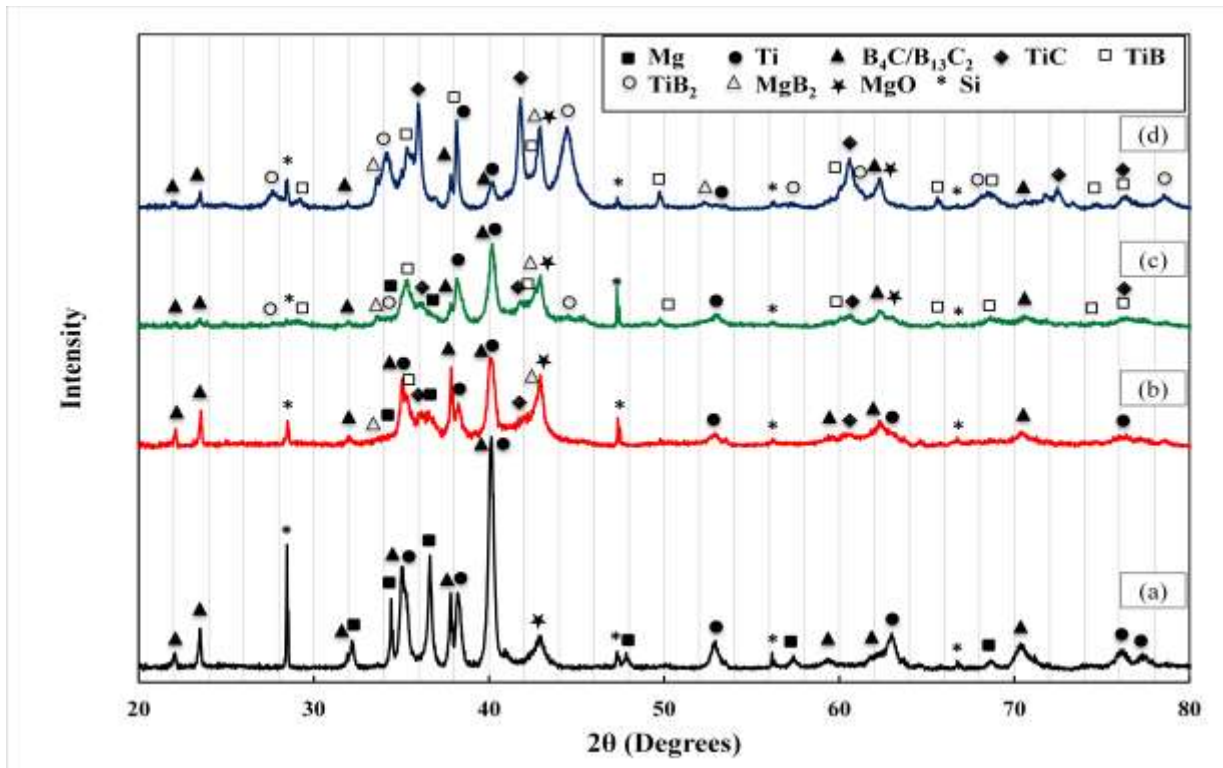
Figure 5.10 XRD patterns of heat-treated Mg-(3Ti-B$_4$C) samples quenched from different temperatures: (a) 600, (b) 700, (c) 800 and (d) 900°C after 1 h holding time

86

The results revealed that no reaction took place at 600ºC where only Mg, Ti and boron carbide peaks are observed beside very small amount of MgO. At 700ºC, the peaks of TiC_x, MgB_2 and very small peaks of TiB beside those of Mg, Ti and boron carbide appeared in the XRD spectra as shown in Figure 5.10. Also, it can be observed that the peaks of Ti, boron carbide and Mg decrease with increasing temperature.

The same scenario as at 700ºC took place at 800ºC with strong appearance of TiB and TiB_2 peaks. When the temperature increased to 900ºC, the retained Ti and boron carbide decreased till it can be said that the retained Ti can be neglected along with disappearance of Mg peaks. On the other hand, the peaks of TiB_2, TiB and MgB_2 increased. However, there are still retained boron carbide and intermediate phases such as TiB and MgB_2.

Based on the XRD results, it was found that the reaction sequence of the Mg-Ti-B_4C system is similar to that of the infiltrated Mg-(Ti-B_4C) system. Thus, Mg powders in the Mg-Ti-B_4C system plays the same role as the infiltrated Mg where it reacts with B_4C forming MgB_2 and liberating C which reacts with Ti to form TiC_x. These reactions are exothermic providing the system with heat which enhances the reaction itself and other reactions in the system such as between Ti and B_4C. This means that the presence of Mg powder in the preform enhances the reaction and its role starts even before the infiltration of molten Mg. After the infiltration of molten Mg, a complete reaction took place without any retained Ti, boron carbide or intermediate phases even after only a short holding time of 1.5 h as shown in Figure 5.11.

5.3.2 The whole Infiltrated Mg-(Mg-Ti-B₄C) System

Figure 5.11 shows the XRD spectra of the 25 wt.% Mg-(3Ti-B₄C) preform mixture compacted at 70% *RD* and heat-treated at 900ºC for 1.5 h in comparison with a AZ91D matrix composite sample fabricated at the same temperature and holding time using a similar preform.
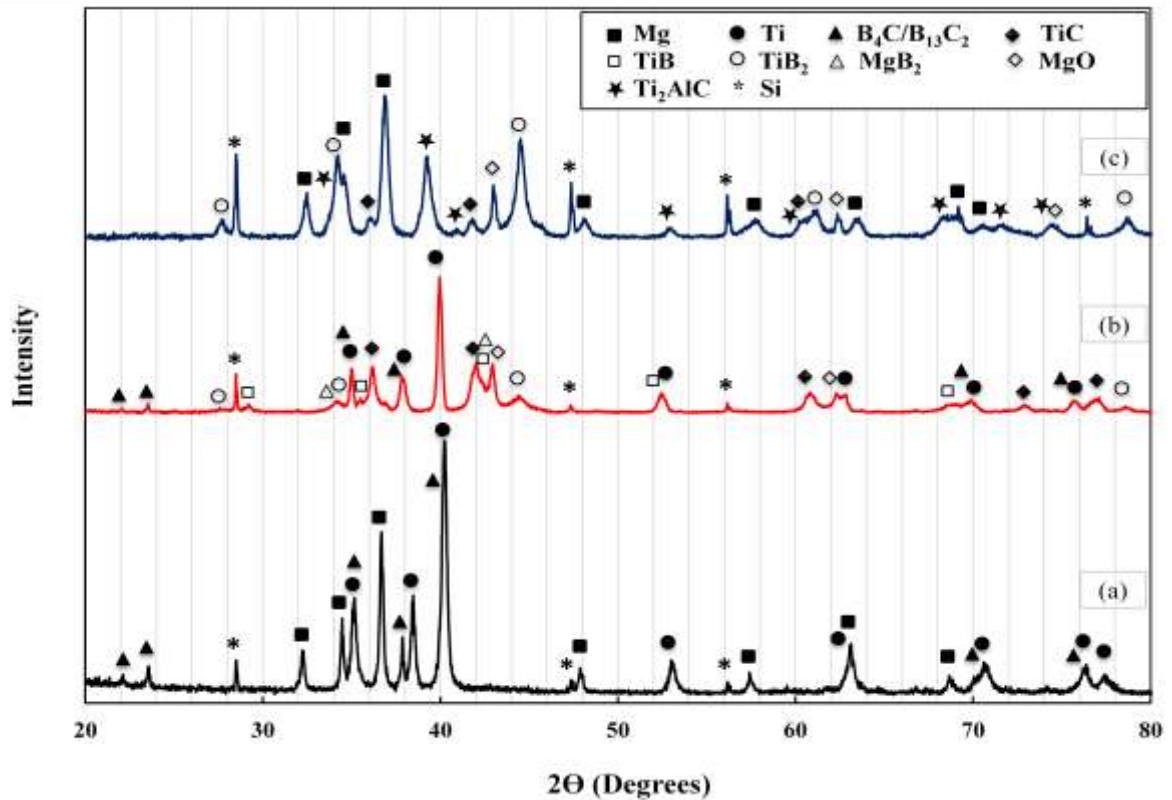
Figure 5.11 XRD pattern of (a) 25 wt.% Mg-(3Ti-B₄C) mixture, (b) 25 wt.% Mg-(3Ti-B₄C) preform heat-treated at 900ºC for 1.5 h and (c) after infiltration of molten AZ91D into this preform

It can be observed that substoichiometric TiC$_x$ formed in both cases while the area under the peaks of the formed TiB₂ in the heat-treated preform is less than those after infiltration of molten AZ91D alloy. Also, there are still peaks of retained Ti and boron carbide and those of the intermediate phases MgB₂ and TiB in case of the heat-treated

88

preform before infiltration of molten AZ91D alloy. This proves that the reaction is incomplete. MgO peaks appear in both cases.

The complete reaction after infiltration of molten magnesium without retained Ti and boron carbide and intermediate phases reveals the role of Mg powder in the reaction. The Mg powder plays a part of the role of the infiltrated Mg where it acts as an intermediary that makes the reaction possible at a lower temperature than that required for solid-state reaction between Ti and B_4C and accelerates the reaction rate.

Based on the XRD results, it can be said that the reaction mechanism of the whole infiltrated Mg-(Mg-Ti-B_4C) system is similar to that of the Mg-Ti-B_4C system. The infiltrated Mg in this system is just to complete the reaction which already has been enhanced due to the presence of Mg powder in the preform and to densify the fabricated composites.

It is worth noting that the ternary Ti_2AlC compound formed with molten AZ91D due to the diffusion of Al into substoichiometric TiC_x at high temperature. This proves that the reaction was enhanced by the presence of Mg powder in the preform making the formation of substoichiometric TiC_x faster, giving Al more time to diffuse into TiC_x. Finally, the formation of this ternary compound takes place in a shorter holding time compared with the case without Mg powder in the preform.

5.4 Reaction Mechanism of Infiltrated Mg-(MgH₂-Ti-B₄C) System

To understand the *in-situ* reaction mechanism of the infiltrated Mg-(MgH_2-Ti-B_4C) system, the reaction mechanism was divided into four subsystems; MgH_2-Ti, MgH_2-B_4C, MgH_2-Ti-B_4C and Mg-Ti-B_4C which was studied before. Mg here is the infiltrated Mg or Mg alloy. Based on the reaction mechanism of these systems, the reaction mechanism of

89

the whole infiltrated Mg-(MgH$_2$-Ti-B$_4$C) system was investigated. It is very important to note that the molar ratio of these individual system matches with 25 wt.% MgH$_2$ powder added to Ti and B$_4$C powders with 3:1 molar ratio.

5.4.1 The MgH$_2$-Ti System

To investigate the reaction mechanism in the MgH$_2$-Ti system experimentally, MgH$_2$-Ti green compacts were prepared with 70% *RD* and placed in a quartz tube under Ar. The encapsulated samples were heat-treated at different temperatures from 400°C to 800°C for 1 h then quenched in water according to the heating cycle shown in Figure 5.3. The XRD patterns of these samples are shown in Figure 5.12.
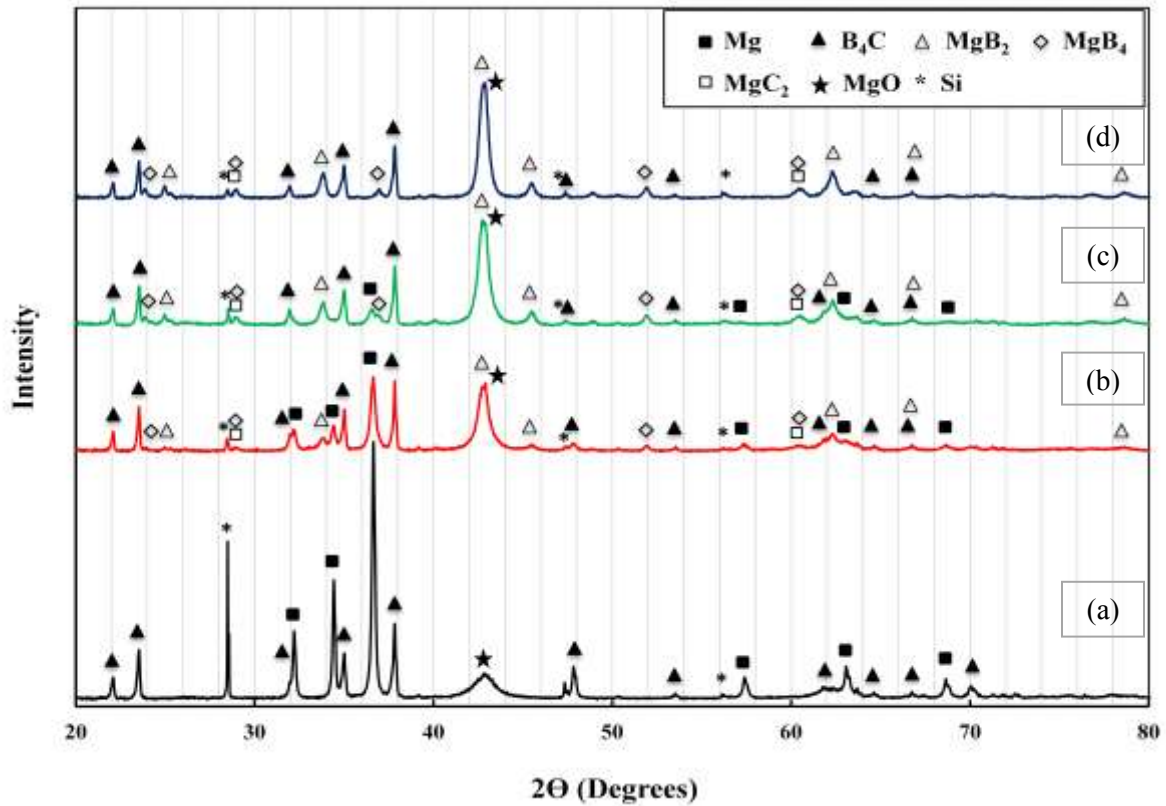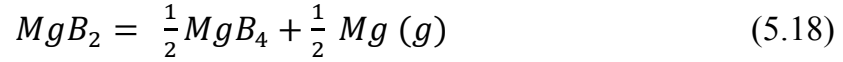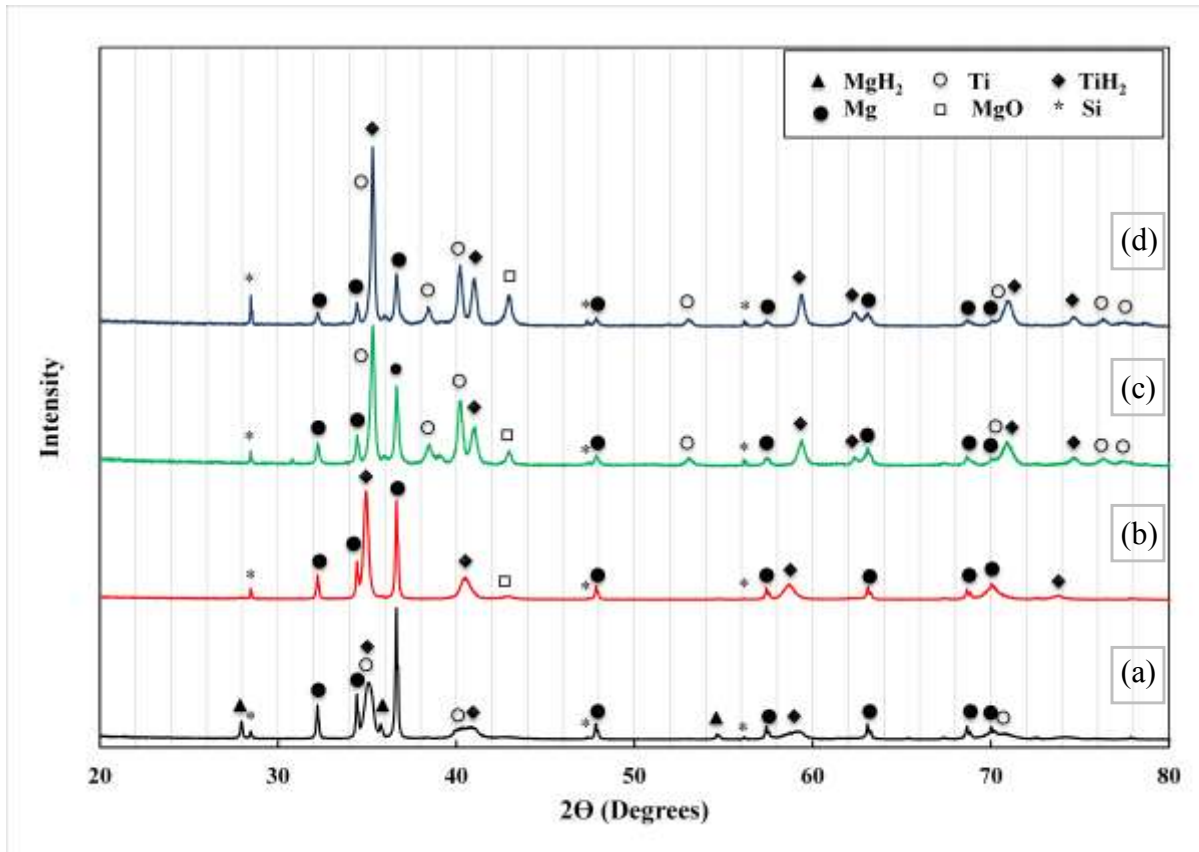

Figure 5.12 XRD patterns of heat-treated MgH$_2$-Ti samples quenched from different temperatures (a) 400, (b) 600, (c) 700 and (d) 800°C after 1 h holding time

The results revealed that at 400°C, the peaks of Mg, MgH$_2$, Ti and TiH$_2$ are the main peaks. However, the only main peaks at 600°C are those of Mg and TiH$_2$ while with increasing temperature, Ti appeared again with TiH$_2$ at 700 and 800°C. The change in the lattice constant for TiH$_2$ as shown in Table 5.3 revealed the highest one at 600°C and decreased with increasing the temperature. Based on this, TiH$_2$ formed at the beginning has a high content of hydrogen which is released by the decomposition of MgH$_2$ and with increasing temperature, the rate of hydrogen release increased due to the decomposition of TiH$_2$.

Table 5.3 Lattice parameters of TiH$_2$ for heat-treated MgH$_2$-Ti samples at different temperatures

Sample	Processing parameters	Lattice constant of TiH$_2$, a, $(\mathring{A})$
MgH$_2$-Ti	400°C/1 h	4.4306
	600°C/1 h	4.453886
	700°C/1 h	4.405647
	800°C/1 h	4.404136

Another investigation of the reaction mechanism of this system was done where an MgH$_2$-Ti green compact with 70% *RD* was kept in the furnace at 900°C for 1.5 holding time (Δt) according to the heating cycle shown in Figure 4.11. This sample was compared with the composite sample fabricated using the same green compact after the infiltration of molten AZ91D at the same processing parameters. The XRD patterns of the MgH$_2$-Ti preform and the sample after infiltration of the molten AZ91D alloy into this preform heated to 900°C for 1.5 h are shown in Figure 5.13.
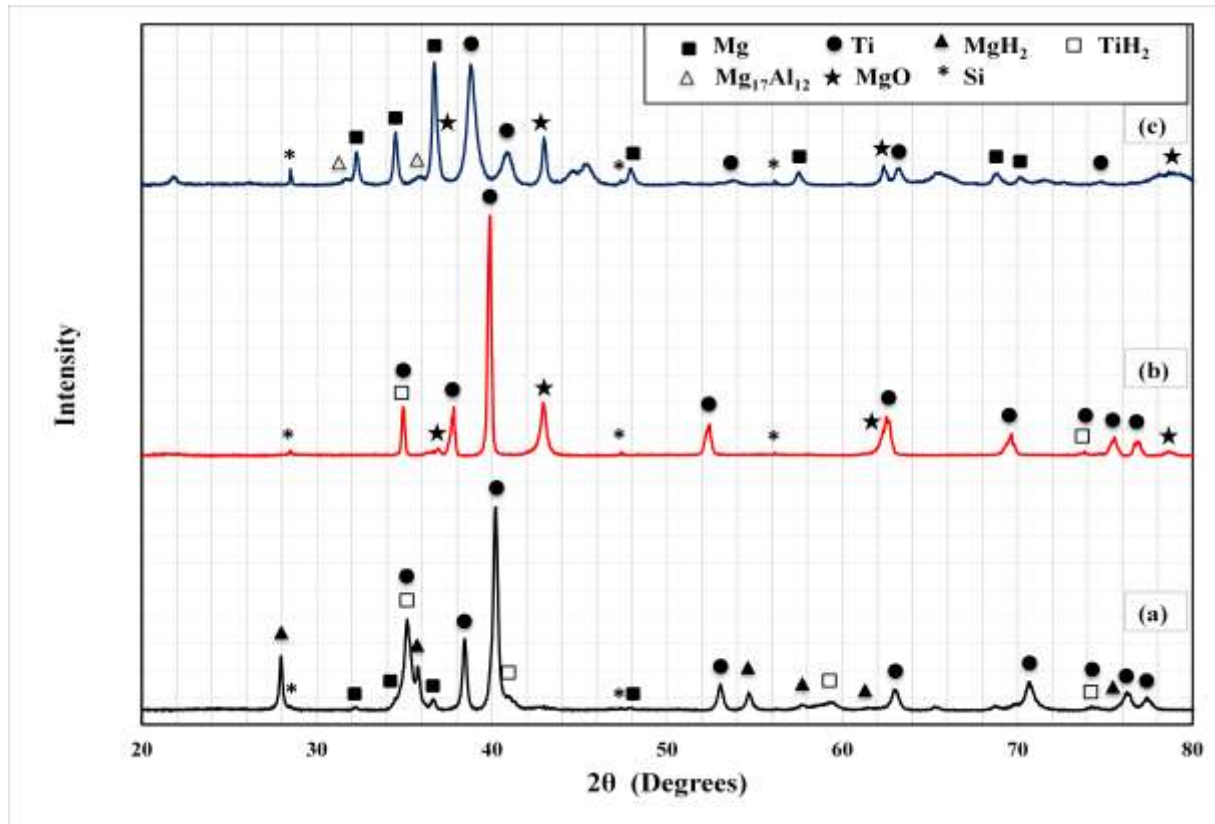
Figure 5.13 XRD pattern of (a) MgH_2-Ti mixture (b) heat-treated MgH_2-Ti preform and (c) after infiltration of molten AZ91D into this preform at 900°C for 1.5 h

Based on the XRD results, it can be observed that MgH_2 decomposed at low temperature ($\leq$400°C) forming Mg and releasing hydrogen according to the following equation:

$$MgH_2 \rightarrow Mg + H_2 \tag{5.25}$$

Then Ti reacts with H_2 to form TiH_2 which decomposes with increasing temperature forming more reactive Ti due to an increase in its surface area and releasing hydrogen as follows:

$$Ti + H_2 \xrightarrow{\leq 600\,°C} TiH_2 \tag{5.26}$$

$$TiH_2 \xrightarrow{\leq 700\,°C} Ti + H_2 \tag{5.27}$$
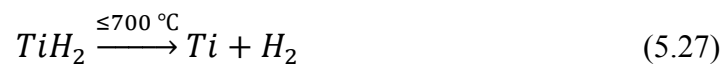
5.4.2 The MgH$_2$-B$_4$C System

To investigate the reaction mechanism of this system, an (MgH$_2$-B$_4$C) green compact with 70% *RD* was kept in the furnace at 900ºC for 1.5 h holding time (Δt) according to the heating cycle shown in Figure 4.11. This sample was compared with the AZ91D composite sample fabricated using the same MgH$_2$-B$_4$C preform and at the same processing parameters. The molar ratio of MgH$_2$ to B$_4$C in these compacts is (2.52:1) which matches with 25 wt.% MgH$_2$ powder in the preform.

The XRD patterns of the MgH$_2$-B$_4$C mixture, the MgH$_2$-B$_4$C preform and the sample after infiltration of molten AZ91D alloy into this preform heated to 900ºC for 1.5 h are shown in Figure 5.14.

Based on the XRD results, it was found that the reaction mechanism of the MgH$_2$-B$_4$C system is similar to that of the Mg-B$_4$C system. The difference between the two cases is that Mg formed by the decomposition of MgH$_2$ is more chemically reactive due to its higher surface area than Mg in the Mg-B$_4$C system. By comparing the MgH$_2$-B$_4$C with the Mg-B$_4$C system, it was found that the magnesium formed by the decomposition of MgH$_2$ is more reactive than Mg powder in the Mg-B$_4$C system. This can be proved by its high affinity for oxygen and forming MgO as shown in Figure 5.14.

During and after complete infiltration of liquid magnesium through the MgH$_2$-B$_4$C preform, some of the molten magnesium reacts with some of the remaining boron carbide as mentioned before in the investigation of the reaction mechanism of 25 wt.% Mg-Ti-B$_4$C system while the rest of molten magnesium just fills the composite sample.
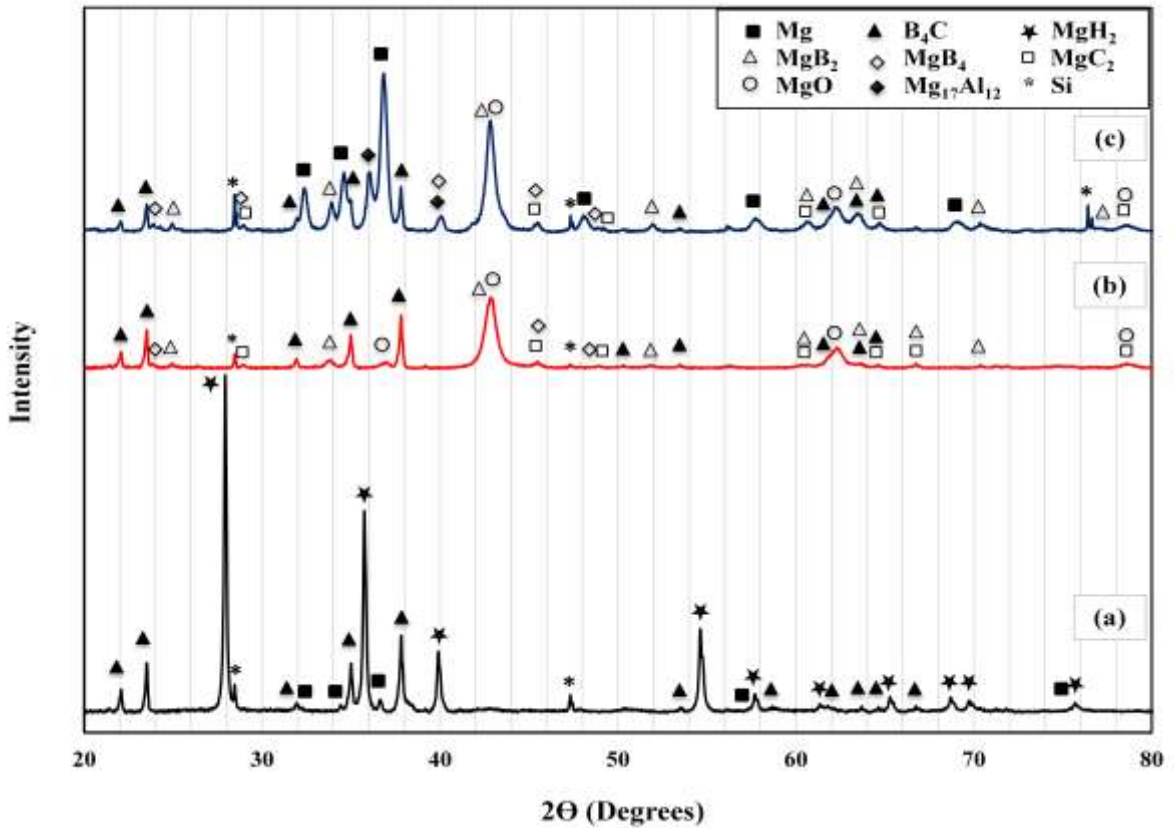
Figure 5.14 XRD pattern of samples (a) MgH_2-B_4C mixture, (b) heat-treated MgH_2-B_4C preform and (c) after infiltration of molten AZ91D into this preform at 900ºC for 1.5 h

5.4.3 The whole Infiltrated Mg-(MgH_2-Ti-B_4C) System

Figure 5.15 shows the XRD spectra of the 25 wt.% MgH_2-($3Ti$-B_4C) preform mixture, that was compacted at 70% *RD* and heat-treated at 900ºC for 1.5 h, and an AZ91D matrix composite sample fabricated at the same temperature, holding time and preform.

It can be observed that substoichiometric TiC_x formed in both cases while TiB_2 formed significantly after infiltration of molten magnesium through the preform. The peaks of the formed TiB_2 before Mg infiltration are very small. Also, there are still peaks of retained Ti and boron carbide and those of the intermediate phases such as MgB_2 and

94

TiB in the case of the heat-treated preform before infiltration of molten AZ91D Mg alloy. This proves that the reaction is incomplete. The complete reaction after infiltration of molten magnesium without retained Ti and boron carbide and intermediate phases reveals the role of MgH_2 in this reaction mechanism. The MgH_2 plays a similar role as the infiltrated magnesium before and during the infiltration process.
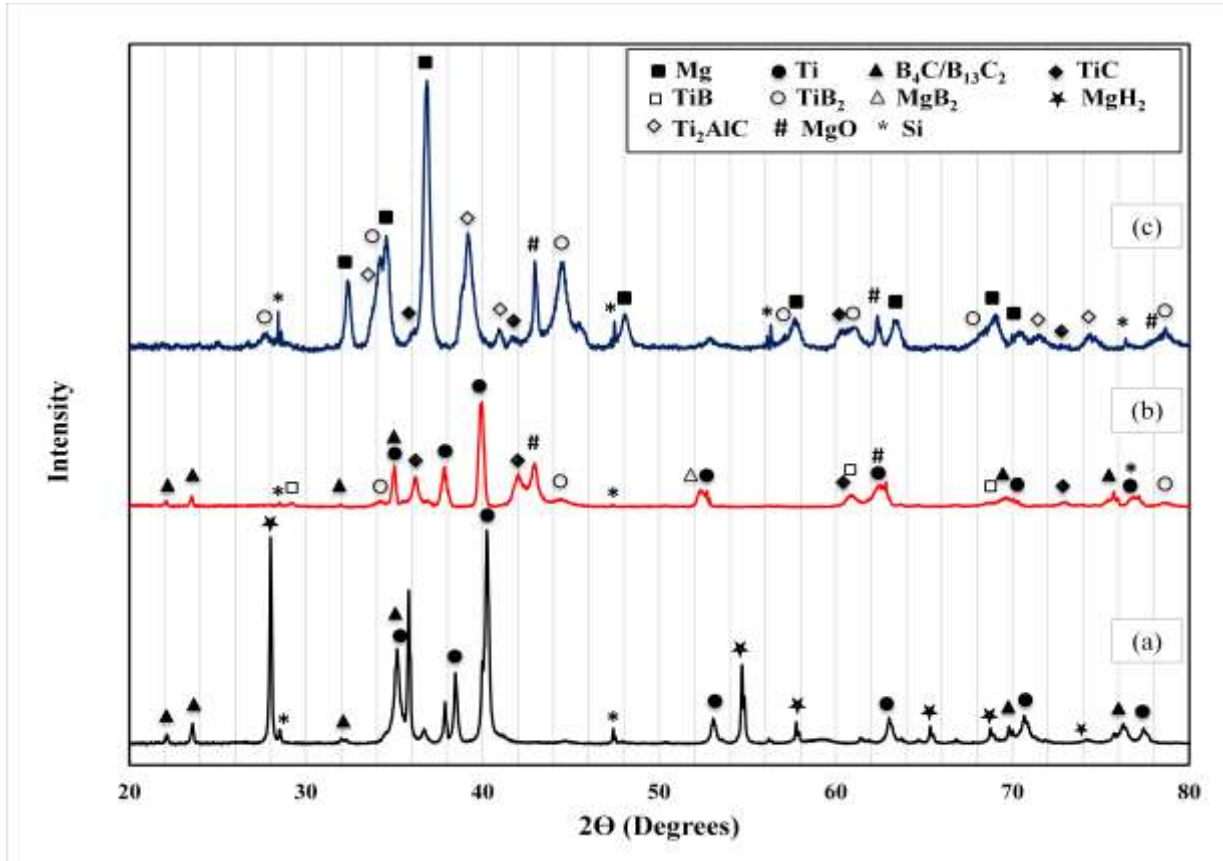
Figure 5.15 XRD pattern of samples (a) 25 wt.% MgH_2-(3Ti-B_4C) mixture, (b) heat-treated 25 wt.% MgH_2-(3Ti-B_4C) preform and (c) after infiltration of molten AZ91D into this preform at 900°C for 1.5 h

Based on these results, the *in-situ* reaction mechanism of the infiltrated Mg-(MgH_2-Ti-B_4C) system was investigated based on the reaction mechanism of the

95

MgH_2-Ti-B_4C system and that of the infiltrated Mg-(3Ti-B_4C) system which was investigated earlier.

It was found that the reaction mechanism of the whole infiltrated Mg-(MgH_2-Ti-B_4C) system is similar to that of infiltrated Mg-(Ti-B_4C) system. The difference between the two cases is that Mg formed by the decomposition of MgH_2 is more chemically reactive due to its higher surface area than Mg in the Mg-Ti-B_4C system. Also, Ti formed after the decomposition of TiH_2 is more chemically reactive due to its higher surface area than Ti in the Mg-Ti-B_4C system making the reaction between Ti and B_4C much faster and the same applies for the case of Mg with B_4C.

Also, it is observed that the ternary Ti_2AlC compound formed when AZ91D is used. Ti_2AlC forms by the diffusion of Al from the molten AZ91D into substoichiometric TiC_x at high temperature. The amount of Ti_2AlC is higher if compared with that formed without MgH_2 in the preform. The reason behind this is that the reaction is faster by the presence of MgH_2 in the preform and then the formation of substoichiometric TiC_x is very fast allowing the formation of this ternary compound in a shorter holding time compared with the case without MgH_2 in the preform.

It can be concluded that MgH_2 after decomposition plays the role of magnesium to react with B_4C before and during the infiltration of molten magnesium or magnesium alloy into the preform. However, the molten Mg or Mg alloy not only infiltrates through the MgH_2-(3Ti-B_4C) preform and thus densifies the fabricated composite as a matrix metal but also acts as intermediary in the reaction making it possible at lower temperature. Hence, Mg and MgH_2 powders accelerate the reaction rate.

Chapter 6

Fabrication of TiC-TiB$_2$/Mg Matrix Composites

Part I: Fabrication of TiC-TiB$_2$/Mg Matrix Composites using a 3Ti-B$_4$C Preform

There are several processing parameters affecting the fabrication of Mg matrix composites via *in-situ* reactive infiltration process such as particle size of the starting powders (Ti and B$_4$C), processing temperature, holding time and the green compact relative density (*RD*). In this work, the influence of the processing temperature, holding time and the green compact relative density have been studied, while the particle sizes of Ti and B$_4$C and conditions of ball milling of the mixture (time and speed) were kept constant. A small particle size of B$_4$C relative to that of Ti has been chosen to enhance the contact and the solid state reaction between them. This study was conducted by changing one factor at a time. The temperature range for fabrication of the composite samples was chosen as 700 to 900ºC ±10ºC at 50ºC intervals based on the results obtained for the heat-treated and quenched 3Ti-B$_4$C samples as shown earlier in Figure 5.5 where below 700ºC, no reaction took place to form TiC and TiB$_2$.

Finding the optimal processing parameters for producing sound magnesium matrix composites reinforced with a network of the *in-situ* formed TiC and TiB$_2$ particles is one of the main objectives of this work. Therefore, to reach this goal, composite samples were fabricated using pure magnesium, AM60B and mainly AZ91D as a matrix metal at different processing parameters as shown in Table 6.1.

97

Table 6.1 The fabricated composite samples at different processing parameters

Sample No.	Matrix Material	Processing Parameters		
		Temperature (ºC)	Holding time (h)	Green compact density (%)
1	AZ91D	700	6	70
2		750	1	70
3			3	70
4			6	70
5		800	1	55
6			1	60
7			1	70
8			3	70
9			6	70
10	Pure Mg		1	70
11			3	70
12			6	60
13			6	70
14	AZ91D	850	1	70
15			3	70
16			6	70
17	Pure Mg		1	70
18			3	70
19			6	70
20	AZ91D	900	1/2	70
21			1	55
22			1	60
23			1	70
24			1.5	55
25			1.5	60
26			1.5	65
27			1.5	70
28			3	70
29			6	70
30	Pure Mg		1/4	70
31			1/2	70
32			1	70
33			1.5	70
34			3	70
35			6	70
36	AM60B		1	70
37			1.5	70
38			3	70
39			6	70

6.1 Influence of the Processing Temperature on the Fabrication of TiC-TiB$_2$/Mg Matrix Composites

Only a sample of the results obtained in this part of the study is presented below. For example, XRD spectra for three composite samples fabricated at 1 h holding time using a 3Ti-B$_4$C preform with 70% *RD* but at different processing temperatures of 800, 850 and 900ºC are presented in Figure 6.1.
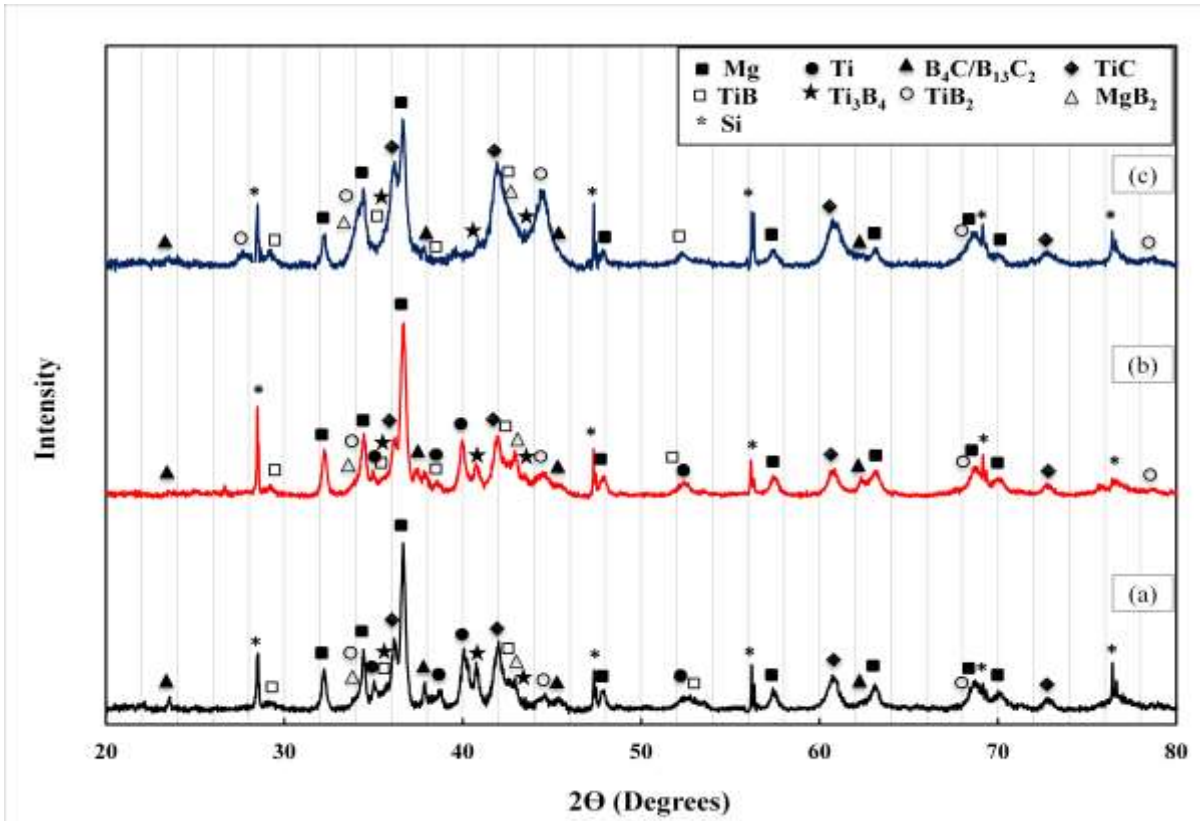
Figure 6.1 XRD pattern of the AZ91D alloy MMCs fabricated using a 3Ti-B$_4$C preform with 70% *RD* at different processing temperatures (a) 800, (b) 850 and (c) 900ºC for 1 h holding time

As shown in Figure 6.1, the main diffraction peaks corresponding to Mg, TiC$_x$ and TiB$_2$ were detected but at the same time there are retained Ti and boron carbide and intermediate phases such as TiB, Ti$_3$B$_4$ and MgB$_2$ as well in all samples. This means that

the reaction is still incomplete in all of them. However, it can be observed that the TiC_x and TiB_2 peak intensities increase as the temperature increases from 800°C to 900°C indicating that the reaction among the Ti, Mg, boron carbide and the intermediate phases did take place during heating and this reflects the effect of processing temperature on the *in-situ* reaction and hence the fabrication of the composites in the end. The volume percentages of the formed phases, based on Rietveld analysis, are presented in Figure 6.2.
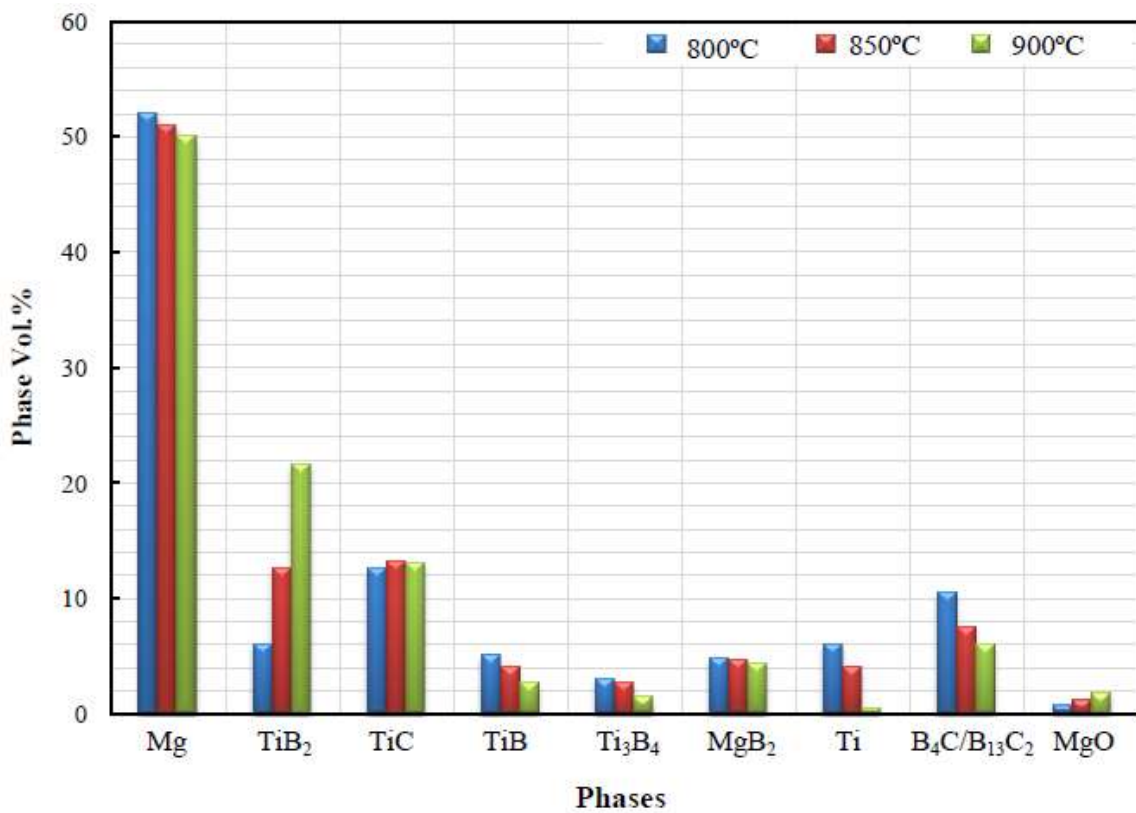
Figure 6.2 Phase volume percentage of the AZ91D alloy MMCs fabricated using a 3Ti-B_4C preform with **70%** *RD* at different processing temperatures: 800, 850 and 900°C for 1 h holding time

The XRD analysis revealed that the percentage of equilibrium phases, TiC_x and TiB_2, at 900°C is higher than that at 800°C or 850°C with lower percentages of retained Ti and boron carbide and the intermediate phases. This means that it is recommended to

fabricate the composite samples at 900ºC rather than at 800ºC or 850ºC to ensure the formation of the required reinforcing phases, TiC_x and TiB_2.

Representative SEM micrographs of the composite samples fabricated at 1 h holding time using a green compact with 70% *RD* but at different processing temperatures of 800, 850 and 900ºC with low and high magnifications are shown in Figures 6.3, 6.4 and 6.5, respectively.
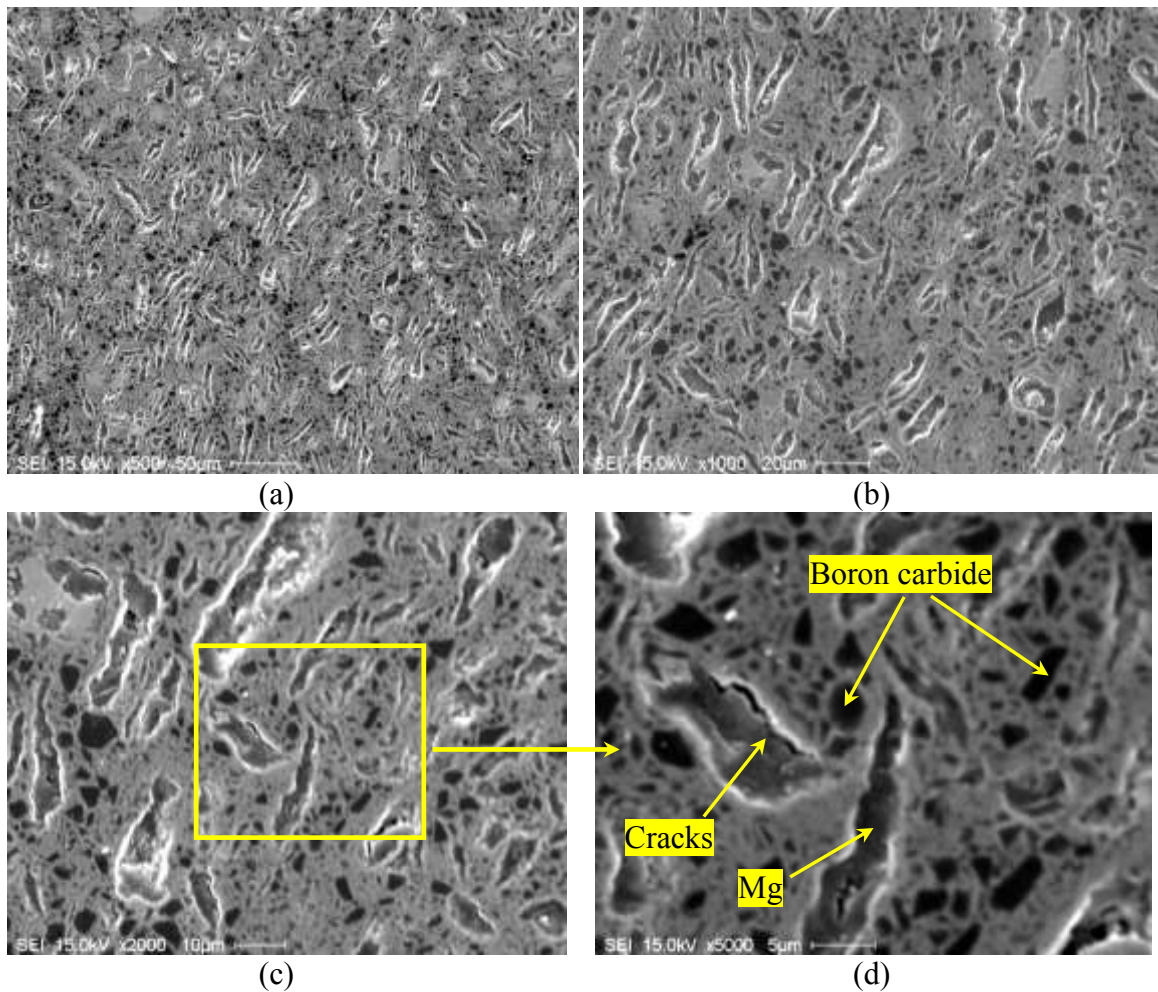
Figure 6.3 SEM microstructure of the AZ91D alloy MMCs fabricated using a 3Ti-B_4C preform with 70% *RD* at 800ºC for 1 h

SEM observations of the sample fabricated at 800ºC reveal a relatively uniform distribution of reinforcing phases as a network of contacting particles in the magnesium matrix and show that no obvious voids are present in the microstructure of the as-fabricated composites. However, some microcracks are indicated in the images of the sample. SEM micrographs also reveal retained boron carbide (dark areas) while retained titanium could not be observed through SEM images. However, retained Ti was observed in the XRD results as shown in Figure 6.1.

(a)   (b)

(c)   (d)
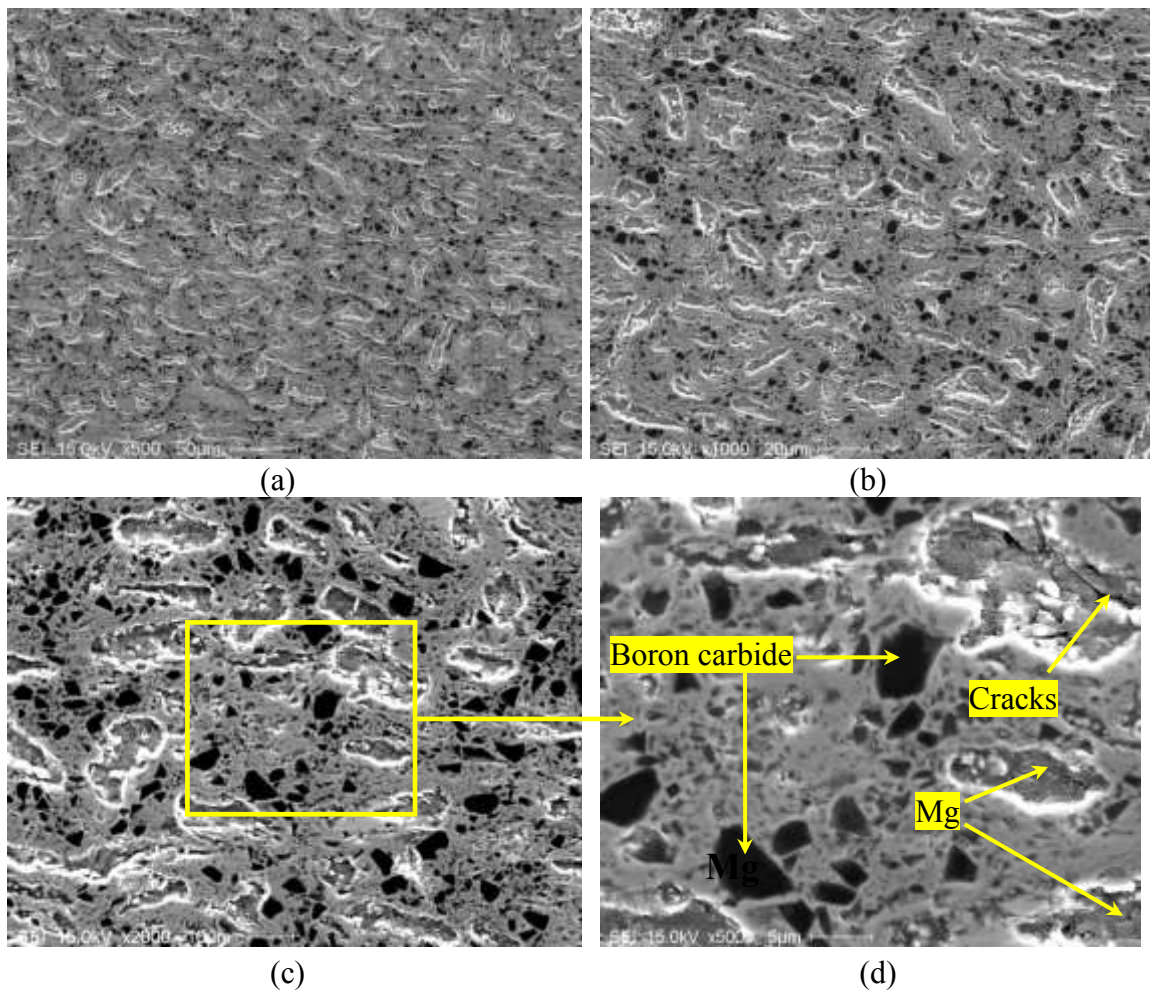
Figure 6.4 SEM microstructure of the AZ91D alloy MMCs fabricated using a 3Ti-B_4C preform with 70% *RD* at 850ºC for 1 h

SEM observations of the sample fabricated at 850ºC also reveal a relatively uniform distribution of reinforcing phases as a network of contacting particles in the magnesium matrix without voids as shown in Figure 6.4. However, the SEM micrographs show less microcracks and retained boron carbide than those in the sample fabricated at 800ºC.

It can be observed that the microcracks at 800ºC are mainly at the ceramic/matrix interface while those at 850ºC are in the Mg matrix. This suggests that the bonding between the matrix and the reinforcing particles for the composites fabricated at 850ºC is stronger than those fabricated at 800ºC. The reason behind these microcracks is most likely the hot tearing of the magnesium during solidification (4.2 vol.% shrinkage [153]).

Finally, SEM observations of the sample fabricated at 900ºC as shown in Figure 6.5 reveal not only a relatively uniform distribution of reinforcing phases as a network of contacting particles in the magnesium matrix but also less retained boron carbide than those in the samples fabricated at 800ºC or 850ºC. Moreover, no voids or microcracks are observed. This indicates that the composites are fully dense.

Also, as shown in Figure 6.6 (b), it is clear from the EDS spectra that this area consists of B, C and Mg. This means that boron carbide is present in the center of this dark phase while MgB_2 lies at its interface (grey phase). These phases were also observed in the XRD results. Also, the presence of Mg in area 3 in the EDS pattern, Figure 6.6 (d), confirms that Mg is present through the network of contacting TiC_x and TiB_2 particles.

(a)　　　　　　　　　　　　(b)

(c)　　　　　　　　　　　　(d)

Figure 6.5 SEM microstructure of the AZ91D alloy MMCs fabricated using a 3Ti-B$_4$C preform with 70% *RD* at 900ºC for 1 h

EDS elemental mapping of the samples fabricated at 850ºC and 900ºC for 1 h holding time are shown in Figures 6.7 and 6.8, respectively. The observed overlap of the titanium, boron and carbon proves the existence of a network of TiC$_x$ and TiB$_2$ in the Mg matrix. Although, there are residual intermediate phases such as TiB and Ti$_3$B$_4$ confirmed by XRD analysis in both samples, it is very difficult to distinguish between TiC$_x$, TiB, Ti$_3$B$_4$, and TiB$_2$ phases in the microstructure. This is because these particles are very small and the difference in their effective atomic numbers is insignificant making the

discernment very difficult by SEM. However, the brightest phase can be considered Ti because it has the highest atomic number of all elements in this system. Also, Mg, boron carbide and MgB_2 phases can be detected more easily due to the significant difference in their effective atomic numbers.

(a)   (b)

(c)   (d)
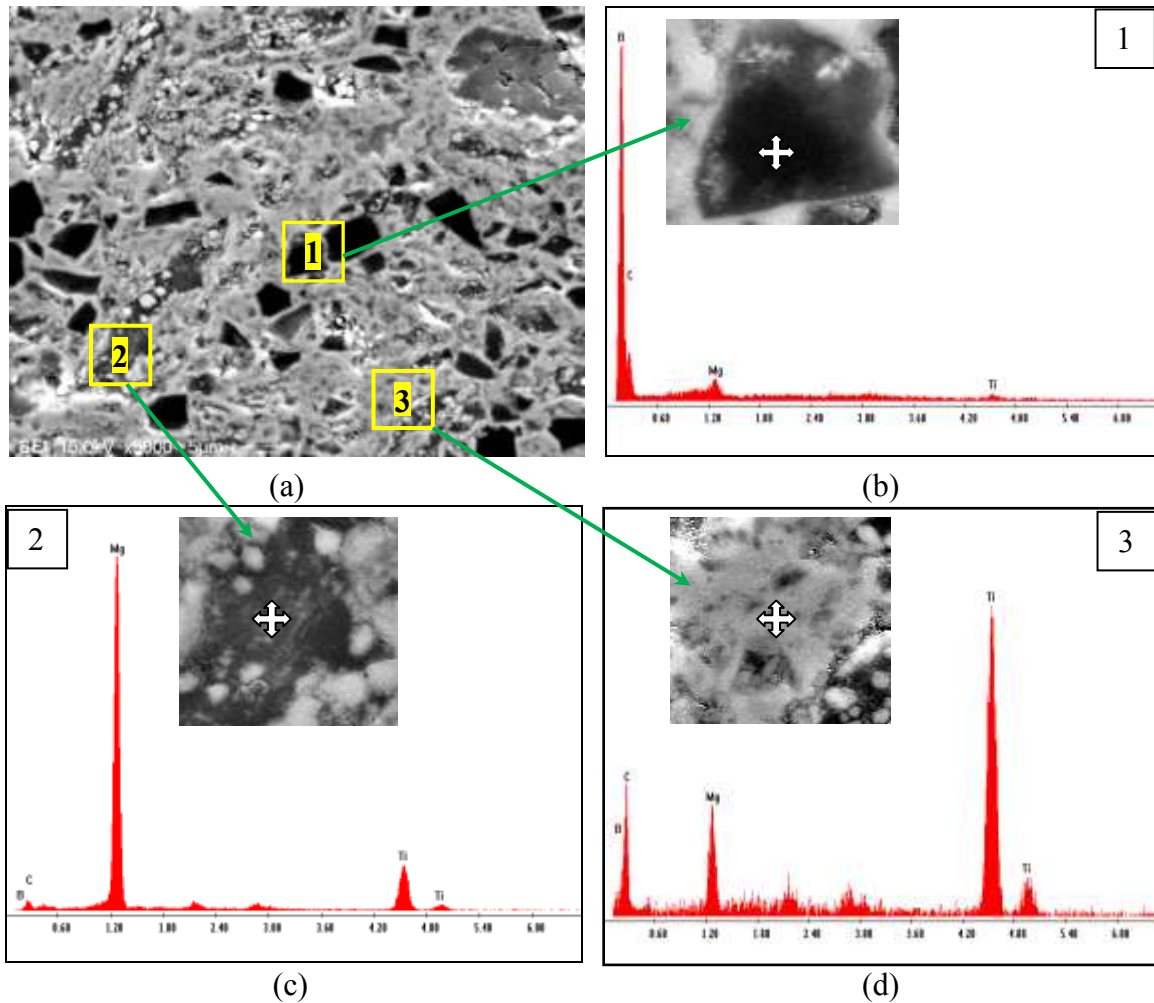
Figure 6.6 SEM-EDS of the AZ91D alloy MMCs fabricated using a 3Ti-B_4C preform with 70% *RD* at 900ºC for 1 h

Furthermore, it can be observed that the retained boron carbide at 900ºC is less than that at 850ºC. The detection of the retained boron carbide in both cases is by the overlap of the elemental mapping of B and C. However, it is very difficult to detect C by

the EDS detector. So, the detection of the retained boron carbide mainly depends on the mapping of boron in its concentrated regions.

SEI Image

Mg-Kα image

Ti-Kα image

C-Kα image

B-Kα image
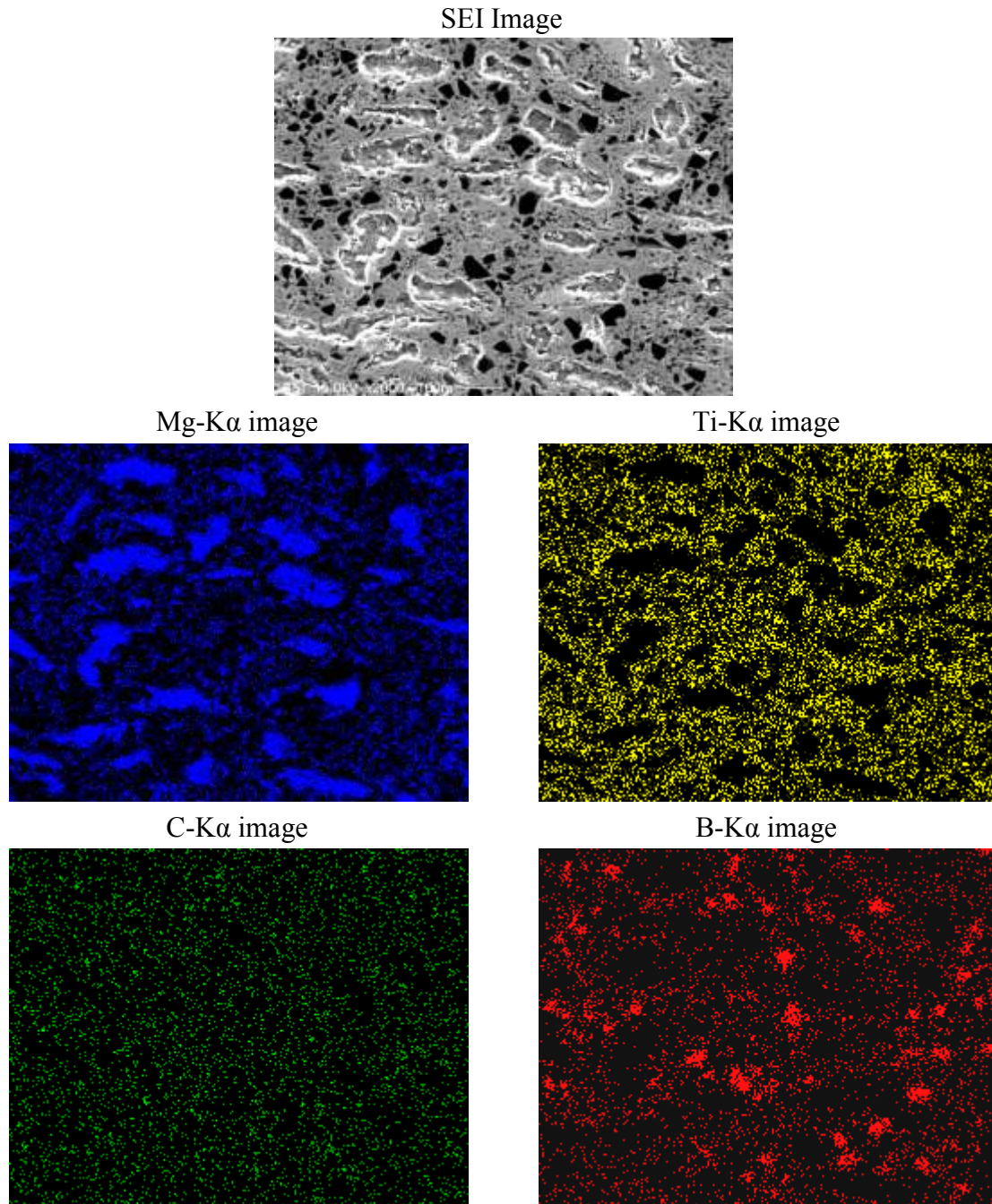
Figure 6.7 SEM microstructure and EDS elemental mapping of the TiC_x-TiB_2/AZ91D composites synthesized at 850ºC for 1 h

SEI Image

Mg-Kα image

Ti-Kα image

C-Kα image

B-Kα image
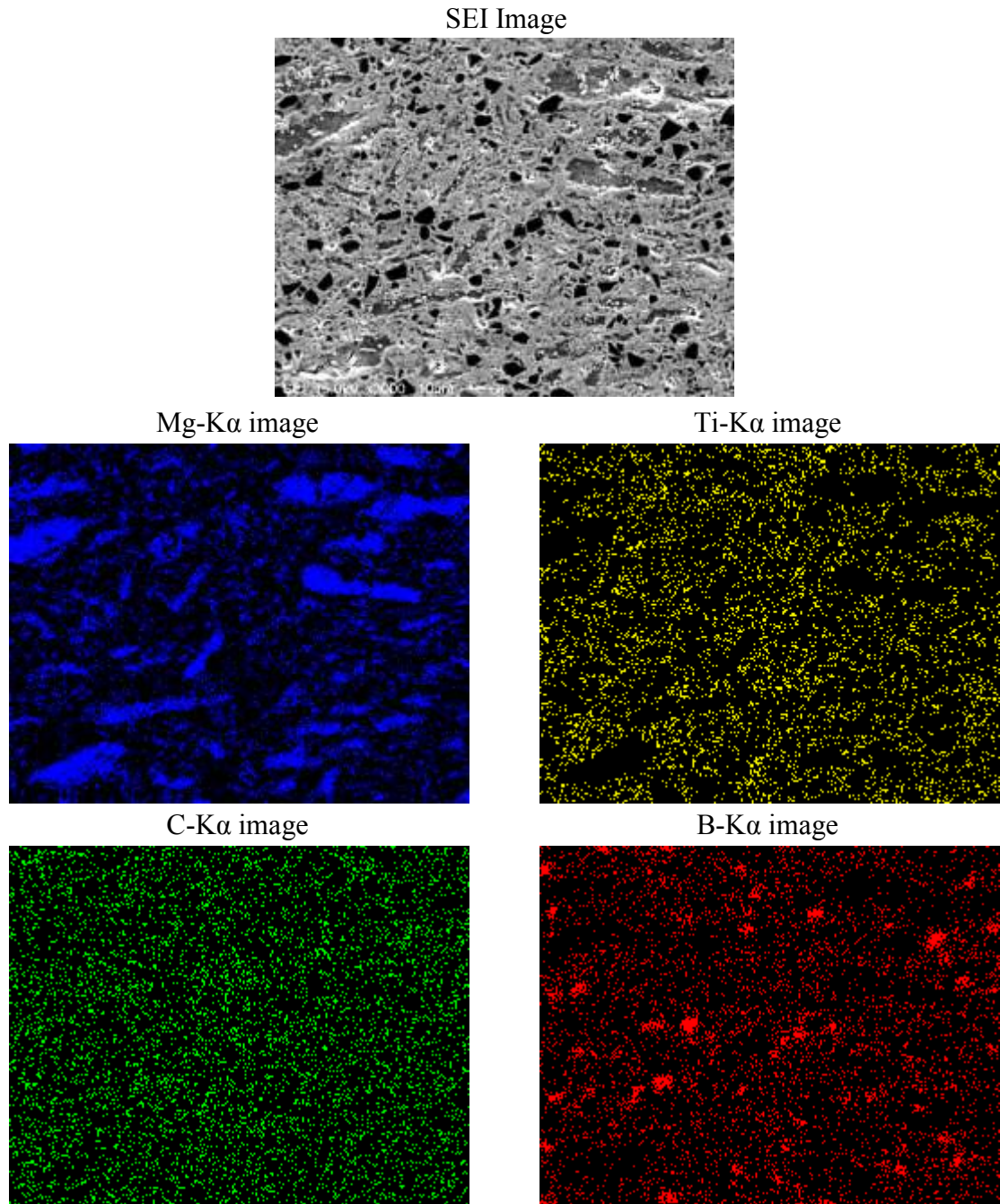
Figure 6.8 SEM microstructure and EDS elemental mapping of the TiC_x-TiB_2/AZ91D composites synthesized at 900ºC for 1 h

The same trend was observed for the samples fabricated at different processing temperatures of 750, 800, 850 and 900ºC while the holding time was kept constant as 6 h.

XRD results showed that TiC_x formed at first in all samples while the percentage of TiB_2 increased with increasing processing temperature and this is clear when comparing the peak areas of the formed phases. Therefore, the processing temperature has a strong effect on increasing the *in-situ* reaction rate. However, fabrication of magnesium matrix composites at 850ºC and higher especially with long holding time is not recommended because of the high rate of oxidation and evaporation of Mg or Mg alloy. As shown in Figure 6.9, the XRD patterns of the samples fabricated at 800 and 900ºC show that MgO peaks can be detected in both cases but are higher at 900ºC. Also, it can be observed that the ternary compound Ti_2AlC formed significantly at 900ºC.
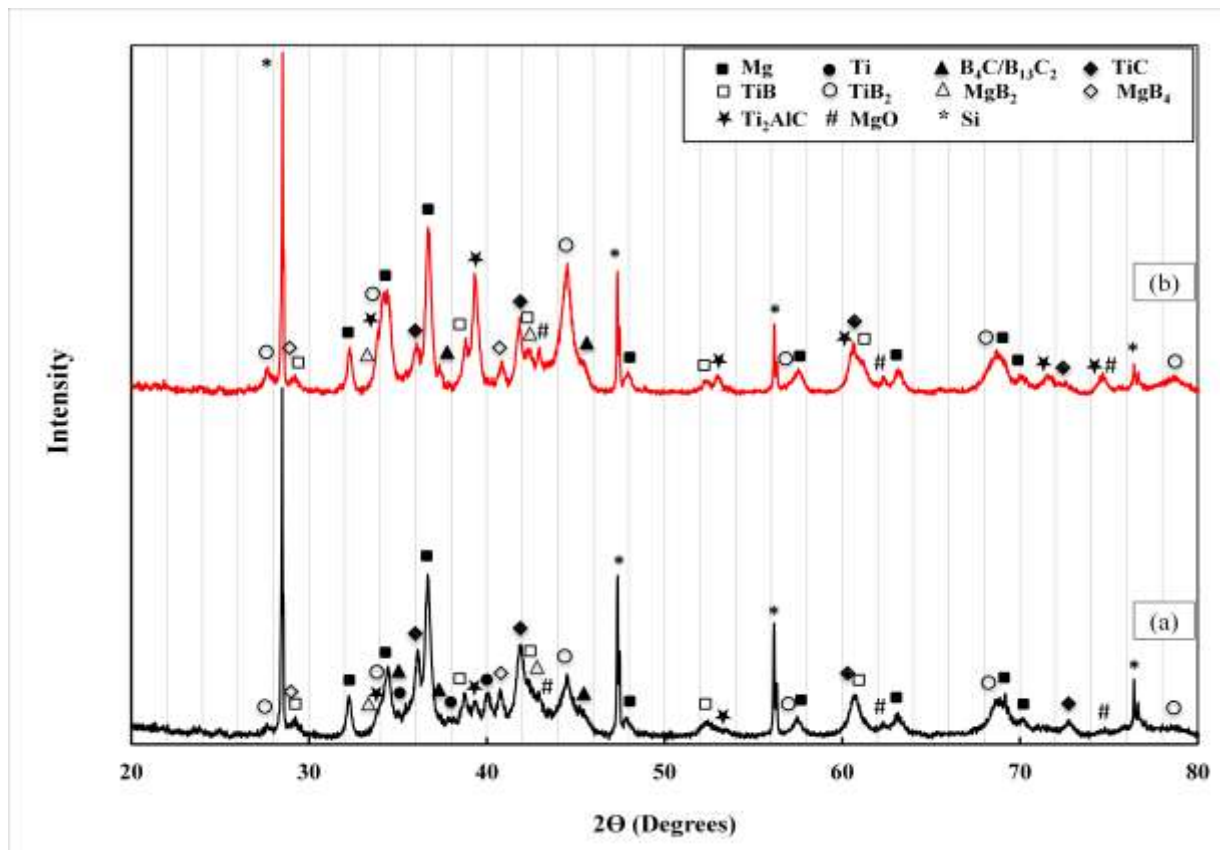
Figure 6.9 XRD patterns of the AZ91D alloy MMCs fabricated using 3Ti-B$_4$C preform with 70% *RD* for 6 h at different temperatures (a) 800 and (b) 900ºC

EDS elemental mapping of the samples fabricated at 800ºC and 900ºC for 6 h holding time are shown in Figure 6.10 and 6.11, respectively.

SEI Image

Mg-Kα image

Ti-Kα image

B-Kα image

Al-Kα image
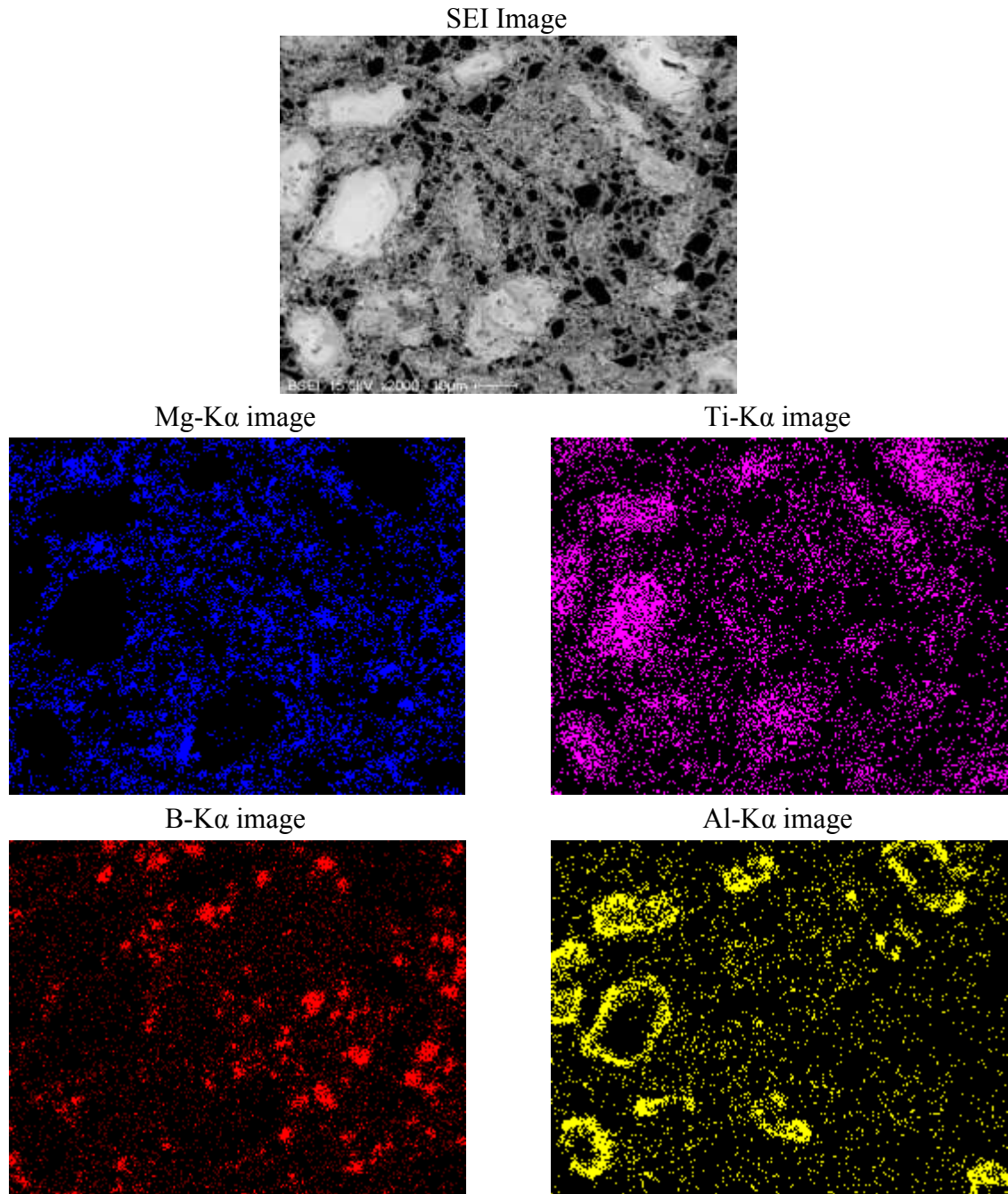
Figure 6.10 SEM microstructure and EDS elemental mapping of the TiC_x-TiB_2/AZ91D composites synthesized at 800ºC for 6 h

SEI Image

Mg-Kα image

Ti-Kα image

B-Kα image

Al-Kα image
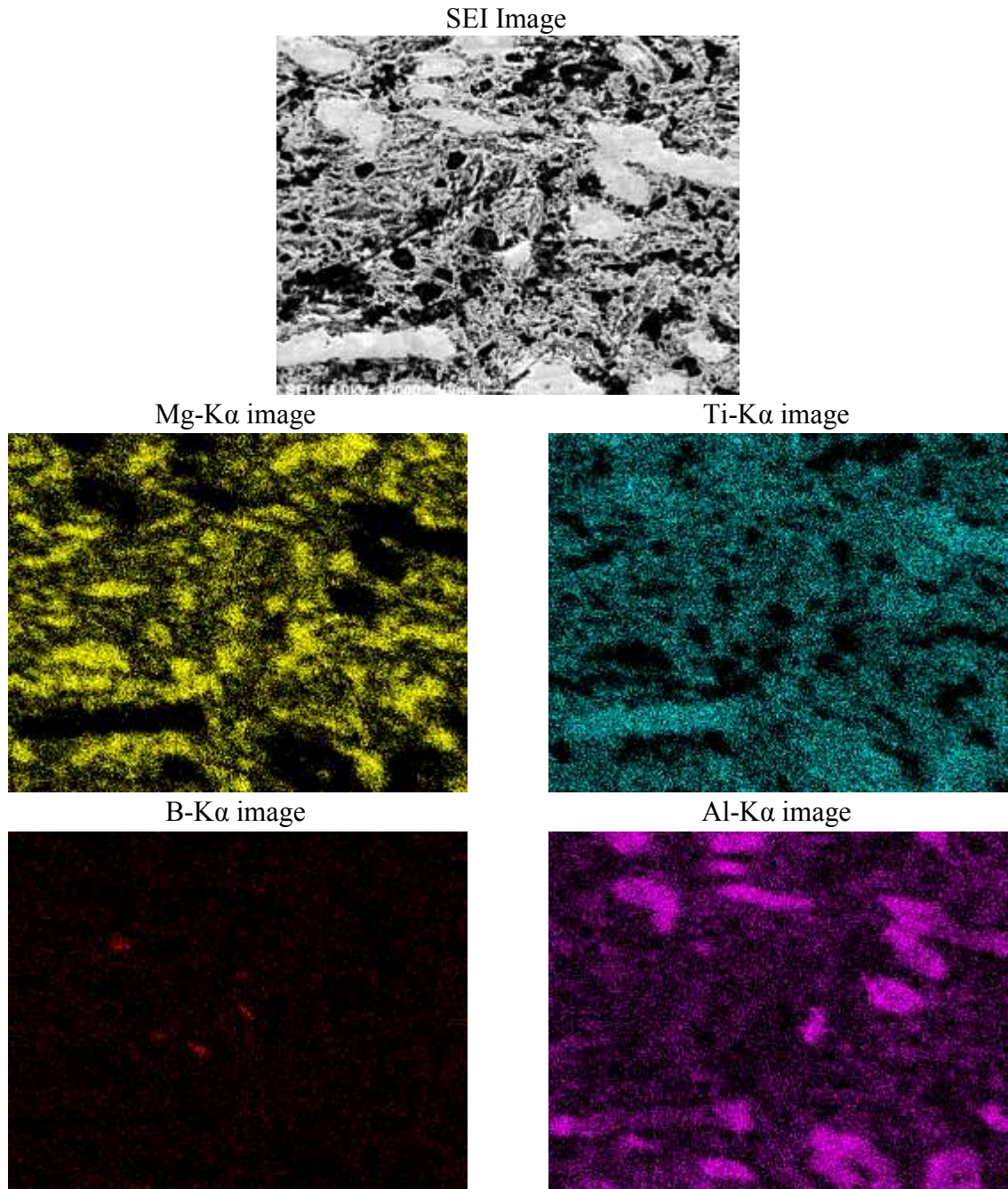
Figure 6.11 SEM microstructure and EDS elemental mapping of the TiC_x-TiB_2/AZ91D composites synthesized at 900°C for 6 h

According to the results obtained, there is a reasonably uniform distribution of the reinforcing phases: TiC_x and TiB_2 with the presence of retained boron carbide with MgB_2 at its interface. Also, it can be observed that the ternary compound, Ti_2AlC, formed at

110

both processing temperatures. At 800ºC, this compound formed at the interface of TiC_x and its percentage increases toward the TiC_x core with increasing the temperature to 900ºC. This ternary compound, Ti_2AlC, forms due to the diffusion of Al from the metal matrix liquid melt into the substoichiometric TiC_x compound especially if the C vacancies in the TiC structure are ordered which is supported by Riley [97, 98]. The formation of the ternary compound, Ti_2AlC, was proved also by the results of XRD for the composite sample fabricated at 900ºC for 6 h using a 3Ti-B₄C preform with 70% *RD* when compared with the XRD pattern of Ti_2AlC from Pearson's crystal database [139] as shown in Figure 6.12.
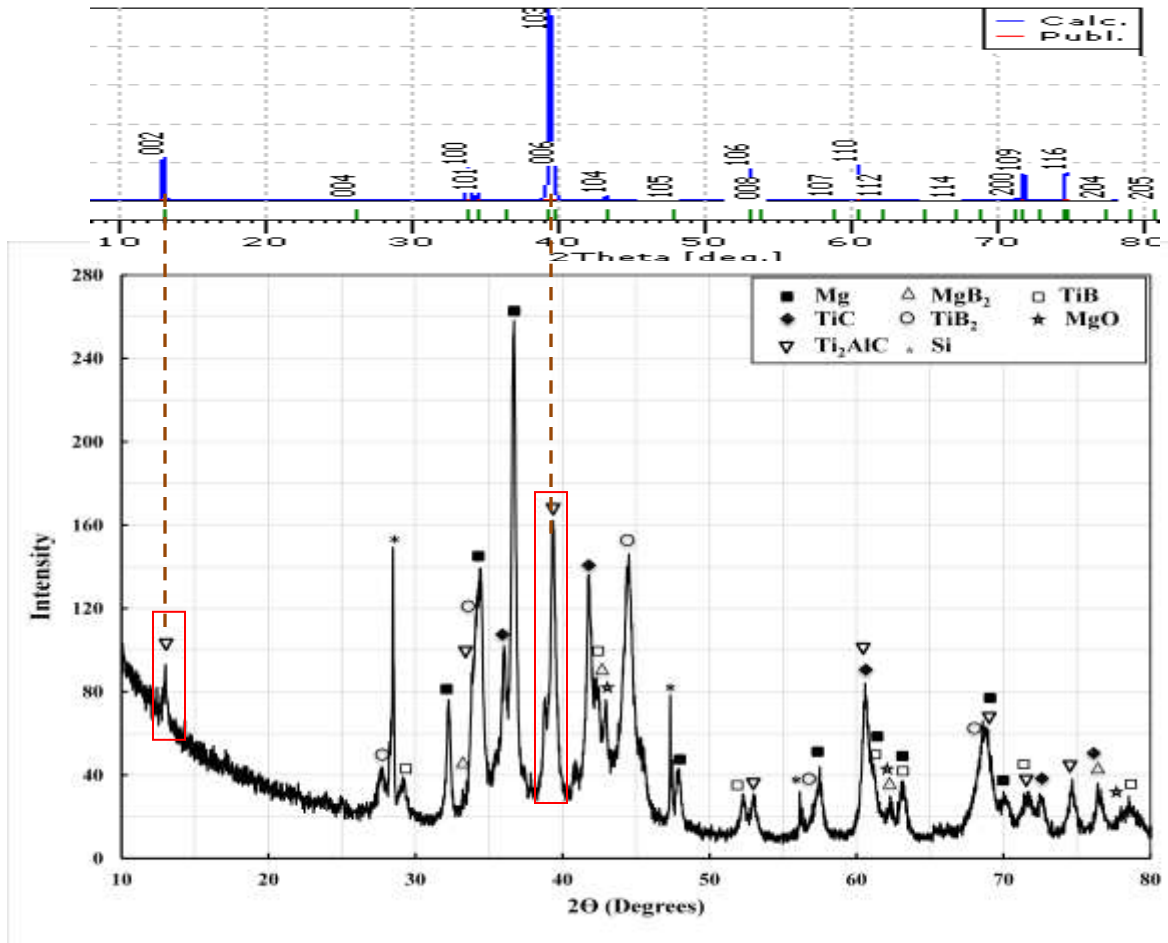
Figure 6.12 XRD pattern of the AZ91D alloy MMCs fabricated using a 3Ti-B₄C preform with 70% *RD* at 900ºC for 6 h

6.2 Influence of the Holding Time on the Fabrication of TiC-TiB$_2$/Mg Matrix Composite

Based on the results obtained so far, it was found that fabrication is more recommended at 900ºC than at 800ºC or 850ºC to obtain sound composites without pores or microcracks and with minimum retained boron carbide and intermediate phases.

To investigate the influence of the holding time on the fabrication of the composites, two sets of experiments were performed; One using pure magnesium and the second using AZ91D alloy as a metal matrix. Both of them were fabricated using a 3Ti-B$_4$C preform with 70% *RD* at 900ºC but for different holding times. In the first set of experiments, composite samples were fabricated at different holding times; 15 min, 30 min, 1 h, 1.5 h, 3 h and 6 h. The XRD analysis of these samples, presented in Figure 6.13, shows the presence of TiC$_x$ in all samples and the stoichiometry of C (x) increases with increasing holding time which can be understood as increasing the time for diffusion of C into Ti.

Also, it can be observed that the TiB$_2$ peak area increases while those of retained Ti and boron carbide decrease with time. The change in the area under the peaks of intermediate phases provides the reaction mechanism and the volume percentage of the phases based on Rietveld analysis as presented in Figure 6.14.

SEM micrographs of the composite samples fabricated at 900ºC using a 3Ti-B$_4$C preform with 70% *RD* but at different holding times of 30 min, 1.5 h and 6 h with low and high magnifications are shown in Figures 6.15 to 6.17.
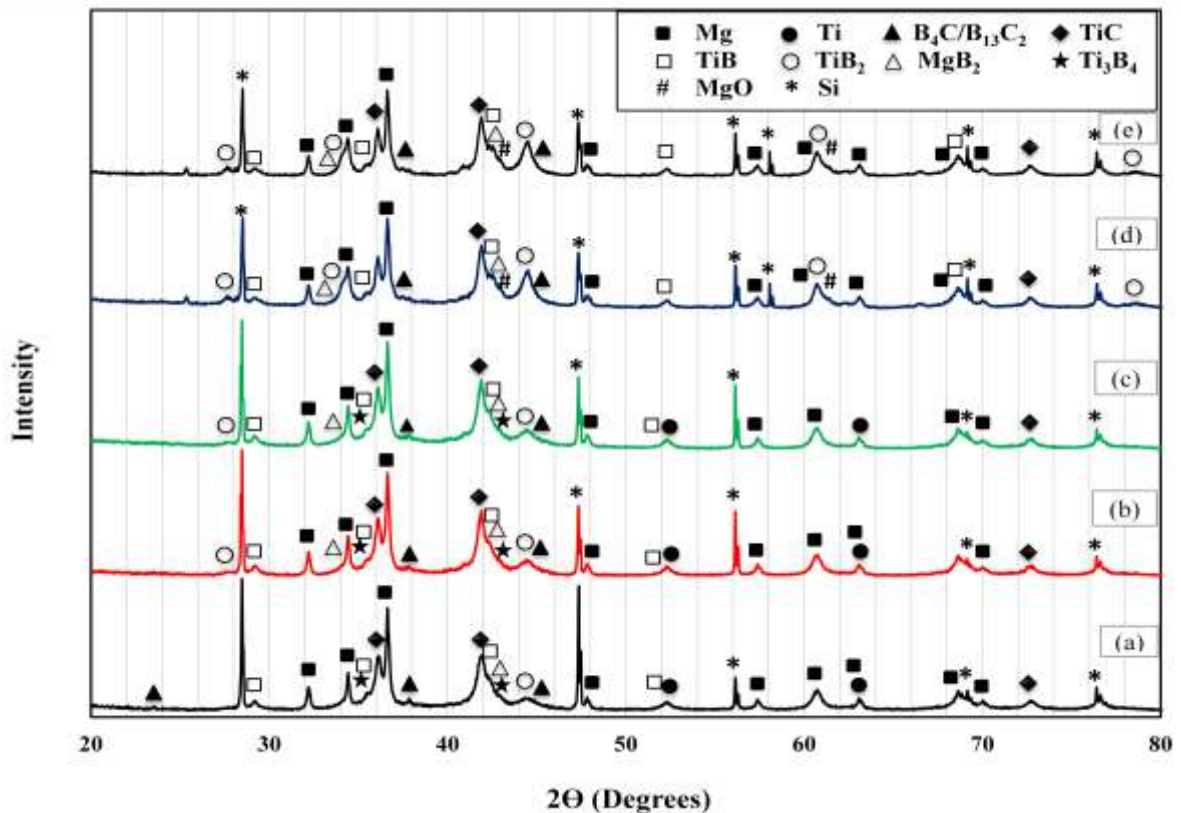
Figure 6.13 XRD pattern of the pure Mg MMCs fabricated using a 3Ti-B$_4$C preform with 70% *RD* at 900ºC for different holding times: (a) 30 min, (b) 1 h (c) 1.5 h, (d) 3 h, and (e) 6 h

SEM observations of the sample fabricated at 30 min show that relatively no pores or microcracks are observed resulting in a dense structure even at this short time. On the other hand, there still exists more residual titanium (bright regions) and boron carbide (dark regions) which remained as particulates in the microstructure at short holding time as shown in Figure 6.15.

With increasing time to 1.5 h, no pores or microcracks are observed as well, as shown in Figure 6.16. Moreover, SEM micrographs reveal less retained boron carbide than those at 30 min while retained Ti is insignificant and very difficult to observe by SEM.

With increasing the holding time to 6 h, and as shown in Figure 6.17, SEM observations reveal some very small microcracks in the Mg matrix. However, no pores are observed. Also, it can be observed that the residual boron carbide decreased compared to the composites fabricated at shorter time, 30 min or 1.5 h. The microcracks were observed only in the Mg matrix. It is possible that these are due to hot tearing in the magnesium during solidification.
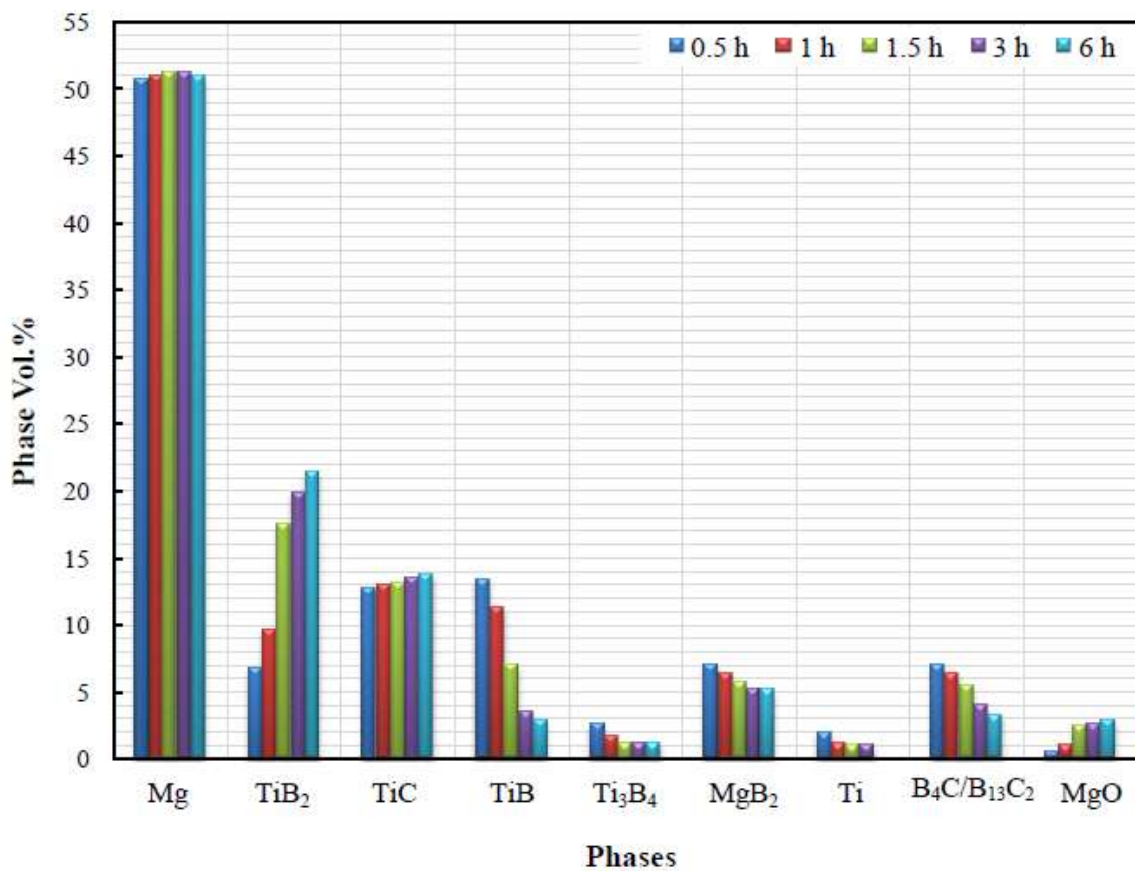
Figure 6.14 Phase volume percentage of pure Mg MMCs fabricated using a 3Ti-B$_4$C preform with 70% *RD* at 900ºC for different holding times of 30 min, 1 h, 1.5 h, 3 h and 6 h
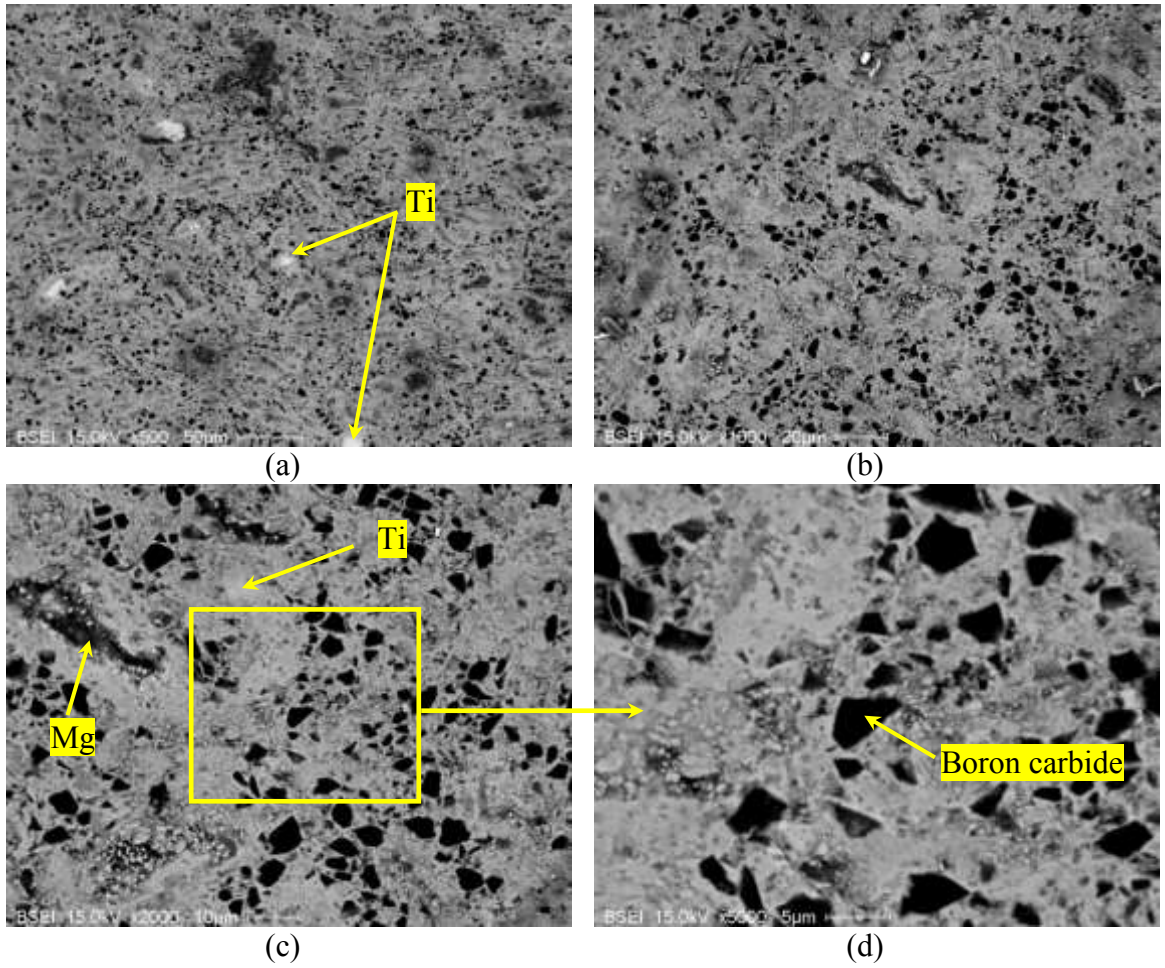
Figure 6.15 SEM microstructure of pure Mg MMCs fabricated using a 3Ti-B₄C preform with 70% *RD* at 900ºC for 30 min
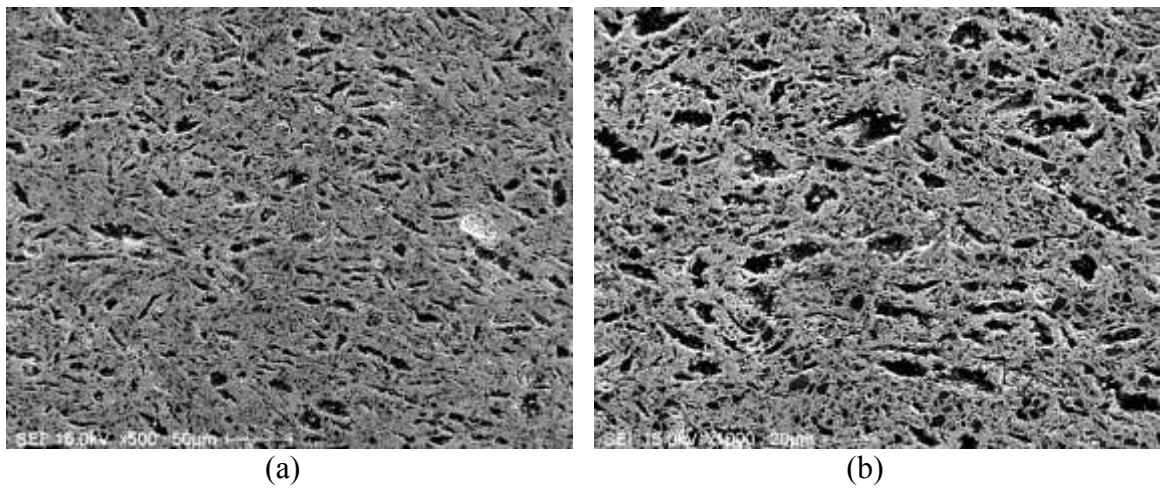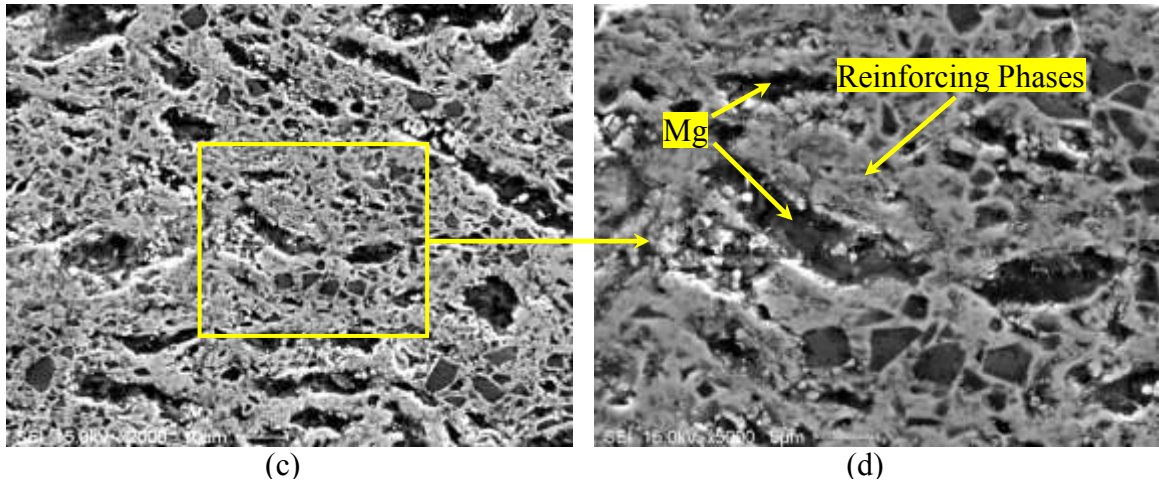
Figure 6.16 SEM microstructure of pure Mg MMCs fabricated using a 3Ti–B$_4$C preform with 70% *RD* at 900ºC for 1.5 h
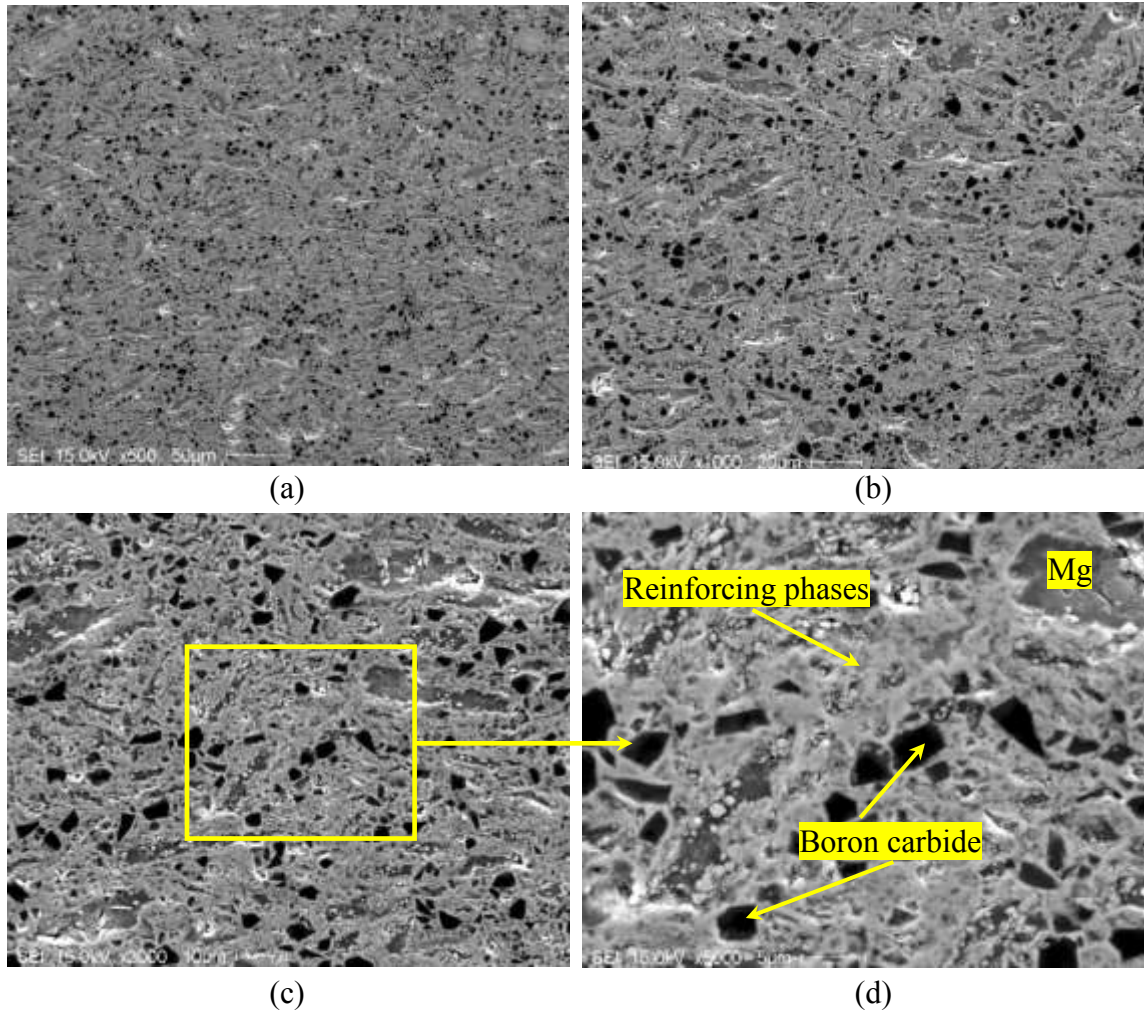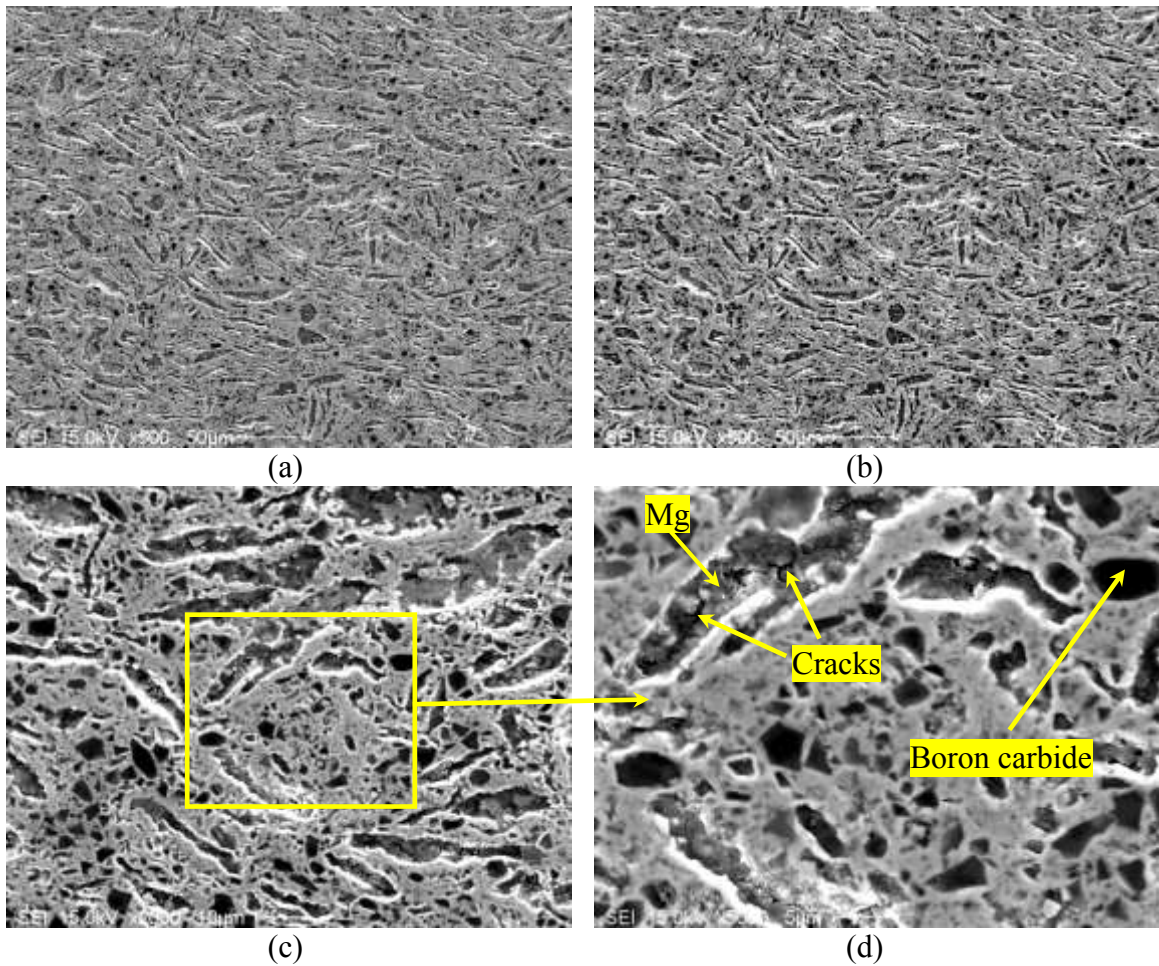

Figure 6.17 SEM microstructure of pure Mg MMCs fabricated using a 3Ti–B$_4$C preform with 70% *RD* at 900ºC for 6 h

EDS elemental mapping of the samples fabricated at 1.5 and 6 h holding time are shown in Figures 6.18 and 6.19. The overlap of boron and carbon reveals that at 6 h, the residual boron carbide is less than that at 1.5 h. However, as mentioned before, it is very difficult to detect carbon by EDS detector. So, the detection of the retained boron carbide mainly depends on the mapping of boron in its concentrated regions.
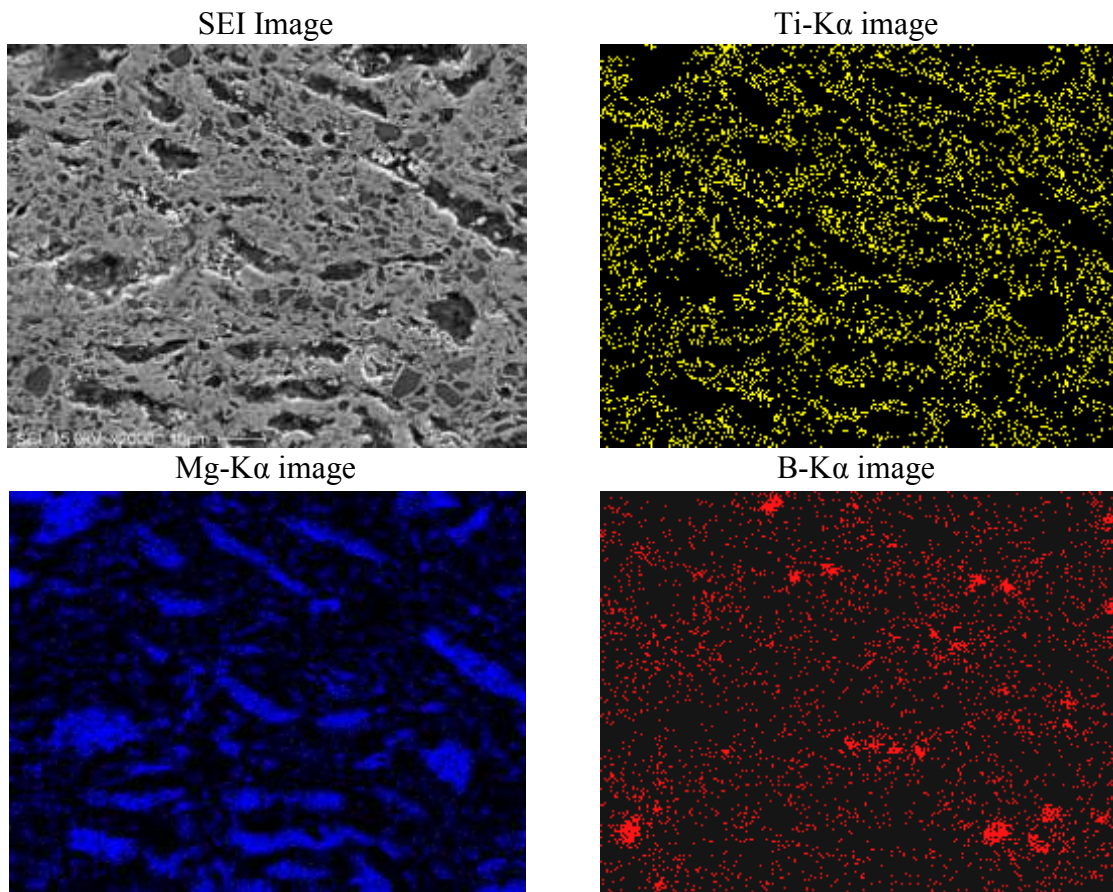
Figure 6.18 SEM microstructure and EDS elemental mapping of the TiC_x-TiB_2/Mg composites synthesized using a 3Ti-B_4C preform with 70% *RD* at 900ºC for 1.5 h
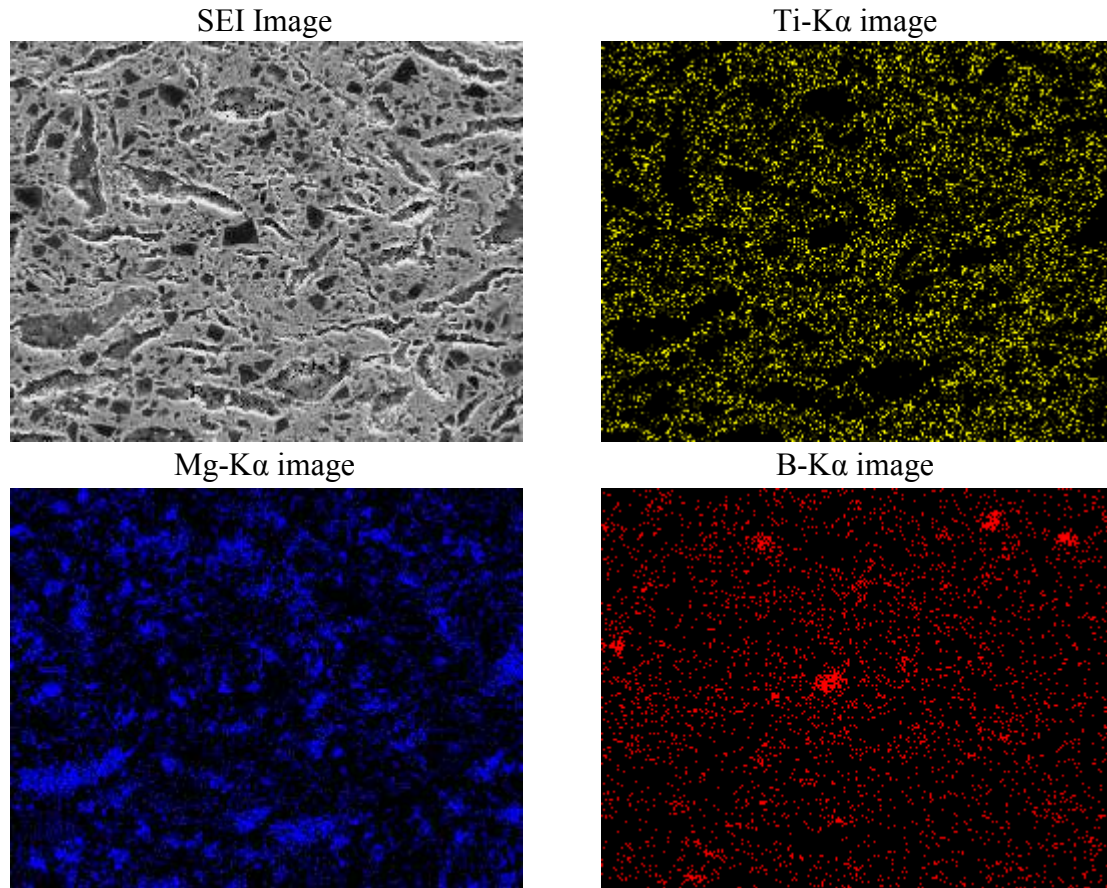
Figure 6.19 SEM microstructure and EDS elemental mapping of the TiC_x-TiB_2/Mg composites synthesized using a 3Ti-B_4C preform with 70% *RD* at 900ºC for 6 h

EDS analysis of the sample fabricated at 900ºC and 6 h, as shown in Figure 6.20 (d), confirms the presence of Mg through the network of TiC_x and TiB_2. On the other hand, oxygen was detected by the EDS analysis which confirms the presence of very small amount MgO which is very difficult to detect by XRD. Hence, it is better to fabricate magnesium matrix composites at lower temperatures and shorter holding times if possible. As shown in Figure 6.20 (c), the retained boron carbide is clear with MgB_2 around it.
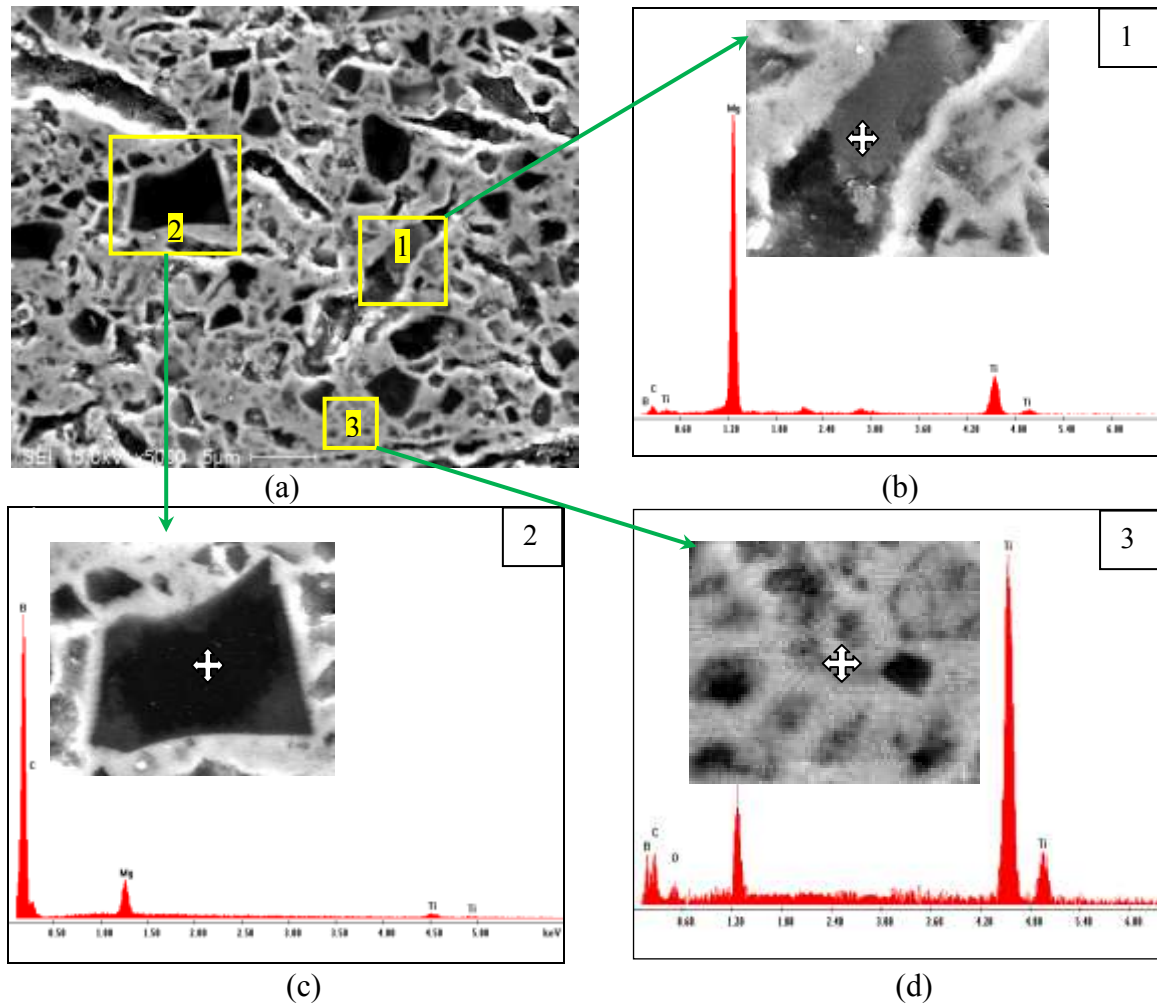
Figure 6.20 SEM-EDS of pure Mg MMCs fabricated using a 3Ti-B$_4$C preform with 70% *RD* at 900ºC for 6 h

In the second set of experiments for this study, composite samples using AZ91D alloy were fabricated at different holding times; 30 min, 1 h, 1.5 h, 3 h, and 6 h while the processing temperature was kept as 900ºC using green compacts with 70% *RD*.

XRD analysis of these samples, as shown in Figure 6.21, reveals the same trend as the samples of the first set of experiments. However, in this case at 3 h holding time and longer, there are peaks of a phase that did not appear in the case of pure magnesium.

As mentioned earlier, these peaks are associated with the MAX ternary compound (Ti$_2$AlC).
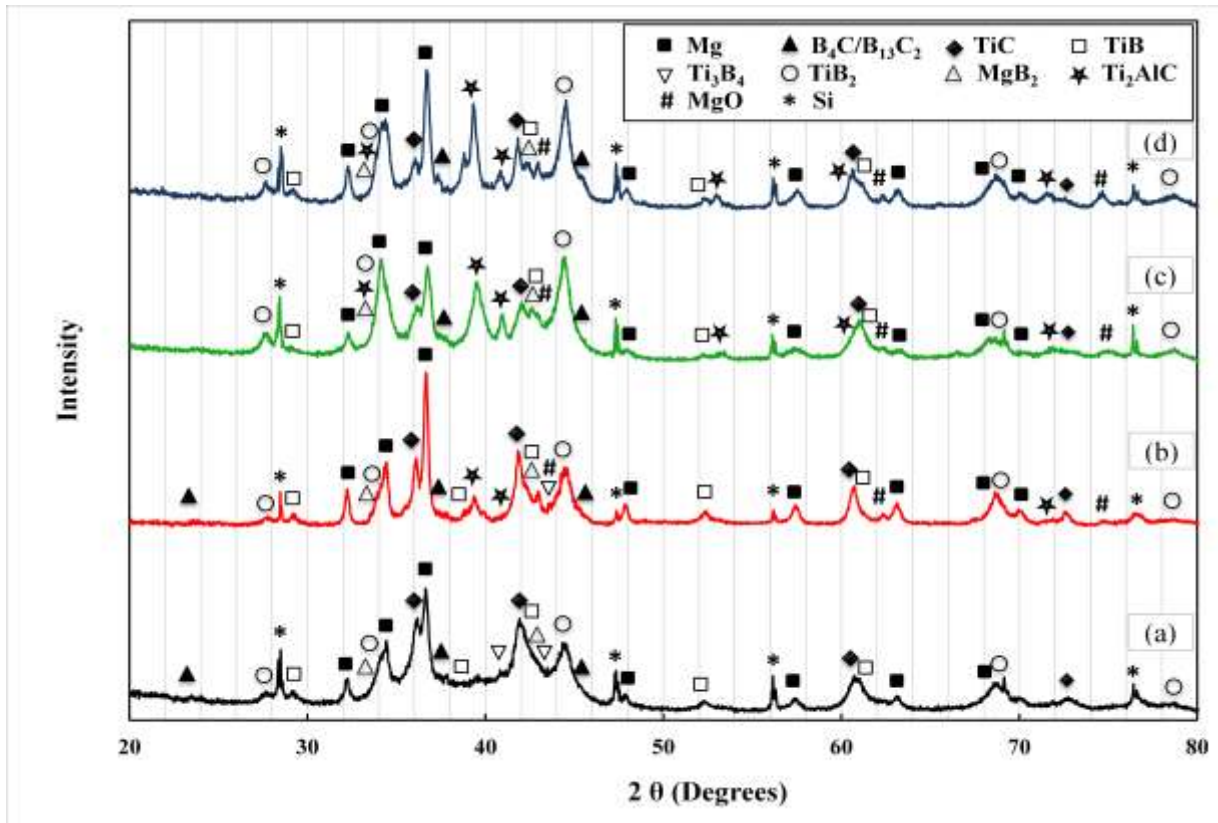
Figure 6.21 XRD pattern of the AZ91D alloy MMCs fabricated using a 3Ti-B$_4$C preform with 70% *RD* at 900°C for different holding times: (a) 1 h, (b) 1.5 h, (c) 3 h, and (c) 6 h

The volume percentages of the formed phases based on Rietveld analysis are presented in Figure 6.22. It is observed that the percentage of TiB$_2$ increases with increasing holding time from 1 h to 6 h. On the other hand, the percentage of TiC$_x$ decreases while that of Ti$_2$AlC increases because this ternary compound forms at the expense of TiC$_x$ and at its interface. Also, it can be observed that the percentages of the residual boron carbide and intermediate phases such as TiB and MgB$_2$ decrease with increasing the holding time.
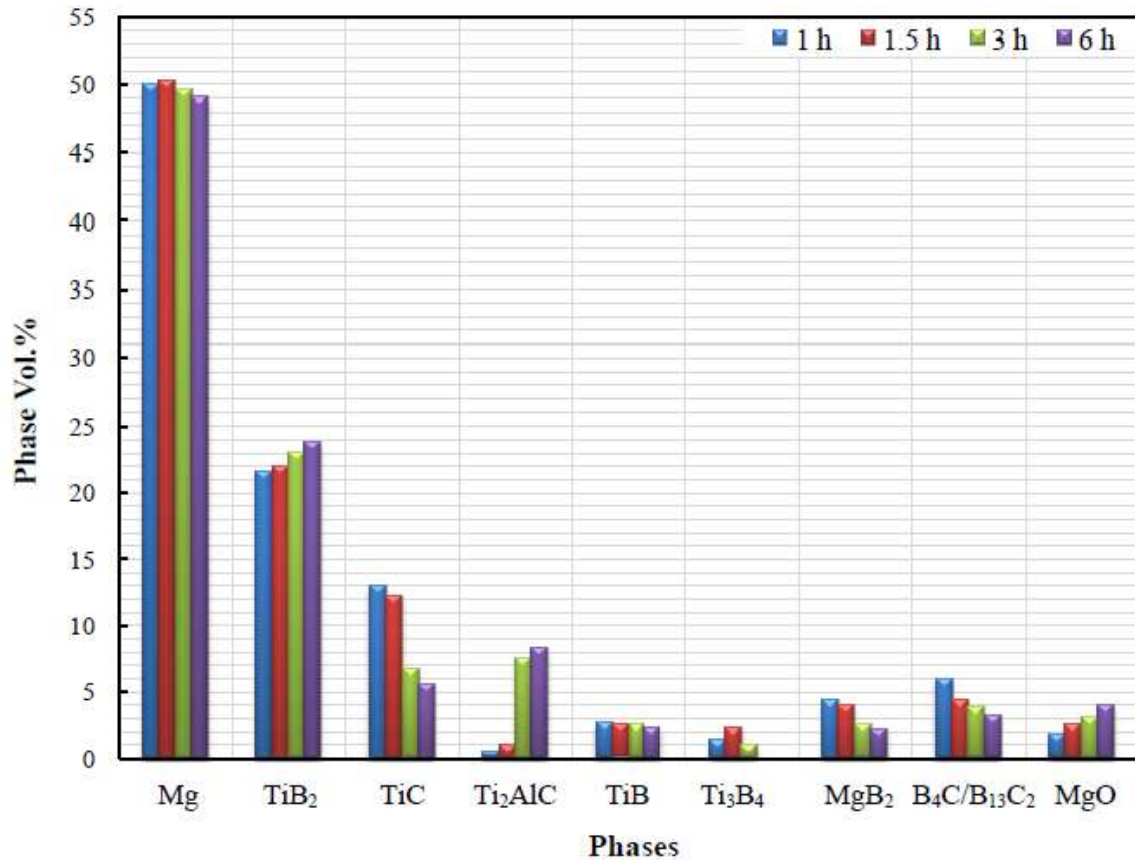
Figure 6.22 Phase volume percentage of the AZ91D alloy MMCs fabricated using a 3Ti-
B$_4$C preform with 70% *RD* at 900ºC for different holding times: 1 h, 1.5 h,
3 h, and 6 h

SEM micrographs of the composite samples fabricated at 900ºC for 30 min as shown in Figure 6.23 reveal a relatively uniform distribution of the reinforcing phases with no voids or microcracks. Also SEM micrographs reveal that there is still residual boron carbide which appears as dark regions in the micrographs.
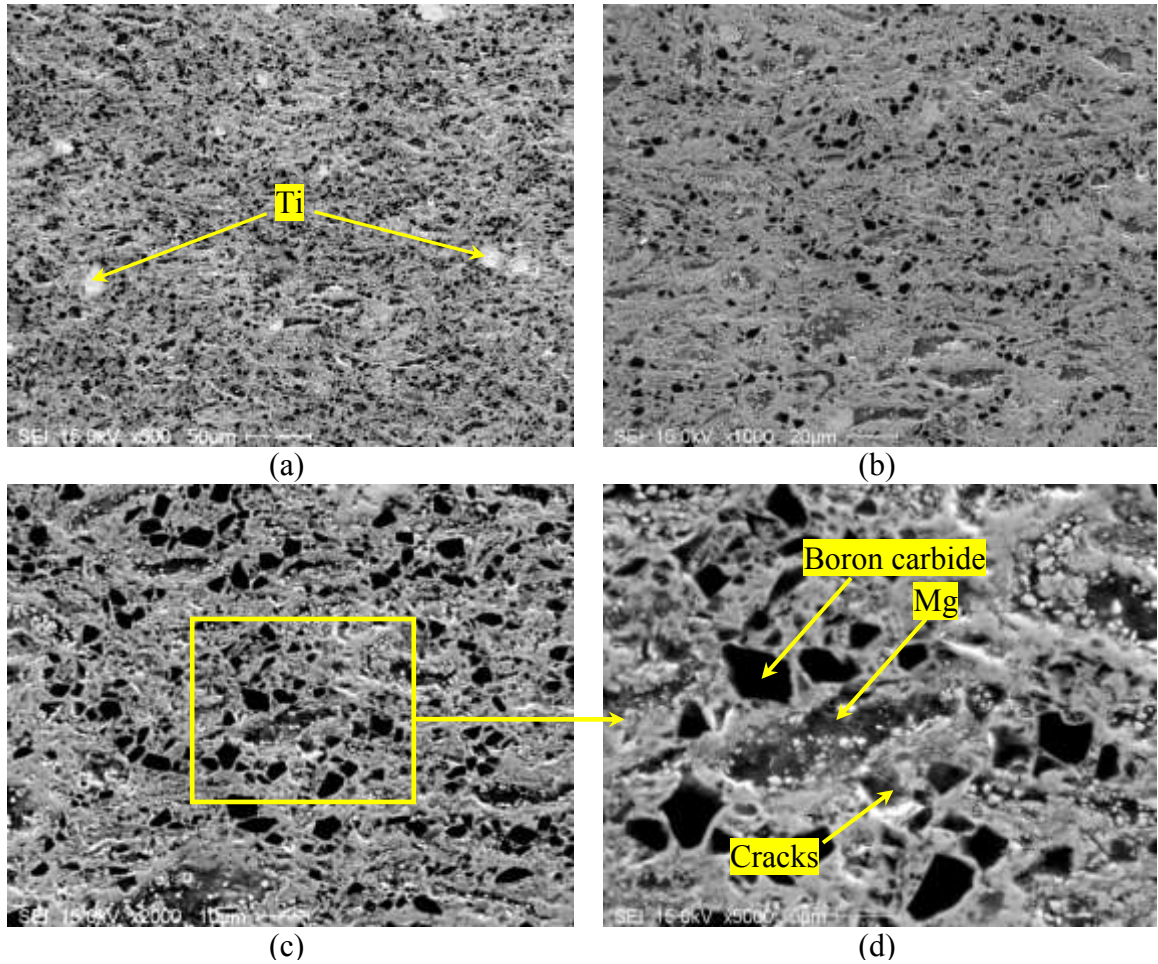
Figure 6.23 SEM microstructure of the AZ91D alloy MMCs fabricated by using a 3Ti-B$_4$C preform with 70% *RD* at 900ºC for 30 min

With increasing the holding time, the retained boron carbide (dark areas) decreased as shown in the microstructures of the samples fabricated at 900ºC for 1.5 and 3 h, Figures 6.24 and 6.25, respectively. No pores or microcracks were detected in all the samples. This suggests that the composites are fully dense.
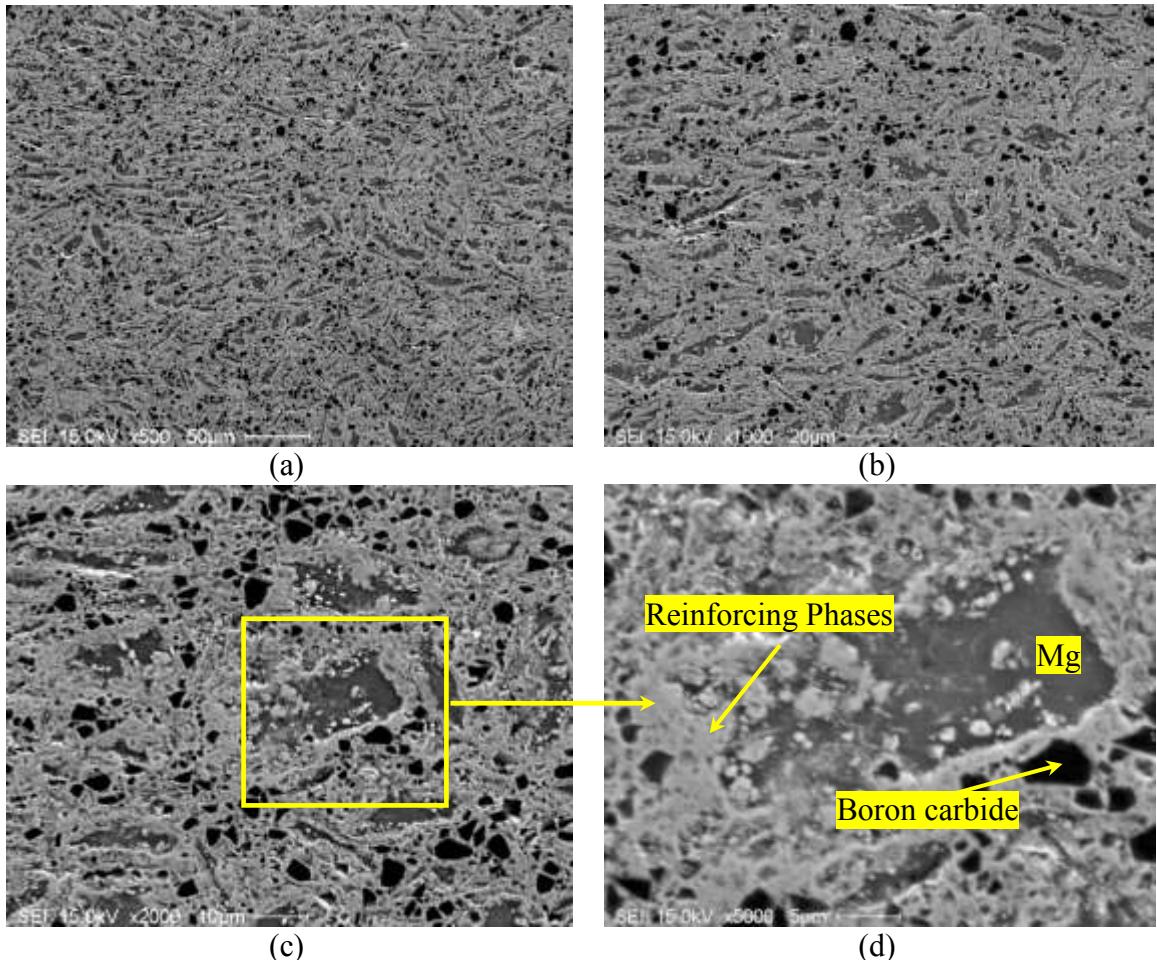
Figure 6.24 SEM microstructure of the AZ91D alloy MMCs fabricated using a 3Ti-B$_4$C preform with 70% *RD* at 900ºC for 1.5 h
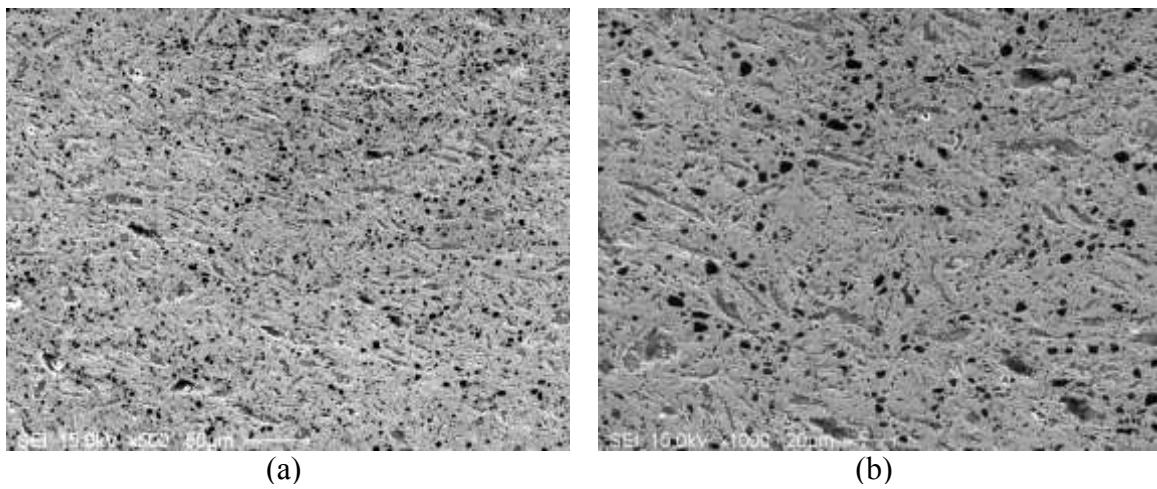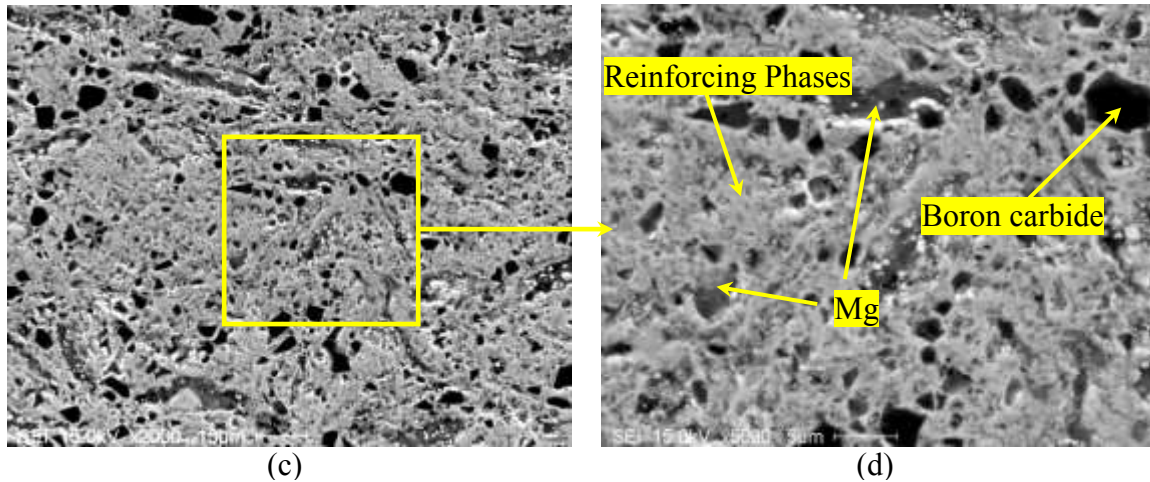
Figure 6.25 SEM microstructure of the AZ91D alloy MMCs fabricated by using a 3Ti-B$_4$C preform with 70% *RD* at 900ºC for 3 h

EDS elemental mappings for these samples are shown in Figures 6.26 to 6.28. The overlap of boron and carbon or the regions of concentrated boron reveal that the retained boron carbide decreased with increased holding time. Also, the overlap of titanium, carbon and boron proves the formation of the reinforcing phases TiC$_x$ and TiB$_2$. Furthermore, the mapping of Al in the samples processed for 1.5 and 3 h reveals its concentration in regions that overlap with Ti suggesting the formation of the ternary compound Ti$_2$AlC which was confirmed by the XRD results.

EDS analysis as shown in Figure 6.29 through a line scan of the sample fabricated at 900ºC for 3 h reveals the presence of the retained boron carbide surrounded by MgB$_2$ phase and also the ternary compound.

SEI Image

Mg-Kα image

Ti-Kα image

B-Kα image

Al-Kα image
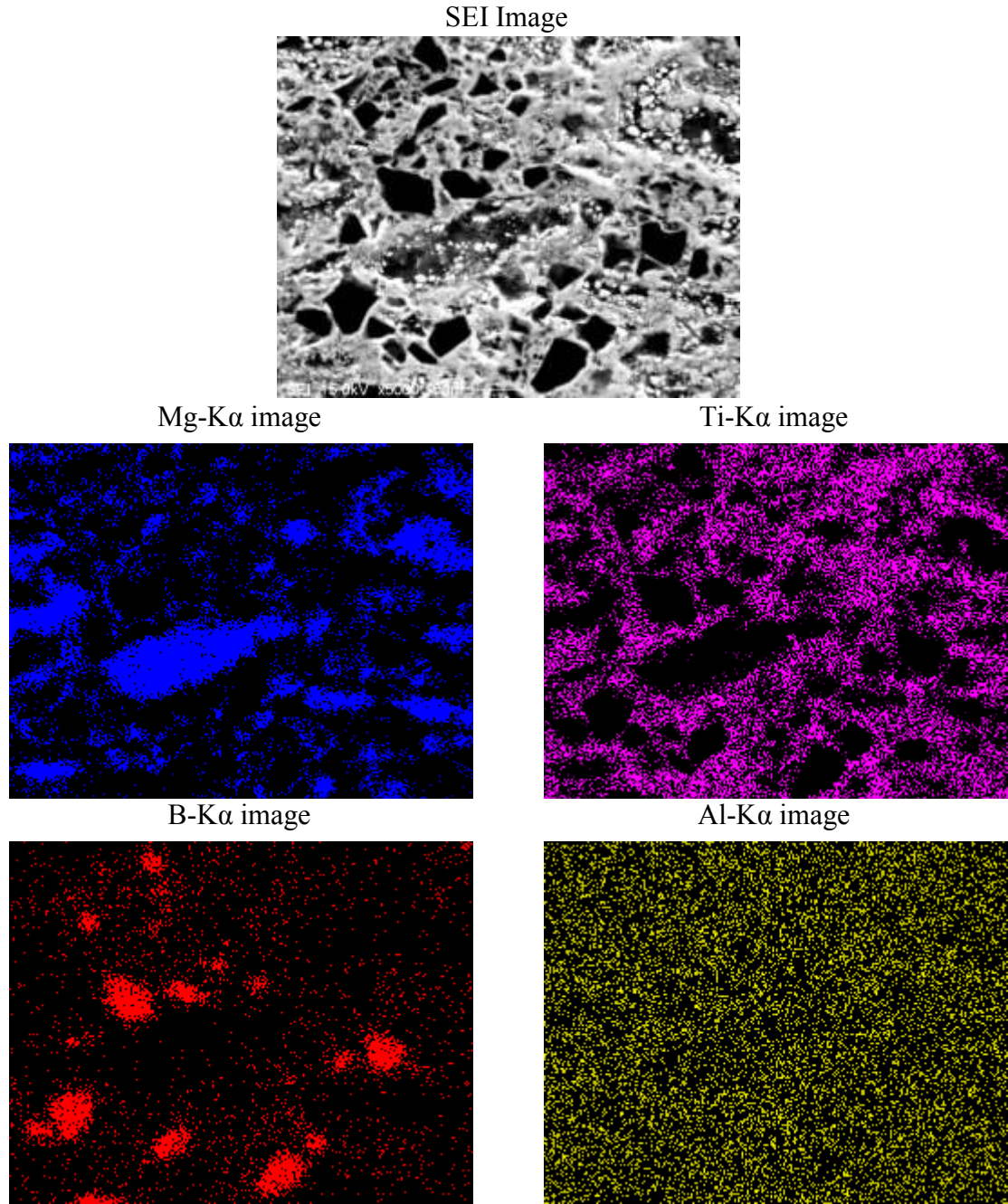
Figure 6.26 SEM microstructure and EDS elemental mapping of the TiC_x-TiB_2/AZ91D composites synthesized at 900ºC for 30 min

SEI Image

Mg-Kα image

Ti -Kα image

B -Kα image

Al-Kα image
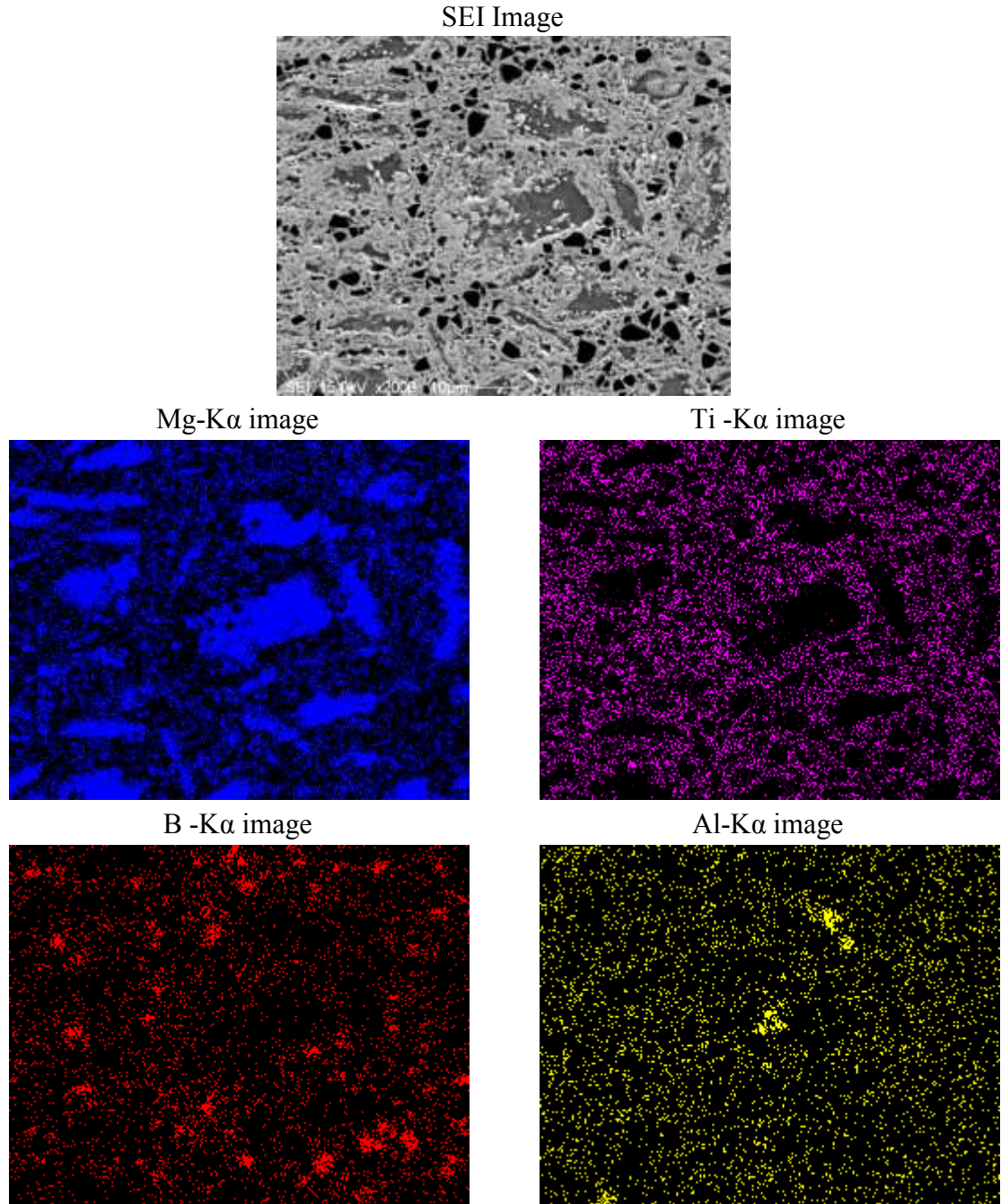
Figure 6.27 SEM microstructure and EDS elemental mapping of the TiC$_x$-TiB$_2$/AZ91D composites synthesized at 900ºC for 1.5 h

SEI Image

Mg-Kα image

Ti-Kα image

B-Kα image

Al-Kα image
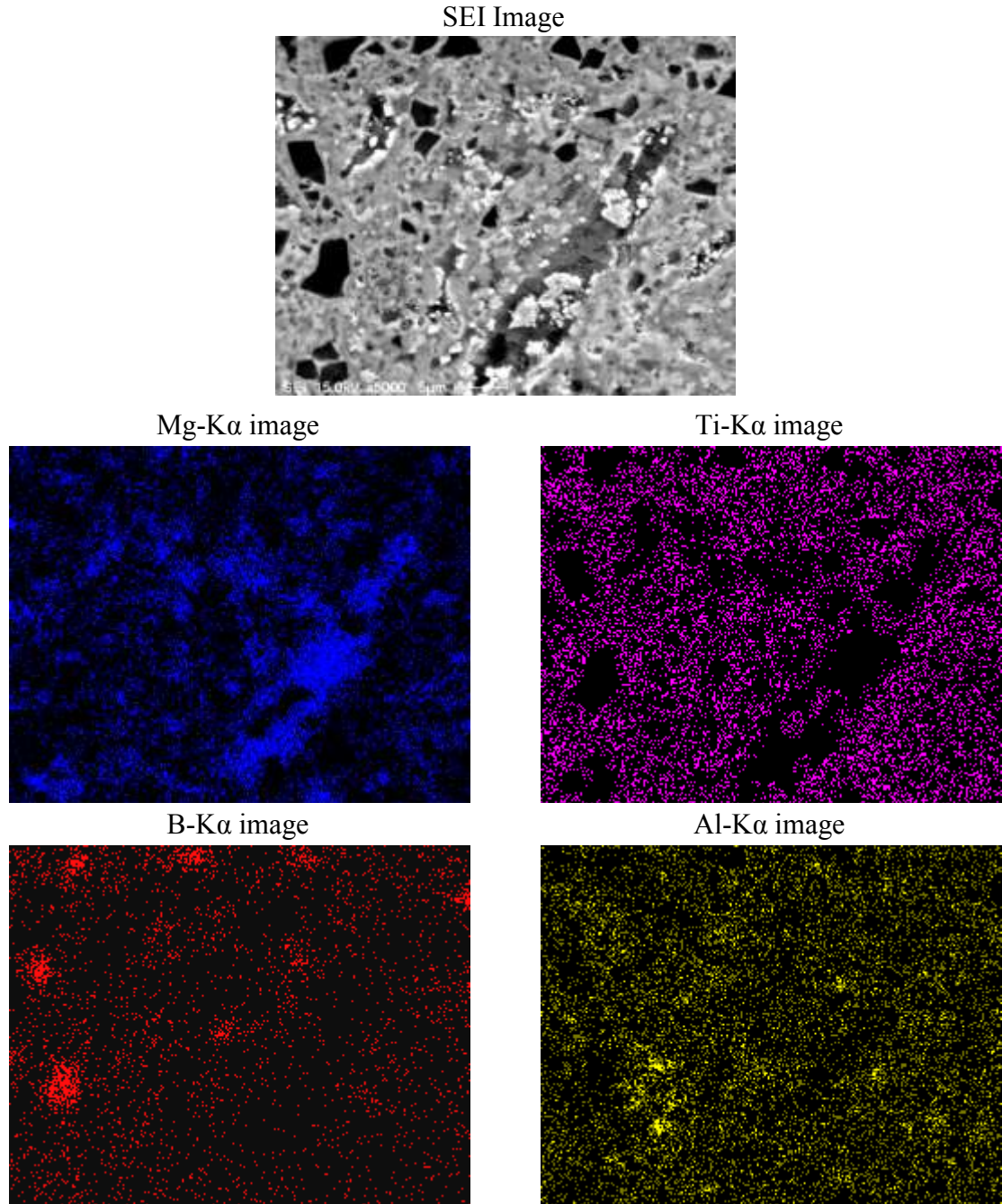
Figure 6.28 SEM microstructure and EDS elemental mapping of the TiC$_x$-TiB$_2$/AZ91D composites synthesized at 900ºC for 3 h

<table>
<tr><td>(a)</td><td>(b)</td></tr>
<tr><td>(c)</td><td>(d)</td></tr>
</table>
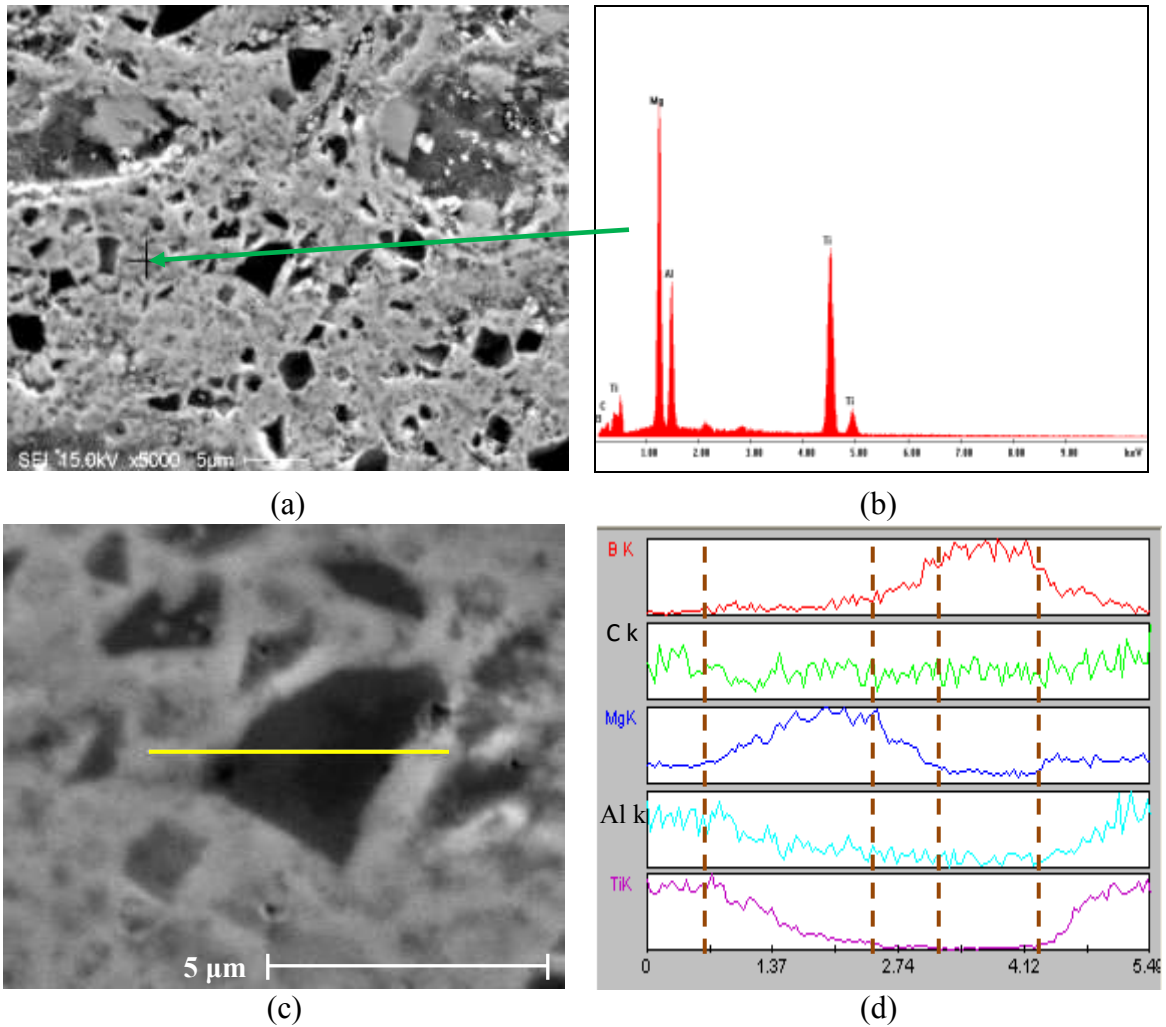
Figure 6.29 SEM-EDS of the AZ91D MMCs fabricated at 900ºC for 3 h holding time

6.3 Influence of the Green Compact Density on the Fabrication of TiC-TiB$_2$/Mg matrix composite

To obtain the influence of the green compact density, composite samples were fabricated using 3Ti-B$_4$C preforms with different relative densities: 55, 60, 65, and 70% while the processing temperature and the holding time were kept constant.

Figure 6.30 shows the XRD spectra for three composite samples prepared at the same temperature, 900ºC, the same holding time 1.5 h and using 3Ti-B$_4$C preforms with different relative densities, 55, 65 and 70%.

128
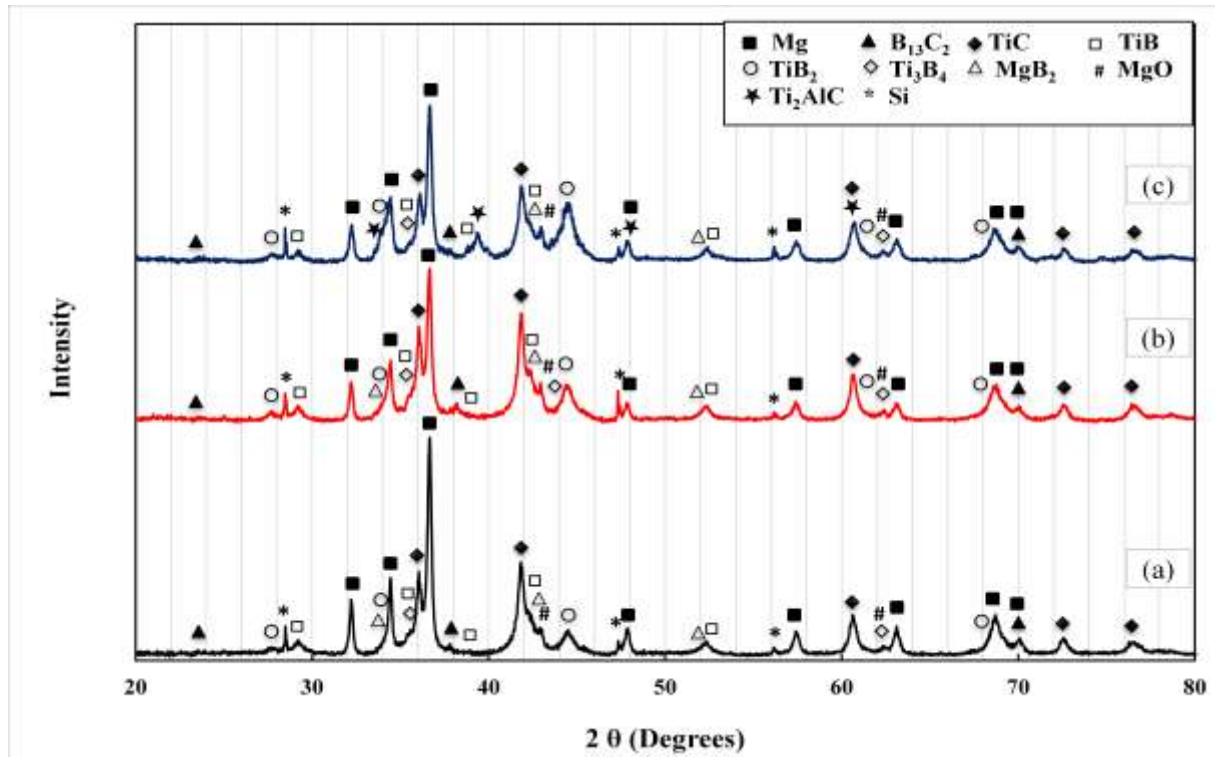
Figure 6.30 XRD patterns of the AZ91D alloy MMCs fabricated at 900ºC for 1.5 h using 3Ti-B$_4$C preforms with different relative densities (a) 55%, (b) 65%, and (c) 70%

It is clear that the peaks of TiC$_x$ and TiB$_2$ are present in all samples and increase with increasing green compact *RD*. On the other hand, the area under the peaks of retained boron carbide and those of the intermediate phases, TiB, Ti$_3$B$_4$, and MgB$_2$, decrease with increasing green compact *RD*. It is important to note that the area under the peaks of Mg at 55% is higher than those at 65% or 70% green compact. Also, the XRD pattern at 70% reveals peaks for the ternary compound (Ti$_2$AlC).

Based on these results, it can be concluded that the higher the green compact *RD*, the higher the contact area between B$_4$C and Ti particles accelerating their reaction through a shorter diffusion path. This is supported by the volume percentage of the phases based on Rietveld analysis as presented in Figure 6.31.

129
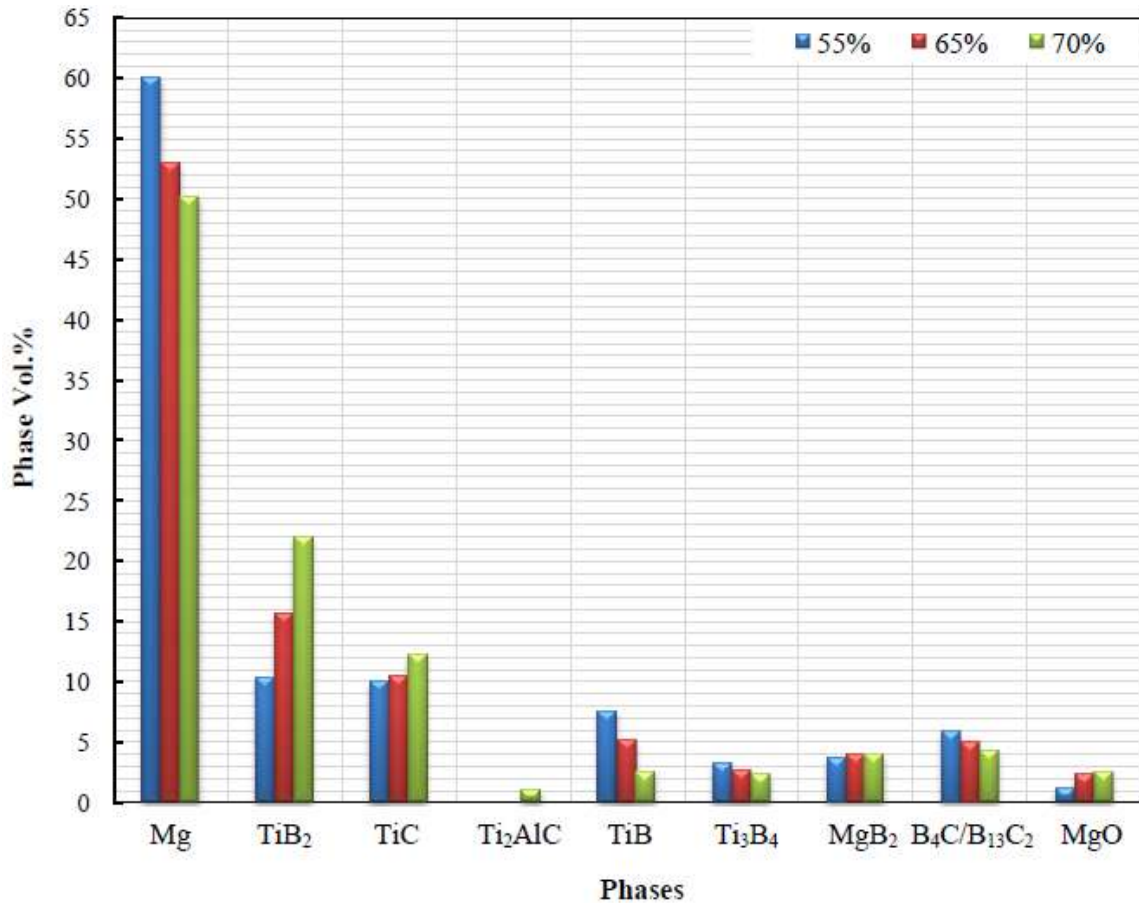
Figure 6.31 Phases volume percentage of the AZ91D alloy MMCs fabricated at 900ºC for 1.5 h using 3Ti-B_4C preforms with different relative densities: 55, 65 and 70%

SEM micrographs of the composite samples fabricated at 900ºC for 1.5 h holding time using different preforms with 55% and 70% *RD* are shown in Figure 6.32.

SEM observations reveal a relatively uniform distribution of the reinforcing phases in the two cases. However, retained boron carbide (dark phase) in the sample fabricated using a 55% *RD* preform is higher than those in the sample fabricated using a 70% *RD* preform. Also, no pores or microcracks are observed in the microstructure of both of them.

(a)	(b)
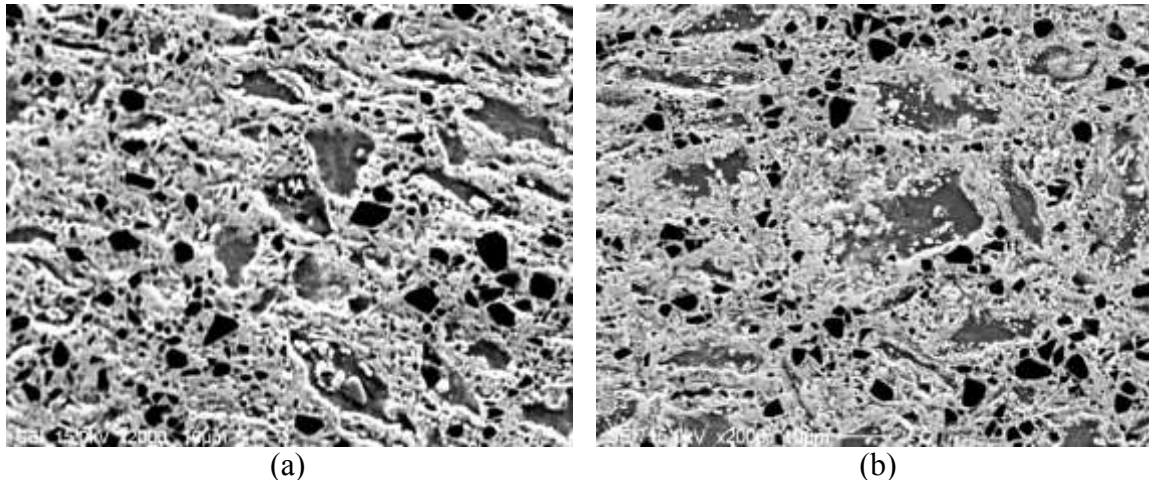
Figure 6.32 SEM micrographs of the AZ91D alloy MMCs fabricated at 900ºC for 1.5 h using a 3Ti-B$_4$C preform with different relative densities: (a) 55% and (b) 70%

It is important to mention that this work tried to increase the volume percentage of magnesium in the composites to improve their ductility by controlling the preform *RD* to obtain the required reinforcement volume percentage in the composites.

For example of the attempts to increase the volume percentage of magnesium by controlling the green compact *RD*, pure Mg matrix composite was fabricated using a 3Ti-B$_4$C preform with 60% *RD* at 800ºC for 6 h. The sample was fabricated at 800ºC to avoid the high oxidation and evaporation of magnesium at higher temperatures and for 6 h to ensure the formation of the equilibrium phases, TiC$_x$ and TiB$_2$ with the least amounts of retained Ti, boron carbide and residual intermediate phases. XRD spectra of two composite samples fabricated using a 3Ti-B$_4$C preform with 60 and 70% relative densities are shown in Figure 6.33.

The results revealed that the volume percentage of Mg inside the composite became higher than that of samples with 70% green compact *RD*. On the other hand, the

peak areas of retained Ti and boron carbide and those of intermediate phases are higher than those of 70% green compact *RD*.
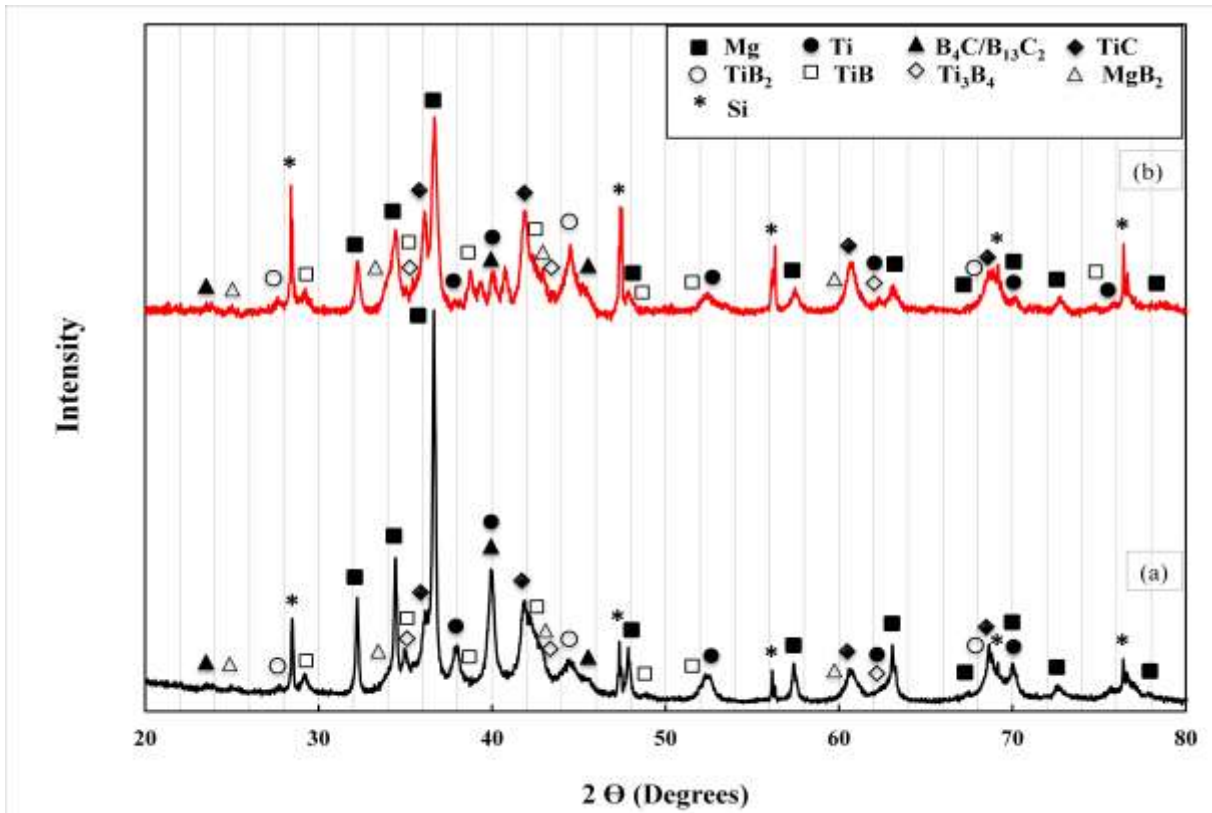
Figure 6.33 XRD patterns of pure Mg MMCs fabricated at 800ºC for 6 h using 3Ti-B$_4$C preforms with different relative densities (a) 60% and (b) 70%

SEM microstructures of the composite sample fabricated using a 3Ti-B$_4$C preform with 60% *RD*, shown in Figure 6.34, reveal a directional distribution of magnesium in the infiltration direction and relatively uniform distribution of the network of TiC$_x$ and TiB$_2$ with residual Ti and boron carbide and intermediate phases. These observations can be supported by EDS analysis as shown also in Figure 6.34 which reveals that Mg penetrates the reinforcing network and proves the presence of residual boron carbide (dark areas) surrounded by MgB$_2$ (dark grey phase) in the microstructure.
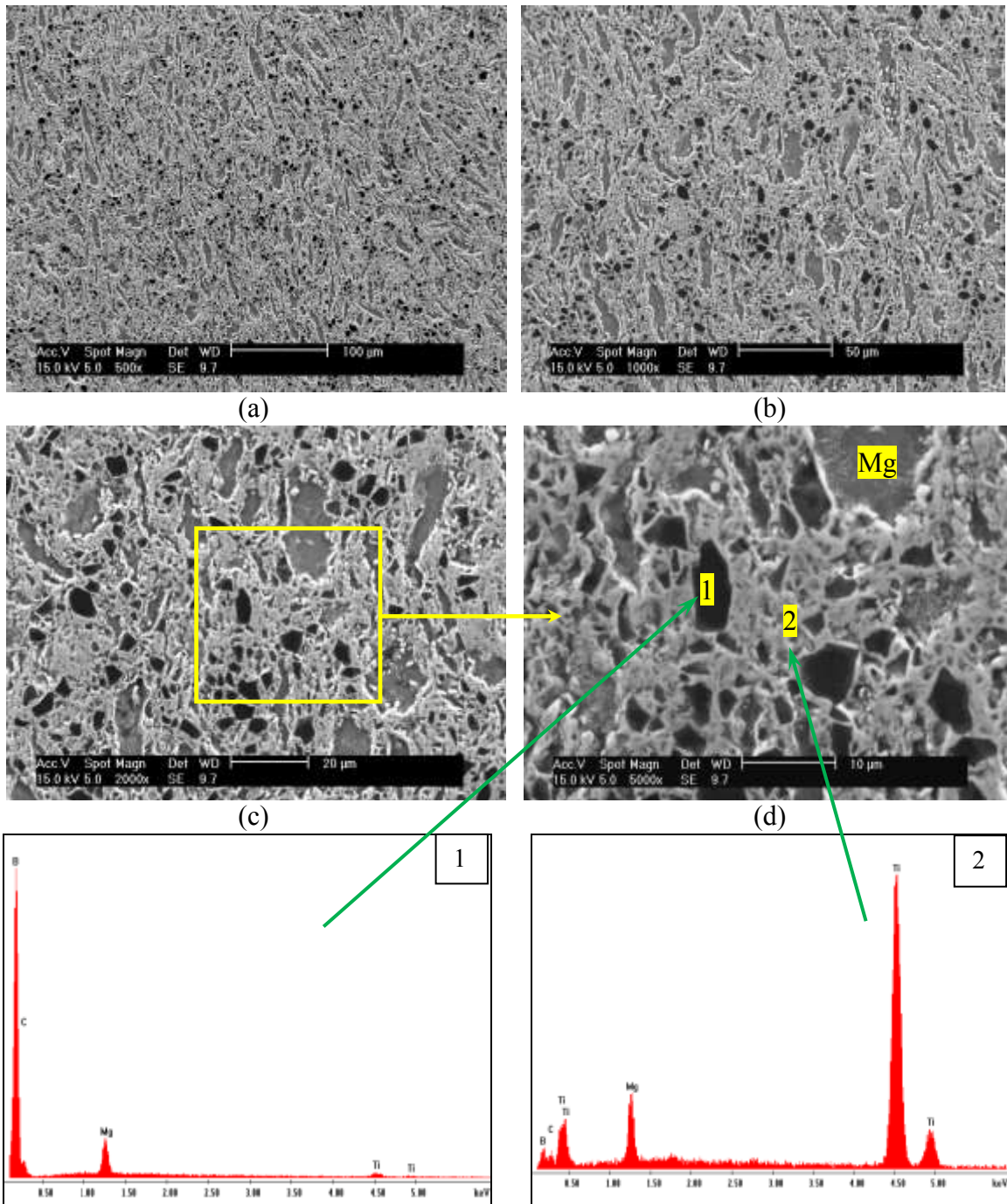
Figure 6.34 SEM-EDS of AZ91D Mg alloy MMCs fabricated at 800ºC for 6 h

Moreover, the elemental mappings for the samples fabricated using different green compact density shown in Figures 6.35 and 6.36 reveal a higher content of Mg in the case of 60% than in the case of 70% green compact *RD*. On the other hand, the

mapping of boron, in its concentrated regions, reveals that the retained boron carbide decreased with increasing green compact *RD*. Also, the overlap of titanium, carbon and boron proves the formation of the reinforcing phases TiC_x and TiB_2. Thus, it can be said that the amount of Mg matrix increased at low green compact *RD* but on the other hand, the reaction to form the reinforcing particles was still incomplete.

Based on the obtained results, it can be mentioned that the volume percentage of the reinforcing phases can be tailored by controlling the preform *RD*.

SEI Image Ti-Kα image

Mg-Kα image B-Kα image
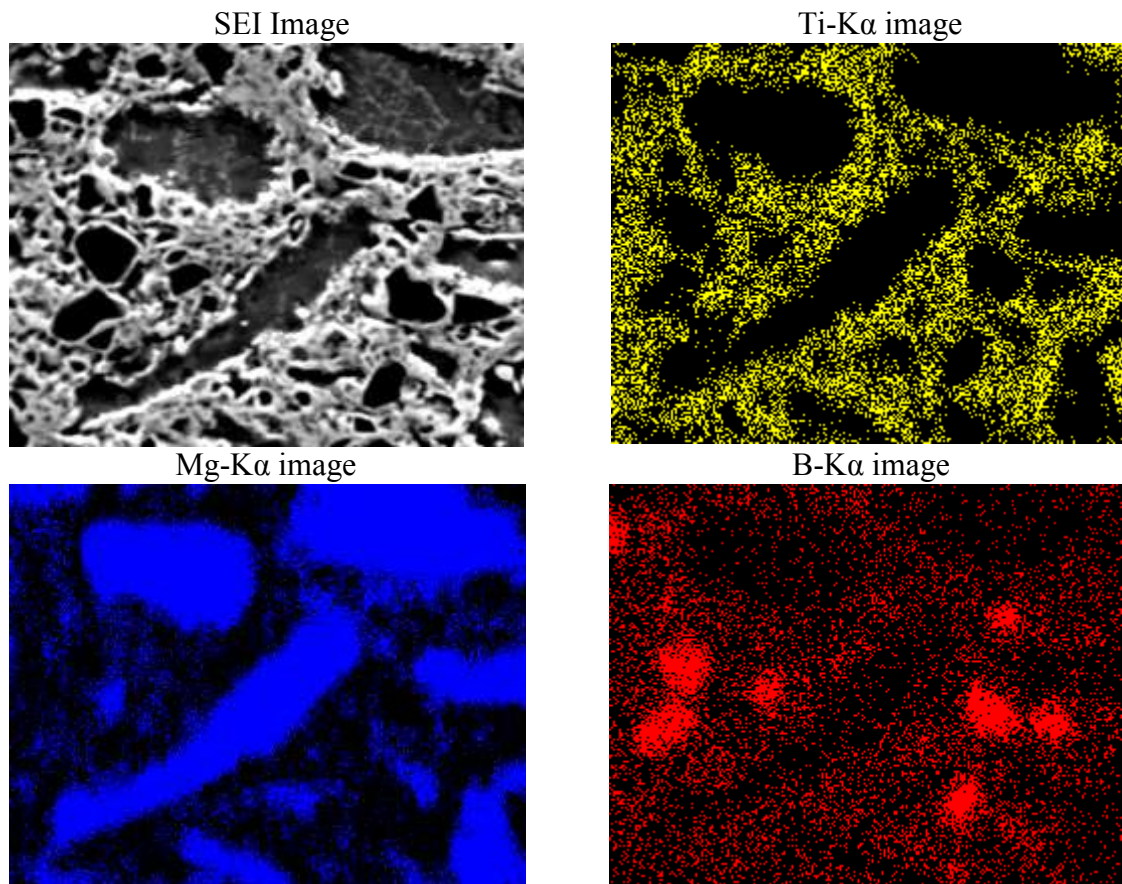
Figure 6.35 SEM microstructure and EDS elemental mapping of the TiC_x-TiB_2/Mg composites synthesized using a 3Ti-B_4C preform with 60% *RD* at 800°C for 6h

SEI Image — **Ti-Kα image** — **Mg-Kα image** — **B-Kα image**
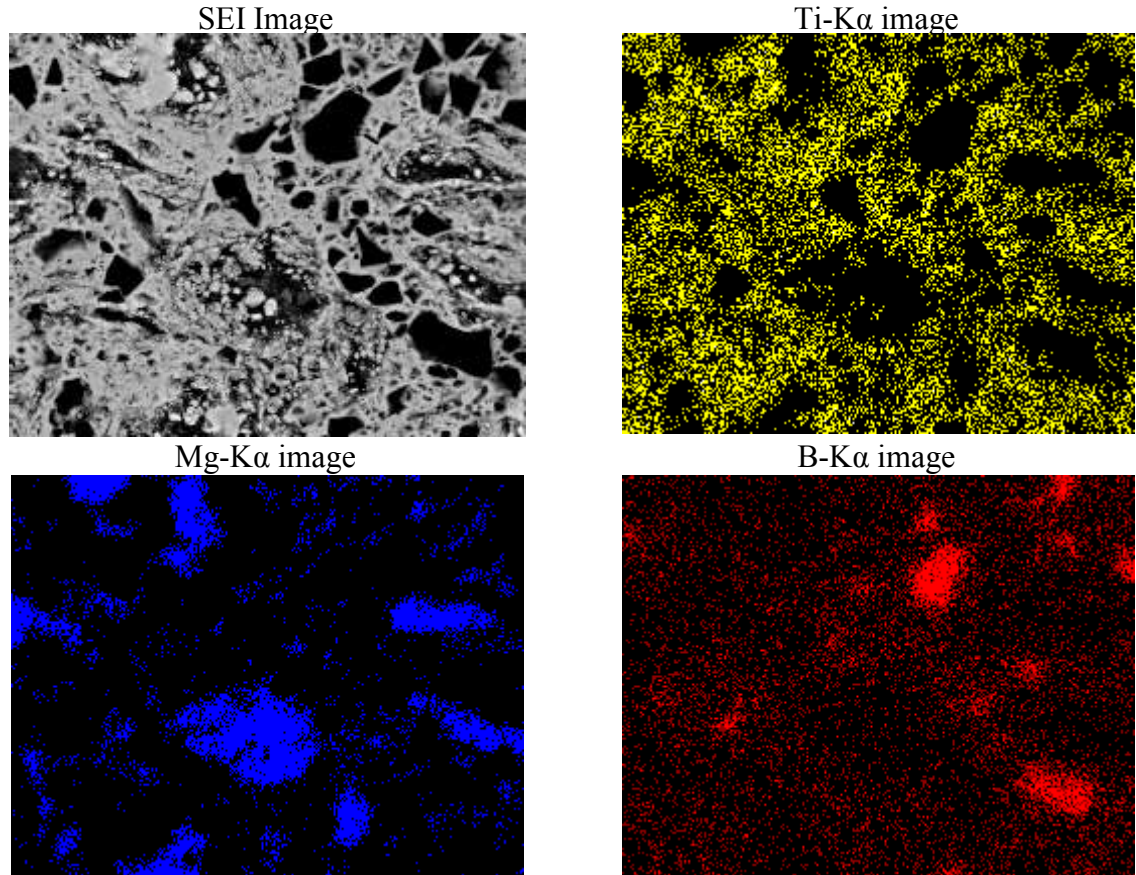
Figure 6.36 SEM microstructure and EDS elemental mapping of the TiC_x-TiB_2/Mg composites synthesized using a 3Ti-B_4C preform with 70% *RD* at 800ºC for 6 h

From the above results, it can be said that the processing parameters such as the processing temperature, holding time and green compact *RD* play an important role in the *in-situ* reaction and hence in the fabrication of the composite.

Based on the results of studying the effect of the processing parameters on the fabrication of composites, it is recommended to fabricate the composites using a green compact of 70% *RD* at 900ºC for 1.5 h. The required equilibrium phases, TiC_x and TiB_2, form in the fabricated composites with very small amount of residual Ti, boron carbide and intermediate phases such as TiB, Ti_3B_4 and MgB_2. Moreover, the fabrication of the

135

composites at these processing parameters avoids significant oxidation of Mg and formation of the ternary compound (Ti$_2$AlC) in the case of AZ91D or AM60B alloy composites which can adversely affect the mechanical properties of the composites.

It can be noted that, in this study, the focus was on AZ91D as a matrix for fabricating the composites. However, what was employed with AZ91D alloy has also been applied with pure Mg and AM60B using the same processing parameters. Figure 6.37 shows SEM micrograph of AM60B composite sample fabricated at 900ºC for 1.5 h using a 3Ti-B$_4$C preform of 70% *RD*.

(a) (b)

(c) (d)
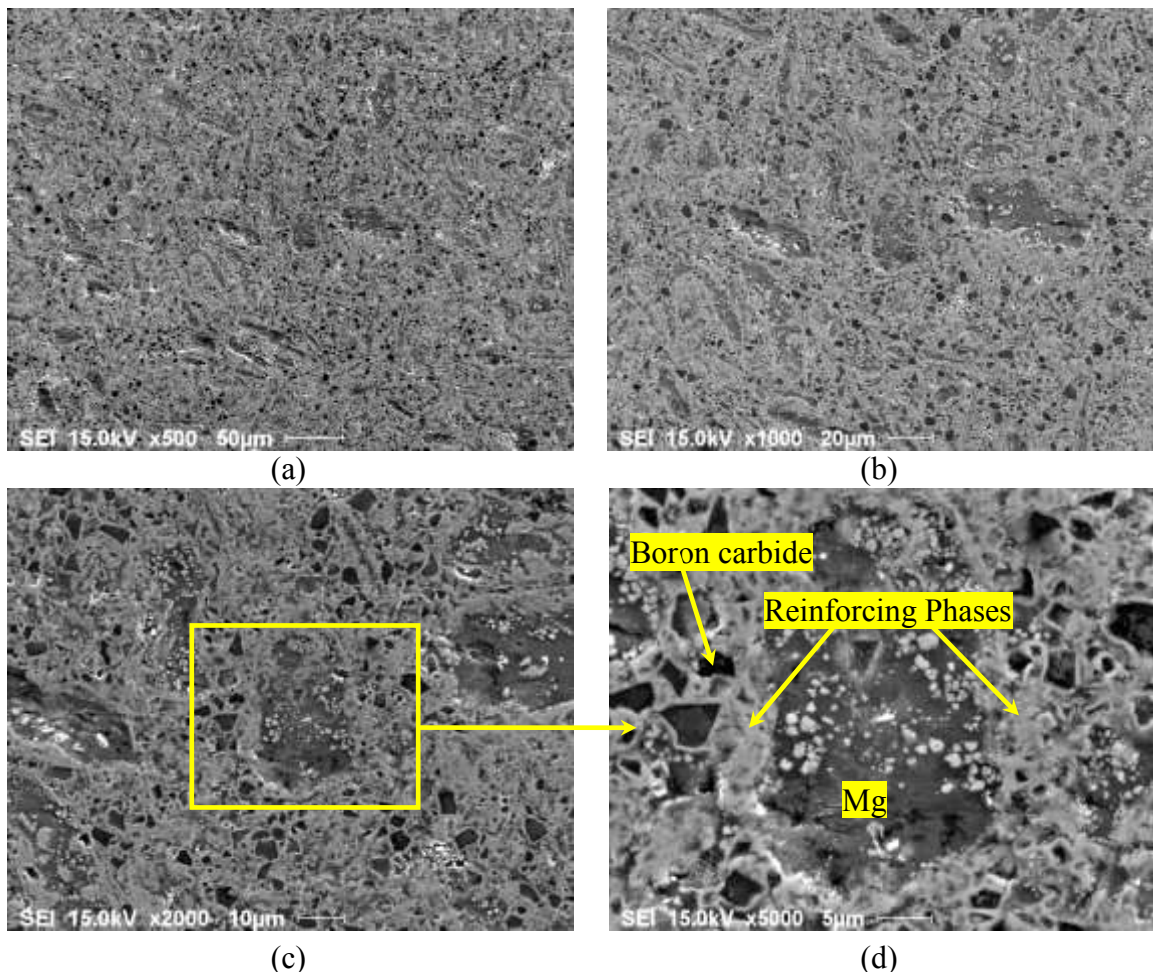
Figure 6.37 SEM micrographs of the AM60B Mg alloy MMCs fabricated using a 3Ti-B$_4$C preform with 70% *RD* at 900ºC for 1.5 h

As in the case of AZ91D composite sample, a relatively uniform distribution of the reinforcing phases is achieved with very small retained boron carbide and intermediate phases such as TiB and Ti_3B_4. As mentioned earlier, it is very difficult to distinguish between these compounds by SEM.

Part II: Fabrication of TiC-TiB$_2$/Mg Matrix Composites using Mg-(3Ti-B$_4$C) or MgH$_2$-(3Ti-B$_4$C) Preform

As mentioned earlier, Mg or MgH_2 powder has been added to the $3Ti$-B_4C preform as an attempt to raise the volume percentage of Mg in the fabricated composites in order to improve the ductility and reduce density. To achieve that, pure Mg, AM60B and AZ91D matrix composites have been fabricated using Mg-($3Ti$-B_4C) or MgH_2-($3Ti$-B_4C) preform with 70% RD and different Mg or MgH_2 weight percentages using the optimum processing parameters: 900ºC and 1.5 h.

6.4 Fabrication of the TiC-TiB$_2$/Mg Composites using Mg-(3Ti-B$_4$C) Preform

Based on the study of the *in-situ* reaction mechanism of the Mg-Ti-B_4C system, Chapter 5, the percentage of magnesium in the composites can be increased. Pure Mg, AM60B and AZ91D matrix composites have been fabricated using an Mg-($3Ti$-B_4C) preform containing different weight percentages of Mg powder at 900ºC, 1.5 h and 70% green compact RD.

Two AZ91D composite samples have been fabricated using a 25 wt.% Mg-($3Ti$-B_4C) preform with 70% RD at 900ºC and for different holding times: 1 and 1.5 h to check if the composite samples can be synthesized with complete formation of TiC_x and TiB_2 at

lower holding time using the Mg-(3Ti-B$_4$C) preform. The XRD patterns of these two samples are shown in Figure 6.38.
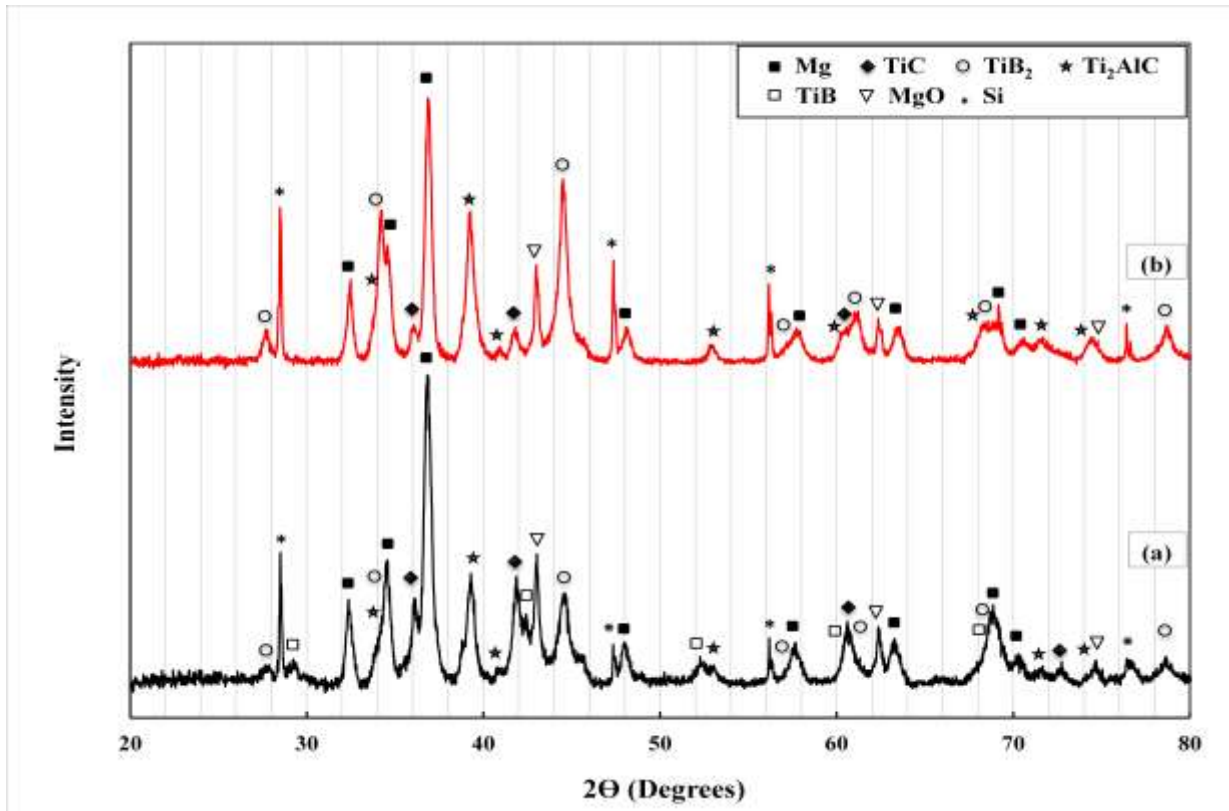
Figure 6.38 XRD pattern of the AZ91D Mg MMCs fabricated using a 25 wt.% Mg-(3Ti-B$_4$C) preform with 70% *RD* at 900ºC for different holding times: (a) 1 h and (b) 1.5 h

The XRD analysis revealed that 1 h holding time is not enough to form the required reinforcing phases, TiC$_x$ and TiB$_2$, completely and very small amounts of retained boron carbide and residual TiB phase were detected. After 1.5 h holding time, TiC$_x$ and TiB$_2$ are completely formed without any retained boron carbide or residual intermediate phases. However, the amount of ternary compound (Ti$_2$AlC) increased while TiC$_x$ decreased. Also, the composite samples have been fabricated at 900ºC for 6 h and the TiC$_x$ and TiB$_2$ are completely formed as well. However, the fabrication of the

composites at 900ºC for 6 h is not recommended because of the higher percentages of the formed ternary compound (Ti_2AlC) and MgO than those in the composites fabricated at 1.5 h. This is due to the diffusion of Al from molten Mg alloy into the substoichiometric TiC_x with increasing holding time resulting in the reduction of the percentage of TiC_x.

SEM micrographs of the composite samples fabricated at 900ºC for 1 h as shown in Figure 6.39 reveal a relatively uniform distribution of the reinforcing phases without pores which means that the as-fabricated composite is fully dense.
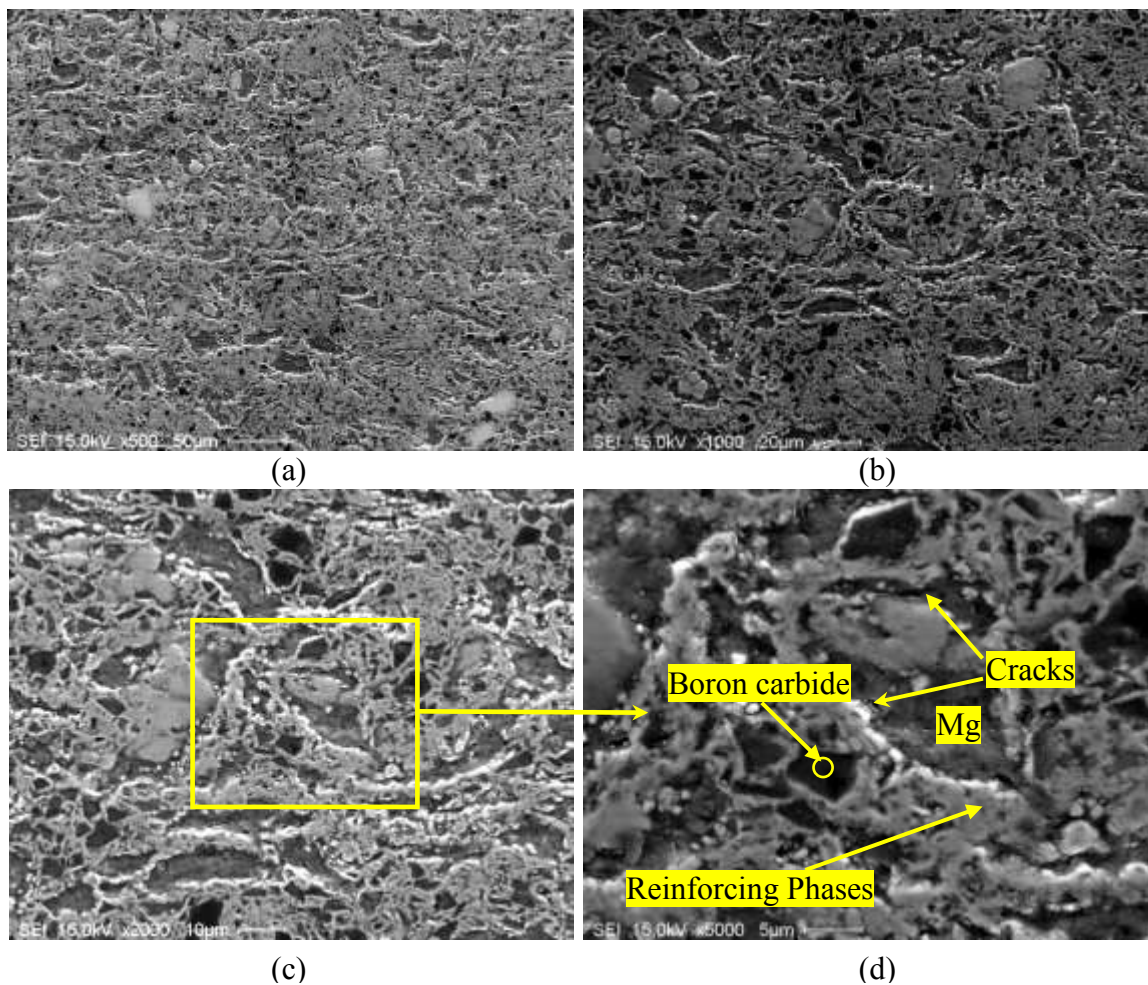
Figure 6.39 SEM microstructure of the AZ91D alloy MMCs fabricated using a 25 wt.% Mg-(3Ti-B_4C) preform with 70% *RD* at 900ºC for 1 h

139

However, there are some very small microcracks in the Mg matrix which are probably due to hot tearing in the magnesium during solidification. Also, very small retained boron carbide can be observed in the microstructure of the sample while it is very difficult to distinguish between TiB and TiB_2 by SEM as mentioned earlier.

On the other hand, with increasing the holding time to 1.5 h, as shown in Figure 6.40, a relatively uniform distribution of the reinforcing phases without any retained boron carbide was obtained, supported by the XRD analysis.
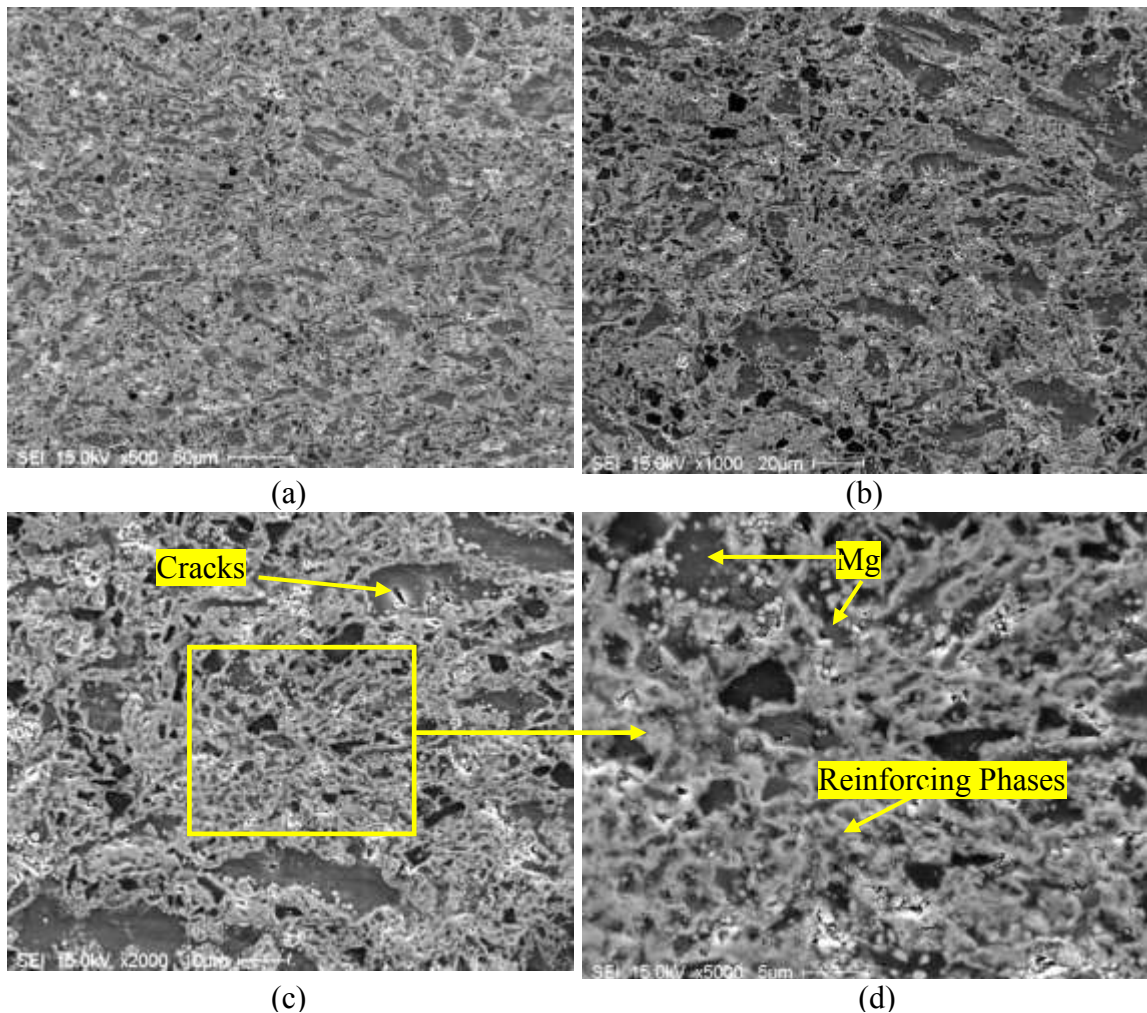
Figure 6.40 SEM microstructure of the AZ91D alloy MMCs fabricated by using a 25 wt.% Mg-(3Ti-B_4C) preform with 70% *RD* at 900ºC for 1.5 h

SEM observations show that no pores are present in the microstructure of the as-fabricated composite and this suggests that the composite is fully dense. However, there are some very small microcracks in the Mg matrix as in the composite sample fabricated at 1 h.

According to the elemental mapping of the composite sample fabricated at 1.5 h as shown in Figure 6.41, the observed overlap of the titanium, carbon and boron proves the existence of the network of TiC_x and TiB_2 in the Mg matrix. Also, the elemental mapping reveals that the dark grey regions are related to Mg or MgO. Moreover, the elemental mapping reveals that Al is distributed not only inside the Mg matrix but also in the Mg-free regions and this means that the ternary compound (Ti_2AlC) is relatively uniformly distributed in the network of the reinforcing phases making its detection by SEM very difficult.

To show the effect of adding Mg powder to the $3Ti-B_4C$ preform on the volume fractions of Mg and the reinforcing phases, XRD analysis was performed. The XRD results, shown in Figure 6.42, reveal that the area under the peaks of magnesium in the fabricated composites increased when the $Mg-(3Ti-B_4C)$ preform was used instead of the $3Ti-B_4C$ preform but on the other hand more MgO was detected as well. This is because Mg powder has a higher affinity for oxygen due to its higher surface area. Also, the presence of Mg powder in the preform enhanced the reaction between Ti and B_4C and as a result, Mg composites were fabricated without any retained Ti, boron carbide or any intermediate phases such as TiB or MgB_2.
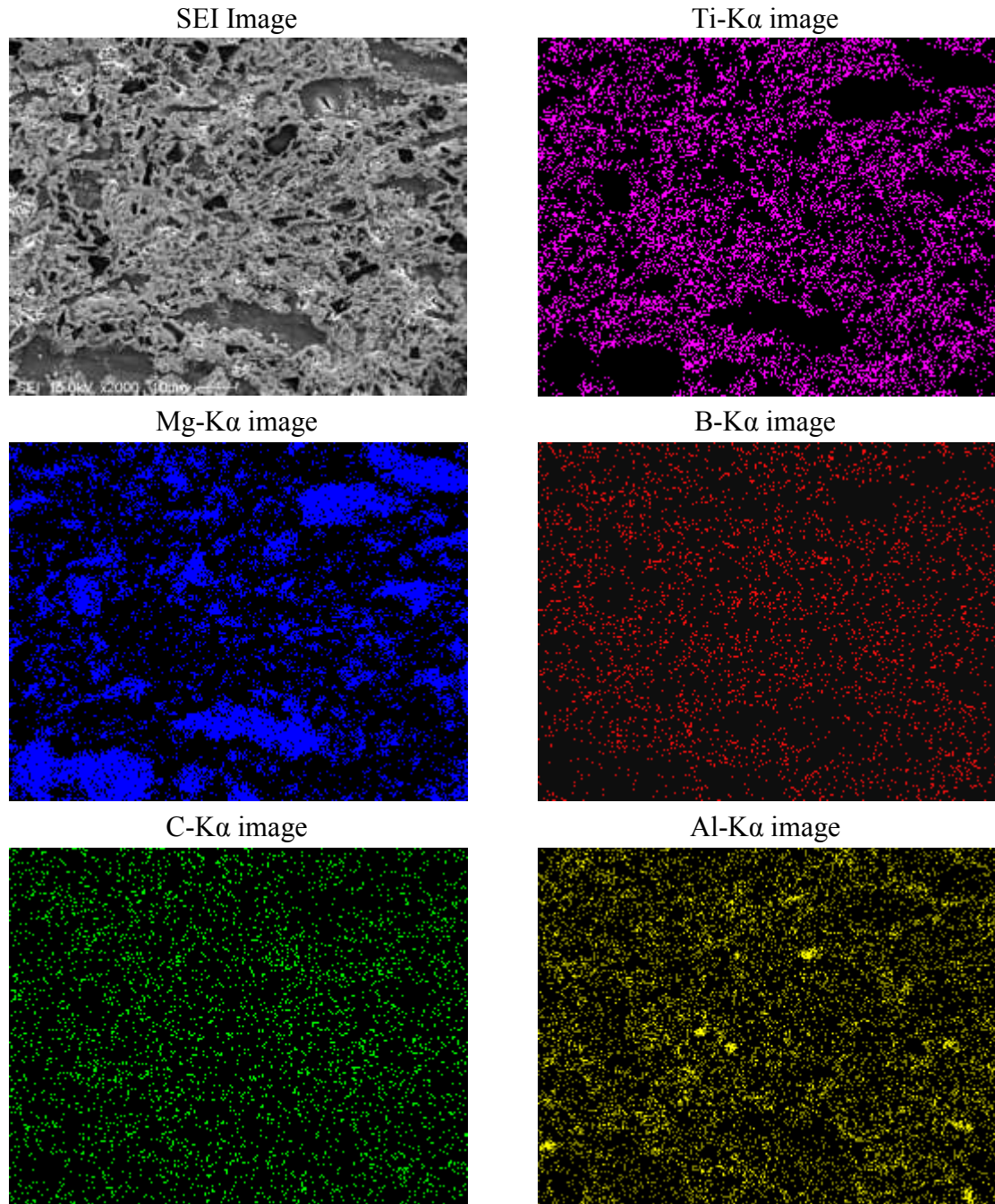
Figure 6.41 SEM microstructure and EDS elemental mapping of the TiC_x-TiB_2/AZ91D composites synthesized at 900ºC for 1.5 h using a 25 wt.% Mg-(3Ti-B_4C) preform with 70% *RD*
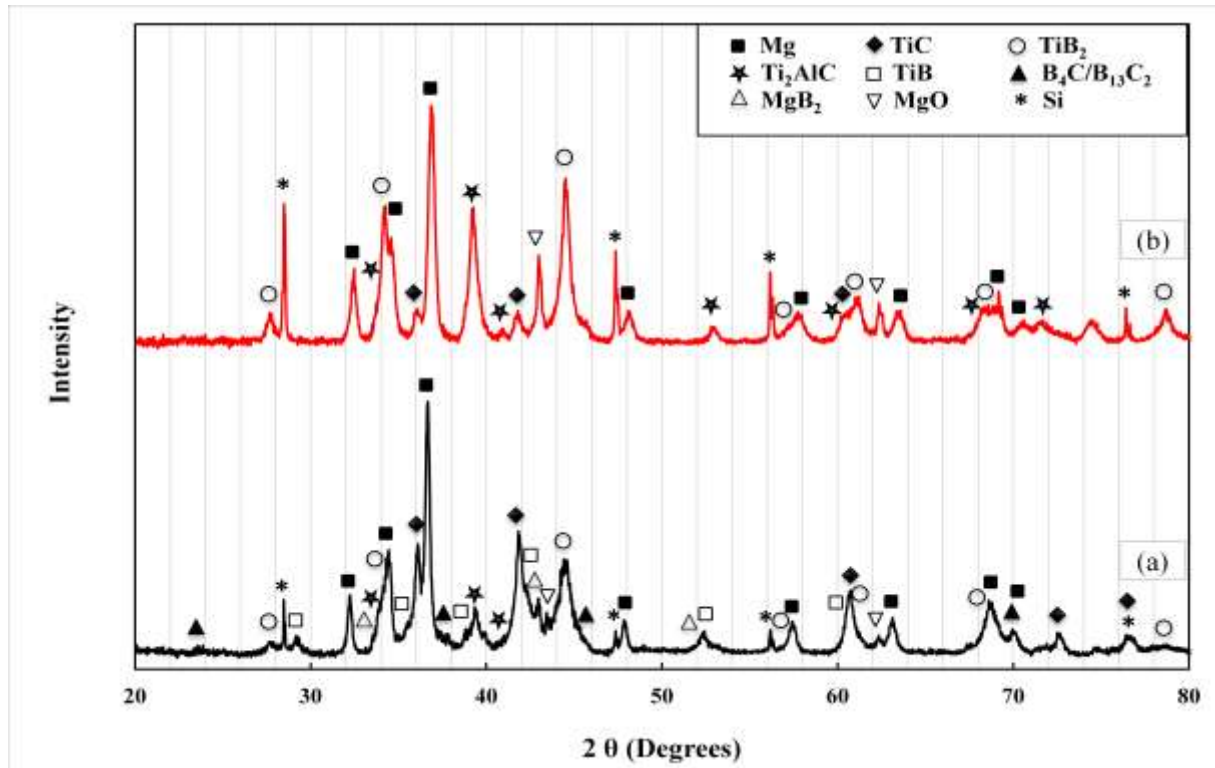
Figure 6.42 XRD pattern of the AZ91D alloy MMCs fabricated at 900ºC for 1.5 h using different preforms (a) 3Ti-B$_4$C and (b) 25 wt.% Mg-(3Ti-B$_4$C) preforms with 70% *RD*

The volume percentages of the phases of the composites synthesized using 3Ti-B$_4$C and 25 wt.% Mg-(3Ti-B$_4$C) preforms are shown in Figure 6.43. A higher percentage of Mg after adding Mg powder to the 3Ti-B$_4$C preform was obtained while the percentage of TiC$_x$ decreased and the amount of the ternary compound Ti$_2$AlC formed in the composite increased after adding Mg powder. Also, the residual boron carbide and intermediate phases such as TiB and MgB$_2$ are still present in the composite made using the 3Ti-B$_4$C preform.
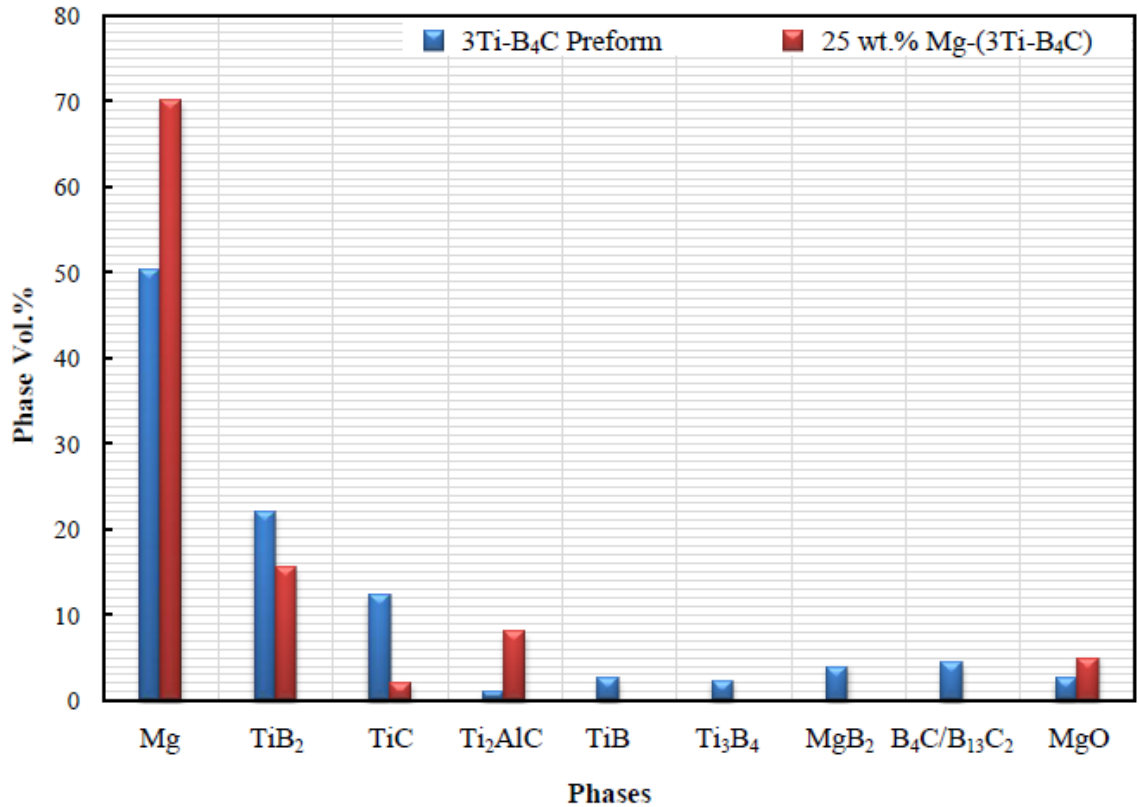
Figure 6.43 Phase volume percentage of the AZ91D alloy MMCs fabricated at 900°C for 1.5 h using different preforms (a) 3Ti-B$_4$C and (b) 25 wt.% Mg-(3Ti-B$_4$C) preforms with 70% *RD*

Comparing the microstructures and elemental mapping of these two cases revealed also the same results: adding Mg powder increases the amount of Mg inside the composites and no residual intermediate phases remain as shown in Figure 6.44.

It can be noted that only one example of using AZ91D alloy as a matrix with a 25 wt.% Mg-(3Ti-B$_4$C) preform has been presented here. However, what is employed with AZ91D alloy has also been applied with pure Mg and AM60B using the same preform with different weight percentages of the Mg powder. It can be concluded that the percentage of reinforcing phases in the Mg matrix can be tailored by adding different amounts of Mg powder to the 3Ti-B$_4$C preform.

144

(a)	(b) Mg-Kα image
(c)	(d) Mg-Kα image
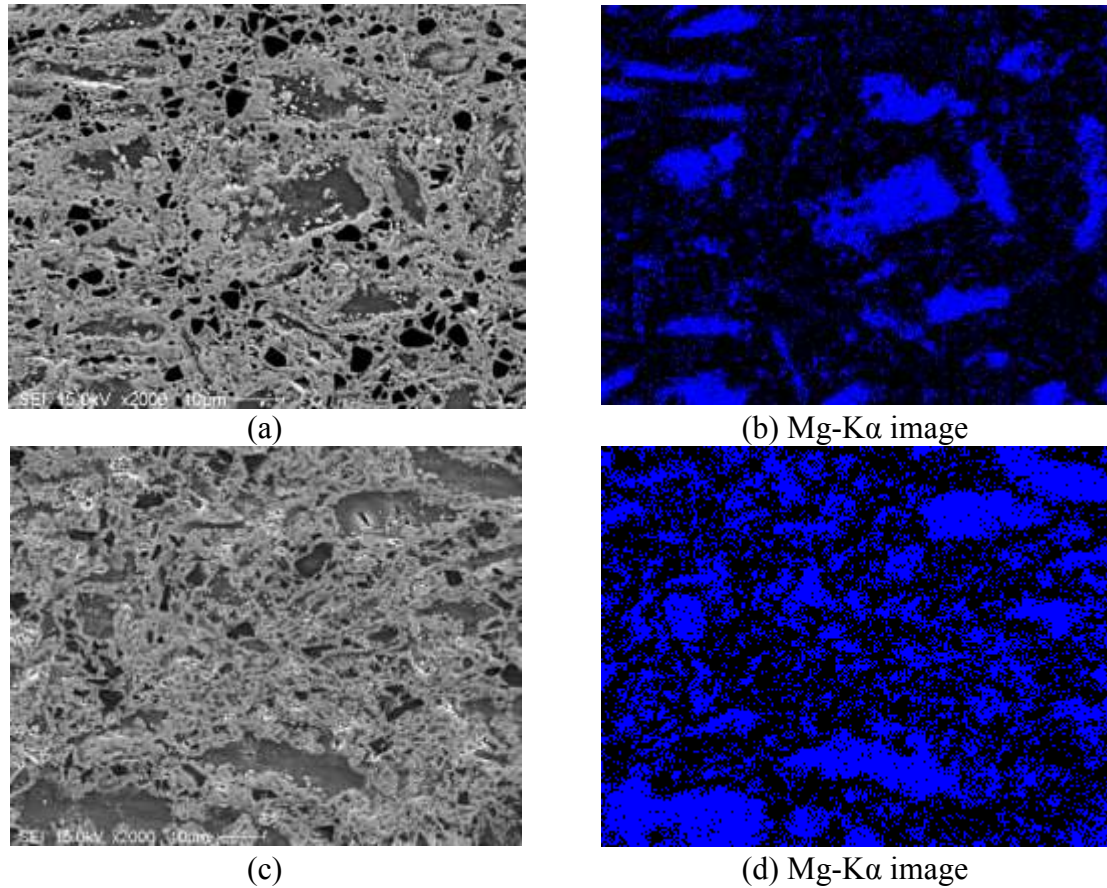
Figure 6.44 SEM microstructure and EDS elemental mapping of the TiC_x-TiB_2/AZ91D composites synthesized at 900ºC for 1.5 h using different preforms: (a) and (b) 3Ti-B_4C and (c) and (d) 25 wt.% Mg-(3Ti-B_4C)

6.5 Fabrication of the Composites using MgH_2-(3Ti-B_4C) Preform

In the same way, and based on the study of the *in-situ* reaction mechanism of the MgH_2-Ti-B_4C system, Chapter 5, the percentage of magnesium in the composites can be increased by magnesium hydride additions. Pure Mg, AM60B and AZ91D matrix composites have been fabricated using an MgH_2-(3Ti-B_4C) preform with 70% *RD* containing different weight percentages of MgH_2 powder at 900ºC for 1.5 h.

6.5.1 AZ91D Matrix

XRD analysis for two composite samples fabricated using a 25 wt.% MgH_2-($3Ti$-B_4C) preform with 70% RD at 900ºC and for 1 and 1.5 h holding times was performed and is presented in Figure 6.45. This analysis was carried out to verify the optimal holding time for composite fabrication using this preform.
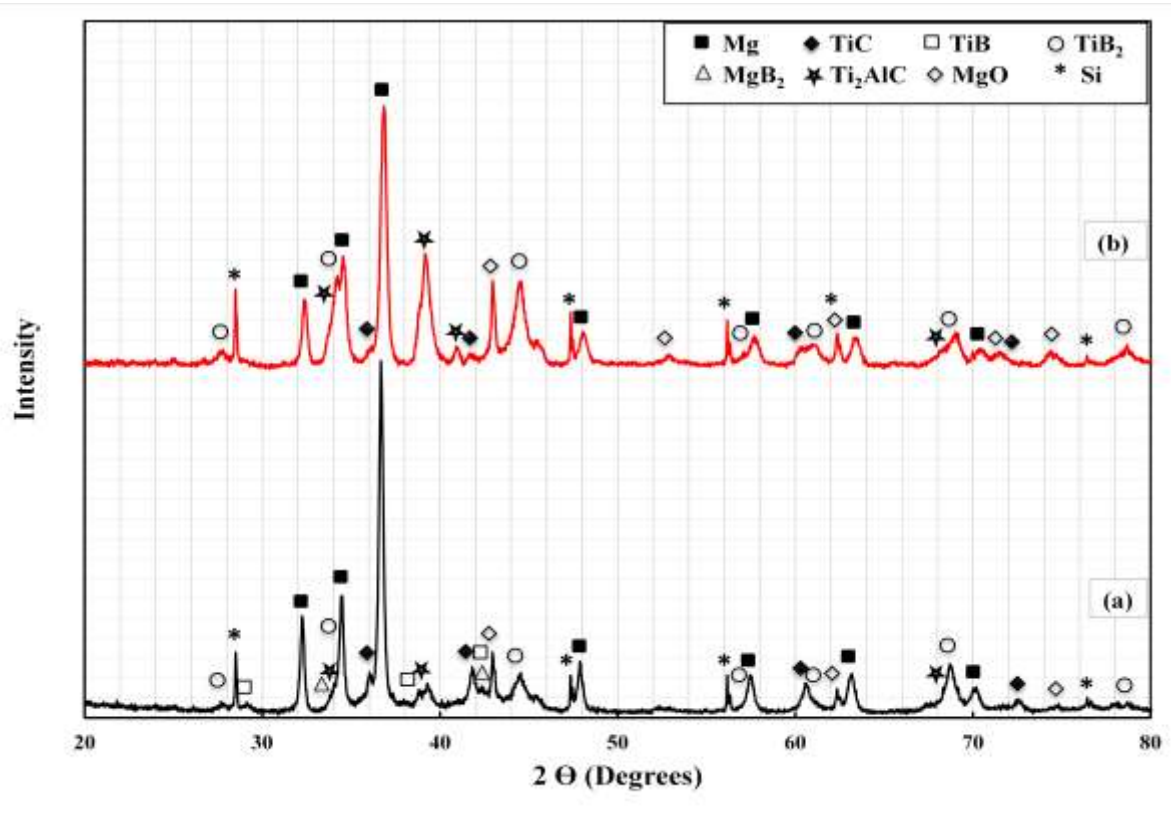
Figure 6.45 XRD pattern of the AZ91D alloy MMCs fabricated using 25 wt.% MgH_2-($3Ti$-B_4C) with 70% RD at 900ºC for different holding times: (a) 1 h and (b) 1.5 h

It can be observed that 1 h holding time is not enough to form the required reinforcing phases, TiC_x and TiB_2, completely and very small amounts of residual intermediate phases such as TiB and MgB_2 were detected. On increasing the holding time to 1.5 h, TiC_x and TiB_2 formed completely without any residual intermediate phases or

only traces of residual TiB which can be neglected. However, higher percentages of the ternary compound (Ti$_2$AlC) and MgO than those in the composites fabricated at 1 h are observed.

Figure 6.46 shows the SEM microstructure of the composite sample fabricated at 900ºC for 1.5 h using a 25 wt.% MgH$_2$-(3Ti-B$_4$C) preform with 70% *RD*.
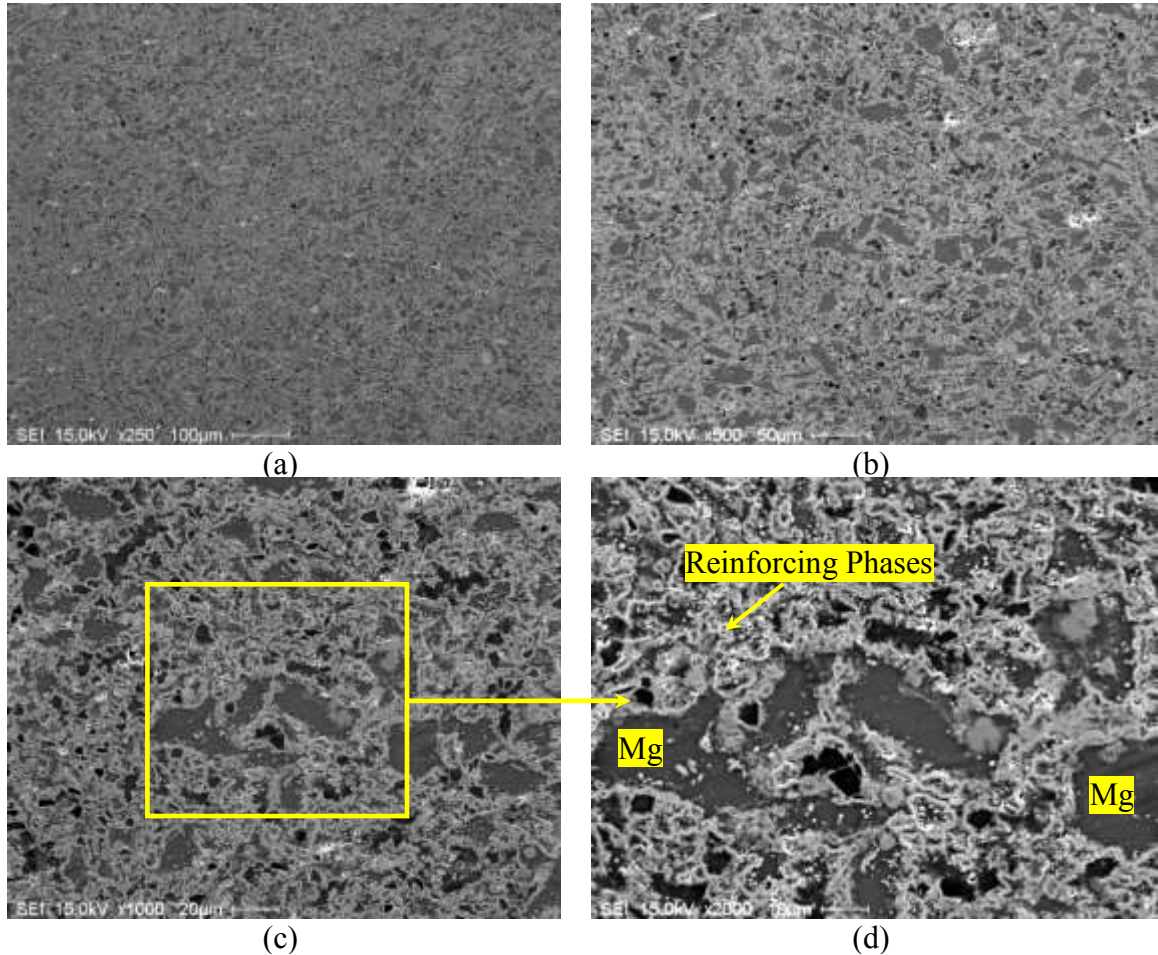
Figure 6.46 Microstructure of the TiC$_x$-TiB$_2$/AZ91D composites synthesized at 900ºC, 1.5 h using a 25 wt.% MgH$_2$-(3Ti-B$_4$C) preform with 70% *RD*

As shown in the figure, a reasonably uniform distribution of reinforcing phases, as a network of TiC$_x$ and TiB$_2$ is observed. However it is very difficult, as mentioned earlier, to distinguish between them especially because their particle sizes are very small in

addition to the insignificant difference in their effective atomic numbers making the discernment very difficult by SEM. Furthermore, SEM observations reveal that no pores or microcracks are present in the microstructure of the as-fabricated TiC_x-TiB_2/AZ91D composites indicating that the composites are fully dense.

According to the elemental mapping for the composite sample fabricated at 1.5 h shown in Figure 6.47, the observed overlap of the titanium, carbon and boron images proves the existence of the network of TiC_x and TiB_2 in the Mg matrix. Furthermore, the elemental mapping reveals that Al is distributed not only inside the Mg matrix but also in the Mg-free regions indicating that the ternary compound (Ti_2AlC) is relatively uniformly distributed in the network of the reinforcing phases making its detection by SEM very difficult. However, the elemental mapping reveals the existence of Al in some concentrated areas as shown in the figure.

EPMA results for the sample at a region of concentrated Al are helpful to analyze the distribution of the *in-situ* reaction products, TiC_x and TiB_2, and infiltrated magnesium, as shown in Figure 6.48. The overlap between titanium, boron and carbon were clearly observed proving the presence of the reinforcing phases, TiC and TiB_2. Also, the overlap between titanium, aluminum and carbon in the region of concentrated aluminum reveals three distinct regions from the interface to the core. It is noticed that Ti increases in the direction of the core while the concentration of Al increases in the opposite direction.
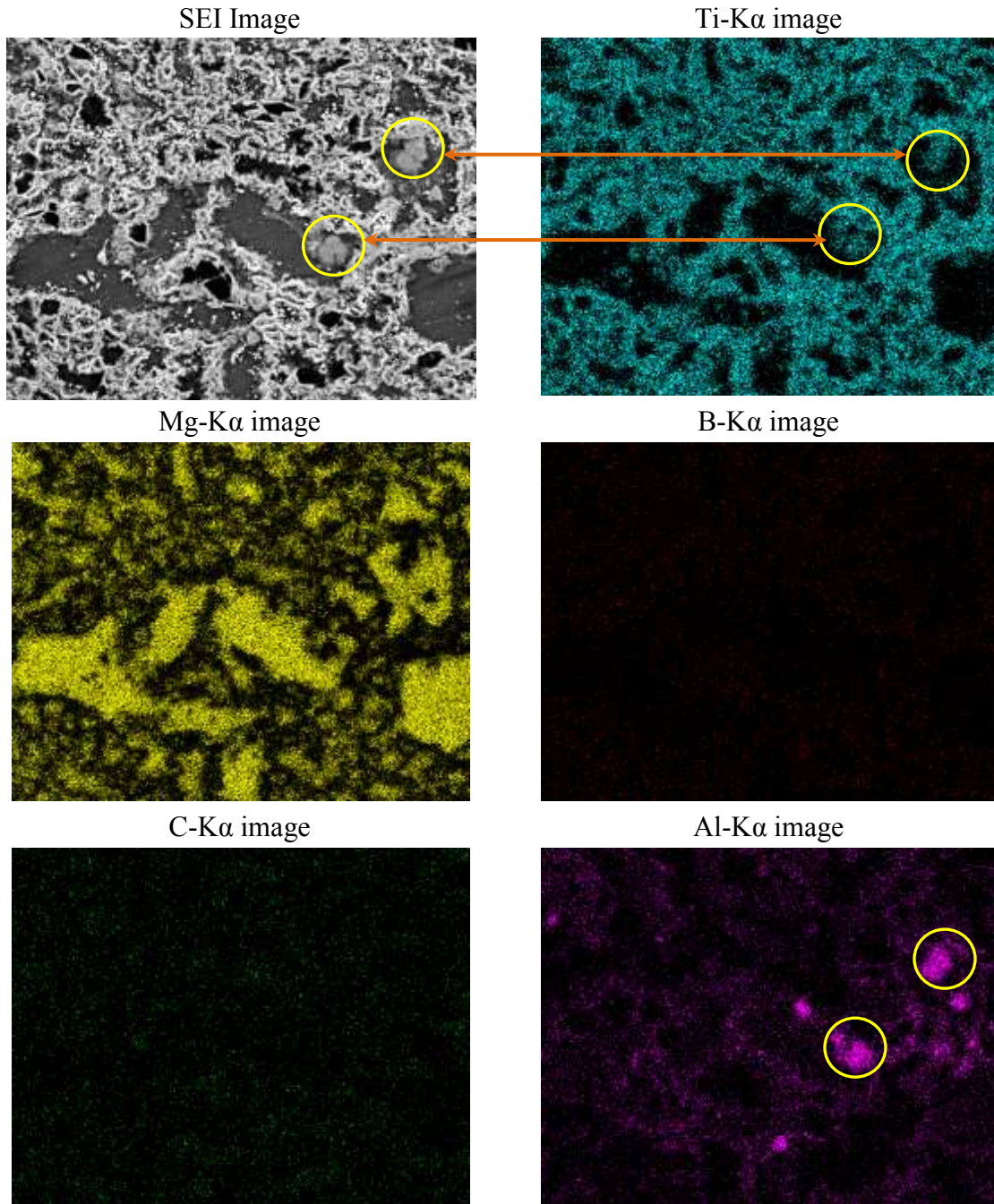
Figure 6.47 SEM microstructure and EDS elemental mapping of the TiC_x-TiB_2/AZ91D composites synthesized at 900ºC for 1.5 h using a 25 wt.% MgH_2-($3Ti$-B_4C) preform with 70% *RD*

BSEI Image

Ti-Kα image

Mg-Kα image

B-Kα image

C-Kα image

Al-Kα image
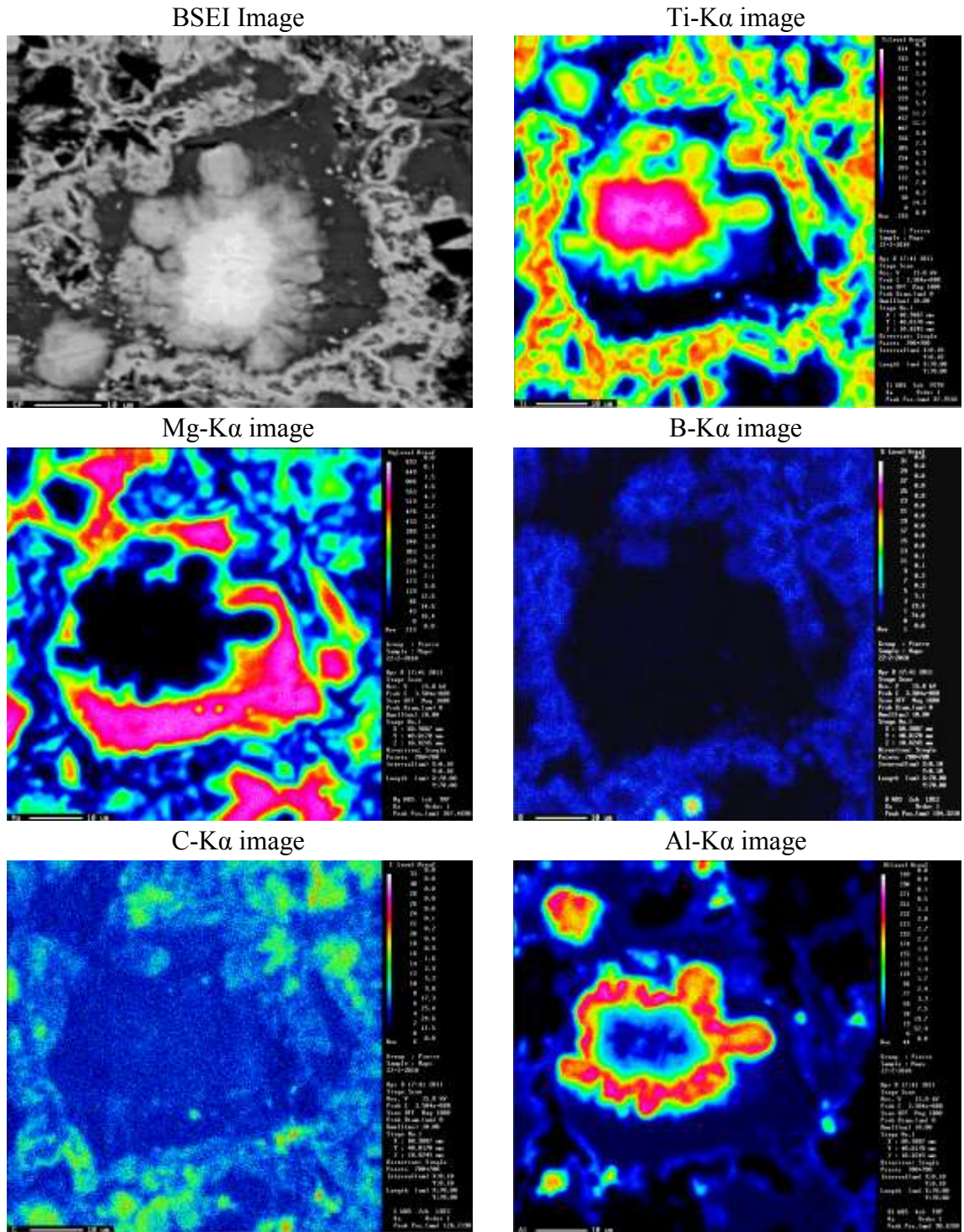
Figure 6.48 EPMA analysis of the TiC-TiB$_2$/AZ91D composites synthesized at 900ºC
for 1.5 h using a 25 wt.% MgH$_2$-(3Ti-B$_4$C) preform with 70% *RD*

Based on these observations, it can be concluded that the ternary compound, Ti_2AlC (Al-rich) formed at the interface followed by a very small layer of another ternary compound, Ti_3AlC_2 and then TiC_x phase in the core. A schematic representation of this process is presented in Figure 6.49.
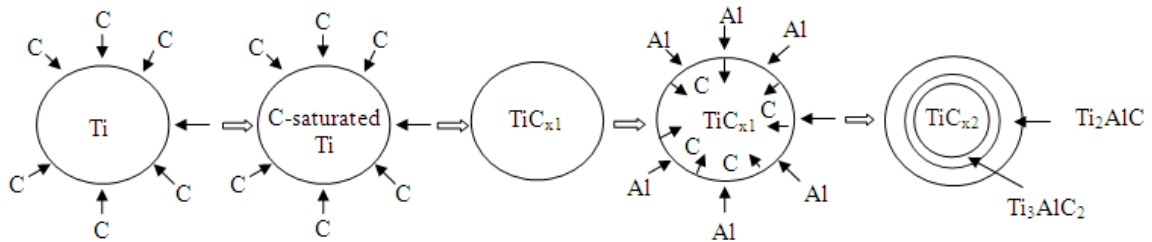
Figure 6.49 Schematic representation of the formation of the ternary compounds in the composite synthesized at 900°C for 1.5 h and using a 25 wt.% MgH_2-($3Ti$-B_4C) with 70% *RD*

To show the influence of adding MgH_2 powder to the $3Ti$-B_4C preform on the volume fractions of Mg and the reinforcing phases, XRD analysis for both scenarios was carried out. The XRD results, shown in Figure 6.50, reveal that the volume percentage of magnesium in the fabricated composites increased after adding MgH_2 powder to the $3Ti$-B_4C preform but on the other hand, more MgO was detected because the decomposition of MgH_2 at low temperature forming Mg with a high affinity for oxygen due to its high surface area. Also, the presence of Mg with high reactivity in the preform enhanced the reaction between Mg, Ti and B_4C and as a result, Mg composites were fabricated without any retained Ti, boron carbide or any intermediate phases such as TiB or MgB_2.

Comparing the volume percentage of the phases in the composites fabricated using 25 wt.% Mg-($3Ti$-B_4C) and 25 wt.% MgH_2-($3Ti$-B_4C) preforms as shown in Figures 6.43

151

and 6.50, respectively, reveal a higher volume fraction of Mg in the composites using MgH$_2$ than those using Mg powder in the preform. This can be interpreted by the higher volume of MgH$_2$ than that of Mg powder when using the same weight percent due to its lower density as presented earlier in Table 4.6. Besides, after the decomposition of MgH$_2$, more channels became available for the infiltrated Mg.
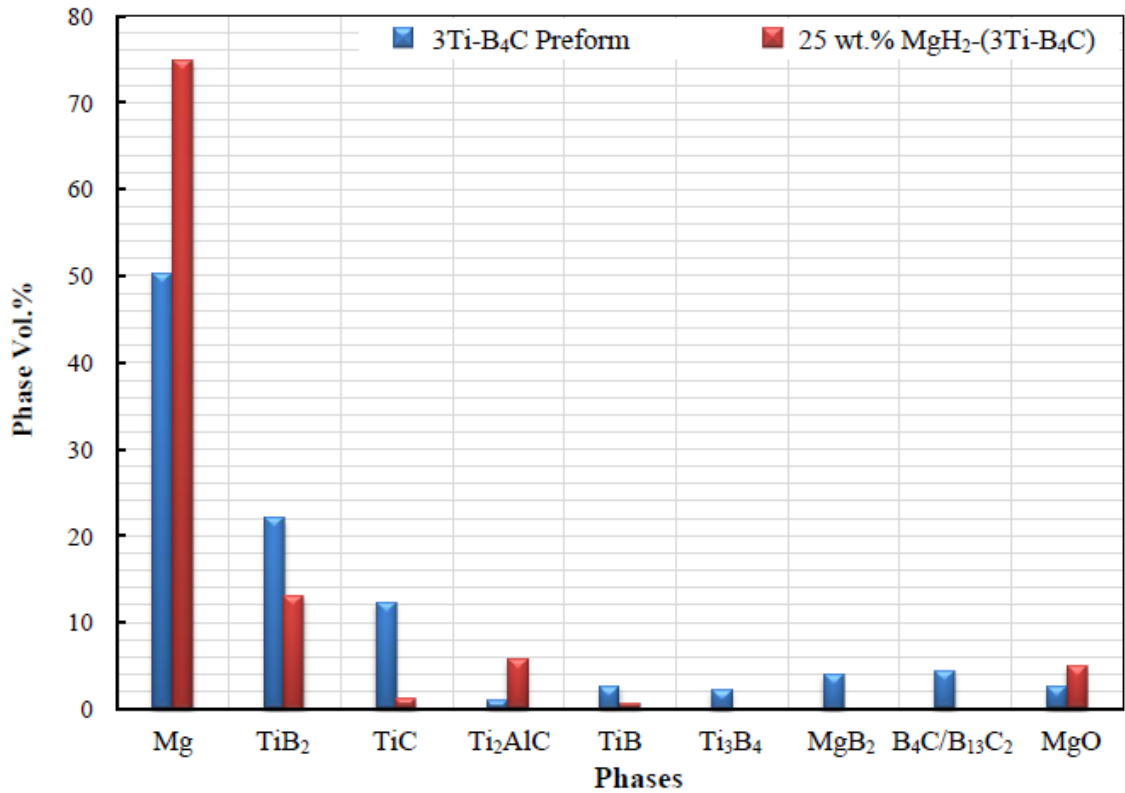
Figure 6.50 Phase volume percentage of the AZ91D alloy MMCs fabricated at 900°C for 1.5 h using different preforms (a) 3Ti-B$_4$C and (b) 25 wt.% MgH$_2$-(3Ti-B$_4$C) preforms with 70 % *RD*

It can be mentioned that the percentage of reinforcing phases in the Mg matrix can be tailored by adding MgH$_2$ powder to the 3Ti-B$_4$C preform. The XRD patterns and the volume percentages of the formed phases in the composite samples synthesized using

an MgH_2-(3Ti-B_4C) preform with 10, 25 and 40 wt.% MgH_2 are shown in Figures 6.51 and 6.52, respectively.

As shown in Figure 6.51, the XRD spectra of the composite sample fabricated using 10 wt.% MgH_2-(3Ti-B_4C) preform reveals the formation of the TiC_x and TiB_2 reinforcing phases with very small residual intermediate phases such as TiB and MgB_2. On the other hand, the XRD patterns of the composite samples fabricated using 25 wt.% or 40 wt.% MgH_2 in the preform reveal the complete formation of the reinforcing phases without intermediate phases. However, the percentage of TiC_x in both cases is lower due to the formation of the ternary compound Ti_2AlC at the expense of TiC_x.
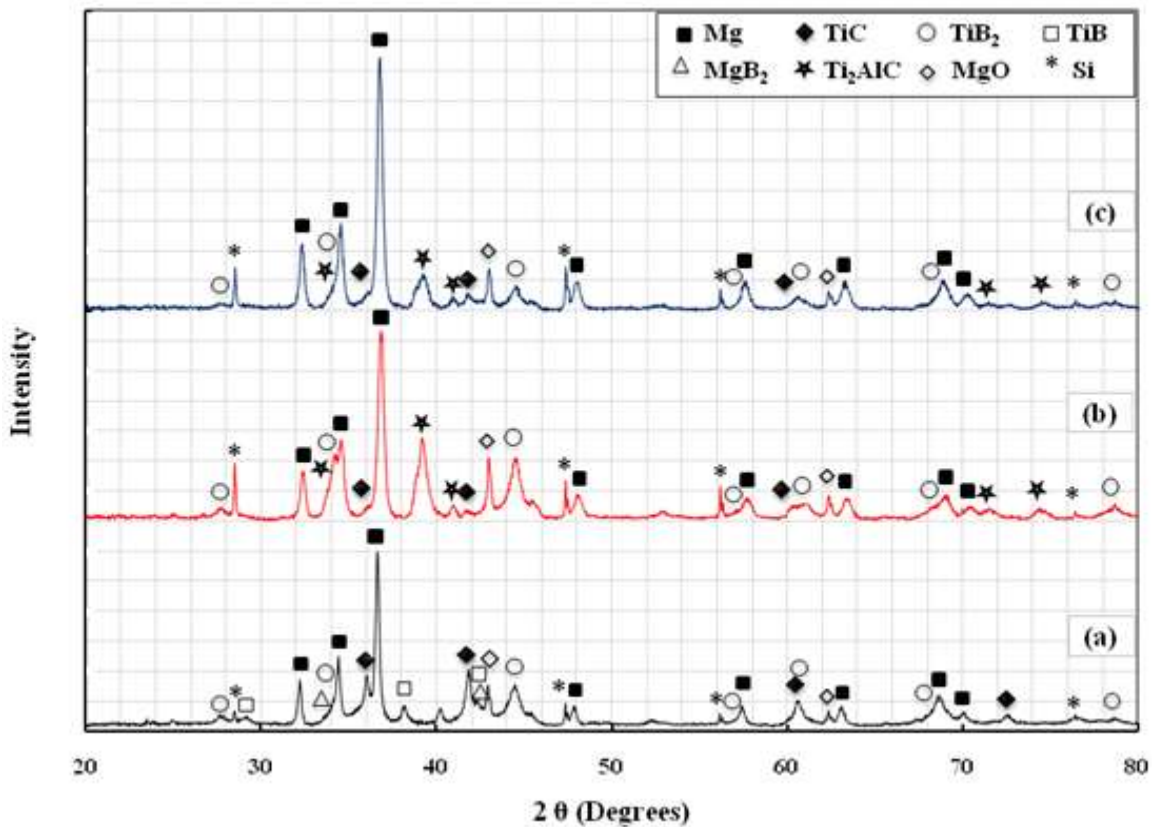
Figure 6.51 XRD pattern of the AZ91D alloy MMCs fabricated at 900ºC for 1.5 h using MgH_2-(3Ti-B_4C) preforms with different MgH_2 weight percentages (a) 10, (b) 25 and (c) 40 wt.%

153
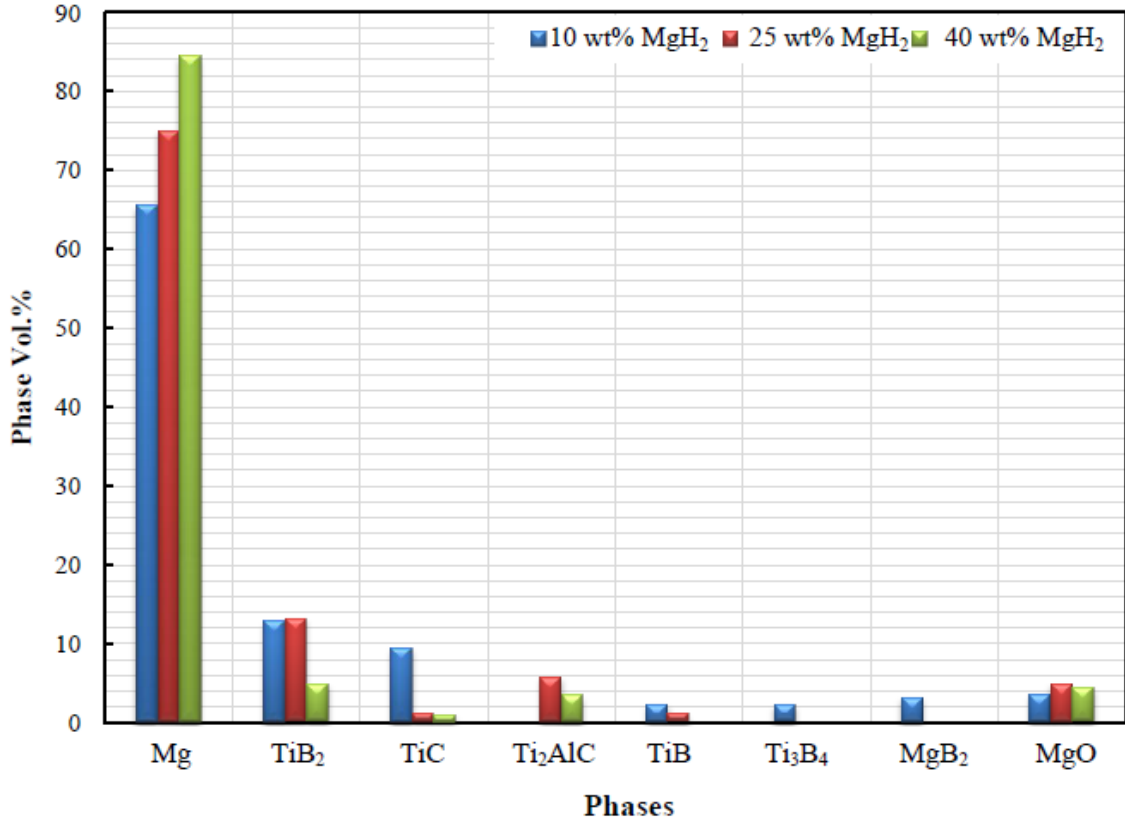
Figure 6.52 Phase volume percentage of the AZ91D alloy MMCs fabricated at 900ºC for 1.5 h using MgH_2-(3Ti-B_4C) preforms with different MgH_2 weight percentages

Moreover, it is obvious that the area under the peaks of the Mg in the composite increased with increasing the weight percentage of MgH_2 powder in the preform which is supported by the calculated volume percentages of the phases in the composite sample as presented in Figure 6.52.

The formation of the ternary compound, Ti_2AlC, was proved also by XRD for the composite sample fabricated using 40 wt.% MgH_2-(3Ti-B_4C) preform with 70% *RD* at 900ºC for 1.5 h compared with the XRD pattern of Ti_2AlC from Pearson's crystal database [139] as shown in Figure 6.53.
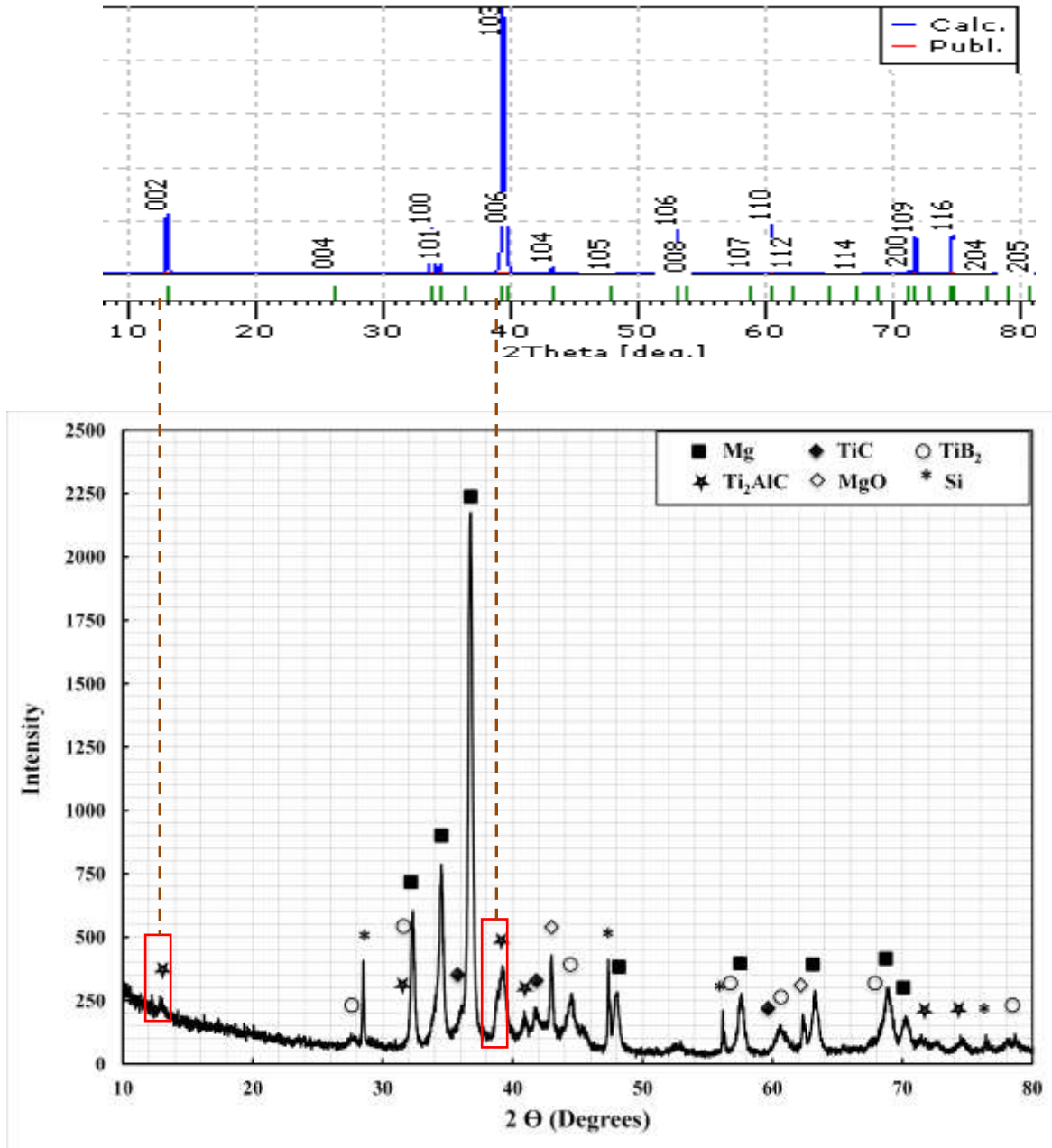
Figure 6.53 XRD pattern of the AZ91D alloy MMCs fabricated at 900ºC for 1.5 h using a 40 wt.% MgH$_2$-(3Ti-B$_4$C) preform with 70% *RD*

6.5.2 AM60B Matrix

Using the same preform consisting of MgH$_2$, Ti and B$_4$C powders at 70% *RD* with different amounts of MgH$_2$ powder, AM60B matrix composites have been fabricated at

900ºC and 1.5 h. In this study, two AM60B composite samples were fabricated using a 25 wt.% MgH_2-(3Ti-B_4C) preform with 70% *RD* at 900ºC and for 1 and 1.5 h different holding times to obtain the optimal holding time to form the required reinforcing phases for this system. The XRD analysis was carried out and presented in Figure 6.54.
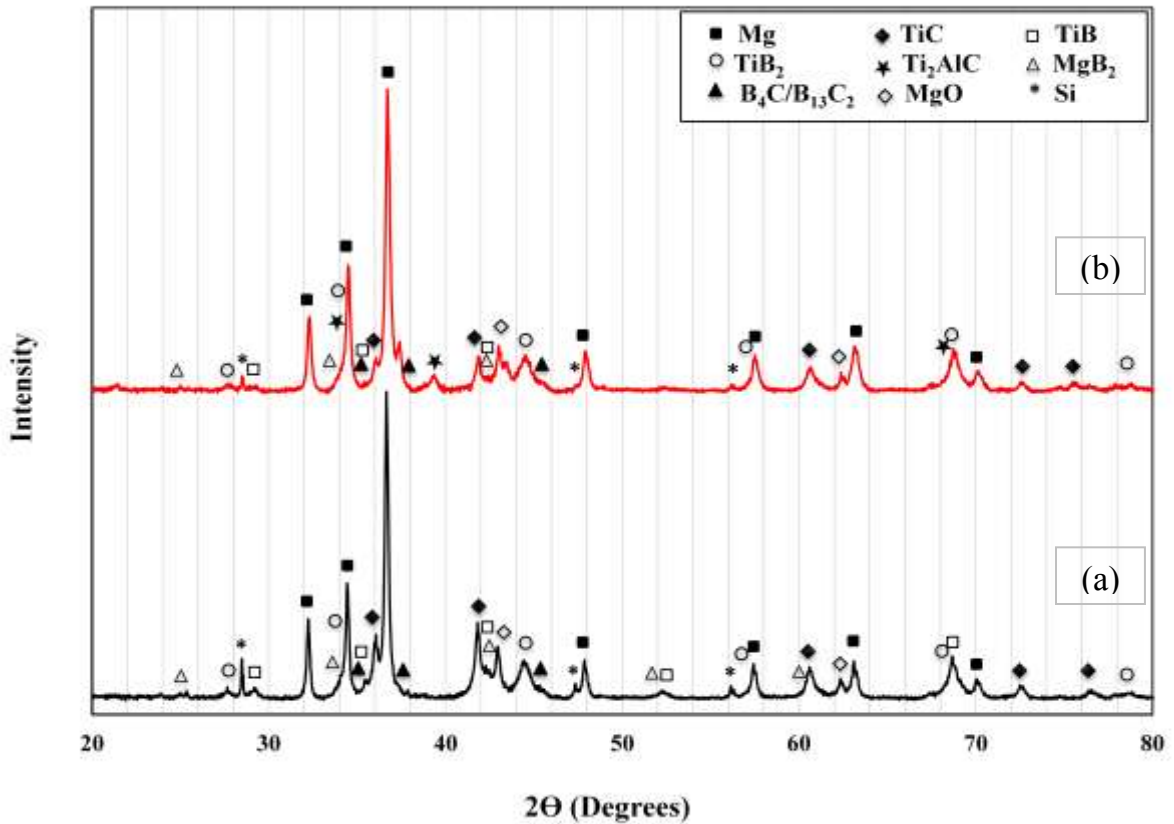
Figure 6.54 XRD pattern of the AM60B alloy MMCs fabricated using a 25 wt.% MgH_2-(3Ti-B_4C) preform with 70% *RD* at 900ºC for different holding times: (a) 1 h and (b) 1.5 h

By comparing the area under the peaks of the phases in the two composites, it can be observed that the equilibrium reinforcing phases, TiC_x and TiB_2, formed in the two samples fabricated at 1 h and 1.5 h with very small amounts of retained boron carbide and residual intermediate phases such as MgB_2 and TiB. However, the sample fabricated

156

at 1.5 h has only traces of these intermediate phases that can be neglected. Furthermore, it can be observed that the ternary compound (Ti$_2$AlC) formed only in the sample fabricated at 1.5 h. To confirm these observations, the volume percentages of the main phases of these two composites fabricated at 1 h and 1.5 h based on Rietveld analysis are analyzed and presented in Figure 6.55.
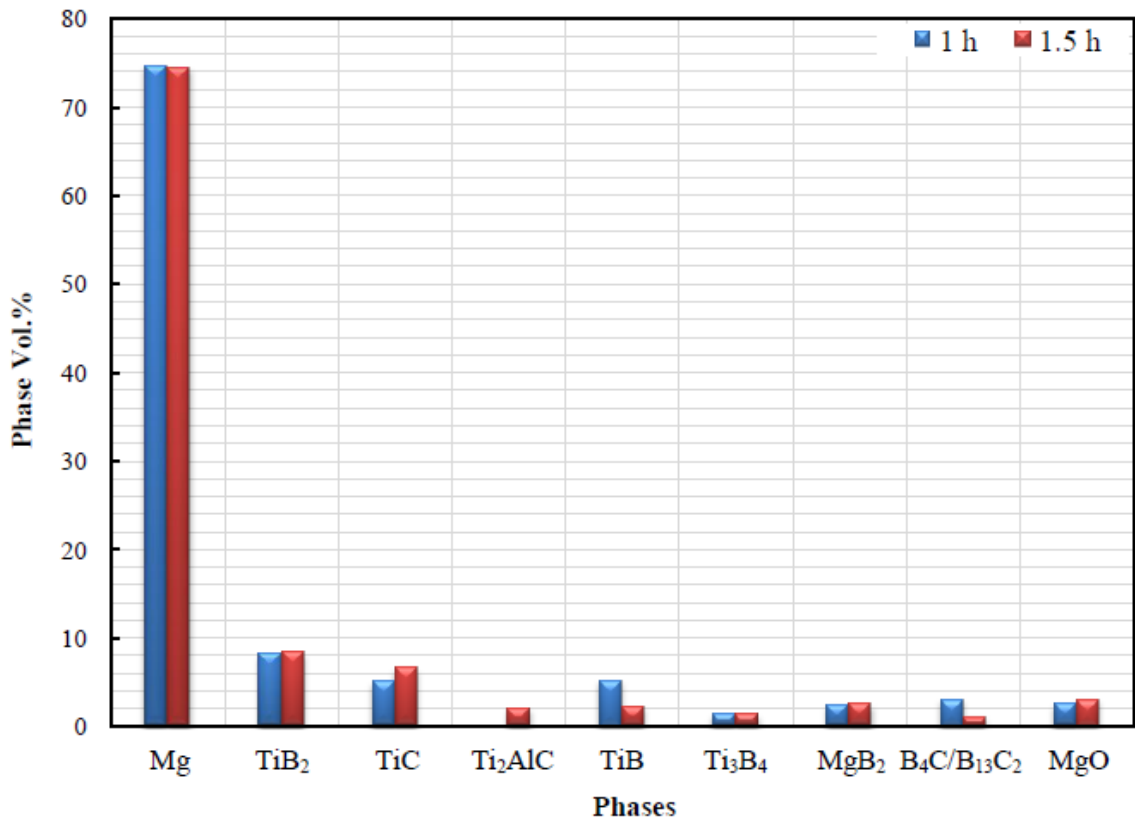
Figure 6.55 Phase volume percentage of the AM60B alloy MMCs fabricated at 900°C using 25 wt% MgH$_2$-(3Ti-B$_4$C) preform with 70% *RD* and at 1 and 1.5 h holding times

SEM observations of the composite samples fabricated at 900°C for 1 h as shown in Figure 6.56 show a relatively uniform distribution of the reinforcing phases without

pores which means that the composite is fully dense. However, there are some very small

microcracks in the Mg matrix for the reason mentioned earlier.

(a) (b)

(c) (d)
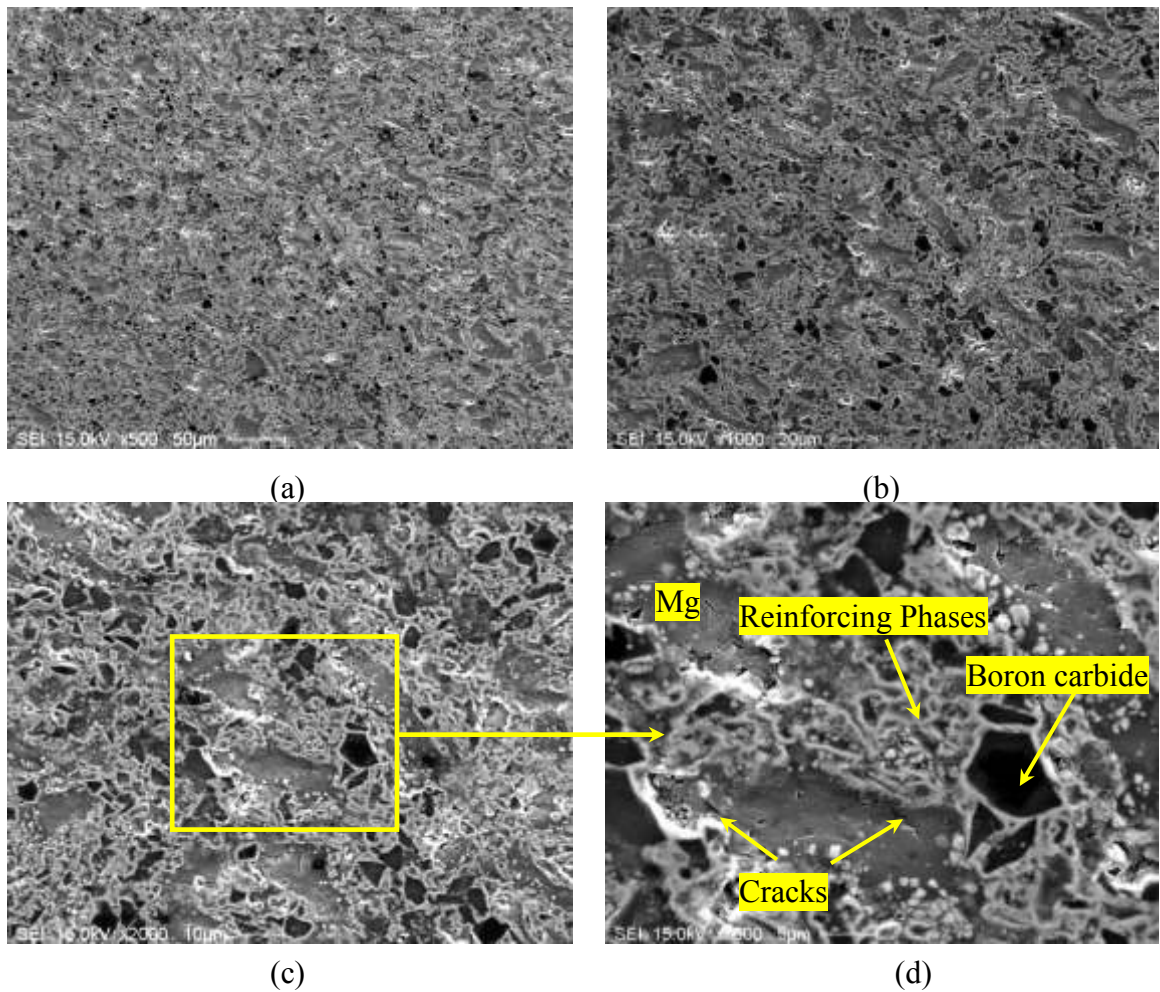
Figure 6.56 SEM microstructure of the AM60B alloy MMCs fabricated using a 25 wt.%

MgH$_2$-(3Ti-B$_4$C) preform with 70% *RD* at 900ºC for 1 h

Also, very small retained boron carbide (dark part) can be observed in the

microstructure of the sample while MgB$_2$ (dark grey part) is present at its interface which

is supported by the EDS analysis through a line scan shown in Figure 6.57.
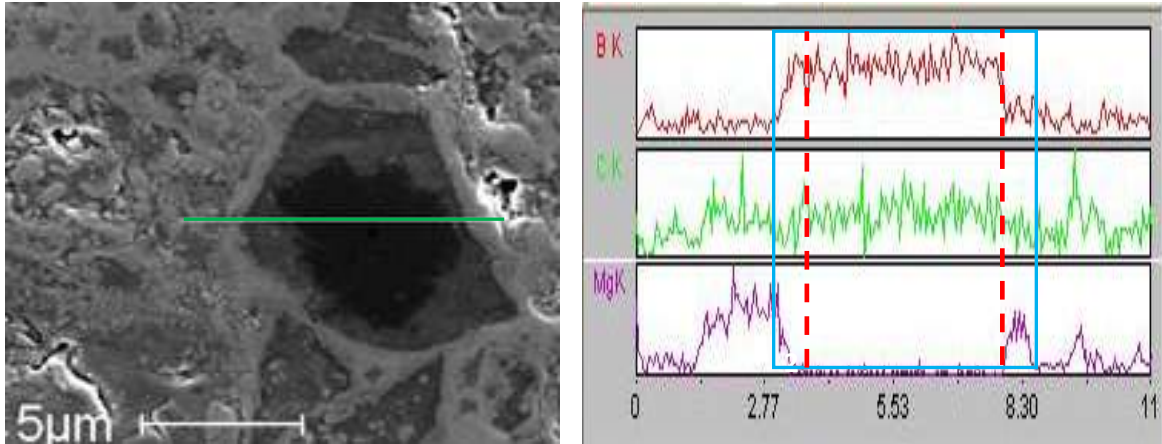
Figure 6.57 SEM-EDS of the AM60B alloy MMCs fabricated using a 25 wt.% MgH$_2$-(3Ti-B$_4$C) preform with 70% *RD* at 900ºC for 1 h

On the other hand, SEM observations of the sample fabricated at 900ºC and 1.5 h using 25 wt.% MgH$_2$-(3Ti-B$_4$C) preform with 70% *RD* reveal, as shown in Figure 6.58, a reasonably uniform distribution of a network of the reinforcing phases. Furthermore, no pores or microcracks were observed in the microstructure of the as-fabricated TiC$_x$-TiB$_2$/AM60B composites.

The elemental mapping for the composite sample fabricated at 1.5 h as shown in Figure 6.59 reveals the overlap between titanium, carbon and boron proving the existence of the network of TiC$_x$ and TiB$_2$ in the Mg matrix. Moreover, the elemental mapping reveals that Al is distributed not only inside the Mg matrix but also in the Mg-free regions. This means that the ternary compound (Ti$_2$AlC) is relatively uniformly distributed in the network of the reinforcing phases. Also, it was observed that the Ti$_2$AlC compound formed with molten AZ91D and AM60B. However, the percentage of this phase with AM60B is lower than that with AZ91D. This becomes clear when the area under the peaks in the two composites is compared as shown in Figure 6.60. This is simply because of the difference in the Al content between the two alloys.
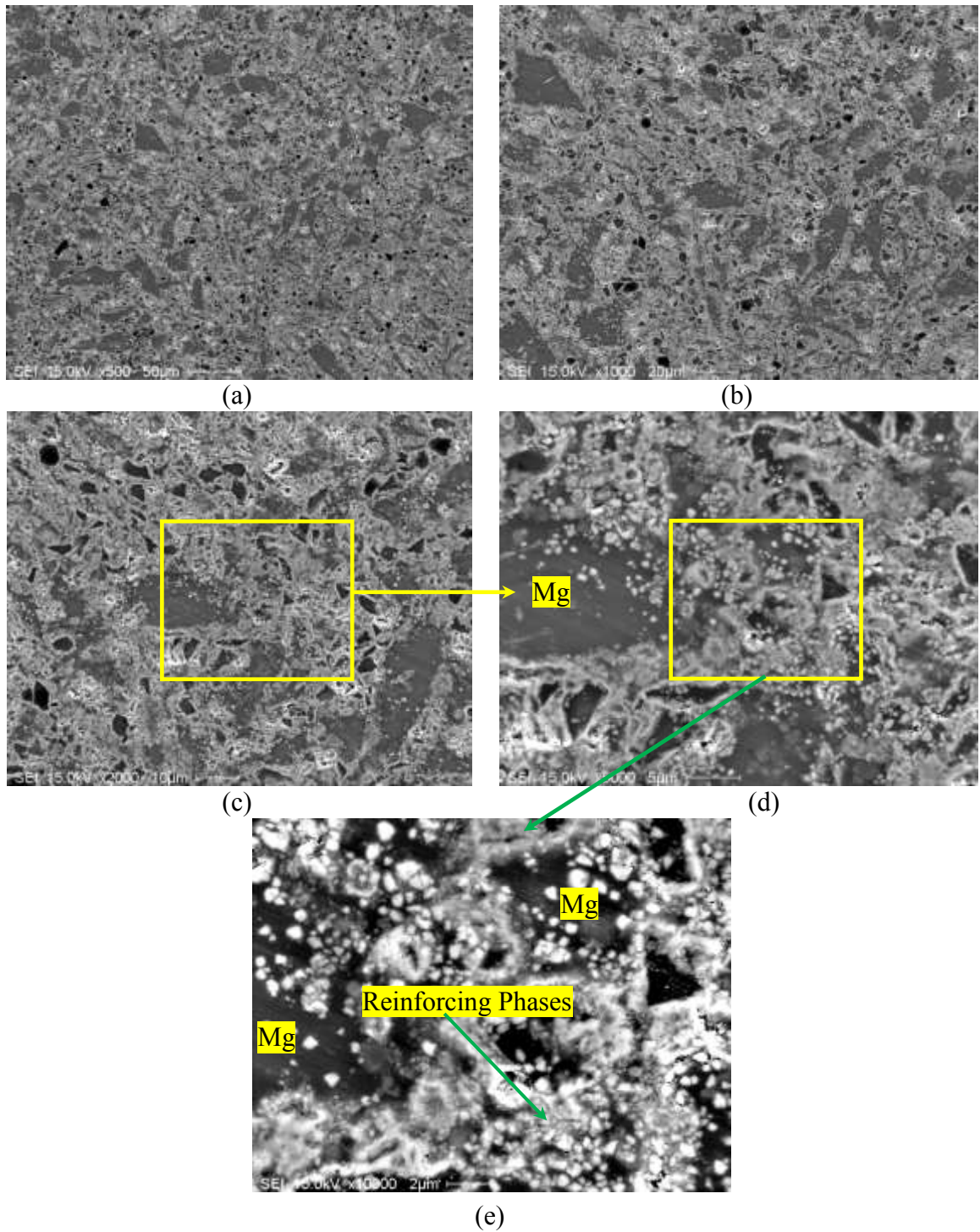
Figure 6.58 SEM microstructure of the AM60B alloy MMCs fabricated using a 25 wt.% MgH_2-($3Ti$-B_4C) preform with 70% *RD* at 900ºC for 1.5 h

SEI Image

Mg-Kα image

Ti-Kα image

B -Kα image

Al-Kα image
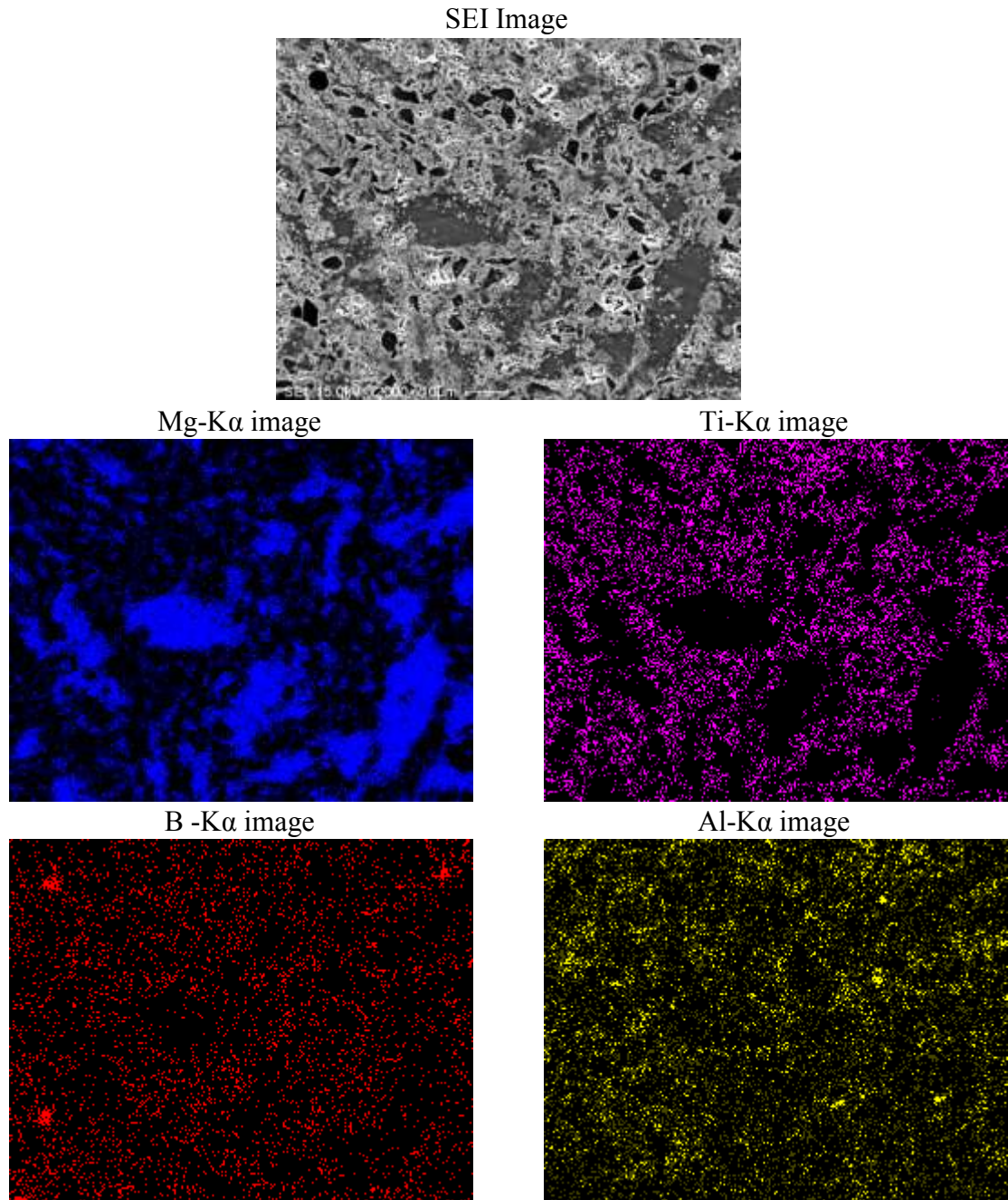
Figure 6.59 SEM microstructure and EDS elemental mapping of the $TiCx$-TiB_2/AM60B composites synthesized at 900ºC for 1.5 h using 25 wt.% MgH_2-(3Ti-B_4C) preform with 70% *RD*
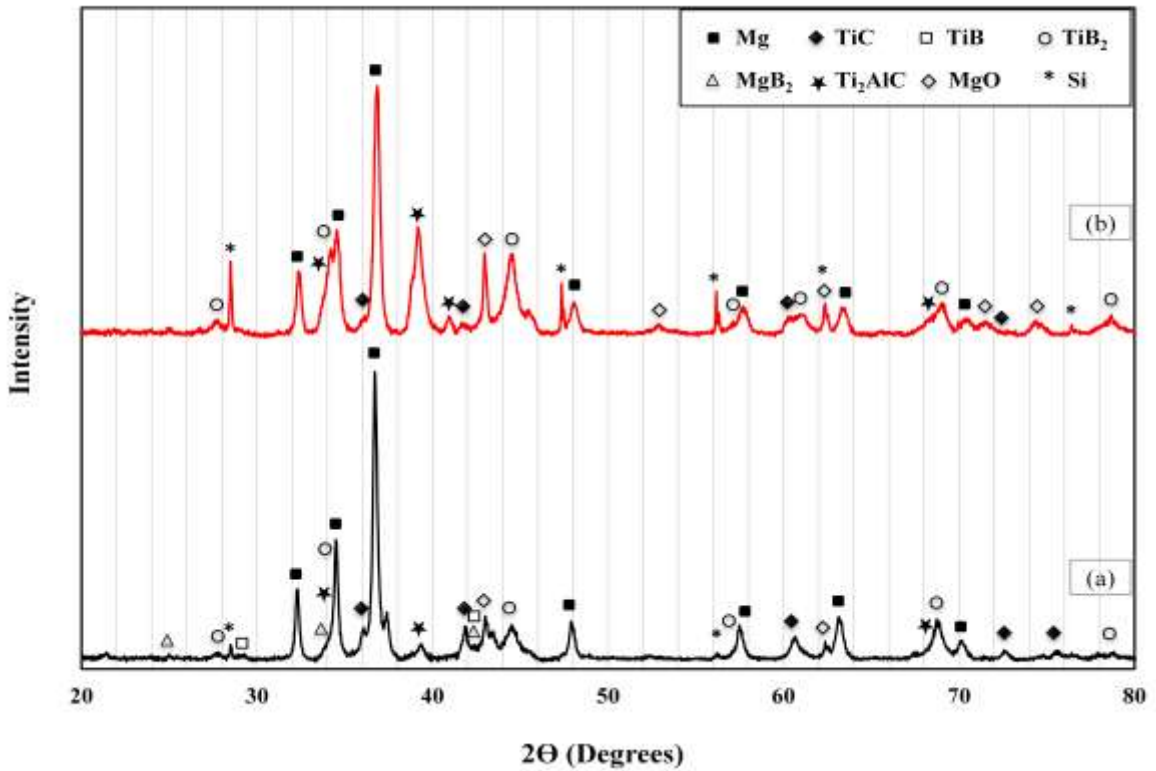
Figure 6.60 XRD pattern of the Mg alloy MMCs fabricated at 900ºC for 1.5 h using a 25 wt.% MgH$_2$-(3Ti-B$_4$C) preform with different matrices (a) AM60B and (b) AZ91D Matrix

The study of the fabrication of composites using MgH$_2$-(3Ti-B$_4$C) preform with AZ91D and AM60B alloy as a matrix was presented. However, what was employed with AZ91D alloy has been applied with pure Mg using the same preform with different weight percentages of the MgH$_2$ powder.

It can be concluded that the percentage of reinforcing phases in the Mg matrix can be tailored by adding different amounts of MgH$_2$ powder to the 3Ti-B$_4$C preform.

Chapter 7

Characterization of the TiC-TiB$_2$/Mg Matrix Composites

7.1 Density and Porosity of the Composite

The bulk density and apparent porosity of the composite samples are measured using Archimedes' principle according to ASTM standard C20-00 [138] as described in Chapter 4.4.1 while the theoretical density was estimated based on the rule of mixtures (ROM) [154]. In practice, Equation 4.3 cannot be used realistically because of the presence of intermediate phases and also due to inaccuracy of volume fraction measurements from XRD.

The bulk density and the apparent density of the fabricated composites using pure Mg, AM60B and AZ91D alloys as a matrix have been measured. However, in this section, the focus is on the results of the AZ91D alloy composites.

The bulk density and apparent porosity of the TiC$_x$-TiB$_2$/AZ91D composites fabricated at the optimal processing parameters, 900ºC and 1.5 h using a 3Ti-B$_4$C preform and after adding different weight percentages of MgH$_2$ powder to the preform were measured. The results are presented in Table 7.1 and shown in Figure 7.1 compared with the density of the unreinforced AZ91D Mg alloy and that of TiC.

It is worth noting that the porosity calculated from Archimedes' principle represents only the open porosity.

The results reveal that the density of the infiltrated composites decreases with increasing MgH$_2$ powder content in the preform due to the increased Mg matrix content.

163

Table 7.1 Bulk density and apparent porosity of the TiC_x-TiB_2/AZ91D composites

MgH$_2$ content in the preform (wt.%)	Reinforcing phases (vol. %)	Bulk density, g/cm^3 ASTM C20-00 [138]	Apparent porosity (%)
0	~ 40	3.19 ±0.12	0.082 ±0.008
10	~ 30	2.78 ±0.088	0.061 ±0.004
25	~ 22	2.56 ±0.066	0.046 ±0.009
40	~ 12	2.30 ±0.045	0.180 ±0.012

[*] The balance is Mg matrix and residual phases and/or MgO
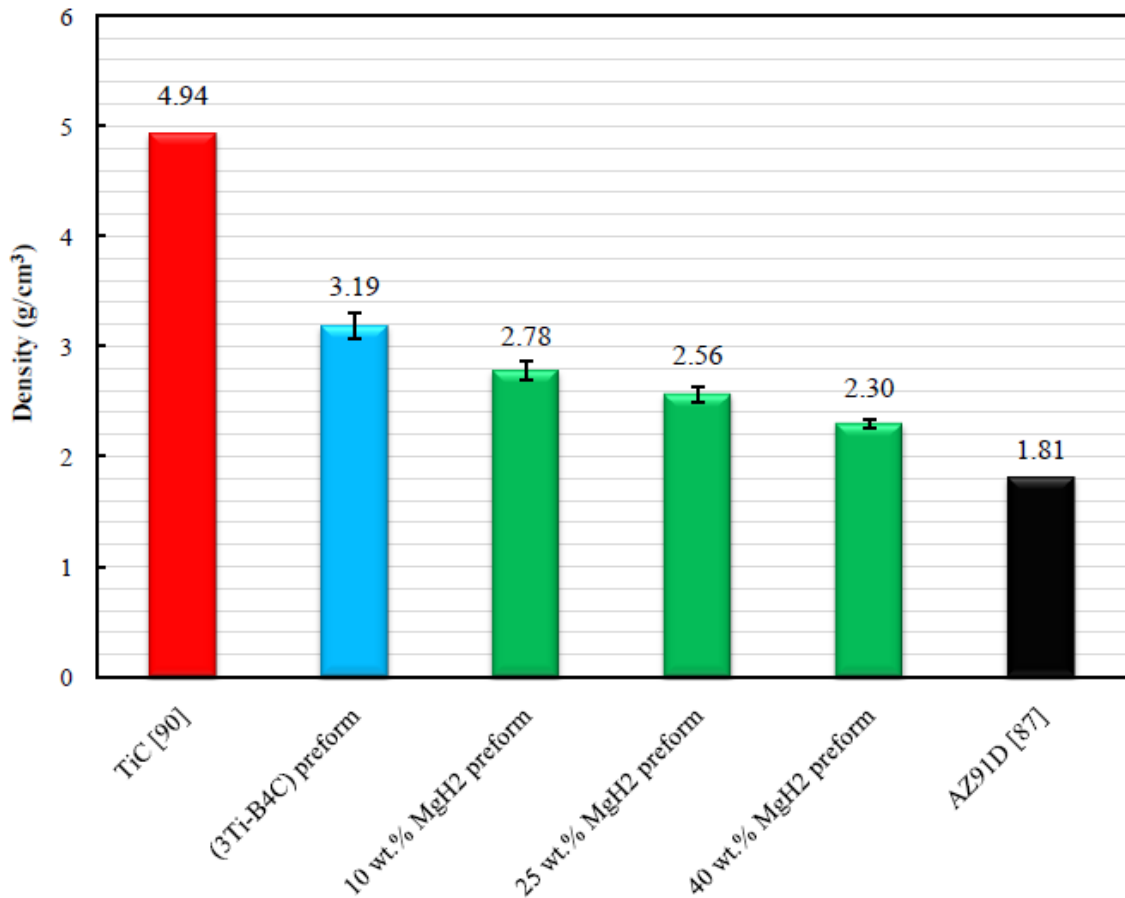
Figure 7.1 Comparison of various bulk density values

Based on these results, the density of the composites can be tailored by controlling the weight percentages of the MgH$_2$ powder added to the 3Ti-B$_4$C preform. For example, the density of TiC_x-TiB_2/AZ91D composites decreased by nearly 13%,

20% and 28% after adding 10 wt.%, 25 wt.%, and 40 wt.% MgH_2 powder to the 3Ti-B_4C preform, respectively.

Furthermore, the bulk density and apparent porosity of the TiC_x-TiB_2/AZ91D composite samples fabricated using 3Ti-B_4C and Mg-(3Ti-B_4C) preforms with 70% *RD* and different Mg powder weight percentages are presented in Table 7.2 and Figure 7.2 compared with the density of the unreinforced AZ91D Mg alloy and that of TiC. The results reveal that the density of the composites decreases with increasing Mg powder weight percentage in the preform due to the increased Mg matrix content.

Based on these results, the density of the composites can be tailored also by controlling the weight percentages of the Mg powder added to the 3Ti-B_4C preform. For example, the density of TiC_x-TiB_2/AZ91D composites decreased by nearly 11% and 17% after adding 10 wt.% and 25 wt.% Mg powder to the 3Ti-B_4C preform, respectively.

The results also show that the density of the composites fabricated using a preform containing Mg powder is higher than those after adding the same weight percentage of MgH_2 powder. As shown in Table 4.6, the density of magnesium is higher than that of MgH_2 which means a higher volume of MgH_2 than Mg for the same weight percent. Thus, the volume fraction of Mg in the composites using MgH_2 is higher than that using Mg powder in the preform.

Table 7.2 Bulk density and apparent porosity of TiC_x-TiB_2/AZ91D composites

Mg content in the preform (wt %)	Reinforcing phases (vol. %)	Bulk density, g/cm^3 ASTM C20-00 [138]	Apparent porosity (%)
0	~ 40	3.19 ±0.12	0.082 ±0.008
10	~ 33	2.84 ±0.08	0.073 ±0.015
25	~ 25	2.65 ±0.052	0.053±0.004

[*] The balance is Mg matrix and residual phases and/or MgO
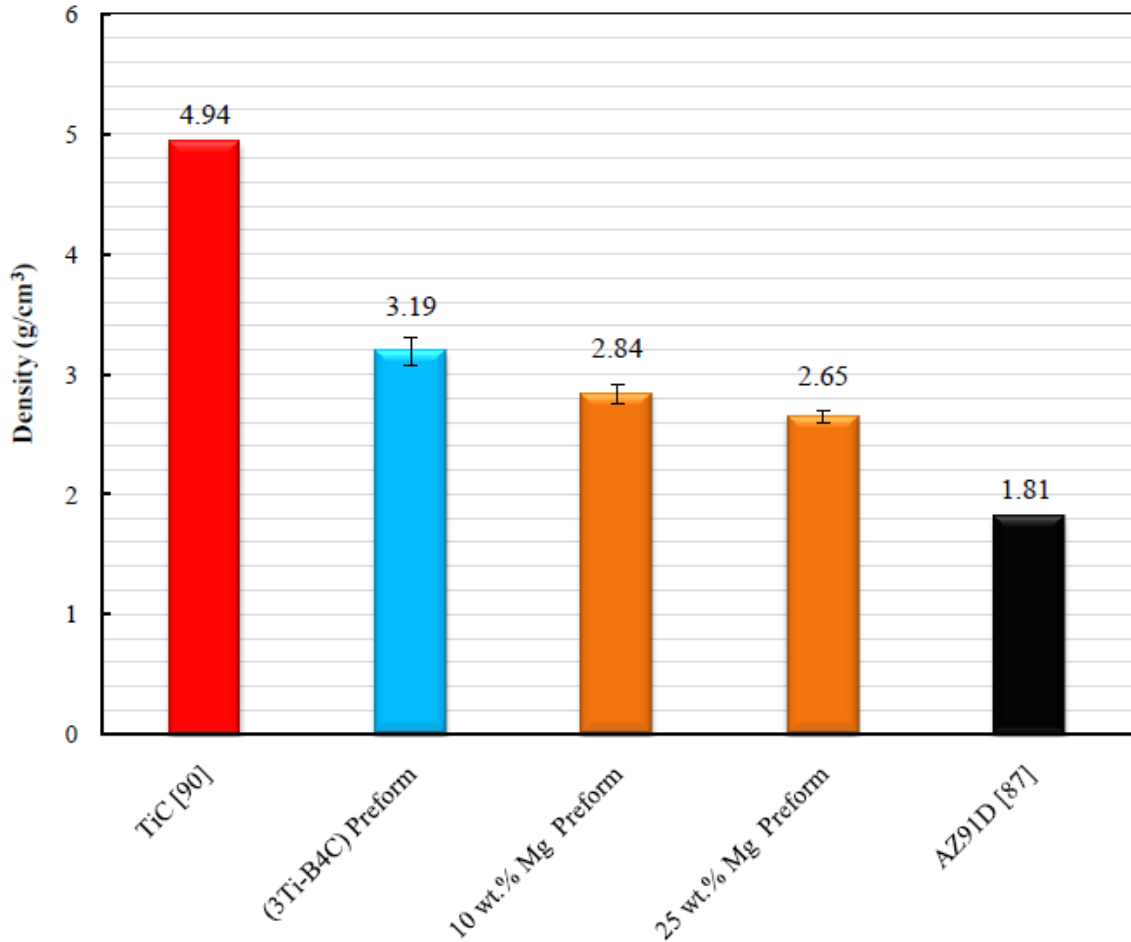
Figure 7.2 Comparison of various bulk density values

The calculated densities of the pure Mg and AM60B composites using Archimedes' principle are 3.01 ± 0.1 and 3.1 ± 0.116, respectively.

In summary, it is important to note that the density and porosity measurements revealed that sound composites with very low porosity have been fabricated at optimal processing parameters and this matches with the microstructural observations shown previously in Chapter 6. Also, it is clear that these fabricated composites are light-weight and their densities can be tailored by controlling the green compact relative density or the weight percentages of the Mg or MgH_2 powder added to the 3Ti-B_4C preform.

7.2 Compression Test Results

The compression behavior of the TiC$_x$-TiB$_2$/Mg composites fabricated at different processing parameters has been studied to obtain the parameters required to fabricate sound composites with improved mechanical properties. Furthermore, the compression behavior of the composites with different volume fractions of the reinforcing particles fabricated at these processing parameters has been investigated.

The engineering stress was obtained by dividing the axial force by the initial cross-sectional area of each sample. The axial strain was evaluated using two strain gages placed in the longitudinal direction as shown in Figure 7.3. Three tests of some samples have been performed to guarantee reliable results and to obtain the standard deviation.
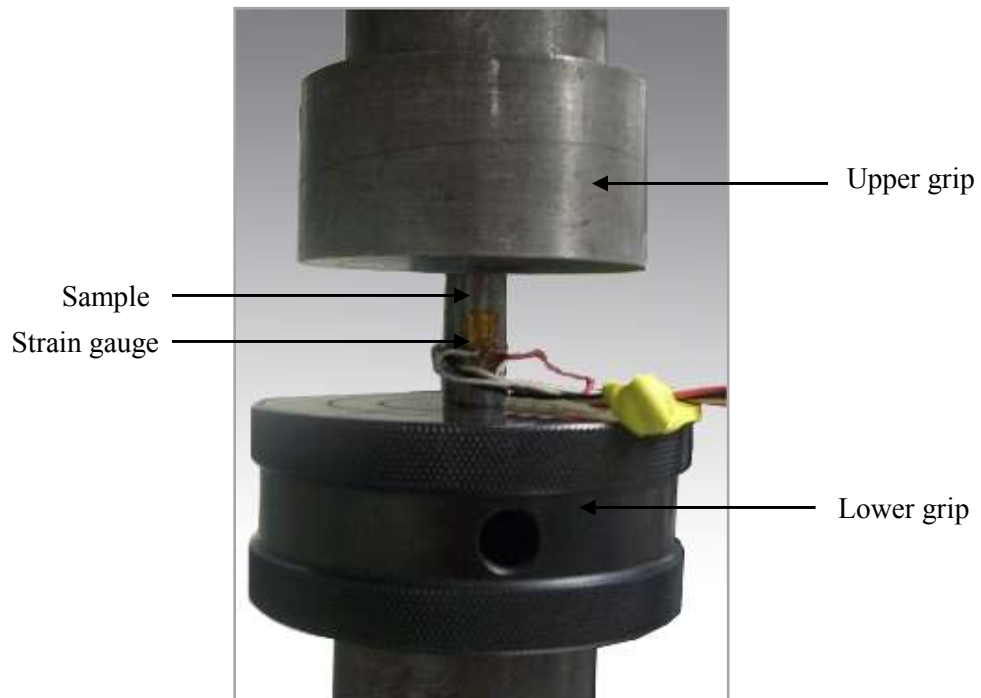
Figure 7.3 Digital photo of compression testing in the MTS machine

7.2.1 Processing Parametric Study

As discussed earlier, the processing parameters such as temperature, holding time and green compact *RD* have a great effect on the *in-situ* reaction mechanism and, therefore, on the fabrication of Mg matrix composites via an *in-situ* reactive infiltration technique. In this section, the effect of these processing parameters on compression test results is investigated focusing on the AZ91D composites. This study was conducted by changing one factor at a time.

7.2.1.1 Effect of Processing Temperature on the Compression Behavior of the Fabricated Composites

The influence of the processing temperature on the compression behavior of the fabricated composites has been studied by testing the composite samples fabricated at different processing temperatures of 800, 850 and 900ºC. These composites were fabricated by using a 3Ti-B$_4$C preform with 70% *RD* at 1.5 h holding time. The compression test was done at room temperature.

Typical stress-strain curves obtained for these composite samples are shown in Figure 7.4. It can be observed that the compressive strength and Young's modulus of the fabricated composite samples are affected significantly by the processing temperature. The average compressive strength, Young's modulus and the percentage of height reduction of the composites fabricated at different processing temperatures are listed in Table 7.3.

The moduli were calculated from the slope of the tangent at a 160 MPa stress level. Moreover, to confirm the moduli values, they were calculated from the linear slope of the stress-strain region between 5 and 25 MPa. For example, for the composite

fabricated at 900ºC for 1.5 h, it corresponds to a strain of about 0.0127% (127 micro-strains) and 25 MPa, as shown in Figure 7.5.
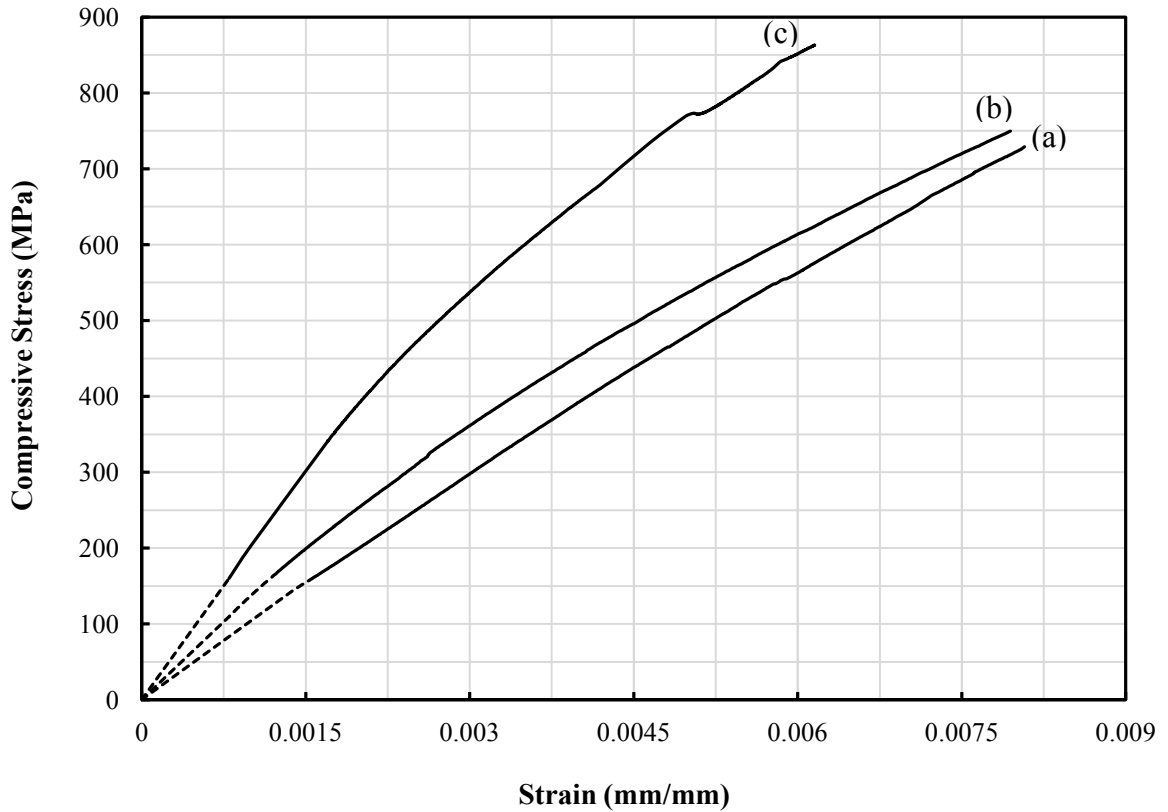
Figure 7.4 Stress-Strain Curves of the TiC_x-TiB_2/AZ91D composites fabricated at different processing temperatures (a) 800ºC, (b) 850ºC, and (c) 900ºC

Table 7.3 Compression test results of AZ91D alloy and TiC_x-TiB_2/AZ91D composites fabricated at different processing temperatures

Sample	Processing Temperature (ºC)	Young's Modulus, E_{T160}, (GPa)	Compressive Strength (MPa)	Height reduction (%)
AZ91D alloy	-----	45	241	3.13
TiC_x-TiB_2/AZ91D Composites	800	104	729	0.81
	850	137	750	0.79
	900 *	195 ±15.69	878 ±19.47	0.66 ±0.04

*Data for this temperature is based on 3 samples.

It is clear that the compressive strength and Young's modulus increased with increasing the processing temperature while the % height reduction decreased. Poor ductility of the composites can be attributed to the presence of brittle ceramic phases, TiC_x and TiB_2, because they prevent the plastic deformation and block the dislocation motion.
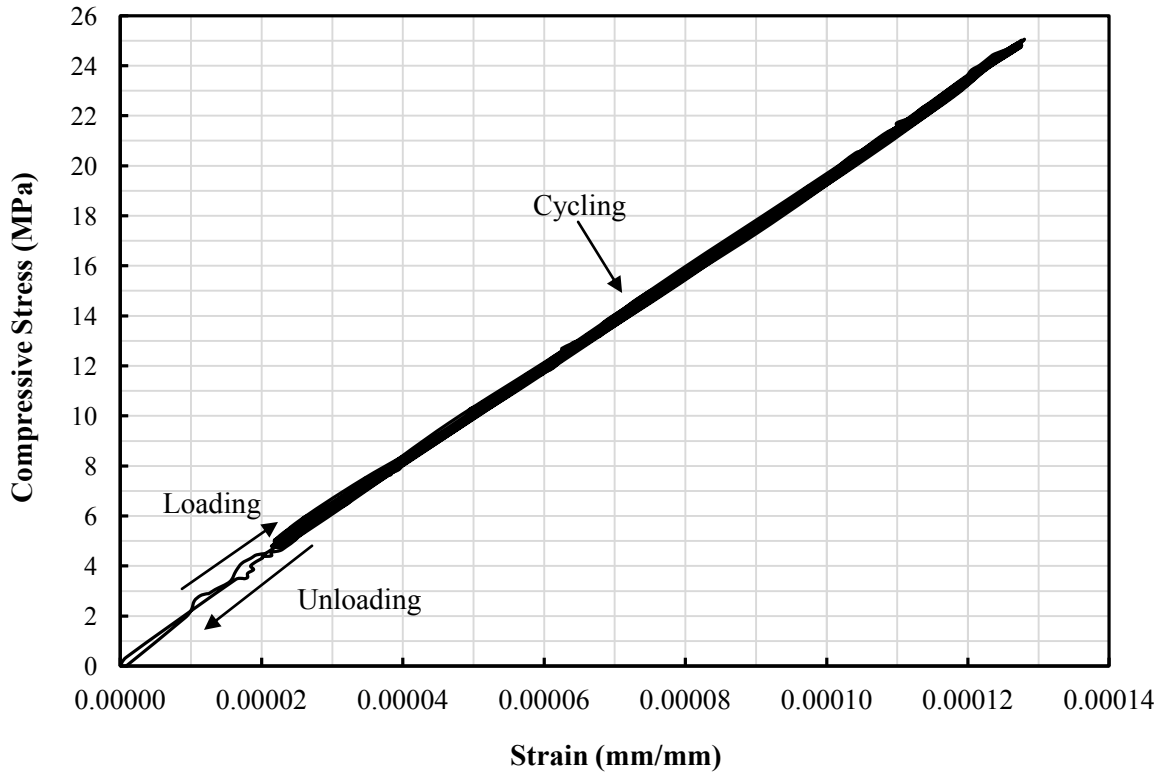
Figure 7.5 Initial region of compression stress-strain curve for the TiC_x-TiB_2/AZ91D composite fabricated at 900°C for 1.5 h

Based on the obtained results, it can be observed that there is a strong relation between the processing temperature and the mechanical properties obtained from the compression test. The effect of the processing temperature on the mechanical properties is attributed to its effect on the *in-situ* reaction and therefore on the volume fractions of the reinforcing phases.

170

According to the volume percentages of the phases from Retvield analysis, shown in Figure 7.6, the highest volume fractions of the reinforcing phases, TiC_x and TiB_2, were found in the sample fabricated at 900°C with very small retained boron carbide and residual intermediate phases compared with those fabricated at 800 or 850°C. Therefore, the composites fabricated at 900°C had the highest compressive strength and Young's modulus but the lowest ductility.
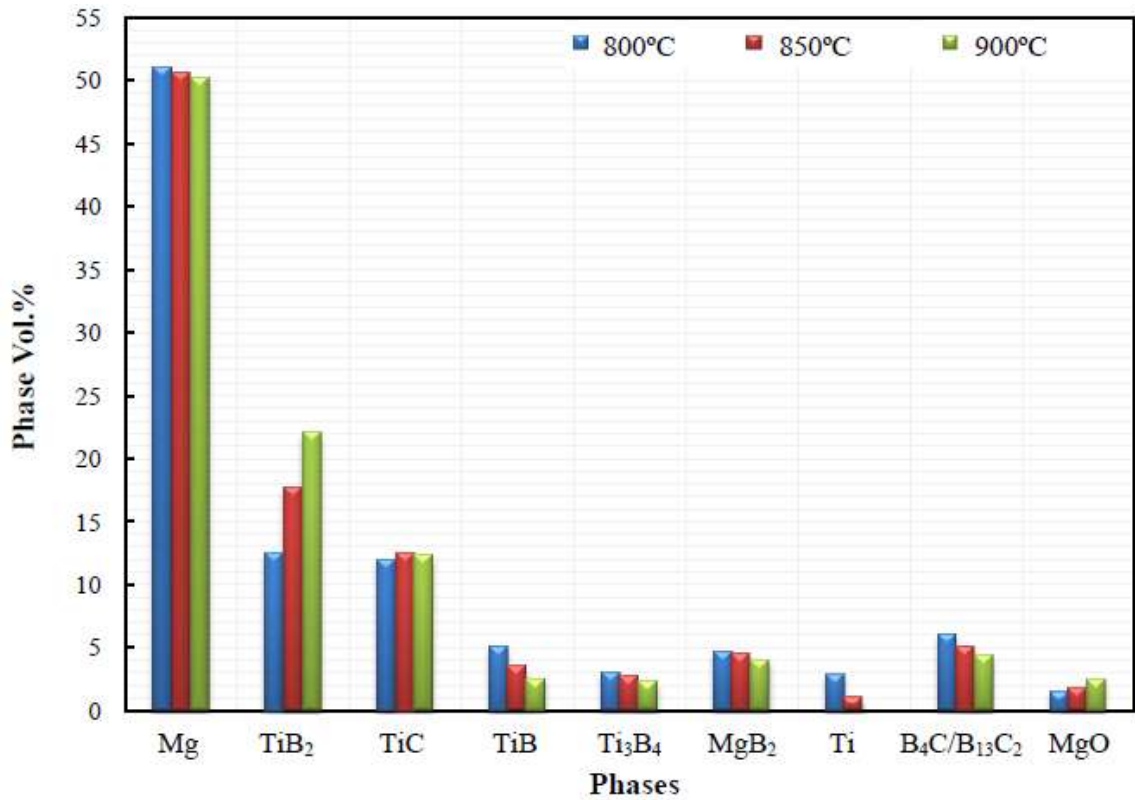
Figure 7.6 Phases volume percentage of the AZ91D alloy MMCs fabricated using a 3Ti-B_4C preform with **70%** *RD* for 1.5 h and different processing temperatures: 800, 850 and 900°C

In general, the strength of the magnesium alloys increased with the addition of the reinforcing phases where the dispersion of fine and hard particles into the matrix blocks the dislocation motion and thus strengthens the material. In this study, the change in the

mechanical properties of the fabricated composites at different processing temperatures is due to the effect of the temperature on the *in-situ* reaction and thereupon the formed reinforcing phases.

7.2.1.2 Effect of Holding Time on the Compression Behavior of the Fabricated Composites

To investigate the effect of the holding time on the compression behavior of the fabricated composites, the compression test has been performed on composites samples which have been fabricated using 3Ti-B$_4$C preforms with 70% *RD* at 900°C for different holding times: 1 h, 1.5 h and 3 h. Typical stress-strain curves for these composites are shown in Figure 7.7.
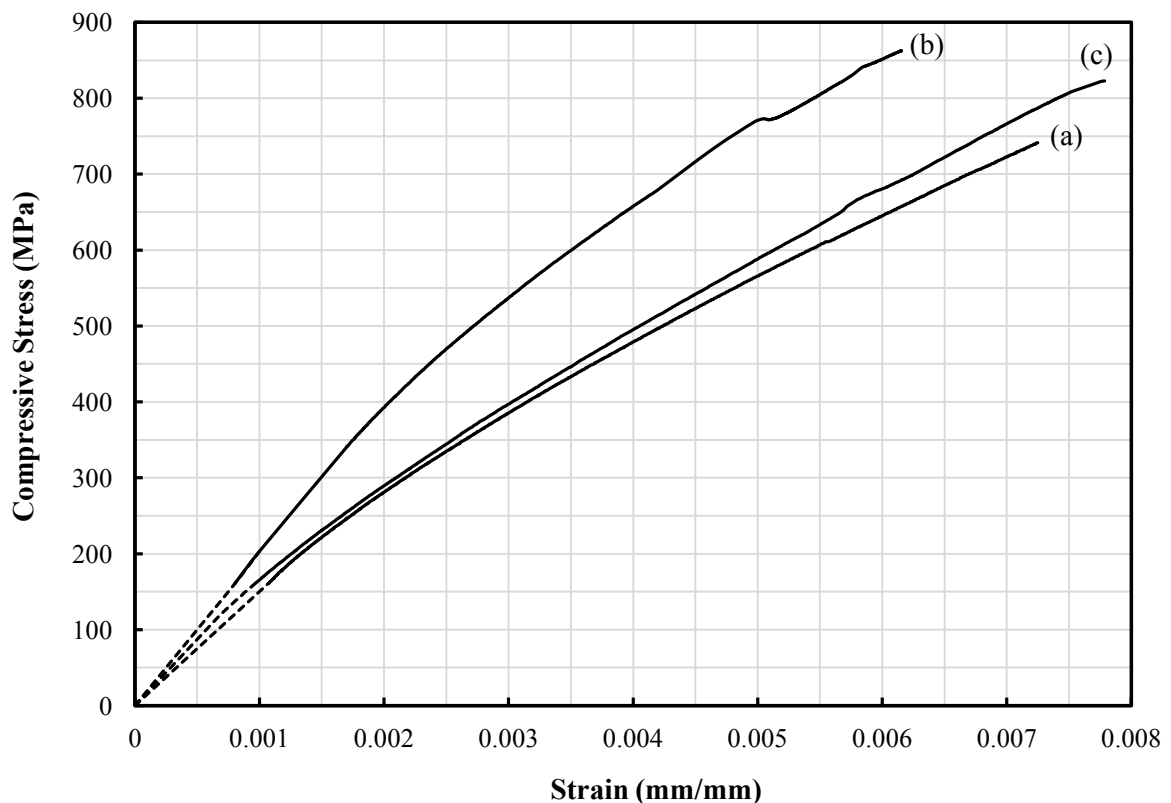
Figure 7.7 Stress-strain curves of the TiC$_x$-TiB$_2$/AZ91D composites fabricated at 900°C and for different holding times (a) 1 h, (b) 1.5 h, and (c) 3 h

172

It can be observed that the compressive strength and Young's modulus of the fabricated TiC_x-TiB_2/AZ91D composites are affected significantly by the holding time. The average compressive strength, Young's modulus and the percentage of height reduction of the composite samples fabricated at different holding times are listed in Table 7.4.

Table 7.4 Mechanical properties of the AZ91D alloy and TiC_x-TiB_2/AZ91D composites fabricated at different holding times

Sample	Holding Time (h)	Young's Modulus, E_{T160}, (GPa)	Compressive Strength (MPa)	Height reduction (%)
AZ91D alloy	-----	45	241	3.13
(TiC-TiB_2)/AZ91D Composites	1	144 ±9.06	737 ±25.26	0.72 ±0.035
	1.5	195 ±15.69	878 ±19.47	0.66 ±0.040
	3	161 ±7.81	826 ±26.80	0.76 ±0.063

Again, the moduli were calculated from the slope of the tangent at a 160 MPa stress level and from the linear slope of the stress-strain region between 5 and 25 MPa as well. For example, Figure 7.8 shows the initial region of the stress-strain curve for the composite fabricated at 900ºC for 3 h. It corresponds to a strain of about 0.015% (150 micro-strains) and 25 MPa.

The holding time plays an important role in the fabrication of the composites and therefore it can significantly affect their mechanical properties. The compression test results revealed that the composite sample fabricated at 1.5 h holding time has a higher compressive strength and Young's modulus than those of the samples fabricated at 1 h or 3 h.

173
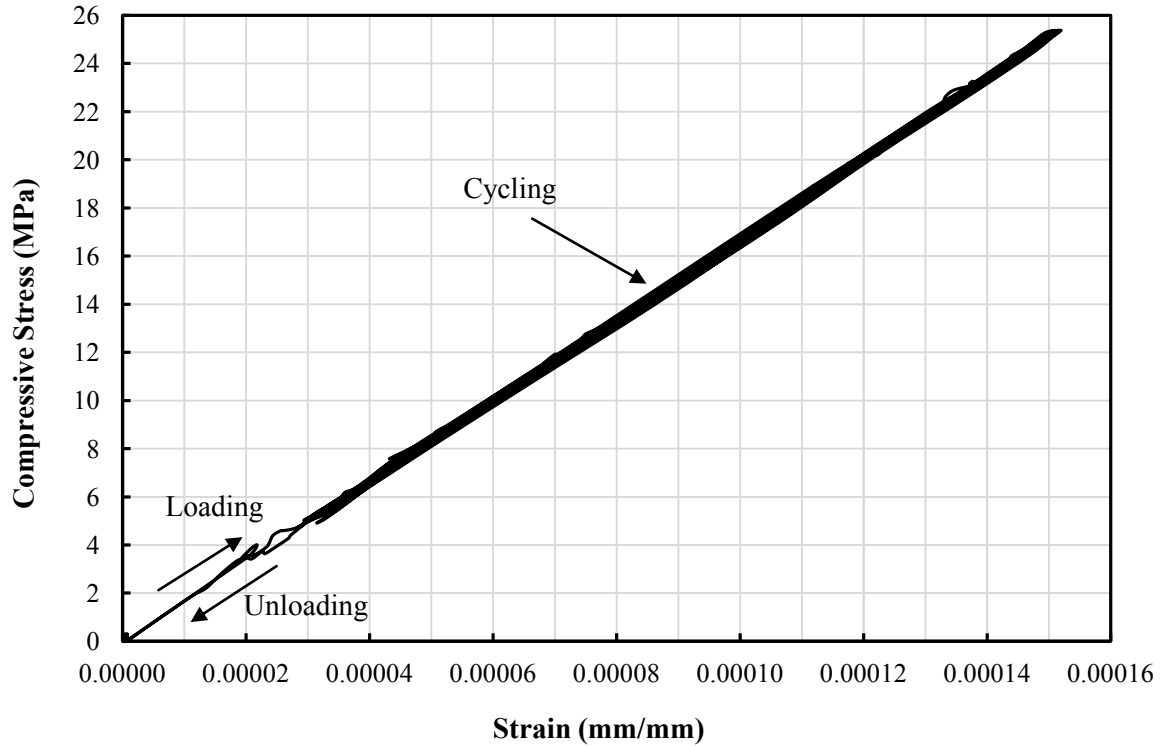
Figure 7.8 Initial region of compression stress-strain curve for the TiC_x-TiB_2/AZ91D composite fabricated at 900°C for 3 h holding time

As mentioned in Section 6.2, for composite samples fabricated at 900°C for 1.5 or 3 h, the required equilibrium phases, TiC_x and TiB_2, formed with very small amounts of residual boron carbide and intermediate phases such as TiB and MgB_2. However, the formation of the ternary compound (Ti_2AlC) at 3 h adversely affects the compressive strength and the Young's modulus of the composite while at the same time can raise its ductility. On the other hand, the residual boron carbide and intermediate phases such as TiB and MgB_2 for composites fabricated at 1 h are higher than those at 1.5 h or 3 h. For this reason, it has a lower compressive strength and Young's modulus than those of composites fabricated at 1.5 h or 3 h. Based on these results, it can be said that the composites fabricated at 900°C for 1.5 h are stiffer and stronger than those fabricated at 900°C for 1 or 3 h but they are more brittle.

174

7.2.1.3 Effect of Green Compact Relative Density on the Compression Behavior of the Fabricated Composites

The influence of the preform relative density (*RD*) on the compression behavior of the fabricated composites was investigated by testing different composite samples which have been fabricated at 900ºC for 1.5 h using 3Ti-B$_4$C preform with different relative densities. Typical stress-strain curves for composite samples fabricated using preforms of 60 and 70% *RD* are shown in Figure 7.9.
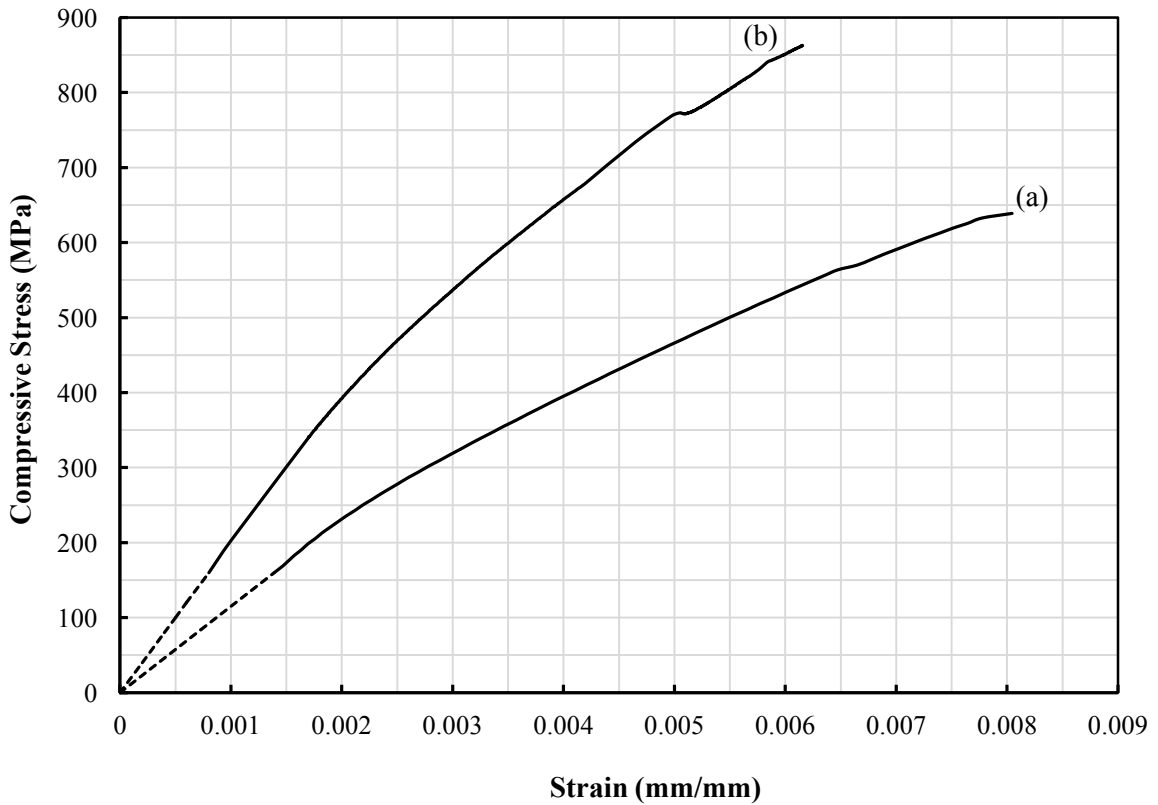
Figure 7.9 Stress-strain curves of the TiC$_x$-TiB$_2$/AZ91D composites fabricated using (3Ti-B$_4$C) preforms with different relative densities (a) 60% and (b) 70%

The results revealed the great effect of the preform RD on the compressive strength and Young's modulus of the fabricated TiC_x-TiB_2/AZ91D composites. Table 7.5 lists the average compressive strength, Young's modulus and the percentage of height reduction where the moduli were calculated from the slope of the tangent at a 160 MPa stress level.

Table 7.5 Compression test results of the AZ91D alloy and TiC_x-TiB_2/AZ91D composites fabricated using $3Ti$-B_4C preforms with different relative densities

Sample	Preform RD (%)	Young's Modulus, E_{T160}, (GPa)	Compressive Strength (MPa)	Height reduction (%)
AZ91D alloy	-----	45	241	3.13
(TiC-TiB$_2$)/AZ91D Composites	60	115	639	0.80
	70 *	195 ±15.69	878 ±19.47	0.66 ±0.04

* Data for this preform RD is based on 3 samples.

The green compact RD plays an important role in the fabrication of the composites and hence it can significantly affect their mechanical properties. The compression test results reveal that the composite sample fabricated using 70% green compact relative density (RD) has a higher compressive strength and Young's modulus than those fabricated using 60% green compact RD. As mentioned in Section 6.3, the higher the green compact RD, the higher the contact area between B_4C and Ti particles thus accelerating the reaction between them through a short diffusion path and hence affecting the microstructure and the formed phases in the system.

176

In summary, considering that the compressive strength and Young's modulus of the unreinforced AZ91D matrix are ~ 240 MPa and 45 GPa, respectively, the compressive strength and Young's modulus of the composites fabricated using a 3Ti-B$_4$C preform with 70% *RD* at 900ºC for 1.5 h increased by nearly 265% and 333%, respectively. However, the composites are brittle due to the high volume fractions of the reinforcing phases of the hard ceramic particles.

7.2.2 Compression Behavior of Composites Fabricated using MgH$_2$-(3Ti-B$_3$C) Preform

In an attempt to improve the ductility of the fabricated composites by increasing the volume percentage of the Mg or Mg alloy matrix, composite samples using MgH$_2$-(3Ti-B$_4$C) preforms with 70% *RD* were fabricated at the optimal processing temperature and holding time, 900ºC and 1.5 h. Different weight percentages of MgH$_2$ powder in the preform have been used while the molar ratio of Ti:B$_4$C was kept at 3:1. This study focused on the AZ91D matrix composites but with some examples of the results of pure Mg and AM60B matrix composites.

7.2.2.1 Mechanical Properties of the TiC$_x$-TiB$_2$/AZ91D Composites

Typical compression behavior of the TiC$_x$-TiB$_2$/AZ91D composites reinforced with different volume percentages of the reinforcing phases due to the use of MgH$_2$ powder in the 3Ti-B$_4$C preform compared with that of the unreinforced AZ91D alloy is given in Figure 7.10.

The compression test results for these composites are summarized in Table 7.6 and represented graphically in Figure 7.11.
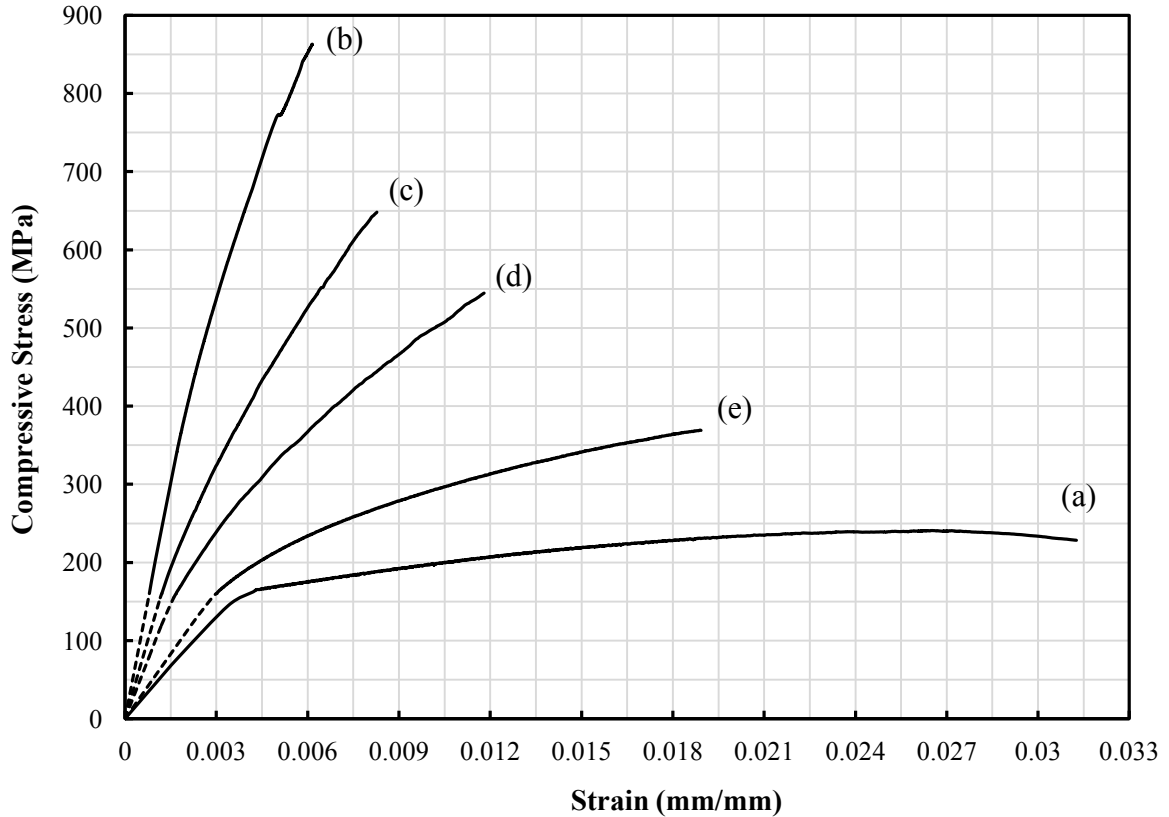
Figure 7.10 Stress-strain curves of (a) the AZ91D alloy and the composites fabricated using MgH_2-($3Ti$-B_4C) preform with different MgH_2 contents: (b) 0 wt.%, (c) 10 wt.%, (d) 25 wt.%, and (e) 40 wt.%

It is clear that the strength and stiffness of the composites increase in response to the higher content of the reinforcing phases, TiC_x and TiB_2. The compression test results show that the composites fabricated using a $3Ti$-B_4C preform are stiffer and stronger than those fabricated after adding MgH_2 powder to the preform. On the other hand, the ductility of the composites was improved substantially by nearly 26%, 81%, and 187% by adding 10 wt.%, 25 wt.%, and 40 wt.% MgH_2 powder to the $3Ti$-B_4C preform, respectively. This is due to the increase of the Mg matrix volume fraction in the fabricated composites compared to the volume fractions of the reinforcing phases.

178

Table 7.6 Compression test results of the AZ91D alloy and TiC_x-TiB_2/AZ91D composites fabricated using MgH_2-(3Ti-B_4C) preform with different MgH_2 contents

Sample	MgH_2 content in the preform	Reinforcing phases (vol. %)	Young's Modulus, E_{T160}, (GPa)	Compressive Strength (MPa)	Height reduction (%)
AZ91D	-----	-----	45	241	3.13
TiC_x-TiB_2/ AZ91D Composites	0 wt.%	~ 40	195 ±15.69	878 ±19.47	0.66 ±0.040
	10 wt.%	~ 30	134	648	0.83
	25 wt.%	~ 22	110 ±10.01	540 ±14.55	1.19 ±0.068
	40 wt.%	~ 12	55	369	1.89
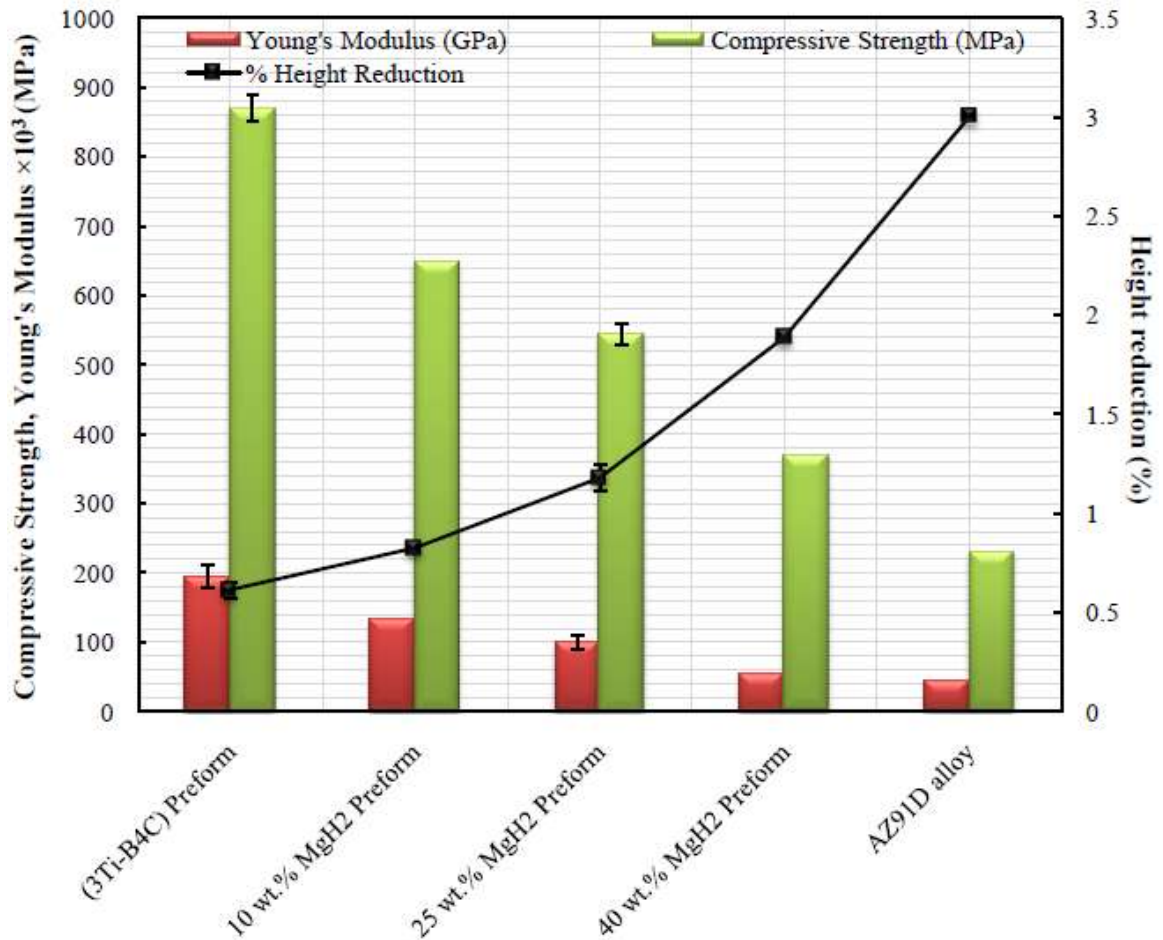
Figure 7.11 Compression test results of the AZ91D alloy and the composites fabricated using an MgH_2-(3Ti-B_4C) preform with different MgH_2 weight percentages

179

The average compressive strength and Young's modulus of the fabricated composites decreased from ~ 878 MPa and 195 GPa, respectively with 0 wt.% MgH$_2$ in the preform to ~ 370 MPa and 55 GPa, respectively when 40 wt.% MgH$_2$ powder is added to the preform. This means that the strength and stiffness decreased by about 58% and 72%, respectively after adding 40 wt.% MgH$_2$ while the ductility was improved by about 187%.

It can be concluded that although the compressive strength and stiffness of the fabricated composites decreased significantly by adding MgH$_2$ powder to the preform, their ductility was significantly improved. Hence, the mechanical properties of the composites can be tailored by controlling the amount of MgH$_2$ addition in the MgH$_2$-(3Ti-B$_4$C) preform.

7.2.2.2　Mechanical Properties of the TiC$_x$-TiB$_2$/AM60B Composites

The same scenario of the effect of the volume fractions of the reinforcing phases on the mechanical properties of AM60B composites by adding different weight percentages of MgH$_2$ to the 3Ti-B$_4$C preform has been obtained. The compression behavior of the TiC$_x$-TiB$_2$/AM60B composites reinforced with different volume fractions of the reinforcing phases using a 3Ti-B$_4$C preform with and without 25 wt.% MgH$_2$ powder compared with that of the AM60B alloy is given in Figure 7.12. The compression test results are listed in Table 7.7 and represented graphically in Figure 7.13.

Figure 7.12 Stress-strain curves of (a) the AM60B alloy and the composites fabricated by adding different weight percentages of MgH_2 powder to the 3Ti-B$_4$C preform: (b) 0 wt.% and (c) 25 wt.%

Table 7.7 Compression test results of the AM60B alloy and the TiC$_x$-TiB$_2$/AM60B composites fabricated using a preform with and without 25 wt.% MgH_2

Sample	MgH_2 content in the preform	Young's Modulus, E_{T160}, (GPa)	Compressive Strength (MPa)	Height Reduction (%)
AM60B alloy	-----	44	195	5.25
TiC$_x$-TiB$_2$ /AM60B Composites	0 wt.%	144 ±8.37	788 ±10.91	1.01 ±0.08
	25 wt.%	90 ±8.30	516 ±15.10	1.6 ±0.10
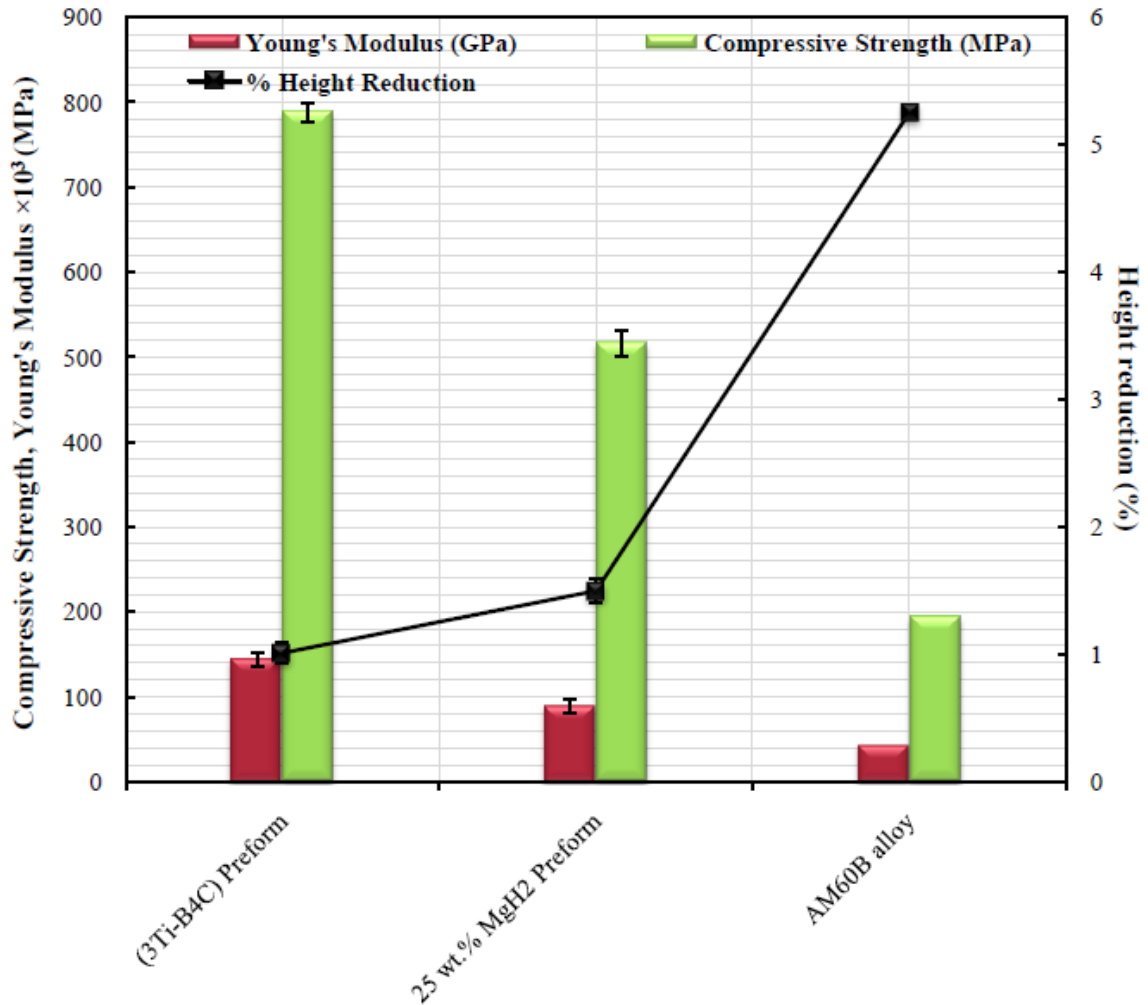
Figure 7.13 Compression test results of the AM60B alloy and the TiC_x-TiB_2/AM60B composites fabricated using a preform with and without 25 wt.% MgH_2

The test results show that the average compressive strength and Young's modulus of the fabricated composites decreased from about 788 MPa and 144 GPa with 0 wt.% MgH_2 in the preform to about 516 MPa and 90 GPa with 25 wt.% MgH_2 in the preform. This means that the strength and stiffness decreased by about 35% and 38%, respectively after adding 25 wt.% MgH_2 while the ductility was improved by about 58%.

In summary, considering that the compressive strength of the unreinforced AM60B matrix is 195 MPa, the compressive strength of the composite samples fabricated using a 3Ti-B$_4$C preform with 70% *RD* at 900°C for 1.5 h increased by nearly 304%.

7.2.2.3 Mechanical Properties of the TiC$_x$-TiB$_2$/ Pure Mg Composites

The compression behavior of the TiC$_x$-TiB$_2$/pure Mg composites reinforced with different volume fractions of the reinforcing phases using a 3Ti-B$_4$C preform with and without 25 wt.% MgH$_2$ powder compared with that for pure Mg is given in Figure 7.14.

Figure 7.14 Stress-strain curves of (a) pure Mg and the composites fabricated by adding different weight percentages of MgH$_2$ powder to the 3Ti-B$_4$C preform: (b) 0 wt.% and (c) 25 wt.%

As can be seen from this figure, the compressive strength and Young's modulus decreased by adding MgH_2 powder to the preform while ductility was improved as in the cases of the AM60B and AZ91D alloy composites. The compression test results are listed in Table 7.8 and graphically represented in Figure 7.15.

Table 7.8 Compression test results of pure Mg and the TiC_x-TiB_2/Mg composites fabricated using MgH_2-(3Ti-B_4C) preform with different amounts of MgH_2

Sample	MgH_2 content in the preform	Young's Modulus, E_{T160}, (GPa)	Compressive Strength (MPa)	Height reduction (%)
Pure Mg	-----	44	150	9.25
(TiC-TiB_2)/Mg Composites	0 wt.%	122 ±9.1	750 ±22	1.1 ±0.10
	25 wt.%	85 ±5.1	461 ±15.18	1.7 ±0.05

The results reveal that the average compressive strength and Young's modulus of the fabricated composites decreased from ~ 750 MPa and 122 GPa with 0 wt.% MgH_2 in the preform to ~ 461 MPa and 85 GPa when 25 wt.% MgH_2 is used in the preform. This indicates that the strength and stiffness decreased by about 38% and 30% after adding 25 wt.% MgH_2 while the ductility was improved by about 55%. It is important to note that the moduli were calculated from the slope of the tangent at the 160 MPa stress level.
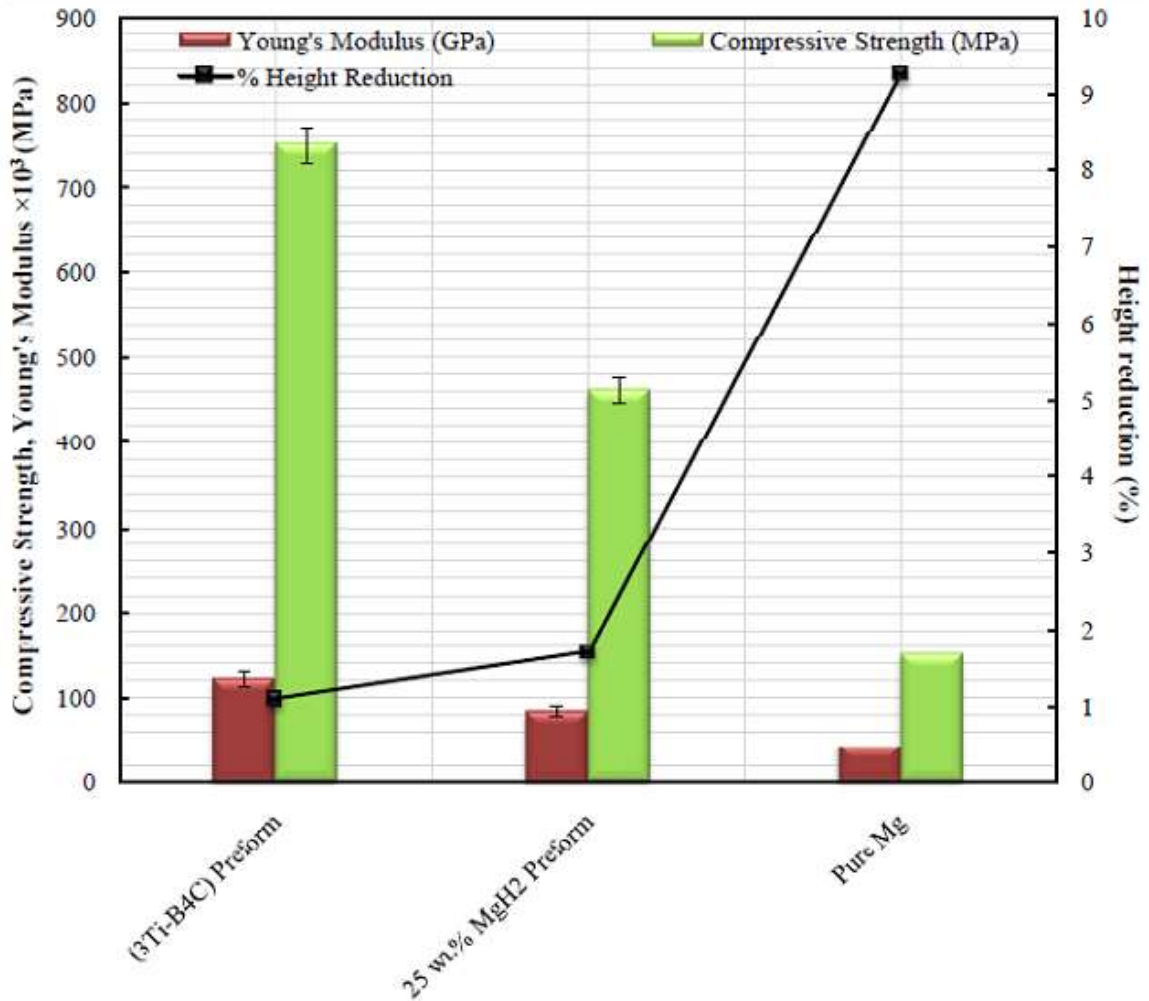
Figure 7.15 Compression test results of pure Mg and the TiC_x-TiB_2/pure Mg composites fabricated using a preform with and without 25 wt.% MgH_2

7.2.3 Compression Behavior of Composites Fabricated using Mg-(3Ti-B_3C) Preform

7.2.3.1 Mechanical Properties of the TiC_x-TiB_2/AZ91D Composites

The stress-strain curves of the TiC_x-TiB_2/AZ91D composites reinforced with different volume percentages of the reinforcing phases due to adding different weight percentages of Mg powder to the 3Ti-B_4C preform are shown in Figure 7.16.

185
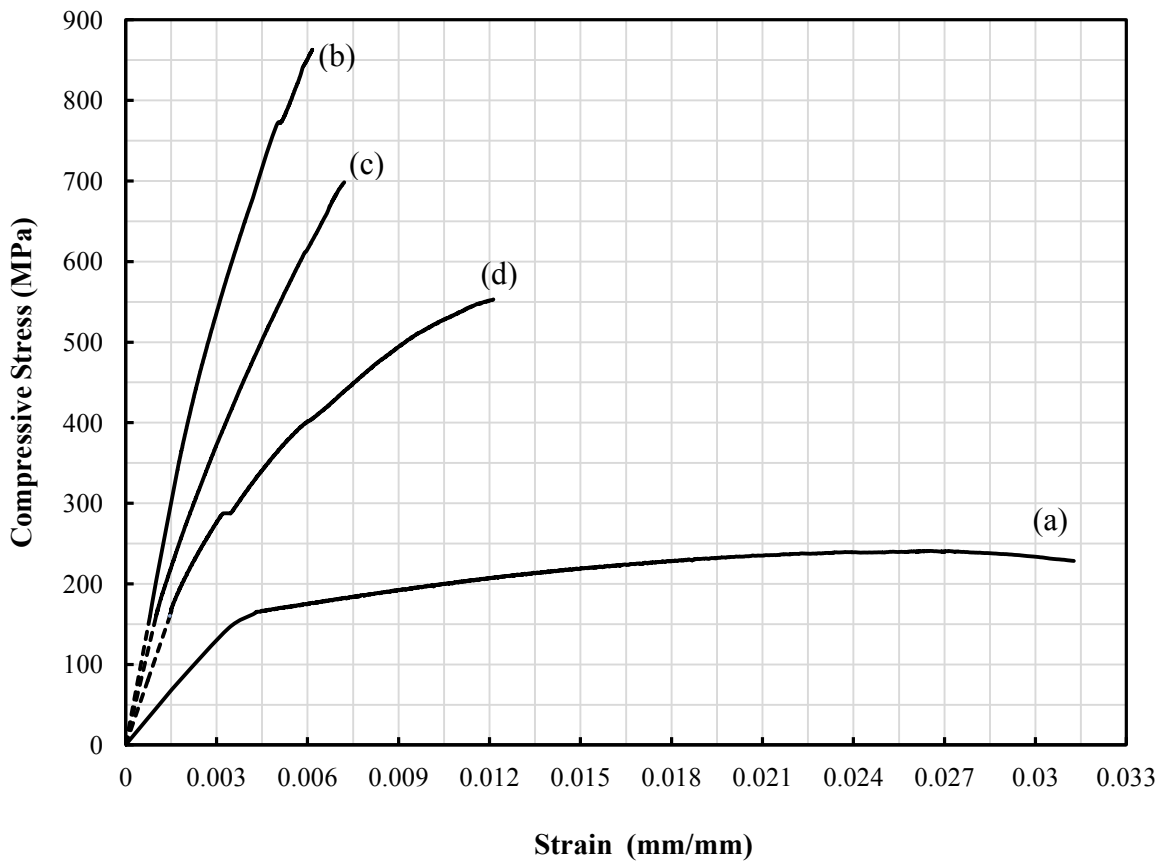
Figure 7.16 Stress-strain curves of (a) the AZ91D alloy and the composites fabricated using different percentages of Mg powder in the preform: (b) 0 wt.%, (c) 10 wt.%, and (d) 25 wt.%

The results shown in Figure 7.16 reveal that the compressive strength and Young's modulus decreased with increasing the weight percentage of Mg powder in the preform, i.e. decreasing the reinforcing phases, while the percentage of height reduction of the composite samples increased. Hence, the composite sample fabricated using a 3Ti-B$_4$C preform has the highest compressive strength and stiffness but on the other hand, it has the lowest ductility as listed in Table 7.9 and shown in Figure 7.17.

186

Table 7.9 Compression test results of the TiC_x-TiB_2/AZ91D composites fabricated using an Mg-(3Ti-B_4C) preform having different Mg powder contents

Sample	Mg content in the preform	Reinforcing phases (vol. %)	Young's Modulus, E_{T160}, (GPa)	Compressive Strength (MPa)	Reduction in height (%)
TiC_x-TiB_2	0 wt.%	~ 40	195 ±15.60	878 ±19.47	0.66 ±0.04
/AZ91D	10 wt.%	~ 33	150	699	0.71
Composites	25 wt.%	~25	132 ±10.17	550 ±10	1.14 ±0.02
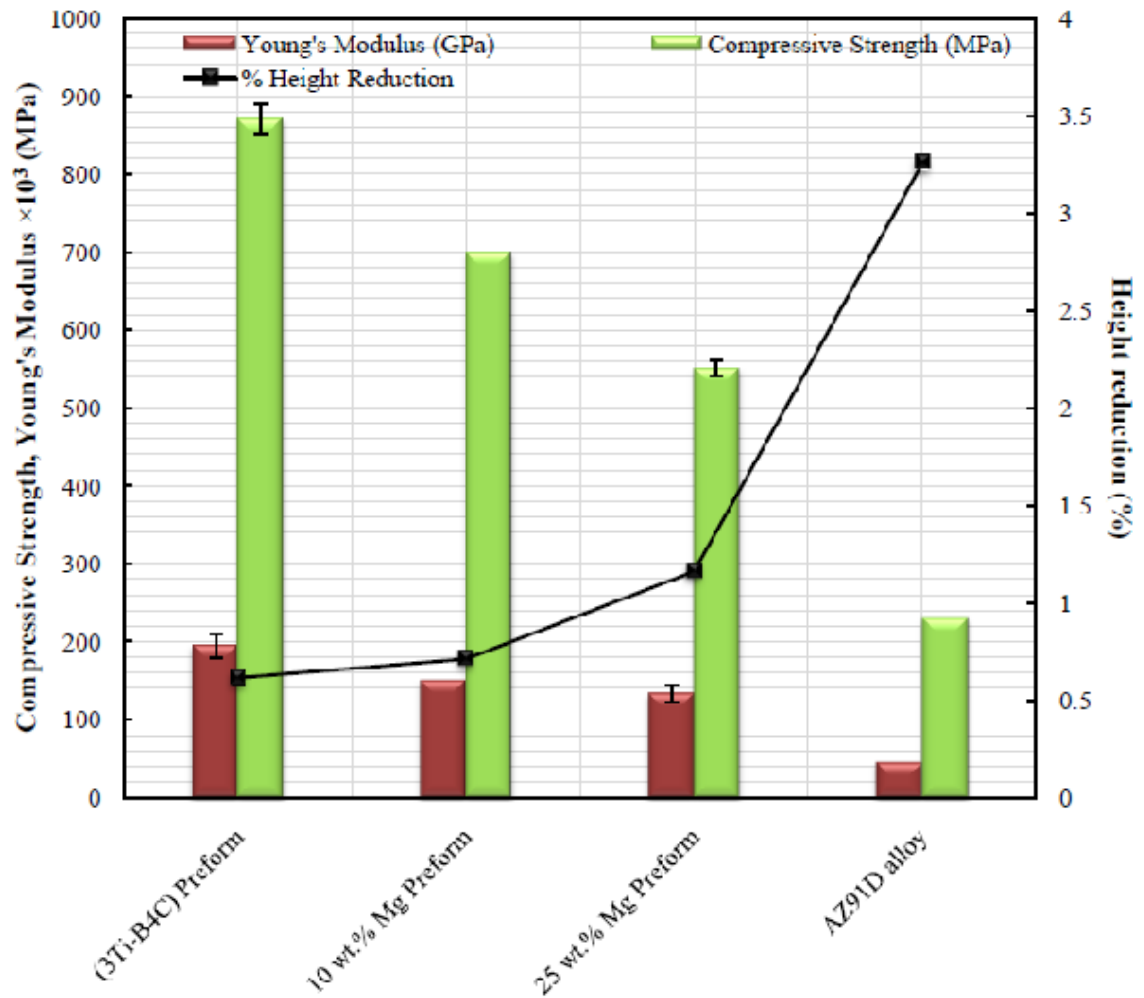
Figure 7.17 Compression test results of the AZ91D alloy and the composites fabricated by adding different weight percentages of Mg powder to the 3Ti-B_4C preform

As in case of the composites fabricated using MgH_2 powder in the preform, the results reveal that the composites fabricated using a $3Ti-B_4C$ preform are stiffer and stronger than those fabricated after adding Mg powder to the preform. For example, the average compressive strength and Young's modulus decreased from $\sim$ 878 MPa and $\sim$ 195 GPa with 0 wt.% Mg powder in the preform to $\sim$ 550 MPa and $\sim$ 132 GPa with 25 wt.% Mg powder in the preform. This indicates that the strength and stiffness decreased by $\sim$ 37% and 32%, respectively after adding 25 wt.% Mg while the ductility was enhanced by about 76%. It is important to note that the moduli were calculated from the slope of the tangent at the 160 MPa stress level.

It is worth noting that the compressive strength and Young's modulus of the composites fabricated using Mg powder in the preform are higher than those using the same weight percent of MgH_2 powder in the preform. This is, as mentioned in Chapter 6, because the volume percentages of the reinforcing phases are higher in case of Mg powder than those in the case of the same weight percentage of MgH_2 in the preform. However, the ductility is lower due to the lower content of Mg matrix but the difference between the two cases is not very significant.

In summary, although the compressive strength and Young's modulus decreased significantly by adding Mg powder to the preform, the ductility of the fabricated composites was improved. Hence, the mechanical properties of the composites can be tailored by controlling the amount of Mg powder in the $Mg-(3Ti-B_4C)$ preform.

7.2.3.2 Mechanical Properties of the TiC$_x$-TiB$_2$/AM60B Composites

As for the case of the AZ91D composites, the same trend took place with the TiC$_x$-TiB$_2$/AM60B composites reinforced with different volume percentages of the reinforcing phases by adding different weight percentages of Mg powder to the 3Ti-B$_4$C preform.

The compression behavior of the TiC$_x$-TiB$_2$/AM60B composites reinforced with different volume fractions of the reinforcing phases using a 3Ti-B$_4$C preform with and without 25 wt.% Mg powder compared with that of the AM60B alloy is given in Figure 7.18. The compression test results are listed in Table 7.10 and shown in Figure 7.19.
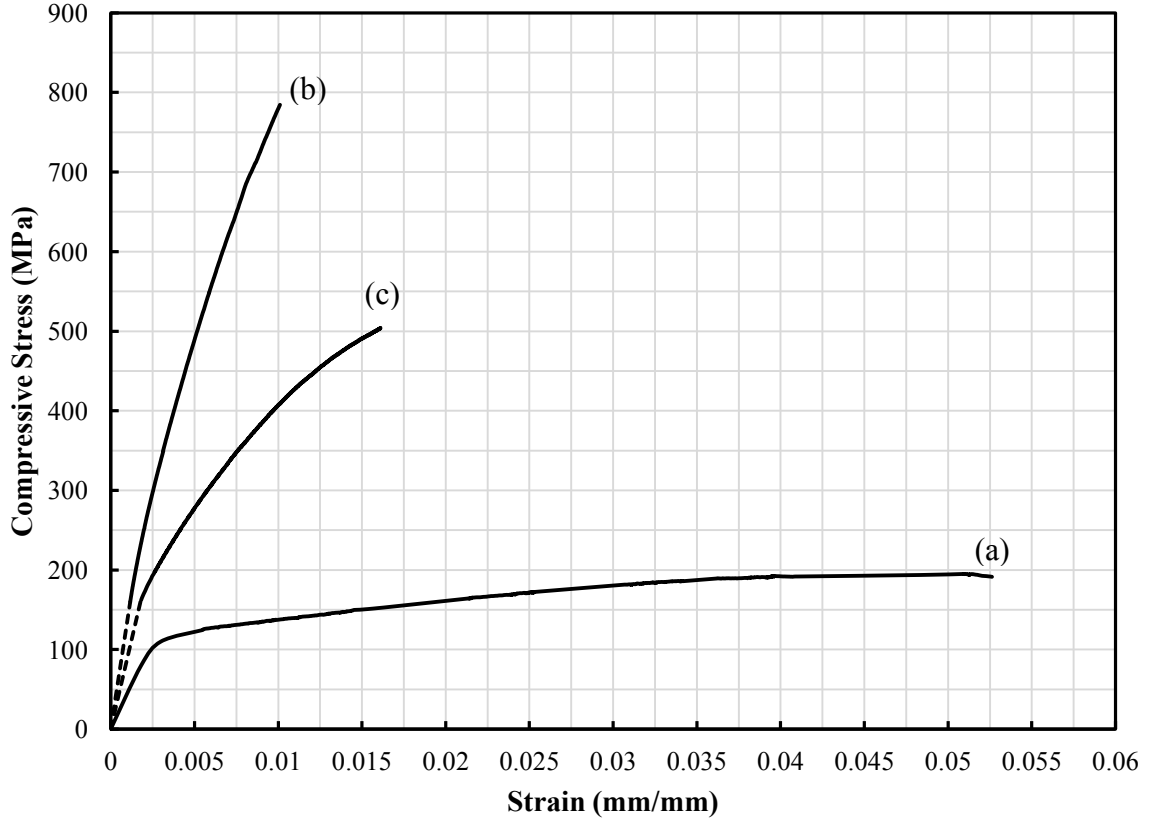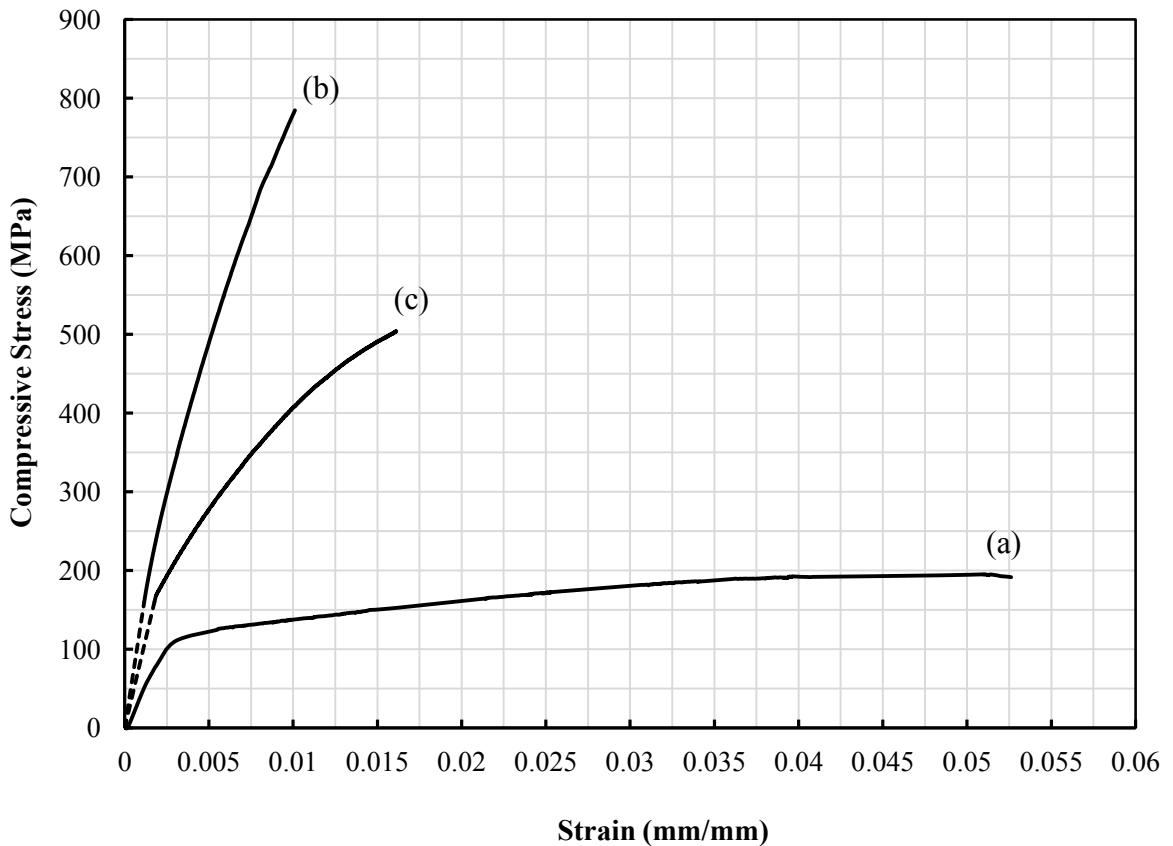

Figure 7.18 Stress-strain curves of (a) the AM60B alloy and the composites fabricated by adding different weight percentages of Mg powder to the 3Ti-B$_4$C preform: (b) 0 wt.% and (c) 25 wt.%

Table 7.10 Compression test results of the TiC_x-TiB_2/AM60B composites fabricated using an Mg-(3Ti-B_4C) preform with different Mg powder contents

|	Preform Mg-3Ti-B_4C	Young's Modulus, E_{T160}, (GPa)	Compressive Strength (MPa)	Height reduction (%)
AM60B alloy	-----	44	195	5.25
TiC_x-TiB_2/AM60B Composites	0 wt.% Mg	144 ±8.37	788 ±10.91	1.01 ±0.08
	25 wt.% Mg	114	518	1.50
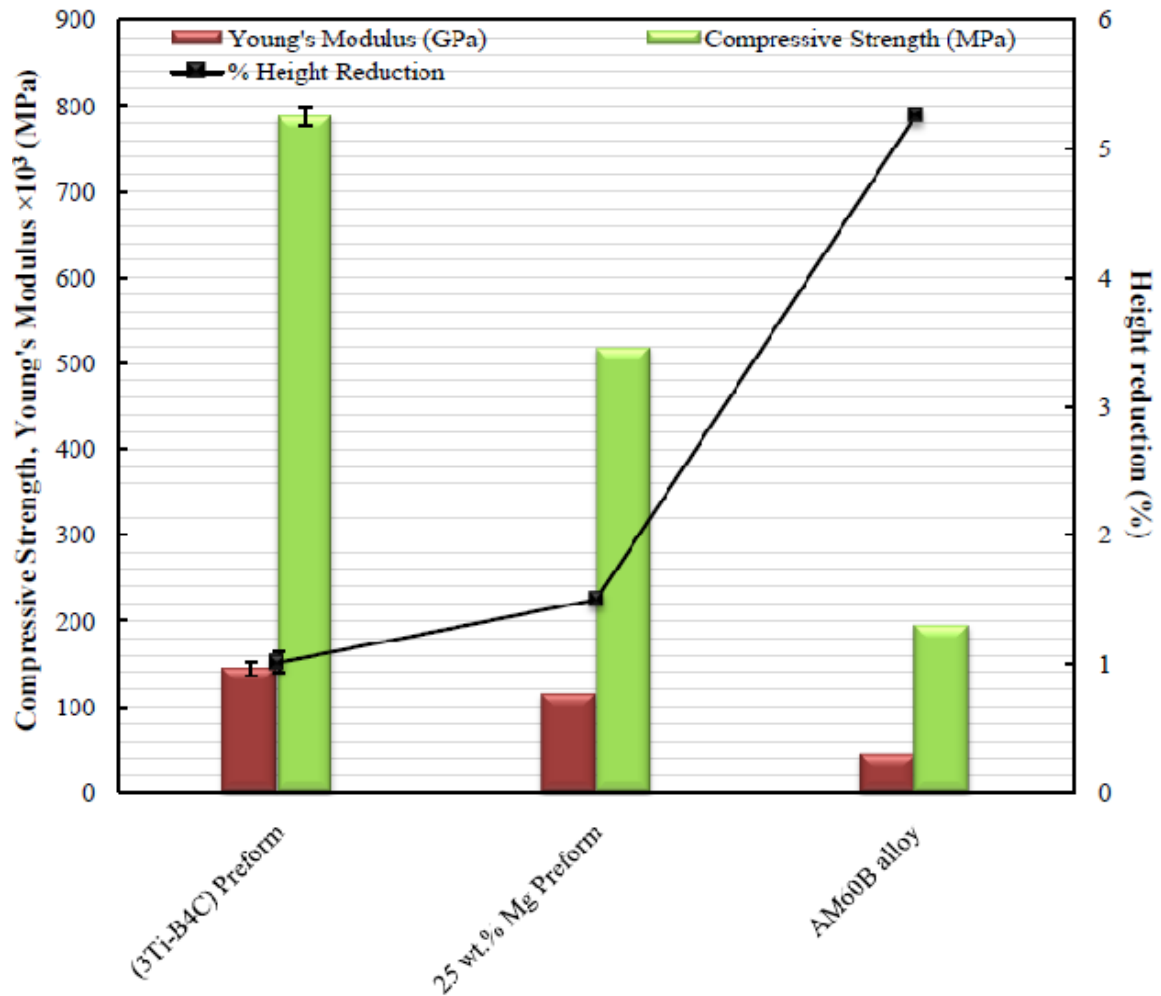
Figure 7.19 Compression test results of the AM60B alloy and the TiC_x-TiB_2/AM60B composites fabricated using a preform with and without 25 wt.% Mg powder

190

The compression test results listed in Table 7.10 and presented in Figure 7.19 show that the average compressive strength and Young's modulus of the fabricated composites decreased from ~ 788 MPa and 144 GPa with 0 wt.% Mg in the preform to ~ 518 MPa and 114 GPa with 25 wt.% Mg powder in the preform. This indicates that the strength and stiffness decreased by ~ 34% and 21%, respectively after adding 25 wt.% Mg powder to the 3Ti-B$_4$C preform while the ductility was improved by about 50%.

7.2.3.3 Mechanical Properties of the TiC$_x$-TiB$_2$/ Pure Mg Composites

Similar to the AZ91D and AM60B composites, pure Mg composites reinforced with different volume percentages of the reinforcing phases by adding different weight percentages of Mg powder to the 3Ti-B$_4$C preform have been studied. The compression behavior of the pure Mg composites reinforced with different volume fractions of the reinforcing phases using a 3Ti-B$_4$C preform with and without 25 wt.% Mg powder in relation to that of pure Mg is shown in Figure 7.20.

The compression test results listed in Table 7.11 and represented graphically in Figure 7.21 show that the average compressive strength and Young's modulus of the fabricated composites decreased from ~ 750 MPa and 122 GPa with 0 wt.% Mg powder in the preform to ~ 490 MPa and 90 GPa with 25 wt.% Mg powder in the preform. This indicates that the strength and stiffness decreased by ~ 35% and 26%, respectively after adding 25 wt.% Mg powder to the 3Ti-B$_4$C preform while the ductility was improved by ~ 48%.
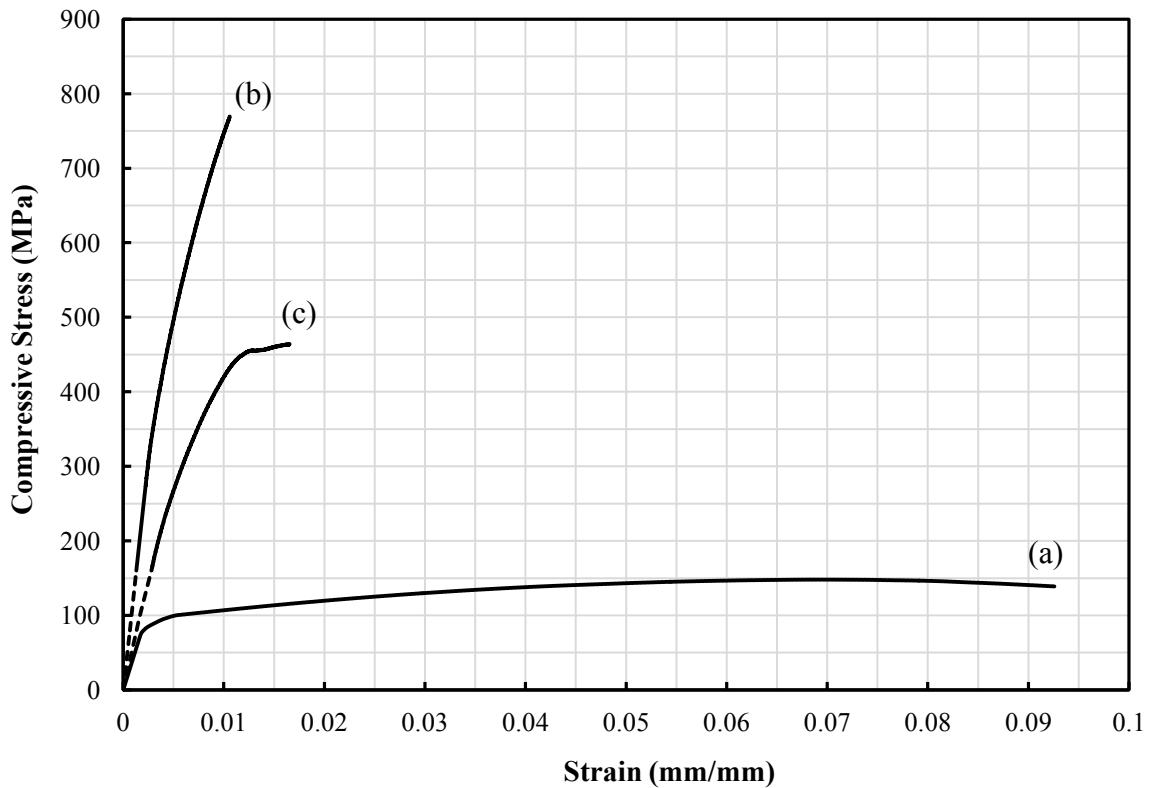
191
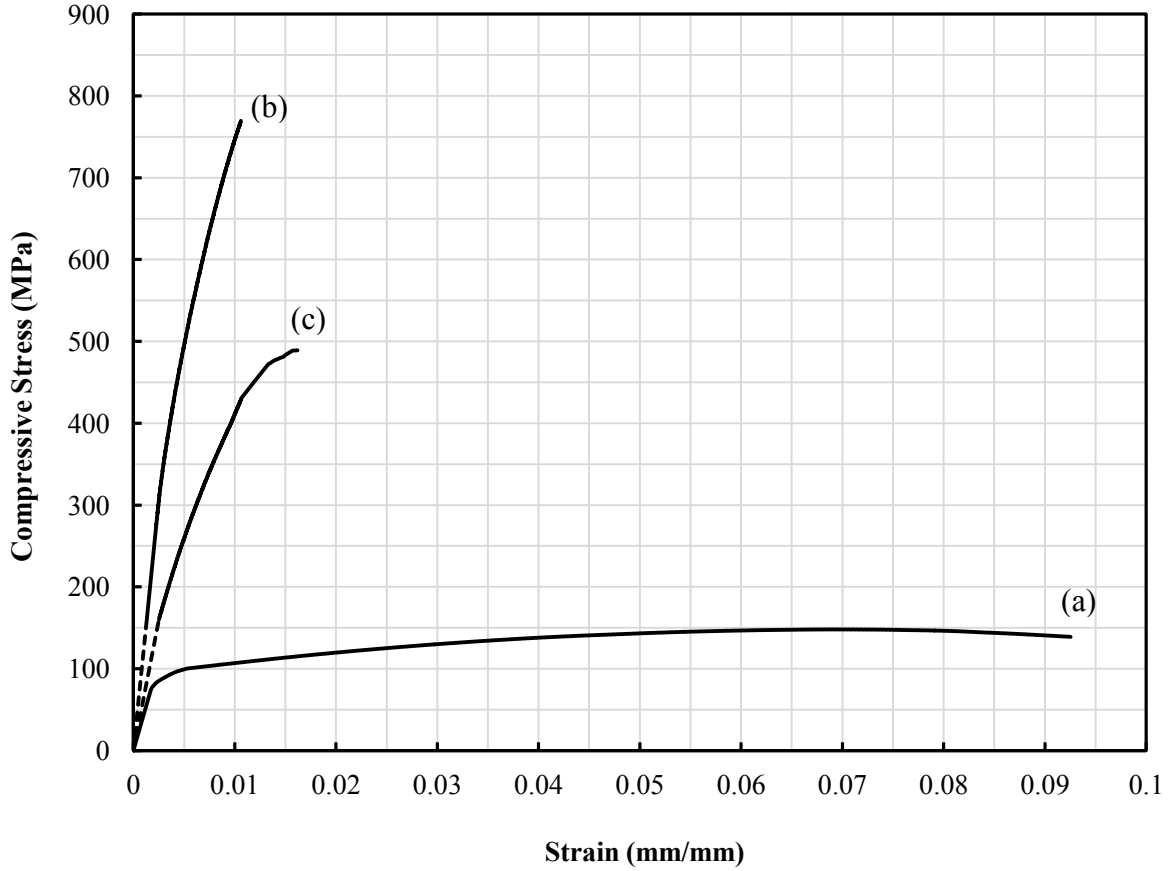
Figure 7.20 Stress-strain curves of (a) pure Mg and the composites fabricated by adding different weight percentages of Mg powder to the 3Ti-B$_4$C preform: (b) 0 wt.% and (c) 25 wt.%

Table 7.11 Mechanical properties of pure Mg and the TiC$_x$-TiB$_2$/Mg composites fabricated using an Mg-(3Ti-B$_4$C) preform with different Mg powder contents

| Sample	Mg content in the preform	Young's Modulus, E_{T160}, (GPa)	Compressive Strength (MPa)	Height reduction (%)
Pure Mg	-----	44	150	9.25
TiC$_x$-TiB$_2$/Mg Composites	0 wt.%	122 ±9.1	750 ±22	1.10 ±0.1
	25 wt.%	90	490	1.62
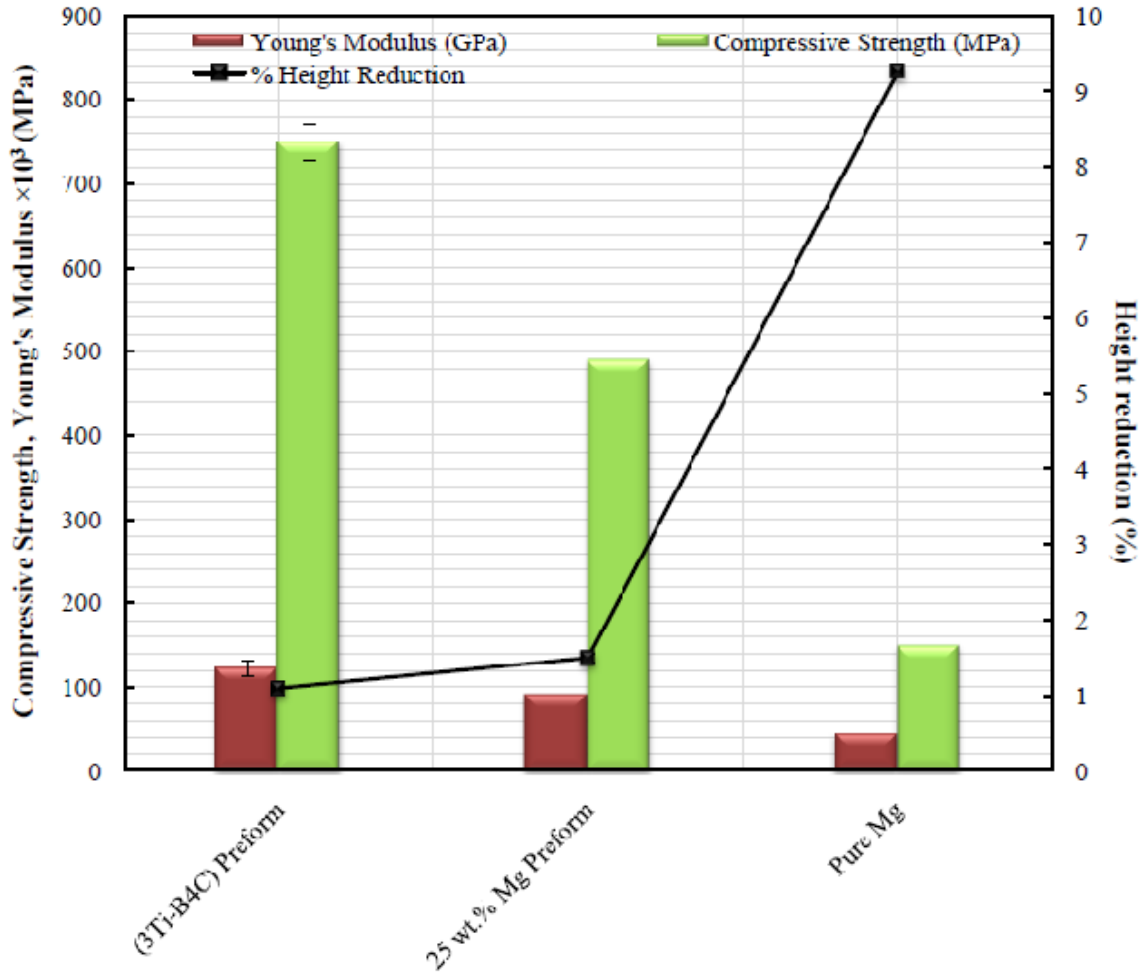
Figure 7.21 Compression test results of pure Mg and the TiC$_x$-TiB$_2$/pure Mg composites fabricated using a preform with and without 25 wt.% Mg powder

Considering that the compressive strength of the unreinforced pure Mg matrix is 150 MPa, the compressive strength of the composites fabricated using a 3Ti-B$_4$C preform with 70% *RD* at 900°C and 1.5 h increased by nearly 400%.

In summary, the compressive strength of pure Mg, AM60B and AZ91D matrix composites is increased because the dispersion of fine and hard TiC$_x$ and TiB$_2$ particles in the matrix drastically blocks the dislocations motion and thus strengthens the material as a whole. On the other hand, the composite material becomes more brittle for the same

reason. Furthermore, the results revealed that the AZ91D matrix composite exhibited a higher compressive strength if it is compared with the pure Mg or the AM60B matrix composites. However, the degree of strength improvement was greater in a pure magnesium composite than that in the AM60B or AZ91D matrix composites. This phenomenon has been ascribed to the higher mechanical properties of AZ91D in comparison to pure magnesium or the AM60B alloy.

7.3 Flexural Strength Test Results

The composite samples were tested using a four-point bending fixture on an MTS machine as shown in Figure 7.22.
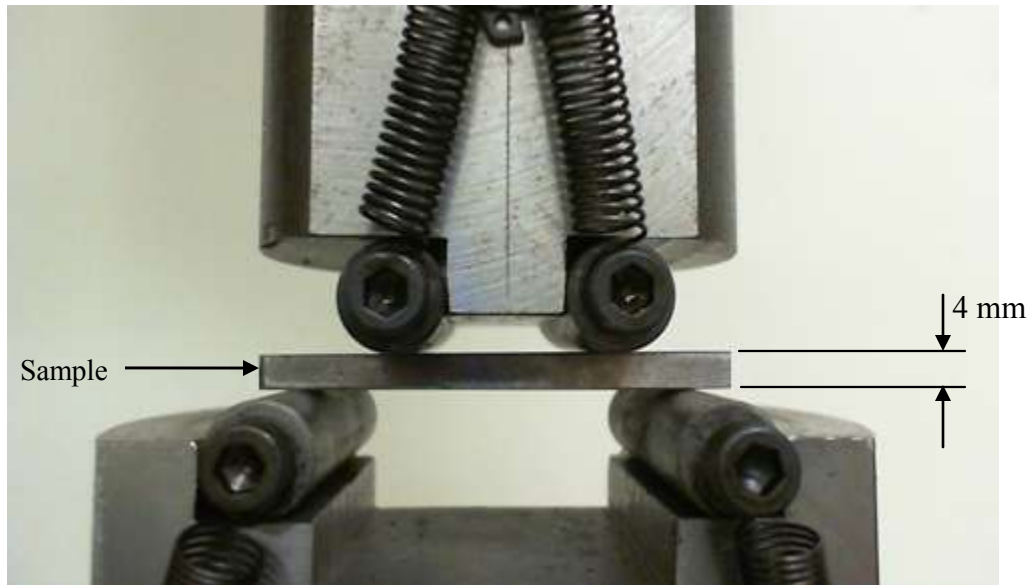
Figure 7.22 Digital image of 4-point bending fixture

All sample geometries were ground finished to 1200 grit silicon carbide paper on four sides to remove any stress concentrations due to cutting or machining. The samples were tested in flexure. The experimental flexural strength results are obtained for three magnesium matrix composites; pure Mg, AM60B and AZ91D alloy reinforced with TiC_x

and TiB_2. For all tests, the maximum or breaking load of each sample was obtained using a data acquisition system.

7.3.1 Flexural Strength Results of the TiC_x-TiB_2/AZ91D Matrix Composites

Composite samples fabricated using a $3Ti$-B_4C preform and with 25 wt.% Mg or MgH_2 powder have been tested to measure their flexural strength. The experimental flexural strength results for these composites are listed in Table 7.12 and compared with the ultimate strength of the AZ91D alloy and the flexural strength of TiC in Figure 7.23.

Table 7.12 Experimental flexural strength results of the TiC_x-TiB_2/AZ91D composites fabricated using different preforms

Samples		Preform	Breaking load (N)	Flexural Strength (σ_{fs}) (MPa)	Average σ_{fs} (MPa)	Standard deviation ($\pm$)
TiC_x-TiB_2/AZ91D Composites	1	$3Ti$-B_4C	1557.36	414.89		
	2		1498.80	409.74		
	3		1782.60	431.10	418.6	11.15
	1	25 wt.% Mg-($3Ti$-B_4C)	1001.92	300.54		
	2		1233.53	327.80		
	3		1166.80	310.07	312.8	13.83
	1	25 wt.% MgH_2-($3Ti$-B_4C)	973.82	326.49		
	2		879.98	303.80		
	3		829.10	294.79	308.4	16.33

The results show that the average flexural strength of the TiC_x-TiB_2/AZ91D composites fabricated using a $3Ti$-B_4C preform is ~ 419 MPa which is higher than the ultimate strength of the AZ91D alloy by ~ 68% while it is lower than the flexural strength of TiC by ~ 25%. Also, the results reveal that the flexural strength of the composites fabricated using a 25 wt.% Mg-($3Ti$-B_4C) and 25 wt.% MgH_2-($3Ti$-B_4C) is 313 and 308 MPa, respectively. Therefore, adding 25 wt.% Mg or 25 wt.% MgH_2 powder to the 3Ti-

B$_4$C preform decreased their flexural strength by about 25% or 26% due to the decrease in the ceramic particle content in the composites.
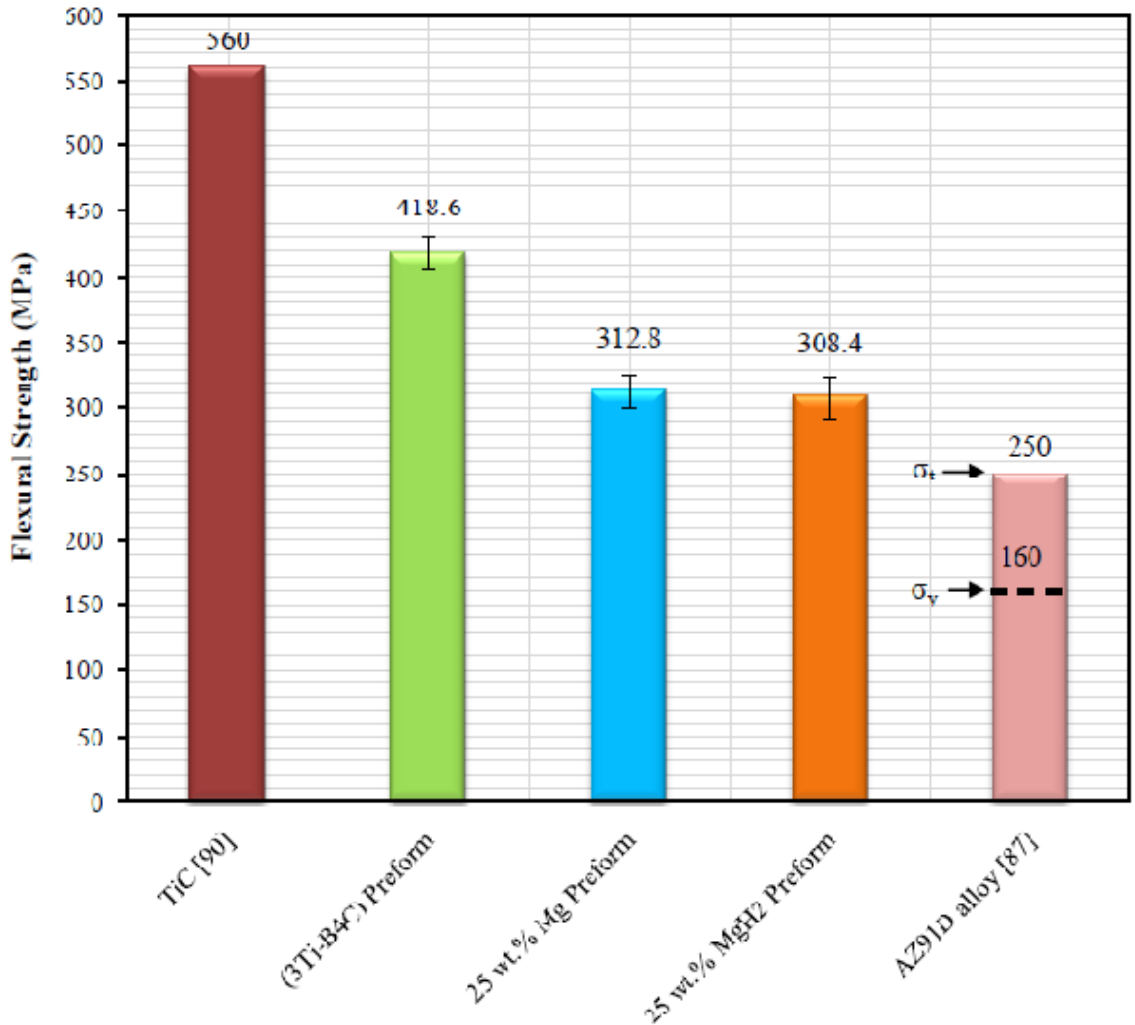
Figure 7.23 Comparison of various flexural strength values

For more investigation about the effect of the volume fraction of the reinforcing particles controlled by varying the weight percentage of MgH$_2$ powder added to the 3Ti-B$_4$C preform, the experimental flexural strength results for the composites fabricated using MgH$_2$-(3Ti-B$_4$C) preforms with different weight percentages of MgH$_2$ powder are presented in Figure 7.24 and summarized in Table 7.13.

Table 7.13 Experimental flexural strength results of the TiC_x-TiB_2/AZ91D composites fabricated using preforms containing different MgH_2 weight percentages

Samples		Preform	Breaking load (N)	Flexural Strength (σ_{fs}) (MPa)	Average σ_{fs} (MPa)	Standard deviation ($\pm$)
	1	10 wt.% MgH_2-(3Ti-B_4C)	1185.37	328.13		
	2		1149.72	322.56		
	3		1334.77	369.49	340.0	25.64
	1	25 wt.% MgH_2-(3Ti-B_4C)	973.82	326.49		
	2		879.98	303.80		
	3		829.10	294.79	308.4	16.33
	1	40 wt.% MgH_2-(3Ti-B_4C)	645.79	239.6		
	2		687.20	254.96		
	3		573.55	212.80	235.8	21.30

(Left vertical label: TiC_x-TiB_2/AZ91D Composites)

The results show that the flexural strength of the composites decreased with decreasing the volume fractions of the reinforcing phases, TiC_x and TiB_2, through adding different weight percentages of MgH_2 powder to the 3Ti-B_4C preform. Looking at the individual results (Figure 7.24), the average flexural strength of the composites decreased by 19%, 26% or 44% due to adding 10 wt.%, 25 wt.% or 40 wt.% MgH_2 powder. These results show that the composites, fabricated using just a 3Ti-B_4C preform, are strong and brittle. However, ductility increased with increasing the volume fraction of Mg matrix in the composites using a 3Ti-B_4C preform with additions of Mg or MgH_2 powder. The digital images of these composite samples at the beginning of the test and just before failure of the samples are shown in Figure 7.25. It is clear that the deflection increases

with increasing the MgH_2 content in the preform indicating that the ductility of the composites increases.
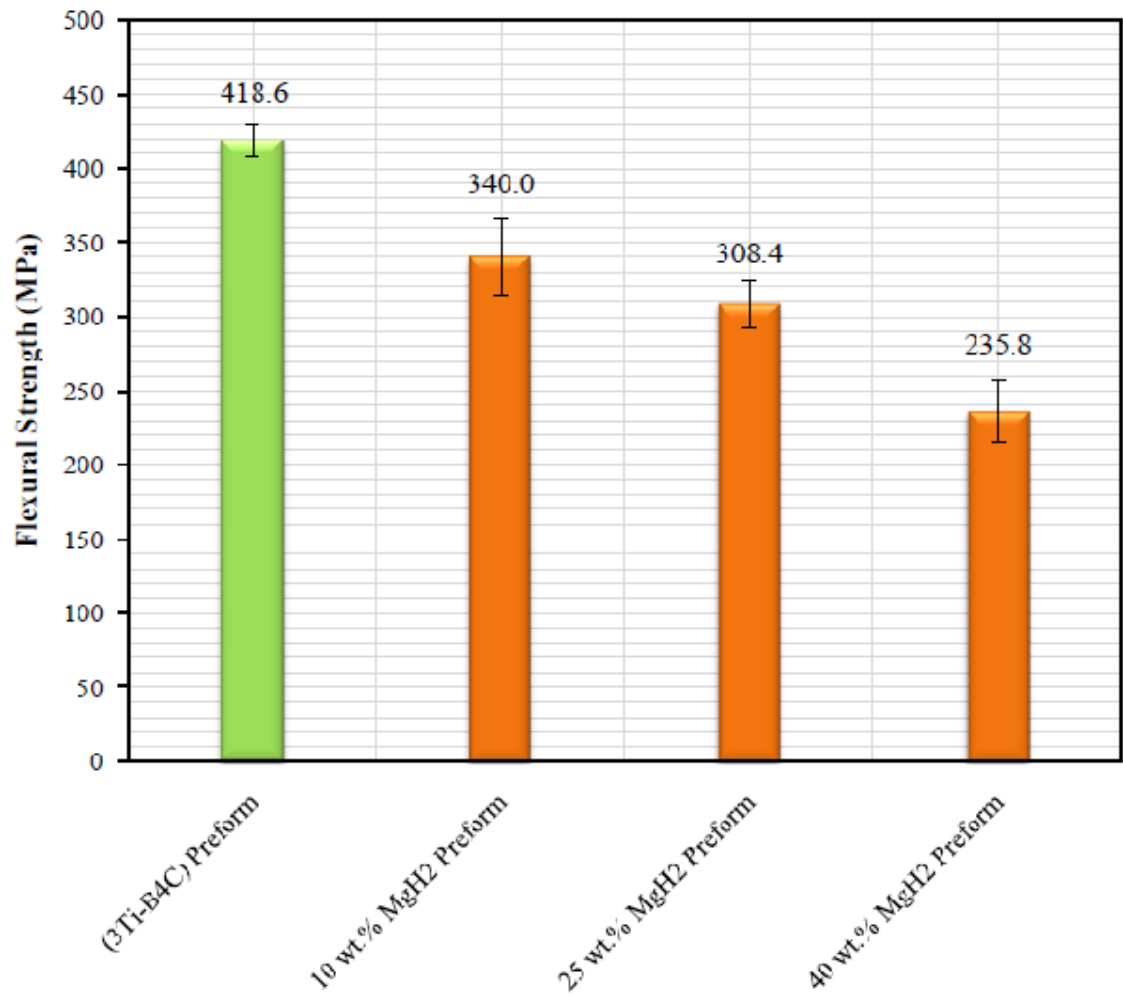
Figure 7.24 Comparison of various flexural strength values of composites fabricated using MgH_2-(3Ti-B$_4$C) preforms with different MgH_2 contents
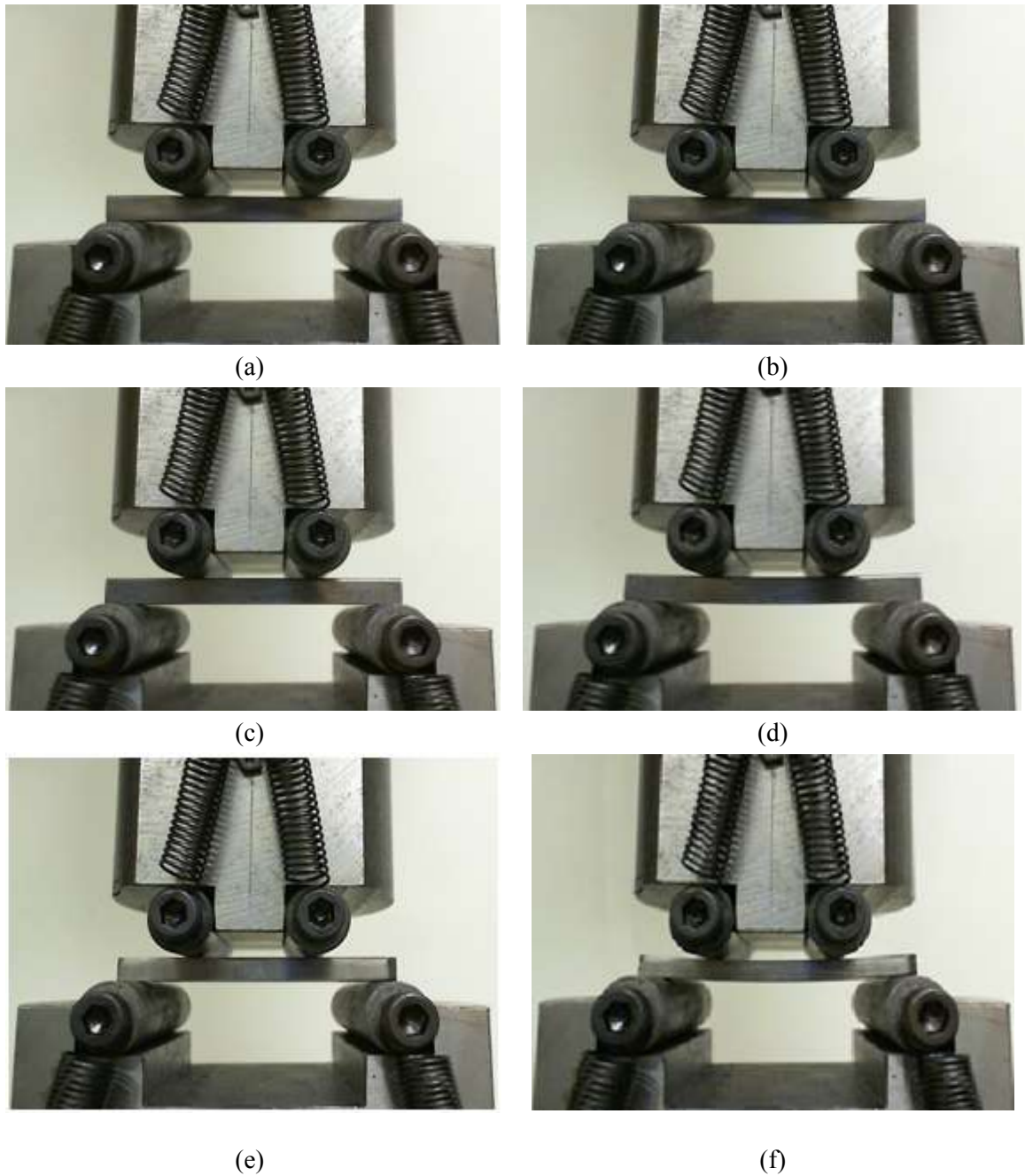
Figure 7.25 Digital images of the 4-point bending test of the TiC$_x$-TiB$_2$/AZ91D composites fabricated using a 3Ti-B$_4$C preform at (a) the beginning of the test and (b) just before failure with 0 wt.% MgH$_2$, (c), (d) with 25 wt.% MgH$_2$ and (e), (f) with 40 wt.% MgH$_2$

7.3.2 Flexural Strength Results of the TiC_x-TiB_2/AM60B Matrix Composites

In the same fashion, composite samples fabricated using a 3Ti-B_4C preform and with 25 wt.% Mg or MgH_2 powder have been tested to measure the flexural strength of the composites. The experimental flexural strength results for these composite samples compared with the ultimate strength of the AM60B alloy and the flexural strength of TiC are listed in Table 7.14 and represented graphically in Figure 7.26.

Table 7.14 Experimental flexural strength results of the TiC_x-TiB_2/AM60B composite samples fabricated using different preforms

Samples		Preform	Breaking load (N)	Flexural Strength (σ_{fs}) (MPa)	Average σ_{fs} (MPa)	Standard deviation ($\pm$)
	1	3Ti-B_4C	1019.18	378.13		
	2		922.84	368.00		
TiC_x-TiB_2/AM60B Composites	3		1321.79	381.80	376.0	7.16
	1	25 wt.% Mg-3Ti-B_4C	1128.40	312.36		
	2		1102.97	305.32		
	3		1032.44	285.80	301.2	13.76
	1	25 wt.% MgH_2-3Ti-B_4C	837.00	272.90		
	2		1157.76	315.00		
	3		844.36	307.67	298.5	22.49

The results show that the TiC_x-TiB_2/AM60B composites have an average flexural strength of 376 MPa and this is higher than the ultimate tensile strength of the AM60B alloy by 57%. Also, the results reveal that the average flexural strengths of the composites fabricated using a 25 wt.% Mg-(3Ti-B_4C) and 25 wt.% MgH_2-(3Ti-B_4C) are 301 and 298.5 MPa, respectively. Therefore, the average flexural strength of the

composites decreased by about 20% or 21% after adding 25 wt% Mg or 25 wt.% MgH_2 powder to the preform.
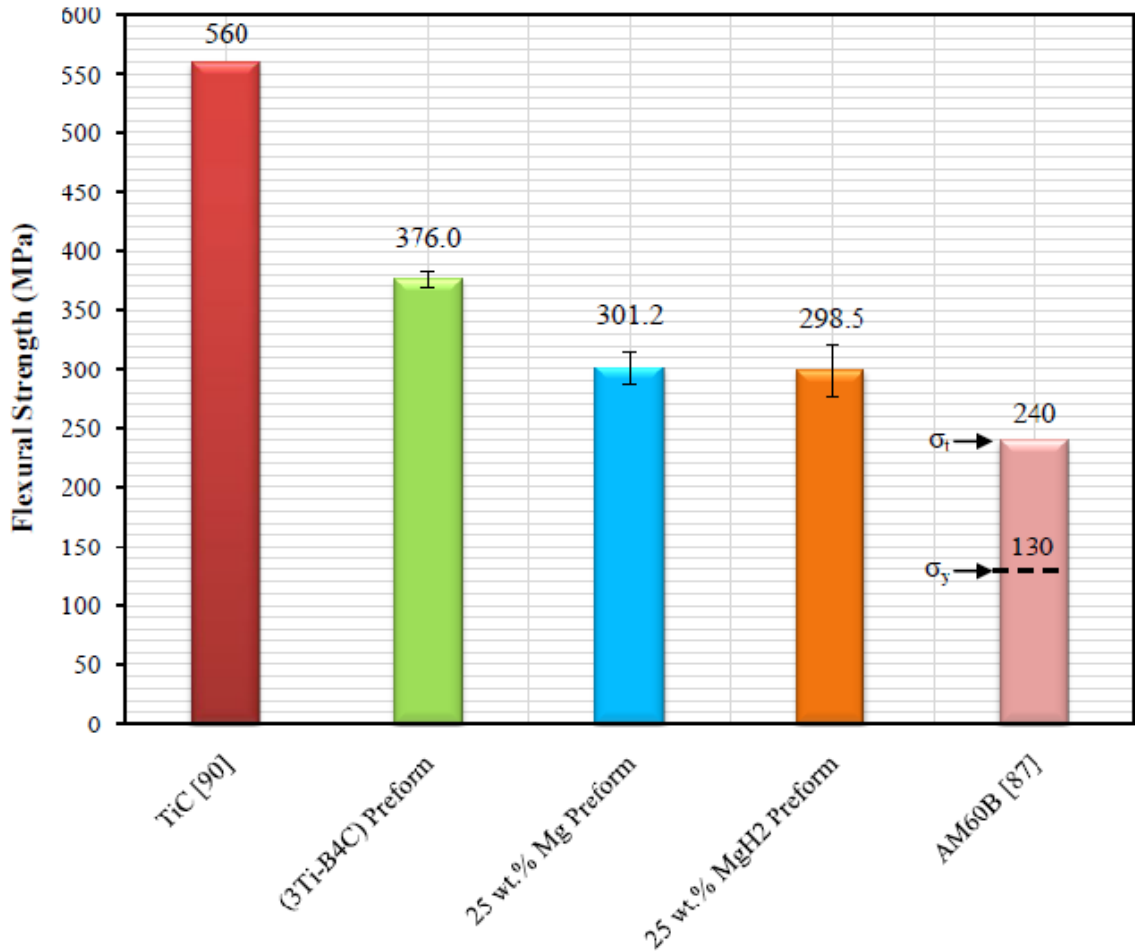
Figure 7.26 Comparison of various flexural strength values

7.3.3 Flexural Strength Results of the TiC-TiB$_2$/Pure Mg Matrix Composites

In this study, composite samples fabricated using a 3Ti-B$_4$C preform and with 25 wt.% Mg or MgH$_2$ powder but using pure Mg as a matrix have been tested. The experimental flexural strength results for these composite samples compared with the ultimate strength of pure Mg and the flexural strength of TiC are listed in Table 7.15 and graphically represented in Figure 7.27.

Table 7.15 Experimental flexural strength results of the TiC$_x$-TiB$_2$/pure Mg composite samples fabricated using different Preforms

Samples			Preform	Breaking load (N)	Flexural Strength (σ_{fs}) (MPa)	Average σ_{fs} (MPa)	Standard deviation ($\pm$)
TiC$_x$–TiB$_2$/Pure Mg Composites		1	3Ti-B$_4$C	920.35	325.30		
		2		847.95	314.60		
		3		950.51	352.65	330.9	19.62
		1	25 wt.% Mg-3Ti-B$_4$C	714.31	237.44		
		2		1005.56	278.36		
		3		822.02	243.82	253.2	22.02
		1	25 wt.% MgH$_2$-3Ti-B$_4$C	967.44	263.80		
		2		953.09	257.09		
		3		596.20	219.28	246.7	24.00

Figure 7.27 Comparison of various flexural strength values

The results show that the average flexural strength of the composite fabricated using a 3Ti-B$_4$C preform is higher than the ultimate tensile strength of pure Mg by 83%. Besides, the results reveal that the average flexural strengths of the composites fabricated using a 25 wt.% Mg or 25 wt.% MgH$_2$ additions are 253 and 247 MPa, respectively. Therefore, the average flexural strength of the composites decreased by 23% or 25% after adding 25 wt.% Mg or 25 wt.% MgH$_2$ powder to the preform.

Furthermore, the results reveal that the AZ91D matrix composite exhibited a higher flexural strength compared with that of the pure Mg or the AM60B matrix

composites. However, the degree of strength improvement was greater in a pure magnesium composite than that in the AM60B or AZ91D matrix composites.

7.4 Fractographic Analysis of Flexural Test

Knowledge about the behavior of magnesium matrix composites under different loading conditions is required especially as these composites are used in different applications. Therefore, the investigation of failure mechanisms of magnesium alloys and magnesium composites is one of the study areas in this field [155].

In this study, the fractured surfaces of the composite samples were analyzed after the four-point bending test. SEM with EDS spot analysis was employed to determine the failure mechanisms of the TiC_x-TiB_2/Mg composite. Figure 7.28 shows the general fracture surface area in the bending of the TiC_x-TiB_2/AZ91D matrix composites fabricated by using a 3Ti-B_4C preform with 70% *RD* at the optimal processing parameters; 900ºC and 1.5 h at low and high magnifications.

Fracture surfaces were flat and parallel to the stress axis when viewed on a macroscopic scale but rough when viewed on a microscopic scale as shown in Figure 7.29. The flat appearance of the fractured surfaces is because of the high TiC_x-TiB_2 content.

(a)

Area 1
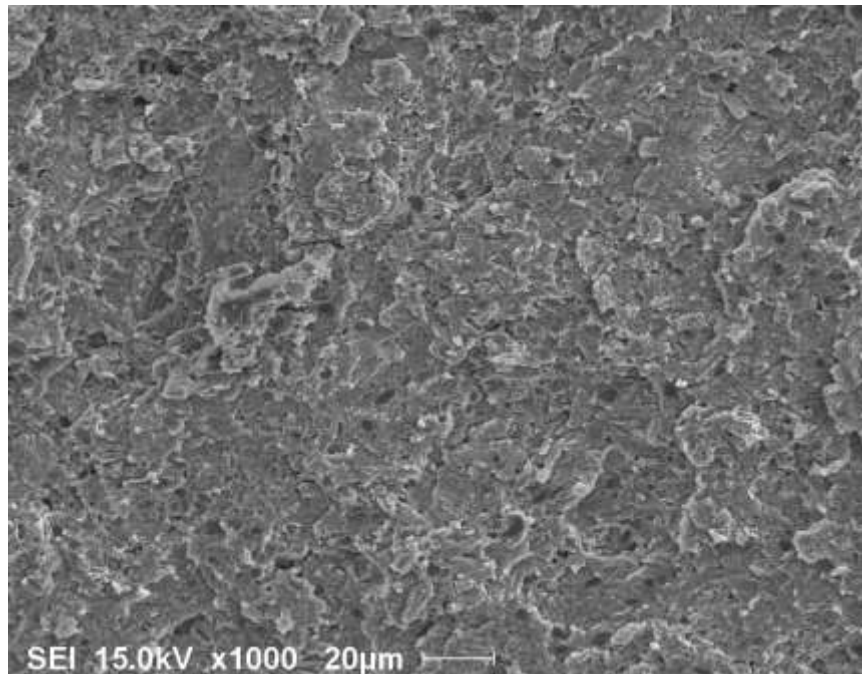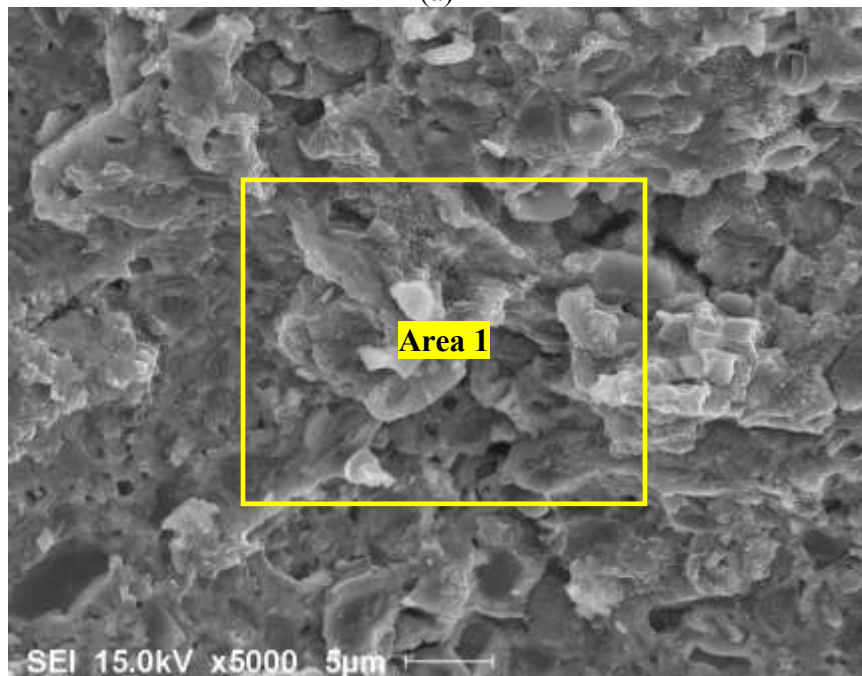
(b)

Figure 7.28 SEM flexural fracture of TiC_x-TiB_2/AZ91D composite (a) at low magnification and (b) at high magnification

At higher magnification as shown in Figure 7.29, signs of mixed fracture are shown in the AZ91D magnesium matrix. SEM observations show cleavage regions as flat

areas which are related to brittle failure while some microdimples also appear and are related to ductile failure. The dimples are small and shallow, consistent with the quite low ductility of the composite. This can be attributed to the HCP crystal structure of magnesium that restricts the slip to the basal plane [14].
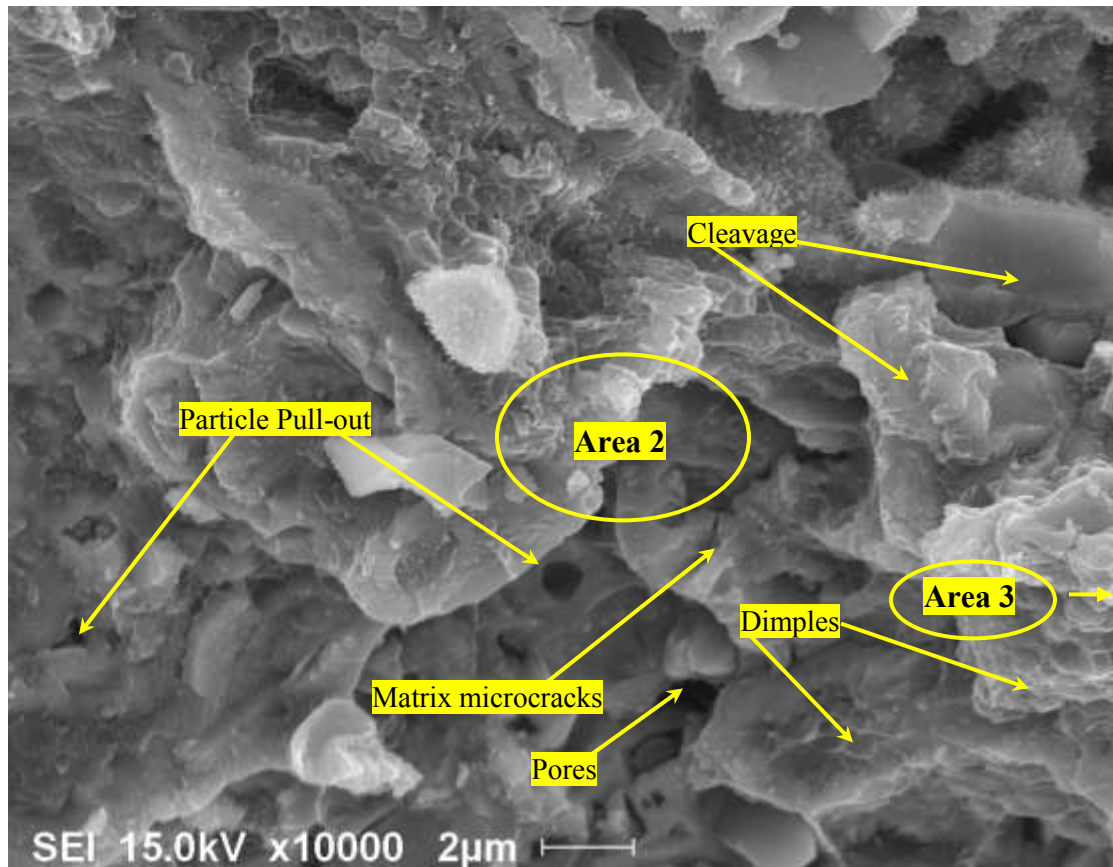
Figure 7.29 SEM flexural fracture of the TiC_x-TiB_2/AZ91D composite at area 1 of Figure 7.28 (b)

For more details about the fracture mechanism, the SEM micrographs have been taken at different areas but at higher magnification with some EDS spot analysis as shown in Figures 7.30-7.32.

Figure 7.30 (the magnified area 2 in Figure 7.29) shows the fracture surface in more detail where the presence of few dimples in the Mg matrix can be observed in some

regions while cleavage appears in other regions in the Mg matrix and in the ceramic particles. However, it is very difficult to notice the fracture in the particles because the particles are very small and some of them are in the nano scale range. This indicates that the bonding between the matrix and the ceramic particle is very strong. Moreover, the SEM observations reveal some microcracks in the Mg and very small pores due to incomplete infiltration in between the particles or the shrinkage of the Mg matrix during cooling.
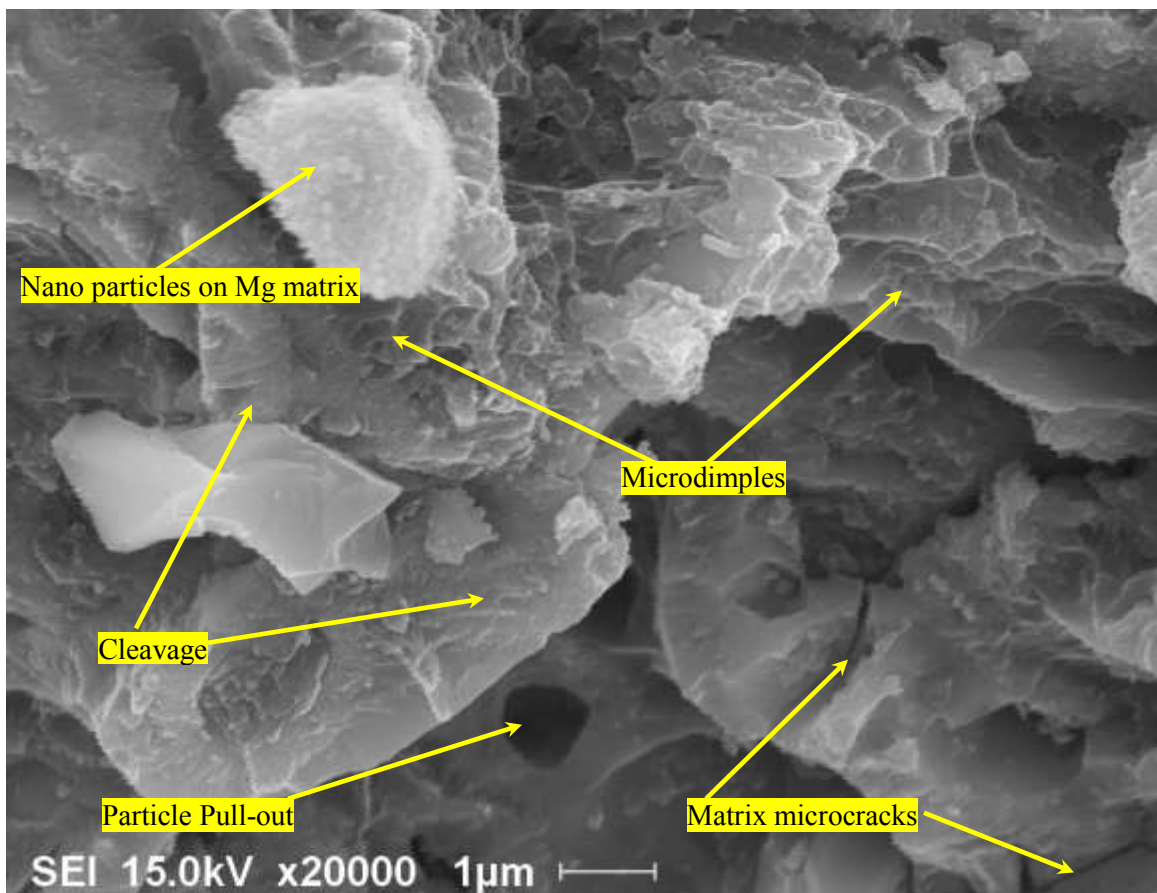
Figure 7.30 SEM flexural fracture of the TiC$_x$-TiB$_2$/AZ91D composite at area 2 in Figure 7.29

Furthermore, as shown in Figure 7.31 (magnified area 3 of Figure 7.29), microdimples and cleavage as well as the presence of microcracks in the Mg matrix are very clear.
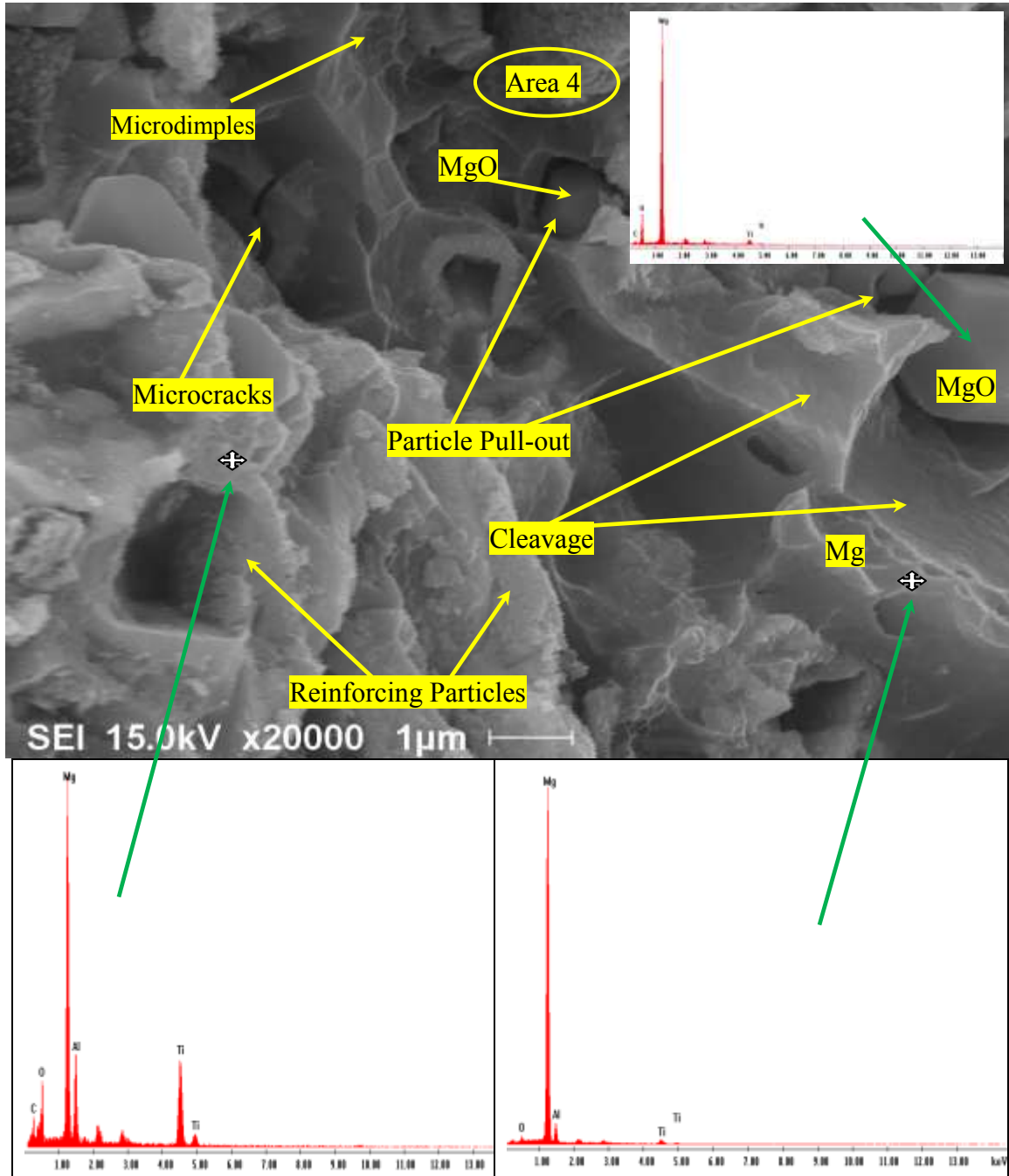
Figure 7.31 SEM flexural fracture and EDS of TiC_x-TiB_2/AZ91D composite at area 3 in Figure 7.29

Also, MgO particle pull-out can be observed indicating that the bonding at the interface between these particles and the Mg matrix is not strong. The existence of the dimples and cleavage in the Mg matrix was confirmed by the EDS spot analysis as shown in the figure. Also, the EDS spot analysis on the particles "pulled-out" proved that these particles are just MgO where Mg and oxygen are the only detected elements. For more details, Figure 7.32 (magnified area 4 of Figure 7.31), reveals not only the presence of microdimples and cleavage besides the presence of microcracks in the Mg matrix but also MgO particle pull-out. On the other hand, the EDS spot analysis in Figure 7.32 (b) reveals the presence of residual particles of MgB_2.

The fracture behavior of the composite samples fabricated using a preform containing Mg or MgH_2 powder is almost the same. However, the higher volume percentage of Mg reveals more microdimples but also more MgO particle pull-out.

Based on these observations of the fracture surfaces through SEM, the composites exhibit a combination of completely brittle fracture regions and brittle-ductile fracture regions. In the brittle-ductile fracture regions, microdimples associated with Mg-enriched zones were observed in the matrix. In addition, microcracks observed in the matrix show that the failure might have initiated in the matrix rather than from the particulates.

Also, it can be observed that the reinforcing particles are very fine, so it is very difficult to see breaking in the particles or the microcracks. However, the high compressive strength and the brittleness of the composites suggest that the flexural cracks might initiate in the matrix from the preexisting microcracks. After that, the cracks propagate in the matrix and through the reinforcing particles till complete failure.
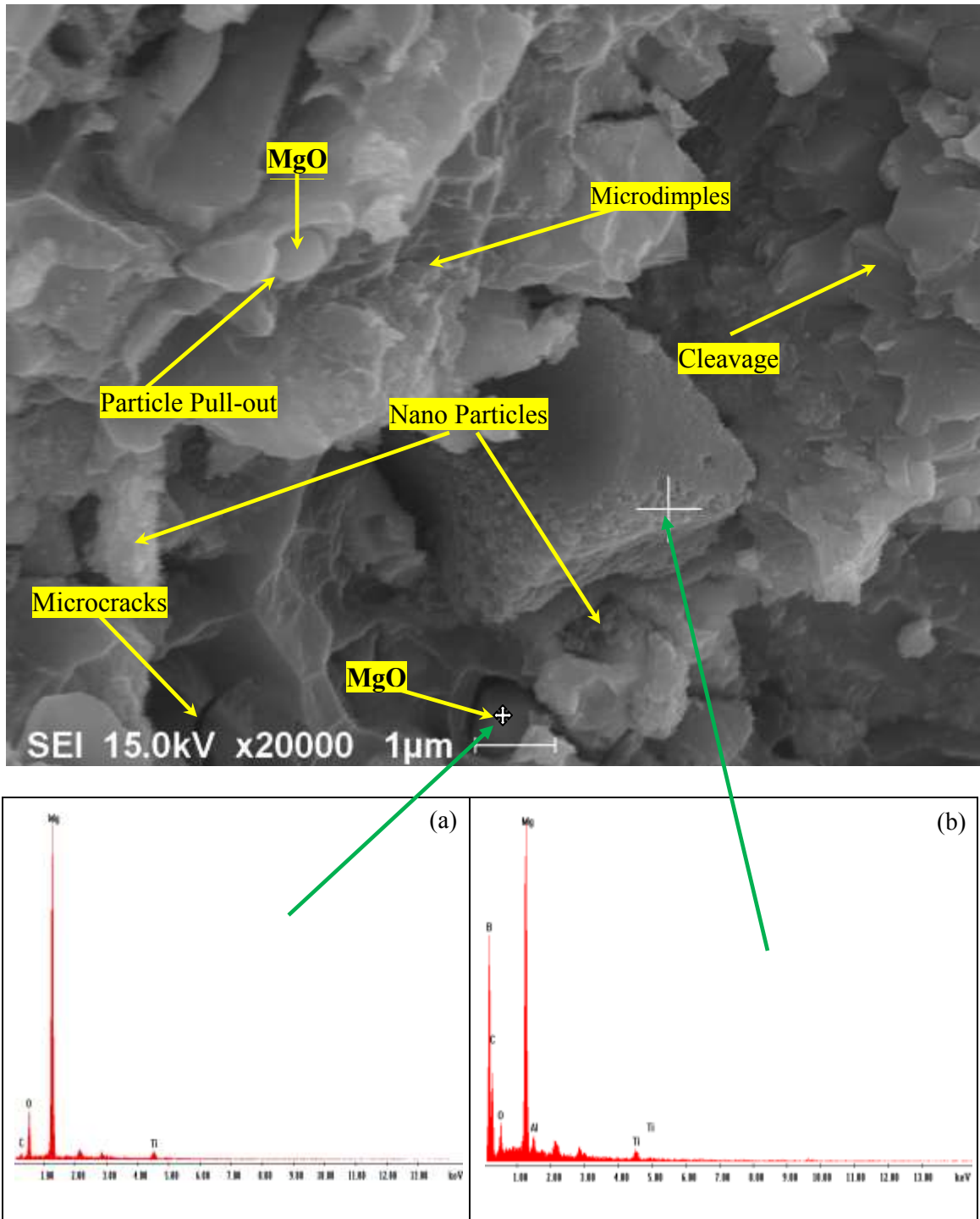
Figure 7.32 SEM flexural fracture and EDS of TiC$_x$-TiB$_2$/AZ91D composite at area 4 in Figure 7.31

7.5 Hardness Test Results

The hardness has been measured for bulk AZ91D composites reinforced with different volume fractions of the reinforcing phases. The average Vickers hardness values of the composite sample fabricated using different weight percentages of MgH_2 powder in the preform compared with the hardness of the AZ91D alloy are summarized in Table 7.16 and shown in Figure 7.33. The hardness value is the average of three measurements of each sample.

Table 7.16 Hardness of bulk AZ91D alloy and TiC_x-TiB_2/AZ91D composites fabricated using MgH_2-(3Ti-B_4C) preform with different MgH_2 contents

Sample		MgH_2 content in the preform	Reinforcing phases (vol. %)	Hardness HV_{10}	Average Hardness HV_{10}	Standard deviation ($\pm$)
AZ91D alloy	1	-----------------	---------------	64.3		
	2			61.7		
	3			61.0	62.3	1.74
TiC_x-TiB_2/AZ91D Composites	1	0 wt.%	~ 40	533.4		
	2			521.8		
	3			512.1	522.4	10.66
	1	10 wt.%	~ 30	357.8		
	2			351.0		
	3			327.3	345.4	16.01
	1	25 wt.%	~ 22	268.2		
	2			273.8		
	3			256.4	266.1	8.82
	1	40 wt.%	~ 12	123.5		
	2			108.5		
	3			115.6	115.9	7.50

The results show a clear rise in the hardness of the TiC_x-TiB_2/AZ91D composites compared with that of the unreinforced AZ91D alloy by nearly 700% showing the role of

the hard ceramic particles of TiC_x and TiB_2 in raising the hardness of the composite material as a whole. Also, the results reveal that the hardness of bulk TiC_x-TiB_2/AZ91D composites is affected by the volume fractions of the Mg matrix and the reinforcing phases, TiC_x and TiB_2. The volume fraction of the reinforcing phases was controlled by varying the weight percentages of MgH_2 powder in the preform as shown in Table 7.16. Thus, the hardness of the composite samples fabricated using 3Ti-B_4C preform having a 522 HV_{10} is higher than those fabricated using MgH_2-(3Ti-B_4C) preform.
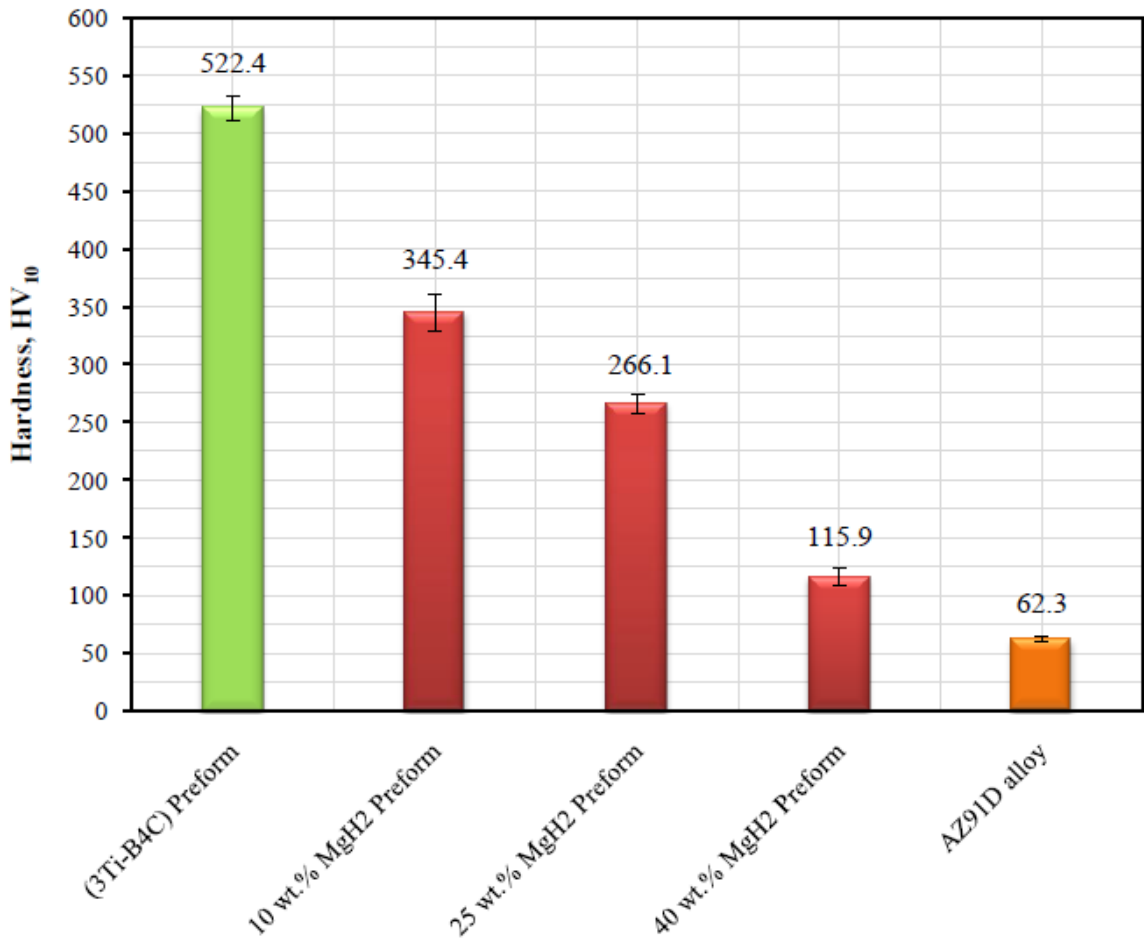
Figure 7.33 Hardness of the AZ91D alloy and TiC_x-TiB_2/AZ91D composites fabricated using preforms with different MgH_2 weight percentages

212

Since the volume fractions of the reinforcing phases decreased with increasing the weight percentage of MgH$_2$ in the preform, the hardness decreased by 34%, 49% or 78% for the composites fabricated using preforms containing 10 wt.%, 25 wt.% or 40 wt.% MgH$_2$ powder as shown in Figure 7.33 and tabulated in Table 7.16.

Figure 7.34 shows the micrographs of the Vickers indentations at 10 kg load for two composite samples: one fabricated using a 3Ti-B$_4$C preform and the other fabricated using a 25 wt. % MgH$_2$-(3Ti-B$_4$C) preform.
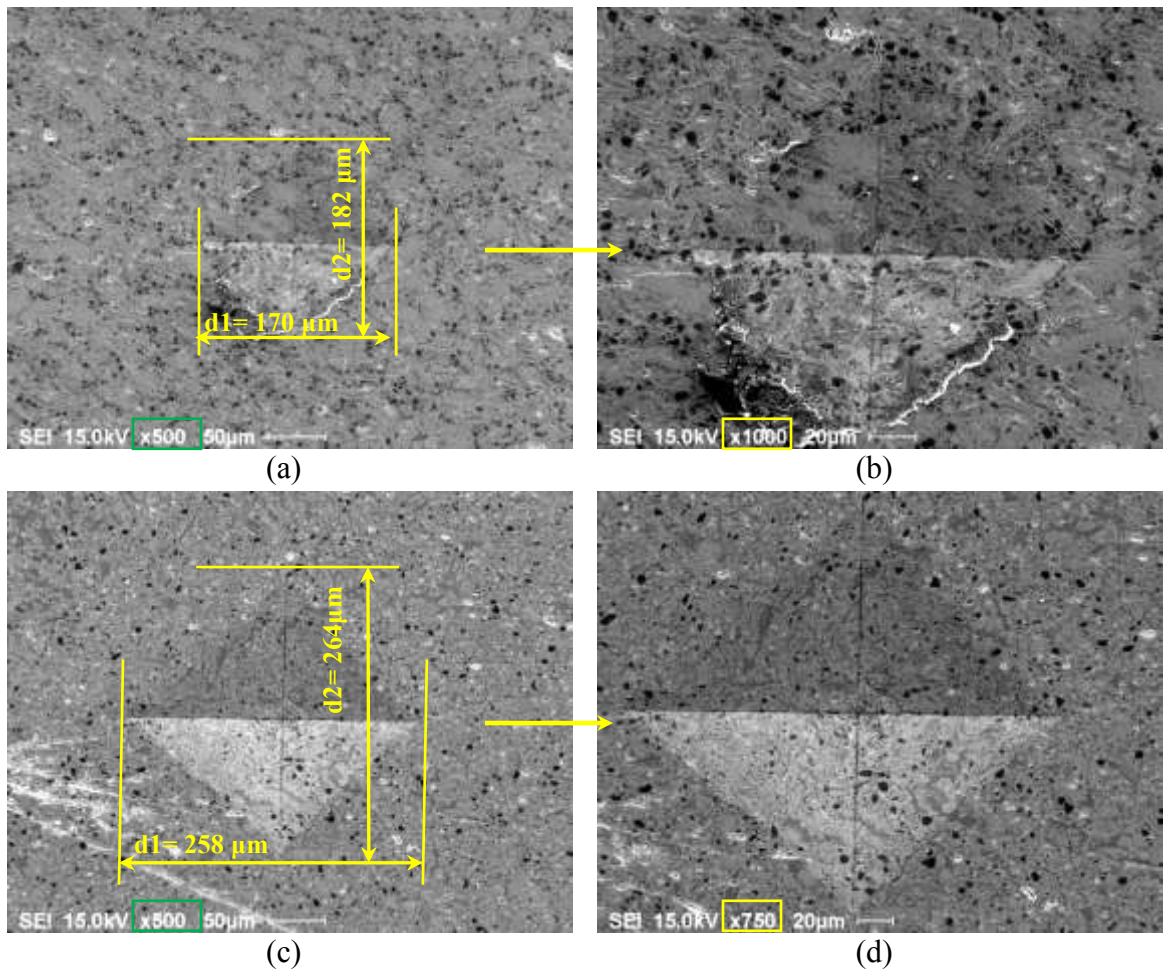
Figure 7.34 SEM micrographs of Vickers indentations obtained under a load of 10 kg for the TiC$_x$-TiB$_2$/AZ91D composites at low and high magnifications (a), (b) 3Ti-B$_4$C preform and (c), (d) 25 wt.% MgH$_2$-(3Ti-B$_4$C) preform

The size of indentations gives an indication about the hardness value. Based on the SEM observations of the indentations produced by testing of these two composites, it can be observed that the standard composite (3Ti-B$_4$C) has an indentation of lower size than that of the composite synthesized with 25 wt.% MgH$_2$ indicating that it has higher Vickers hardness value as listed in Table 7.16 and shown in Figure 7.33.

The same scenario of the change in the bulk hardness of the TiC$_x$-TiB$_2$/AZ91D composites fabricated using Mg-(3Ti-B$_4$C) preform was observed. The hardness decreased by 27% or 45% when the composites fabricated using a preform containing 10 wt.% or 25 wt.% Mg powder, respectively. The hardness results are listed in Table 7.17 and shown in Figure 7.35.

Table 7.17 Hardness of bulk TiC$_x$-TiB$_2$/AZ91D composites fabricated using an Mg-(3Ti-B$_4$C) preform with different Mg powder contents

Sample		Mg content in the preform	Reinforcing phases (vol. %)	Hardness HV$_{10}$	Average Hardness HV$_{10}$	Standard deviation (±)
TiC$_x$-TiB$_2$/AZ91D composites						
	1			533.4		
	2	0 wt.%	~ 40	521.8		
	3			512.1	522.4	10.66
	1			390.6		
	2	10 wt.%	~ 33	355.4		
	3			400.5	382.2	23.70
	1			293		
	2	25 wt.%	~ 25	281.6		
	3			285.8	286.8	5.77

It is clear that the values of the bulk hardness of the composites are higher when they are fabricated by adding Mg powder to the preform than MgH_2 powder because of the higher volume fractions of the reinforcing phases for Mg than MgH_2 additions.
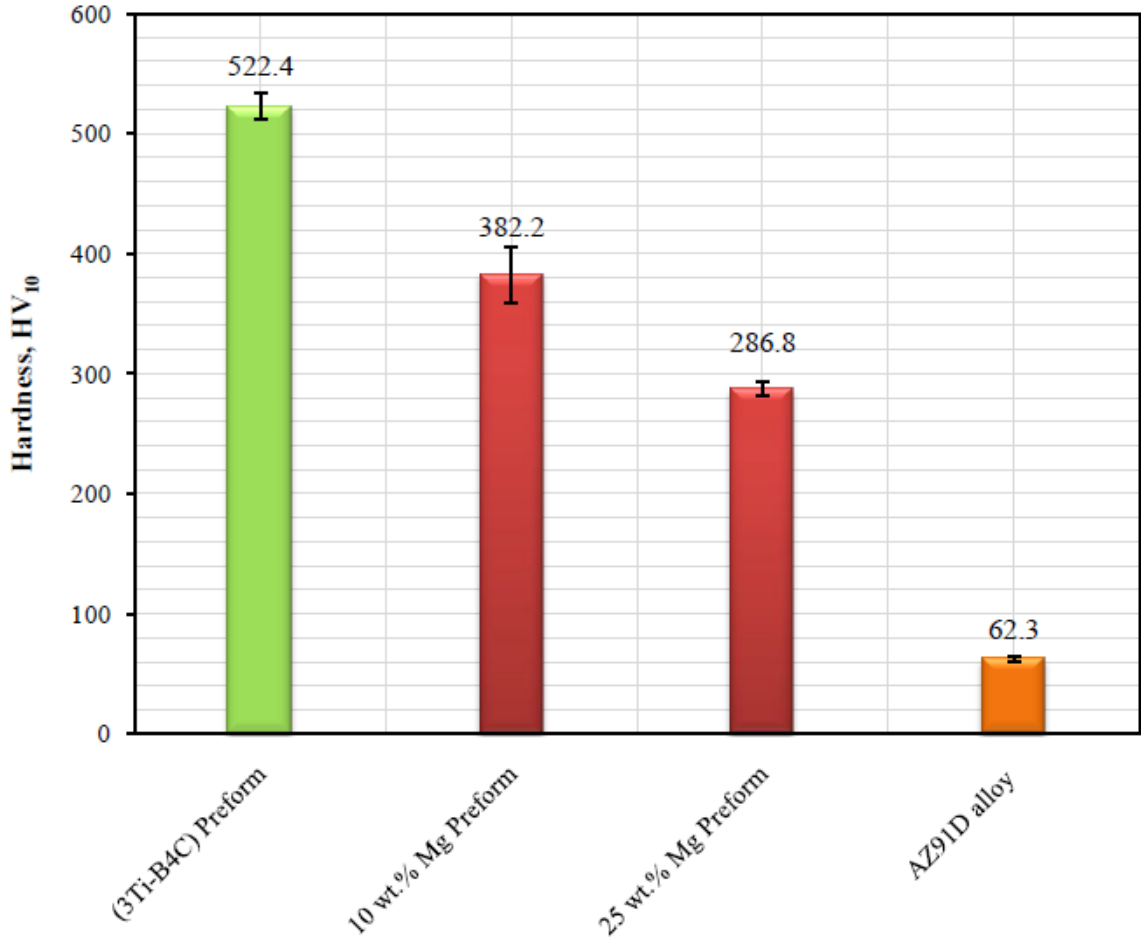
Figure 7.35 Hardness of the AZ91D alloy and TiC_x-TiB_2/AZ91D composites with different weight percentages of Mg powder in the preform

Also, the hardness of bulk pure Mg and the AM60B composites has been measured. The presence of TiC_x and TiB_2 reinforcing phases in pure Mg matrix leads to an increase in hardness. The results revealed that the hardness of bulk pure Mg composites reinforced with TiC_x-TiB_2 particles has an average value of 406 ±22 HV_{10} while that of unreinforced pure Mg is in the range of 35.9 ±2.75 HV_{10}.

215

Because of the high volume percentages of the reinforcing particles in the magnesium matrix especially in the composites fabricated using a 3Ti-B$_4$C preform without Mg or MgH$_2$ powder, it was very difficult to measure the microhardness in the particle-free regions to determine the properties of the matrix material only. Also, it is very difficult to measure the microhardness of the reinforcing particles since they are very small and it is very difficult to distinguish between them. However, the Vickers microhardness was measured for the unreinforced AZ91D and AZ91D matrix composites under different loads of 0.2, 0.5 and 1 kg. Ten measurements were taken for each sample along a line with a distance of almost 3 times the indentation size between every two points as shown in Figure 7.36.

Figure 7.37 shows the microhardness measurements of the TiC$_x$-TiB$_2$/AZ91D composites under different applied loads compared with those of the unreinforced AZ91D alloy. The lines of the measurements are different. It is clear that the microhardness varies from point to point due to the change of the phases and their percentages from point to point. Some points are rich in magnesium so give lower microhardness value while some points are rich in ceramic particles making the value higher. Hence, as observed in Figure 7.36, there is a difference in the size of the three indentations shown under the same load of 1 kg.
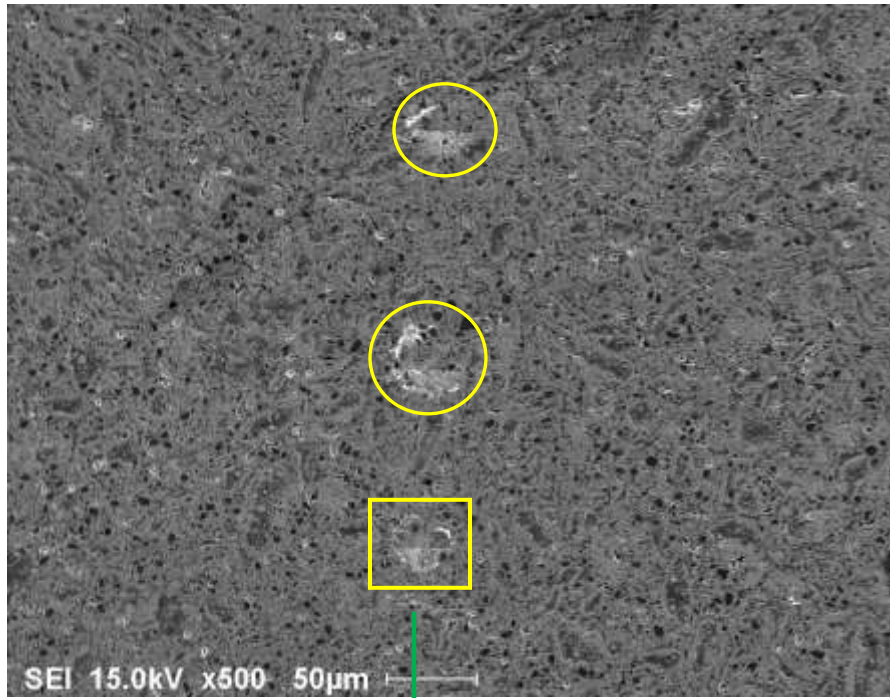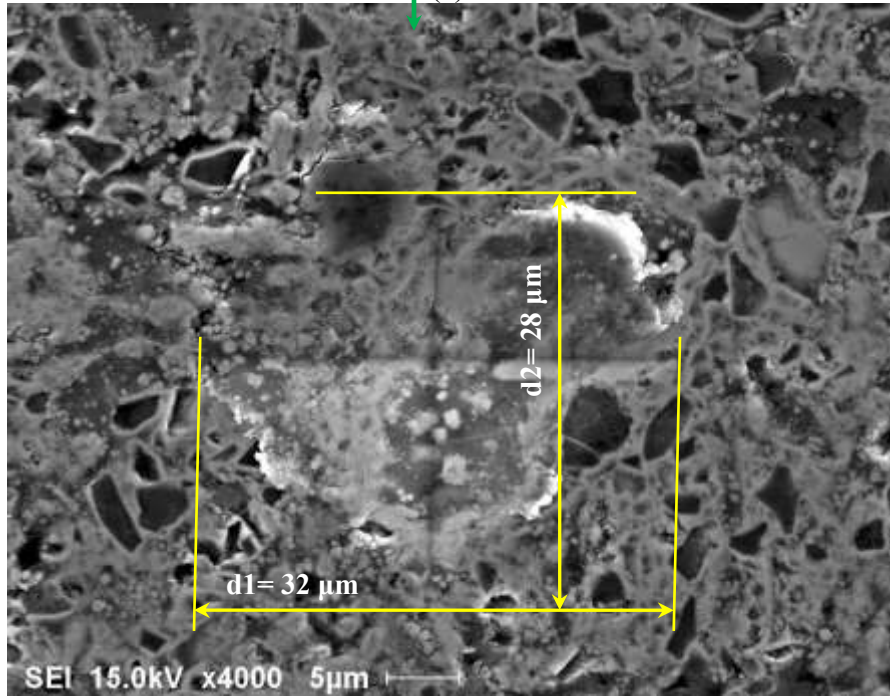
Figure 7.36 SEM micrographs of the microindentaion on the TiC$_x$-TiB$_2$/AZ91D composites
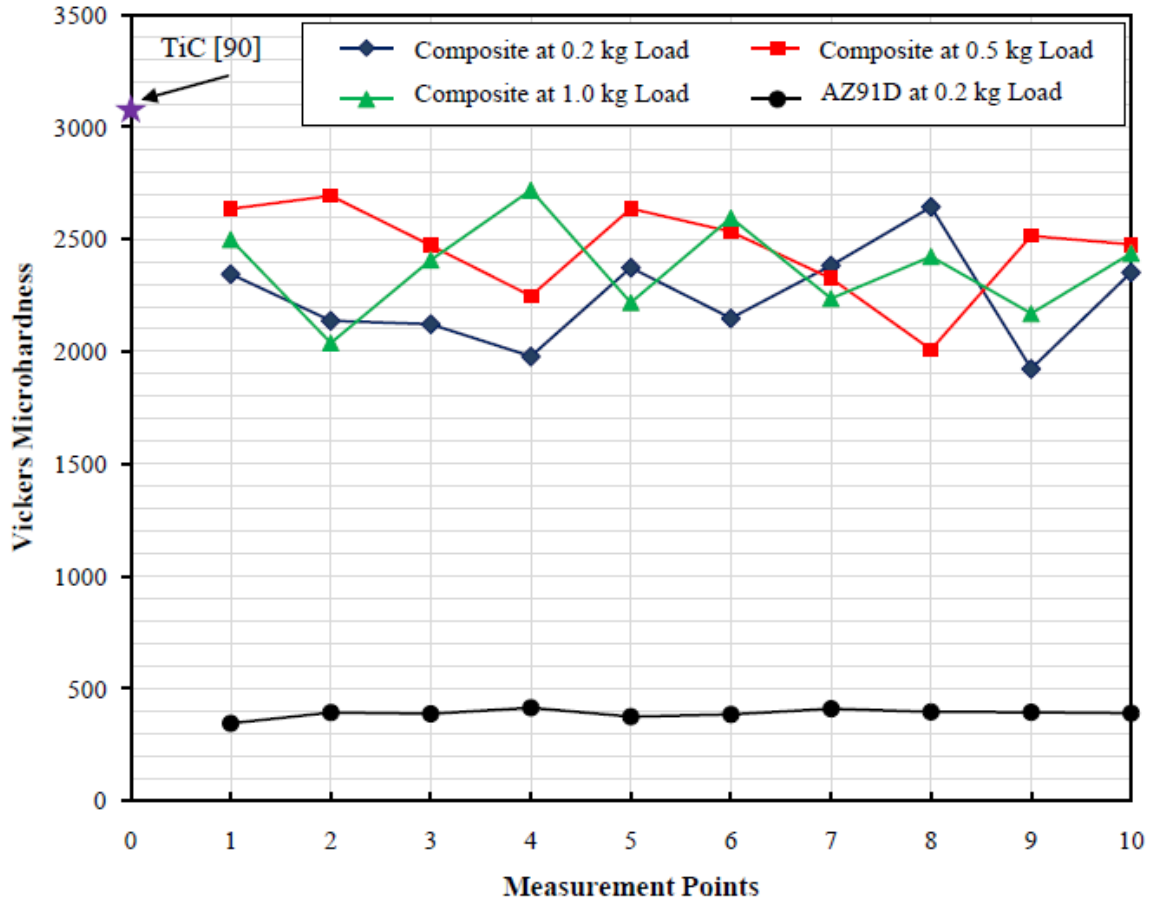
Figure 7.37 Vickers microhardness of the AZ91D alloy under 0.2 kg and its composites under different loads

Based on the these results, the average Vickers microhardness of the fabricated composite using 3Ti-B$_4$C preform at the optimal processing parameters was calculated to be 2356 ±108 HV$_{1.0}$ while that of the unreinforced AZ91D alloy is 388 ±21 HV$_{1.0}$. Therefore, the higher hardness of the composite compared with that of the unreinforced AZ91D matrix is due to the presence of the hard ceramic particles of TiC$_x$ and TiB$_2$ dispersed in the Mg matrix.

218

7.6 Wear Resistance Test Results

The wear rates for AZ91D and its composite at a constant load of 10 N and 500 m sliding distance but at different sliding speeds are plotted in Figure 7.38. As clear in the figure, both the wear rate of AZ91D alloy and the TiC_x-TiB_2/AZ91D composite increases with the increase of the sliding speed, but the TiC_x-TiB_2/AZ91D composite has lower wear rate than the unreinforced AZ91D alloy. The improvement of the wear resistance of the composites results from the presence of the network of the TiC and TiB_2 particles.
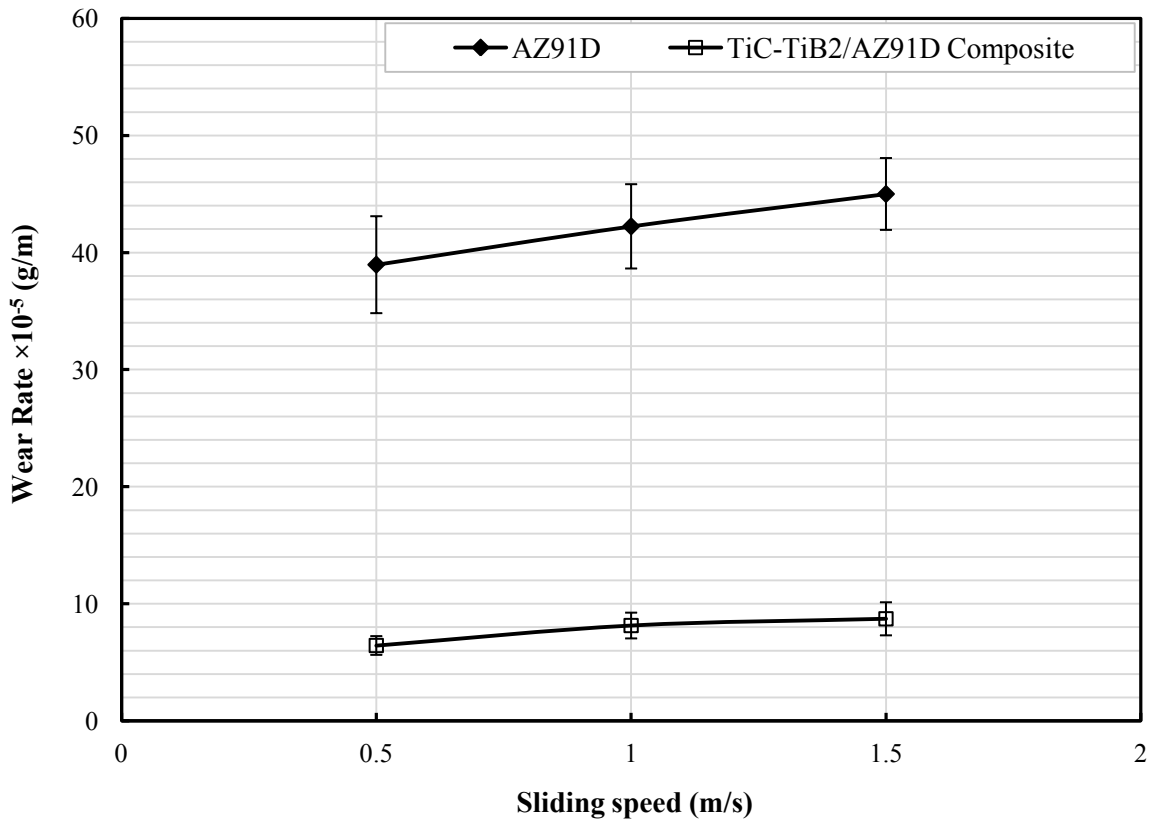
Figure 7.38 The variation of wear rate of the AZ91D alloy and TiC-TiB_2/AZ91D composites with the sliding speed

The influence of applied load on the wear rate of the AZ91D alloy and its composite is investigated by performing the wear test at the same sliding speed of 1 m/s and sliding distance of 500 m. The results, shown in Figure 7.39 reveal that an increase in

219

applied load increases the wear rate. However, the increase in wear rate with increasing

load is much more dramatic in the AZ91D alloy than the composite. The AZ91D alloy

exhibits very high wear rate and seizes at 45 N. In the case of composites, seizure was not

observed at 45 N, which is due to the presence of the reinforcing particles which restricts

the flow of metal during sliding.
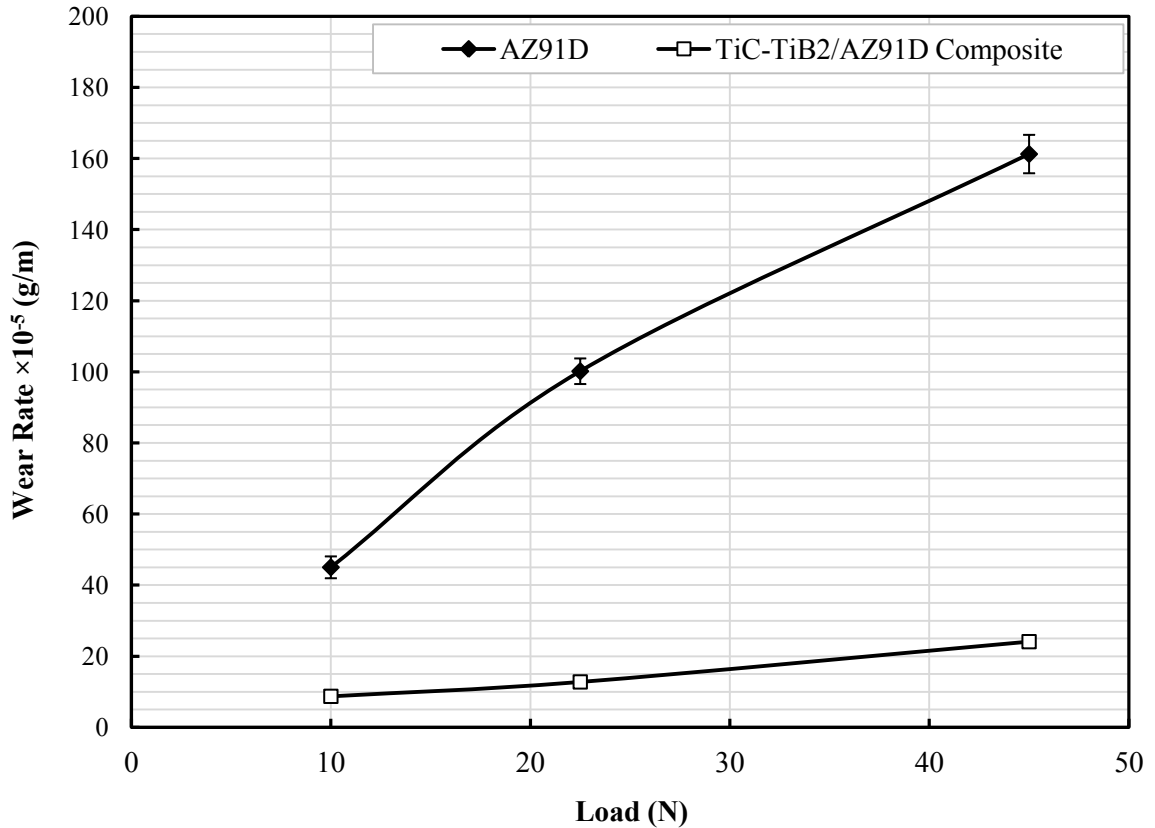
Figure 7.39 The variation of wear rate of the AZ91D alloy and TiC-TiB$_2$/AZ91D composites with the applied load

To investigate the wear mechanism, the surfaces of the worn samples were

examined under SEM. Figure 7.40 shows typical worn surfaces of the AZ91D alloy and

the TiC$_x$-TiB$_2$/AZ91D composite under an applied load of 10 N, 1.5 m/s sliding speed

and after 500 m sliding distance.

(a)   (b)

(c)   (d)
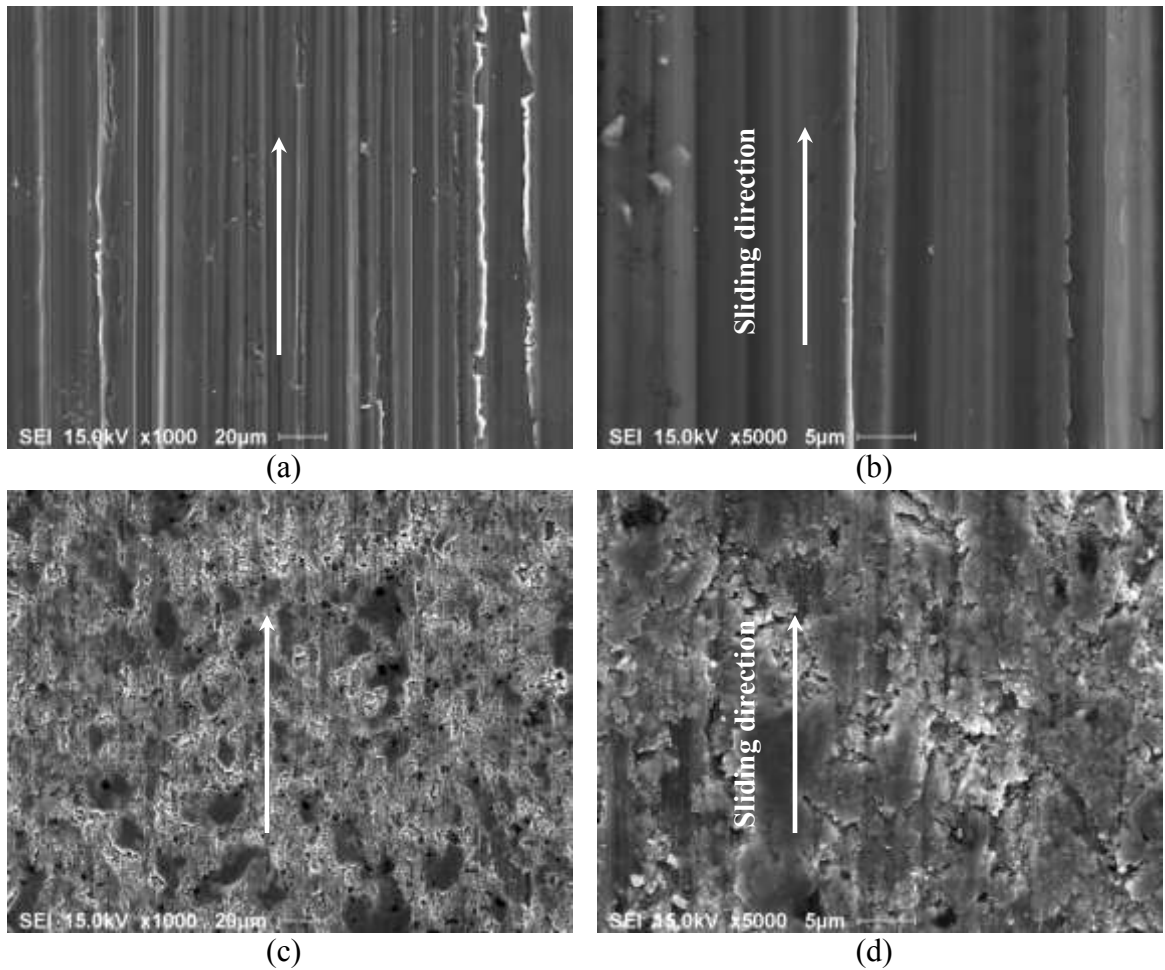
Figure 7.40 SEM micrographs of the worn surfaces of the AZ91D magnesium alloy and
the TiC$_x$-TiB$_2$/AZ91D composite at the sliding speed of 1.5 m/s and under a
normal load of 10 N at low and high magnification (a), (b) AZ91D alloy and
(c), (d) composite

As shown in the figure, many ploughed grooves produced by the harder asperities
on the surface of the counterface can be observed on the worn surfaces of the AZ91D
alloy. These grooves are deep and wide. On the contrary, the appearance of the worn
surface of the composite is significantly different from that of the unreinforced AZ91D
alloy; only shallow and thin ploughed grooves are observed on the worn surfaces of the
composite. It is clear that the reinforcing particles stand above the worn surface after the

magnesium alloy matrix has worn out in the ploughed grooves region. These observations reveal the role of the reinforcing particles, TiC and TiB$_2$, to strengthen the magnesium matrix and protect it against wear.

Because of the high wear resistance of TiC and TiB$_2$, the wear resistance of the composites is improved where these particles are relatively uniformly distributed as a network in the magnesium matrix and they are well bonded with the magnesium matrix as well.

In summary, the results reveal that the TiC$_x$-TiB$_2$/AZ91D composites have a lower wear rate and hence higher wear resistance than those of the unreinforced AZ91D alloy. This is directly related to the higher hardness and strength of the composites. Also, this is predicted by Archard's equation [133]. Enhancements in the hardness and strength could be due to the presence of the network of contacting particles of TiC$_x$ and TiB$_2$ in the relatively soft AZ91D matrix.

Chapter 8

Conclusions and Suggestions for Future Work

8.1 Conclusions

Magnesium matrix composites reinforced with a network of TiC_x and TiB_2 particles were successfully synthesized using a practical and low cost *in-situ* reactive infiltration technique. The *in-situ* reaction mechanism was studied and the effect of the processing parameters: temperature, holding time and green compact *RD* on the fabrication of the composites was investigated as well. Finally, the density, porosity and mechanical properties of the fabricated composites were evaluated.

8.1.1 *In-situ* Reaction Mechanism

- The microstructure of TiC_x-TiB_2/AZ91D composites is essentially evolved from the reaction between Ti, B_4C and the Mg melt. The substoichiometric TiC_x forms prior to TiB_2 because the diffusion of carbon in Ti is much faster than that of boron.

- Studying the *in-situ* reaction mechanism revealed the role of the Mg melt in the system where it not only infiltrates through the $3Ti-B_4C$ preform and thus densifies the fabricated composites as a matrix metal but also acts as an intermediary that makes the reaction possible at a lower temperature than that is required in the case of the solid-state reaction between Ti and B_4C.

- The addition of Mg or MgH_2 powder to the $3Ti-B_4C$ preform significantly accelerates the reaction between Ti and B_4C since Mg, or MgH_2 after decomposition, plays the

role of magnesium which reacts with B_4C before and during the infiltration of molten magnesium. However, the molten Mg or Mg alloy not only infiltrates through the Mg or MgH_2-(3Ti-B_4C) preform and thus densifies the fabricated composite as a matrix metal but also acts as intermediary in the reaction making the reaction faster.

8.1.2 Fabrication of TiC_x-TiB_2/Mg Matrix Composites

- Studying the effect of the processing parameters on the composite fabrication revealed that the composites synthesized using a 3Ti-B_4C preform with 70% *RD* at 900ºC for 1.5 h results in a relatively uniform distribution of the reinforcing phases with relatively no pores or microcracks.

- Based on XRD analysis, the required equilibrium phases, TiC_x and TiB_2, were formed in the fabricated composites with very small amounts of residual Ti, boron carbide and intermediate phases such as TiB, Ti_3B_4 and MgB_2. However, it is very difficult by SEM to distinguish between TiC_x, TiB, Ti_3B_4 and TiB_2 because these particles are very small and the difference in their effective atomic numbers is insignificant.

- SEM observations and XRD analysis revealed significant formation of the ternary compound (Ti_2AlC) in the composites fabricated using a 3Ti-B_4C preform with 70% *RD* at 900ºC for 3 h and longer. This ternary compound, Ti_2AlC, forms due to the diffusion of Al from the Mg alloy melt into the substoichiometric TiC_x compound.

- Fabrication of composites at 900ºC for 1.5 h avoids significant oxidation of Mg, and formation of the ternary compound (Ti_2AlC) in the cases of AZ91D or AM60B alloy composites which can adversely affect the mechanical properties.

224

- The volume percentage of the reinforcing phases in the composites can be tailored by controlling either the green compact RD or by adding Mg or MgH_2 powder to the 3Ti-B_4C preform.

- Although, the amount of Mg matrix in the composites using a 3Ti-B_4C preform with 60% RD was higher than that in the composites using the same preform but with 70% RD, the reaction to form the reinforcing particles for 60% RD was still incomplete since there were still significant amounts of retained Ti, boron carbide and intermediate phases such as TiB and MgB_2.

- Also, the addition of Mg or MgH_2 powder to the 3Ti-B_4C preform raised the volume percentage of Mg matrix compared to the reinforcing phases, TiC_x and TiB_2. For example, the volume percentage of Mg increased from ~ 52% in the composites fabricated using a 3Ti-B_4C preform to ~ 72% or 75% when 25 wt.% Mg or 25 wt.% MgH_2 powder is added to the 3Ti-B_4C preform, respectively.

- The ternary compound, Ti_2AlC, was formed in the composites fabricated using a preform containing Mg or MgH_2 powder at 900°C for a short time (even after 1 h holding time) and this is because the reaction was accelerated by the additions of Mg or MgH_2 promoting faster formation of TiC_x than in those fabricated without Mg/ MgH_2 additions.

8.1.3 Characterization of the TiC_x-TiB_2/Mg Matrix Composites

- The density measurements revealed that the fabricated composites are dense. Moreover, the density of the composites can be tailored by controlling the weight percentages of the Mg or MgH_2 powder added to the 3Ti-B_4C preform. For example,

the density of TiC_x-TiB_2/AZ91D composites decreased by nearly 13%, 20% and 28% after adding 10 wt.%, 25 wt.% and 40 wt.% MgH_2 powder to the 3Ti-B_4C preform, respectively.

- The results of the mechanical characterization revealed that TiC_x-TiB_2/Mg matrix composites developed in this study exhibit higher modulus and compressive strength compared with the unreinforced Mg matrix while the ductility is reduced. For example, the compressive strength and Young's modulus of the composites fabricated using a 3Ti-B_4C preform with 70% *RD* at 900ºC and 1.5 h increased by nearly 265% and 333%, respectively compared with those of the unreinforced AZ91D alloy while the ductility decreased by $\sim$ 79%.

- The strength and stiffness of the composites are significantly increased due to the presence of a network of the reinforcing phases, TiC_x and TiB_2, in the Mg matrix which blocks the dislocations motion and thus strengthens the material as a whole.

- It is clear that the strength and stiffness of the composites increase in response to the higher content of the reinforcing phases, TiC_x and TiB_2. The compression test results show that the composites fabricated using a 3Ti-B_4C preform are stiffer and stronger than those fabricated after adding Mg or MgH_2 powder to the preform. For example, the compressive strength and Young's modulus of the fabricated composites decreased from $\sim$ 878 MPa and 195 GPa, respectively with 0 wt.% MgH_2 in the preform to $\sim$ 370 MPa and 55 GPa, respectively with 40 wt.% MgH_2 in the preform. This means that the strength and stiffness decreased by $\sim$ 58% and 72% after adding 40 wt.% MgH_2 to the 3Ti-B_4C preform.

- On the other hand, the ductility was improved substantially when Mg or MgH$_2$ powder was added to the preform. For example, the ductility increased by nearly 26%, 81% and 187% by adding 10 wt.%, 25 wt.% and 40 wt.% MgH$_2$ powder, respectively. Hence, the mechanical properties of the composites can be tailored by controlling the weight percentages of Mg or MgH$_2$ powder added to the 3Ti-B$_4$C preform.

- AZ91D matrix composite exhibited a higher compressive strength compared with the pure Mg or AM60B matrix composites. However, the degree of strength improvement was greater in a pure magnesium composite than that in AM60B or AZ91D matrix composites. This phenomenon has been ascribed to the higher base mechanical properties of AZ91D in comparison to pure magnesium or AM60B alloy.

- The flexural strengths of the composites were higher than the tensile strength of the unreinforced pure Mg or Mg alloys and decreased with increasing the weight percentage of Mg or MgH$_2$ powder in the preform.

- The fracture surfaces through SEM of the composite samples after the flexural test revealed that the composites exhibit a combination of completely brittle fracture regions and brittle-ductile fracture regions. In the brittle-ductile fracture regions, microdimples associated with Mg-enriched zones were observed in the matrix. In addition, microcracks observed in the matrix show that the failure might have initiated in the matrix rather than from the particulates. Also, MgO particle pull-out was observed especially in the composites fabricated using a preform containing Mg or MgH$_2$ powder.

- The results show a clear rise in the hardness of TiC_x-TiB_2/AZ91D composites compared with that of the unreinforced AZ91D alloy by nearly 700% showing the role of the hard ceramic particles of TiC_x and TiB_2 in raising the hardness of the composite material as a whole.

- Also, the results reveal that the hardness of bulk TiC_x-TiB_2/AZ91D composites is affected by the volume fractions of the Mg matrix and the reinforcing phases. The volume fraction of the reinforcing phases was controlled by controlling the weight percentages of Mg or MgH_2 powder in the preform.

- Furthermore, the results revealed that the TiC_x-TiB_2/AZ91D composites have a lower wear rate and hence higher wear resistance than those of the unreinforced AZ91D alloy. This is directly related to the higher hardness and strength of the composites due to the presence of the network of TiC_x and TiB_2 phases in the soft AZ91D matrix.

- SEM observations revealed deep and wide grooves on the worn surface of the AZ91D alloy while shallow and thin ploughed grooves are found on the worn surfaces of the composite. These observations reveal the role of the reinforcing particles to strengthen the magnesium matrix and protect it against wear.

8.2 Suggestions for Future Work

- Studying the infiltration kinetics by investigating the infiltration length with time at different temperatures.

- Studying the effect of the heat treatment on the mechanical properties of the composites.

- Studying the effect of the particle size of the starting powders, Ti, B_4C, Mg, MgH_2, on the reaction mechanism, infiltration rate and hence the fabrication of the composites.

- Since, these composites are attractive for automotive applications, studying the damping capacity is very important.

Since Magnesium and magnesium alloys have HCP structure, they should present different mechanical property response to temperature change. The following would be interesting to investigate:

- Compressive behavior of magnesium matrix composites at different temperatures and strain rates.

- Creep behavior of magnesium matrix composites reinforced with TiC and TiB_2 particles.

8.3 Original Contributions to Knowledge

- For the first time, Mg matrix composites reinforced with a network of the TiC_x and TiB_2 particles are fabricated starting with Ti and B_4C materials without adding Al using a simple, practical and cost-effective *in-situ* reactive infiltration technique.

- The study of the reaction mechanism of the Mg-($3Ti$-B_4C) is considered to be a major contribution in this work, especially as this is the first investigation of the reaction mechanism of $3Ti$-B_4C and the effect of the infiltrated Mg on this reaction.

- This thesis constitutes the first attempt to add Mg or MgH_2 powder to the $3Ti$-B_4C preform for increasing the Mg content in the composites to improve their ductility and to investigate the effect of these additions on the reaction mechanism.

- This work reports on the formation of the Ti_2AlC ternary compound in the AZ91D alloy composites fabricated using $3Ti$-B_4C preform.

- This work succeeded to fabricate Mg matrix composites with tailored density and mechanical properties by controlling the weight percentages of Mg or MgH_2 powder added to the $3Ti$-B_4C preform.

- This work provides details of the mechanical behavior and wear resistance of the TiC_x-TiB_2/Mg composites. Significant enhancements in these properties have been achieved.

- Last but not least, pure Mg and Mg alloys, AZ91D and AM60B, are used in this work as a metal matrix and this work succeeds in controlling the mechanical properties for three magnesium matrix composites.

REFERENCES

[1]   K.G. Satyanarayana: Aluminum Cast Metal Matrix Composites, Handbook of Ceramics and Composites, Cheremisinoff N. P., New York, USA, 1989, pp. 555-599.

[2]   S.F. Hassan and M. Gupta: Development of a novel magnesium-copper based composite with improved mechanical properties, *Materials Research Bulletin*, Vol. 37, No. 2, 2002, pp. 377-389.

[3]   S.C. Tjong and Z.Y. Ma: Microstructural and mechanical characteristics of in situ metal matrix composites," *Materials Science and Engineering: R: Reports*, Vol. 29, No. (3-4), 2000, pp. 49-113.

[4]   Q.F. Guan, H.Y. Wang, X.L. Li, and Q.C. Jiang: Effect of compact density on the fabrication of Mg-TiC composites, *Journal of Materials Science*, Vol. 39, No. 16, 2004, pp. 5569-5572.

[5]   Q.C. Jiang, X.L. Li, and H.Y. Wang: Fabrication of TiC particulate reinforced magnesium matrix composites, *Scripta Materialia*, Vol. 48, No. 6, 2003, pp. 713-717.

[6]   B.L. Mordike, and T. Ebert: Magnesium: Properties-applications-potential, *Materials Science and Engineering A*, Vol. 302, No. 1, 2001, pp. 37-45.

[7]   A. Luo: Processing, microstructure, and mechanical behavior of cast magnesium metal matrix composites, *Metallurgical and Materials Transactions A: Physical Metallurgy and Materials Science*, Vol. 26A, No. 9, 1995, pp. 2445-2455.

[8]   M. Kulekci: Magnesium and its alloys applications in automotive industry, *The International Journal of Advanced Manufacturing Technology*, Vol. 39, No. 9, 2008, pp. 851-865.

[9]   H.Y. Wang, Q.C. Jiang, X.L. Li, J.G. Wang, Q.F. Guan, and H.Q. Liang: *In-situ* synthesis of TiC from nanopowders in a molten magnesium alloy, *Materials Research Bulletin*, Vol. 38, No. 8, 2003, pp. 1387-1392.

[10] Y. Wang, H.Y. Wang, K. Xiu, H.Y. Wang, and Q. C. Jiang: Fabrication of TiB$_2$ particulate reinforced magnesium matrix composites by two-step processing method, *Materials Letters*, Vol. 60, No. 12, 2006, pp. 1533-1537.

[11] L.Q. Chen, Q. Dong, M.J. Zhao, J. Bi, and N. Kanetake: Synthesis of TiC/Mg composites with interpenetrating networks by *in-situ* reactive infiltration process, *Materials Science and Engineering: A*, Vol. 408, No. (1-2), 2005, pp. 125-130.

[12] G. Wen, S.B. Li, B.S. Zhang, and Z.X. Guo: Reaction synthesis of TiB$_2$-TiC composites with enhanced toughness, *Acta Materialia*, Vol. 49, No. 8, 2001, pp. 1463-1470.

[13]   W.J. Li, , R. Tu, and T. Goto: Preparation of directionally solidified TiB$_2$-TiC eutectic composites by a floating zone method, *Materials Letters*, Vol. 60, No. 6, 2006, pp. 839-843.

[14] X. Zhang, H. Wang, L. Liao, and N. Ma: New Synthesis Method and Mechanical Properties of Magnesium Matrix Composites, *Journal of ASTM International*, 2005, Vol. 3, No. 10.

[15] B. Ma, H. Wang, Y. Wang, and Q. Jiang: Fabrication of (TiB$_2$−TiC)$_p$/AZ91 magnesium matrix hybrid composite, *Journal of Materials Science*, Vol. 40, No. 17, 2005, pp. 4501-4504.

[16] X. Zhang, H. Wang, L. Liao, X. Teng, and N. Ma: The mechanical properties of magnesium matrix composites reinforced with (TiB$_2$+TiC) ceramic particulates, *Materials Letters*, Vol. 59, No. 17, 2005, pp. 2105-2109.

[17] K.U. Kainer: *Magnesium-Alloys and Technology*, Wiley-VCH Verlag GmbH & Co, Weinheim, Germany, 2003.

[18] Y.Z. Lü, Q.D. Wang, W.J. Ding, X.Q. Zeng, and Y.P. Zhu: Fracture behavior of AZ91 magnesium alloy, *Materials Letters*, Vol. 44, No. 5, 2000, pp. 265-268.

[19] L. Chen, J. Guo, , B. Yu, , and Z. Ma: Compressive Creep Behavior of TiC/AZ91D Magnesium-matrix Composites with Interpenetrating Networks, *Journal of Materials Science and Technology*, Vol. 23, No. 2, 2007, pp. 207-212.

[20] Q. Dong, L.Q. Chen, M.J. Zhao, and J. Bi: Synthesis of TiC_p reinforced magnesium matrix composites by *in-situ* reactive infiltration process, *Materials Letters*, Vol. 58, No. 6, 2004, pp. 920-926.

[21] D. Qun, L. Chen, Z. Mingjiu, and B. Jing: Analysis of *in-situ* reaction and pressureless infiltration process in fabricating TiC/Mg composites, *Journal of Materials Science and Technology*, Vol. 20, 2004, pp. 3-7.

[22] L. Chen, J. Guo, J. Wang, X. Yongbo, and B. Jing: Tensile Deformation and Fracture Behavior of AZ91D Magnesium Alloy and TiC/Mg Magnesium Matrix Composites Synthesized by *in-situ* Reactive Infiltration Technique, *Journal of Rare Metal Materials and Engineering*, Vol. 35, No. 1, 2006, pp. 29-32.

[23] J.J. Wang, J.H. Guo, and L.Q. Chen: TiC/AZ91D composites fabricated by *in-situ* reactive infiltration process and its tensile deformation, *Transactions of Nonferrous Metals Society of China*, Vol. 16, No. 4, 2006, pp. 892-896.

[24] W. Cao, C. Zhang, T. Fan, and D. Zhang: *In-Situ* Synthesis and Compressive Deformation Behaviors of TiC Reinforced Magnesium Matrix Composites, *Materials Transactions*, Vol. 49, No. 11, 2008, pp. 2686-2691.

[25] A. Chaubey, B. Mishra, N. Mukhopadhyay, and P. Mukherjee: Effect of compact density and preheating temperature of the Al–Ti–C preform on the fabrication of *in-situ* Mg–TiC composites, *Journal of Materials Science*, Vol. 45, No. 6, 2010, pp. 1507-1513.

[26] N. Chawla and K.K. Chawla: *Metal Matrix Composites*, Springer+Busness Media, Inc., New York, 2006.

[27] H. Ye, and X. Liu: Review of recent studies in magnesium matrix composites, *Journal of Materials Science*, Vol. 39, No. 20, 2004, pp. 6153-6171.

[28] S.R. Nutt: Defects in Silicon Carbide Whiskers, *Journal of the American Ceramic Society*, Vol. 67, No. 6, 1984, pp. 428-431.

[29] A. Evans, C. San Marchi, and A. Mortensen: Metal matrix composites in industry: an introduction and a survey, Kluwer Academic Publishers, Dordrecht, Netherlands, 2003.

[30] I.A. Ibrahim, F.A. Mohamed, and E.J. Laverina: Particulate reinforced metal matrix composites-a review, *Journal of Materials Science*, Vol. 26, 1991, pp. 1137-1156.

[31] A.L. Geiger and M. Jackson: Low-expansion MMCs boost avionics, *Advanced Materials Process*, Vol. 136, No. 1, 1989, pp. 23-30.

[32] C.A. Leon-Patino: Infiltration Processing of Metal Matrix Composites using Coated Ceramic Particulates, Ph.D. diss., McGill university, Montreal, Canada, 2000.

[33] K.U. Kainer: Influencee of the Production Technique and Type of Reinforcement on the properties of Magnesium Matrix Composites, *Composite Material technology, ASME,* Vol. 37, 1991, pp. 191-197.

[34] R.W. Cahn, P. Haasen, and E.J. Kramer: *Structure and Properties of Composites*, VCH, New York, USA, 1993.

[35] P.K. Rohatgi: *Cast Metal Matrix Composites*, ASM International, Ohio, USA, 1988.

[36] H.Y. Wang, Q.C. Jiang, Y.G. Zhao, and F. Zhao: In situ synthesis of TiB_2/Mg composite by self-propagating high-temperature synthesis reaction of the Al-Ti-B system in molten magnesium, *Journal of Alloys and Compounds*, Vol. 379, No. (1-2), 2004, pp. L4-L7.

[37] B.W. Chua, L. Lu, and M.O. Lai: Influence of SiC particles on mechanical properties of Mg based composite, *Composite Structures*, Vol. 47, No. (1-4), 1999, pp. 595-601.

[38] Q.C. Jiang, H.Y. Wang, B.X. Ma, Y. Wang, and F. Zhao: Fabrication of B_4C particulate reinforced magnesium matrix composite by powder metallurgy, *Journal of Alloys and Compounds*, Vol. 386, No. (1-2), 2005, pp. 177-181.

234

[39] K. Xiu, Q. Jiang, B. Ma, Y. Wang, H. Sui, and E. Shang: Fabrication of TiC/Mg composites by powder metallurgy, *Journal of Materials Science*, Vol. 41, No. 5, 2006, pp. 1663-1666.

[40]   H.Y. Wang, Q.C. Jiang, Y. Wang, B.X. Ma, and F. Zhao: Fabrication of TiB$_2$ particulate reinforced magnesium matrix composites by powder metallurgy, *Materials Letters*, Vol. 58, No. (27-28), 2004, pp. 3509-3513.

[41] J. Hashim, L. Looney, and M.S.J. Hashmi: Metal matrix composites: production by the stir casting method, *Journal of Materials Processing Technology*, Vol. 92-93, 1999, pp. 1-7.

[42] M.K. Surappa: Microstructure evolution during solidification of DRMMCs: state of art, *Journal of Materials Processing Technology*, Vol. 63, 1997, pp. 325-333.

[43]   D.M. Skibo, D.M. Schuster, and L. Jolla: Process for preparation of composite materials containing nonmetallic particles in a metallic matrix and composite materials made thereby, US Patent 4786467, 1988.

[44]   G.S. Hanumanth, and G.A. Irons: Particle incorporation by melt stirring for the production of metal-matrix composites, *Journal of Materials Science*, Vol. 28, No. 9, 1993, pp. 2459-2465.

[45]   R.A. Saravanan and M.K. Surappa: Fabrication and characterisation of pure magnesium-30 vol.% SiC$_P$ particle composite, *Materials Science and Engineering A*, Vol. 276, No. (1-2), 2000, pp. 108-116.

[46] P. Poddar, V.C. Srivastava, P.K. De, and K.L. Sahoo: Processing and mechanical properties of SiC reinforced cast magnesium matrix composites by stir casting process, *Materials Science and Engineering: A*, Vol. 460-461, 2007, pp. 357-364.

[47] R. Asthana: Reinforced cast metals: Part I Solidification microstructure, *Journal of Materials Science*, Vol. 33, No. 7, 1998, pp. 1679-1698.

[48] T.W. Clyne: 3.7.12. Metal Matrix Composites: Matrices and Processing," Encyclopedia of Materials: Science and Technology, Composites: MMC, CMC, PMC, ed. A Mortensen, Elsevier, 2001, pp. 1-14.

[49] D.J. Lloyd: Particle reinforced aluminium and magnesium matrix composites, *International Materials Reviews*, Vol. 39, 1994, pp. 1-23.

[50] T.W. Clyne and P.J. Withers: *An Introduction to Metal Matrix Composites*, Cambridge University Press, London, England, 1995.

[51] T. Ebert, F. Moll, and K.U. Kainer: Spray forming of magnesium alloys and composites, *Powder Metallurgy*, Vol. 40, No. 2, 1997, pp. 126-130.

[52] A. Noguchi, I. Ezawa, J. Kaneko, and M. Sugamata: SiC_p/Mg-Ce and Mg-Ca alloy composites obtained by spray forming, *Keikinzoku*, Vol. 45, No. 2, 1995, pp. 64-69.

[53] P.J. Vervoort and J. Duszczyk: Spray deposited magnesium alloy and composite, *In Procceedings of International Conference on PM Aerospace Materials*, 1991.

[54] H.Y. Wang, Q.C. Jiang, X.L. Li, and J.G. Wang: In situ synthesis of TiC/Mg composites in molten magnesium, *Scripta Materialia*, Vol. 48, No. 9, 2003, pp. 1349-1354.

[55] Q.C. Jiang, H.Y. Wang, J.G.Wang, Q.F. Guan, and C.L. Xu: Fabrication of TiC_p/Mg composites by the thermal explosion synthesis reaction in molten magnesium, *Materials Letters*, Vol. 57, No. (16-17), 2003, pp. 2580-2583.

[56] M.J. Koczak and M.K. Premkumar: Emerging technologies for the in situ production of MMC's, *The Journal of the Minerals, Metals, and Materials Society*, Vol. 45, No. 1, 1993, pp. 44-48.

[57] R.J. LaBotz and D.R. Mason: The thermal conductivities of Mg_2Si and Mg_2Ge, *Journal of the Electrochemical Society*, Vol. 110, No. 2, 1963, pp. 121-126.

[58] S. Beer, G. Frommeyer, and E. Schmid: Development of Mg-Mg$_2$Si light weight alloys, Magnesium Alloys Their Applications, DGM conference paper, 1992, pp. 317-324.

[59] E.E. Schmid, K. Von Oldenburg, and G. Forommeyer: Microstructure and properties of as-cast intermetallic Mg$_2$Si-Al alloys, *Z. fur Metallkunde*, Vol. 81, No. 11, 1990, pp. 809-815.

[60] M. Mabuchi, K. Kubota, and K. Higashi: Tensile strength, ductility and fracture of magnesium-silicon alloys, *Journal of Materials Science*, Vol. 31, No. 6, 1996, pp. 1529-1535.

[61] M. Mabuchi, K. Kubota, and K. Higashi: Development of Mg-Si alloys by I/M and R/S routes, *Proceedings of the Third Symposium on Light Weight Alloys for Aerospace Applications*, Las Vegas, Nevada, USA, 1995, pp. 463-470.

[62] M. Mabuchi, K. Kubota, and K. Higashi: High strength and high strain rate superplasticity in a Mg-Mg$_2$Si composite, *Scripta Metallurgica et Materialia*, Vol. 33, No. 2, 1995, pp. 331-335.

[63] H. Yu, G. Min, and X. Chen: The microstructure and mechanical properties of Mg-11Li composites reinforced by the self-nascent MgO/Mg$_2$Si particulates, *Metallofizika I Noveishie Tekhnologii*, Vol. 20, No. 1, 1998, pp. 61-64.

[64] T. Choh, M. Kobashi, H. Nakata, and H. Kaneda: Fabrication of metal matrix composites by spontaneous infiltration and subsequent in-situ reaction process, *Materials Science Forum*, Vol. 217-222, 1996, pp. 353-358.

[65] K. Yamada, T. Takahashi, and M. Motoyama: EPMA state analysis of formation of TiC during mechanical alloying on a Mg-Ti-graphite powder mixture, *Journal of the Japan Institute of Metals*, Vol. 60, No. 1, 1996, pp. 100-105.

[66] A. Contreras, V.H. López, and E. Bedolla: Mg/TiC composites manufactured by pressureless melt infiltration, *Scripta Materialia*, Vol. 51, No. 3, pp. 249-253.

[67] M.A. Matin, L. Lu, and M. Gupta: Investigation of the reactions between boron and titanium compounds with magnesium, *Scripta Materialia*, Vol. 45, No. 4, 2001, pp. 479-486.

[68] D. Muscat, K. Shanker, and R.A.L. Drew: Al/TiC Composites Produced by Melt Infiltration, *Materials Science & Technology*, Vol. 8, No. 11, 1992, pp. 971-976.

[69] S.T. Mileiko: *Fabrication of Metal Matrix Composites*, Elsevier Science Publishers, 1983.

[70] D. Muscat and R.A.L. Drew: Infiltration Kinetics of Aluminum in Titanium Carbide Preforms, *In Proceedings of International Conference High Temperature Capillarity*, Cracow, Poland, 1997.

[71] D. Kopeliovich, "Liquid state fabrication of Metal Matrix Composites", http://www.substech.com, Apr. 2009.

[72] F. Delannay, L. Froyen, and A. Deruyttere: The wetting of solids by molten metals and its relation to the preparation of metal-matrix composites composites, *Journal of Materials Science*, Vol. 22, No. 1, 1987, pp. 1-16.

[73] H. Lianxi, and W. Erde: Fabrication and mechanical properties of SiCw/ZK51A magnesium matrix composite by two-step squeeze casting, *Materials Science and Engineering A*, Vol. 278, No. (1-2), 1999, pp. 267-271.

[74] A. Lu, J. Renaud, I. Nakatsugawa, and J. Plourde: Magnesium Castings for Automotive Applications, *JOM*, Vol. 47, No. 7, 1995, pp. 28-31.

[75] K. Wu, M. Zheng, C. Yao, T. Sato, H. Tezuka, A. Kamio, and D.X. Li: Crystallographic orientation relationship between SiC_w and Mg in squeeze-cast SiC_w/Mg composites, *Journal of Materials Science Letters*, Vol. 18, No. 16, 1999, pp. 1301-1303.

[76] M. Zheng, K. Wu, and C. Yao: Effect of interfacial reaction on mechanical behavior of SiC_w/AZ91 magnesium matrix composites, *Materials Science and Engineering A*, Vol. 318, No. (1-2), 2001, pp. 50-56.

[77] G.A. Chadwick, and A. Bloyce: Squeeze cast magnesium alloys and magnesium based composites, *Magnesium Alloys Their Applications, DGM Conference Paper*, 1992, pp. 93-100

[78] K.U. Kainer: *Magnesium-Alloys and Technology*, Wiley-VCH, Weinheim, Germany, 2000.

[79] M.M. Schwartz: *Composite Materials, Volume I: Properties, Non-Destructive Testing, and Repair*, Prentice Hall, New Jersey, USA, 1997.

[80] C. Toy, and W.D. Scott: Ceramic-metal composites produced by melt infiltration, *Journal of American Ceramic Society*, Vol. 73, No. 1, 1990, pp. 97-101.

[81] S. Valdez, B. Campillo, R. Pérez, L. Martínez, and H.A. García: Synthesis and microstructural characterization of Al-Mg alloy-SiC particle composite, *Materials Letters*, Vol. 62, No. (17-18), 2008, pp. 2623-2625.

[82] H. Kaneda, and T. Choh: Fabrication of particulate reinforced magnesium composites by applying a spontaneous infiltration phenomenon, *Journal of Materials Science*, Vol. 32, No. 1, 1997, pp. 47-56.

[83] E. Aghion, B. Bronfin, and D. Eliezer: The role of the magnesium industry in protecting the environment, *Journal of Materials Processing Technology*, Vol. 117, No. 3, 2001, pp. 381-385.

[84] X. Zhang, L. Liao, N. Ma, and H. Wang: New In-situ synthesis method of magnesium matrix composites reinforced with TiC particulates, *Materials Research*, Vol. 9, 2006, pp. 357-360.

[85] J.N. Fridlyander, and I.H. Marshall: *Metal Matrix Composites*, Caphman & Hall, London, England, 1995.

[86] M. Taya, and R.J. Arsenault: *Metal Matrix Composites*, Pergamon Press, New York, USA, 1989.

[87] M.M. Avedesian and H. Baker: *Magnesium and magnesium alloys*, ASM International. Ohio, US, 1999.

[88] Y. Liang, and S.P. Dutta: Application trend in advanced ceramic technologies, *Technovation*, Vol. 21, No. 1, 2001, pp.61-65.

[89] N. Durlu: Titanium carbide based composites for high temperature applications, *Journal of the European Ceramic Society*, Vol. 19, No. (13-14), 1999, pp. 2415-2419.

[90] J.F. Shackelford and W. Alexander: *CRC Materials Science and Engineering Handbook*, Third edition, CRC Press, Boca Raton, Florida, 2001.

[91] R.G. Munro: Material Properties of Titanium Diboride, *Journal of Research of the National Institute of Standards and Technology*, Vol. 105, No. 5, 2000, pp. 709-720.

[92] F. De Mestral and F. Thevenot: Ceramic composites: TiB-TiC-SiC, *Journal of Materials Science*, Vol. 26, No. 20, 1991, pp. 5547-5560.

[93] H. Holleck, H. Leiste, E. Nold, H. Schulz, and A. Skokan: Multiphase ceramic materials and coatings for fusion reactor applications, *Journal of Nuclear Materials*, Vol. 155-157, No. 1, 1988, pp. 221-224.

[94] H.O. Pierson: *Handbook of Refractory Carbides and Nitrides*, Noyes Puplications, Westwood, New Jersey, USA, 1996.

[95] Y. Zhou, and Z. Sun: Crystallographic relations between Ti_3SiC and TiC, *Materials Research Innovations*, Vol. 3, No. 5, 2000, pp. 286-291.

[96] W.H. Gitzen: *Alumina as a Ceramic Material*, American Ceramic Society. Westerville, Ohio, USA, 1970.

[97] D.P. Riley and E.H. Kisi: A New Solid State Synthesis Methodology for Ternary and Higher Order Compounds, *Journal of the American* Ceramic *Society*, Vol. 90, 2007, pp. 102-109.

[98] D. Music, D.P. Riley, and J.M. Schneider: Energetics of Point Defects in TiC, *Journal of the European* Ceramic *Society*, Vol. 29, 2009, pp. 773-777.

[99]   Y. Zhou, and Z. Sun: Electronic structure and bonding properties of layered machinable Ti_2AlC and Ti_2AlN ceramics, *Physical Review B*, Vol. 61, No. 19, 2000, pp. 12570-12573.

[100] Z. Sun, D. Music, R. Ahuja, S. Li, and , J.M. Schneider: Bonding and classification of nanolayered ternary carbides, *Physical Review B*, Vol. 70, No. 9, 2004, pp. 1-3.

[101] Y.C. Zhou and X.H. Wang: Deformation of polycrystalline Ti_2AlC under compression, *Materials Research Innovations*, Vol. 5, No. 2, 2001,pp. 87-93.

[102] W.B. Zhou, B.C. Mei, and J.Q. Zhu: Rapid reactive synthesis of Ti_2AlC-TiB_2 composites by spark plasma sintering, *Journal of Ceramic Processing Research*, Vol. 10, No. 1, 2009, pp. 102-104.

[103] P. Wang, B.C. Mei, X.L. Hong, and W.B. Zhou: Synthesis of Ti2AlC by hot pressing and its mechanical and electrical properties, *Transactions of Nonferrous Metals Society of China*, Vol. 17, No. 5, 2007, pp. 1001-1004.

[104] H. Holleck, H. Leiste, and W. Schneider: Significance of phase boundaries in wear resistant TiC/TiB_2 materials, *Materials Science Monographs*, Vol. 38C (High Tech Ceram., Pt. C), 1987, pp. 2609-2622.

[105] V. Milman and M.C. Warren: Elastic properties of TiB_2 and MgB_2, *Journal of Physics: Condensed Matter*, Vol. 13, 2001, pp. 5585-5595.

[106] Q.C. Jiang: In-situ Synthesis of TiB_2 Particulate Locally Reinforced Steel Matrix Composite by the Self-propagating High-temperature Synthesis Reaction of Al-Fe-Ti-B System during Casting, *ISIJ international*, Vol. 44, No. 11, 2004, pp. 1847-1851.

[107] J. Molina, J. Tian, J. Narciso, and E. Louis: Fabrication of Al/TiB composites through gas pressure infiltration, *Journal of Materials Science*, Vol. 45, No. 10,2010, pp. 2816-2821.

[108] H.Y. Wang, Q.C. Jiang, Y. Wang, B.X. Ma, and F. Zhao: Fabrication of TiB_2 particulate reinforced magnesium matrix composites by powder metallurgy, *Materials Letters*, Vol. 58, No. (27-28), 2004, pp. 3509-3513.

[109] S. Sugiyama, K. Asari, and H. Taimatsu: Synthesis of Ti-B-C composites by reactive spark plasma sintering of B_4C and Ti, *Journal of the Ceramic Society of Japan*, Vol. 108, 2000, pp. 747-752.

[110] W.S.M. Williams: Transition metal carbides, nitrides, and borides for electronic applications," *JOM*, Vol. 49, No. 3, 1997, pp. 38-42.

[111] A.G. Merzhanov and I.P. Borovinskaya: Self-propagating high-temperature synthesis of refractory inorganic compounds, *Doklady Akademii Nauk SSSR*, Vol. 204, No. 2, 1972, pp. 366-369.

[112] A.G. Merzhanov and A.K. Filonenko: New phenomena during the combustion of condensed systems, *Doklady Akademii Nauk SSSR*, Vol. 208, No. 4, 1973, pp. 892-894.

[113] A.G. Merzhanov, G.G. Karyuk, I.P. Borovinskaya, S.Y. Sharivker, E.I. Moshkovskii, V.K. Prokudina, and E.G. Dyad'ko: Titanium carbide produced by self-propagating high-temperature synthesis-Valuable abrasive material, *Powder Metallurgy and Metal Ceramics*, Vol. 20, No. 10, 1981, pp. 709-713.

[114] I. Borovinskaya, A. Merzhanov, N. Novikov, and A. Filonenko: Gasless combustion of mixtures of powdered transition metals with boron, *Combustion, Explosion, and Shock Waves*, Vol. 10, No. 1, 1974, pp. 2-10.

[115] N.D. Corbin, W. James, and A.L. Command: *Self-Propagating High-Temperature Synthesis (SHS): Current Status and Future Prospects*, MTL MS 86-1, Watertown, MA, 1986.

[116] Y. Wang, H.Y. Wang, B.X. Ma, K. Xiu, and Q.C. Jiang: Effect of Ti/B on fabricating $TiB_2p/AZ91$ composites by employing a TiB_2p/Al master alloy, *Journal of Alloys and Compounds*, Vol. 422, No. (1-2), 2006, pp. 178-183.

[117] H.Y. Wang, Q.C. Jiang, Y.Q. Zhao, F. Zhao, B.X. Ma, and Y. Wang: Fabrication of TiB_2 and TiB_2-TiC particulates reinforced magnesium matrix composites, *Materials Science and Engineering A*, vol. 372, No. (1-2), 2004, pp. 109-114.

[118] P.J. Davies, J.L.F. Kellie, and J.V. Wood: UK Patent no. 2 257985A, ASM, September 1992.

[119] J. Kellie, and J.V. Wood: Reaction processing in the metals industry, *Materials World*, Vol. 3, No. 1, 1995, pp. 10-12.

[120] J.L.F. Davies, J.L.F. Kellie, and J.V. Wood: Development of cast aluminum MMC's, *Key Engineering Materials*, Vol. 77-78, 1993, pp. 357-361.

[121] J.V. Wood, P. Davies, and J.L.F. Kellie: Properties of reactively cast aluminum-TiB$_2$ alloys, *Materials Science Technology*, Vol. 9, No. 10, 1993, pp. 833-840.

[122] L. Lu, M.O. Lai, and F.L. Chen: Al-4 wt% Cu Composite reinforced with in-situ TiB$_2$ particles, *Acta Materialia*, Vol. 45, No. 10, 1997, pp. 4297-4309.

[123] Y. Chen, and D.D.L. Chung: In situ Al-TiB composite obtained by stir casting, *Journal of Materials Science*, Vol. 31, No. 2, 1996, pp. 311-315.

[124] Y. Chen, and D.D.L. Chung: Ductile and strong aluminium-matrix titanium aluminide composite formed from aluminium, titanium dioxide and sodium hexafluoroaluminate, *Journal of Materials Science*, Vol. 30, No. 18, 1995, pp. 4609-4616.

[125] W. Cao, C. Zhang, T. Fan, and D. Zhang: In-situ synthesis of TiB$_2$/Mg composites by flux-assisted synthesis reaction of the Al-Ti-B in molten magnesium, *Journal of Key Engineering Materials*, Vol. 351, 2007, pp. 166-170.

[126] X. Zhang, L. Liao, N. Ma, and H. Wang: Effect of aging hardening on in situ synthesis magnesium matrix composites, *Materials chemistry and physics*, Vol. 96, No. 1, 2006, pp. 9-15.

[127] K. Kondoh, M. Kawakami, H. Imai, J. Umeda, and H. Fujii: Wettability of pure Ti by molten pure Mg droplets, *Acta Materialia*, Vol. 58, 2010, pp. 606- 614.

[128] W. Cao, C. Zhang, T. Fan, and D. Zhang: In situ synthesis and damping capacities of TiC reinforced magnesium matrix composites, *Materials Science and Engineering: A*, Vol.496, No. (1-2), 2008, pp. 242-246.

[129] X. Zhang, D. Zhang, R. Wu, Z. Zhu, and C. Wang: Mechanical properties and damping capacity of (SiC whisker + B_4C particle)/ZK60A Mg alloy matrix composite, *Scripta Materialia*, Vol. 37, No. 11, 1997, pp. 1631-1635.

[130] X. Zhang, X. Li, and H. Wang: Research of Mechanical Properties on In-Situ TiC/AZ91 Composites, *Zhuzao (Foundry)*, Vol. 56, No. 11, 2007, pp. 1178-1181

[131] X. Zhang, L. Liao, N. Ma, and H. Wang: Mechanical properties and damping capacity of magnesium matrix composites, *Composites Part A: Applied Science and Manufacturing*, Vol. 37, No. 11, 2006, pp. 2011-2016.

[132] R. Colaco, and R. Vilar: Abrasive wear of metallic matrix reinforced materials, *Wear*, Vol. 255, No. 1, 2003, pp. 643-650.

[133] J.F. Archard: Contact and Rubbing of Flat Surfaces, *Journal of Applied Physics Letters*, Vol. 24, 1953, pp. 981-988.

[134] B. Bhushan: *Principles and applications of tribology*, John Wiley, New York, USA, 1999.

[135] K. Xiu, H. Wang, H. Sui, Y. Wang, C. Xu, J. Wang, and Q. Jiang: The sliding wear behavior of TiC/AZ91 magnesium matrix composites, *Journal of Materials Science*, Vol. 41, No. 21, pp. 7052-7058.

[136] J. Yao, W. Li, L. Zhang, F. Wang, M. Xue, H. Jiang, and J. Lu: Wear Mechanism for In Situ TiC Particle Reinforced AZ91 Magnesium Matrix Composites, *Tribology Letters*, Vol. 38, No. 3, 2010, pp. 253-257.

[137] M. Merola: Theoretical evaluation of the physical properties of copper-lead rheocast alloys, *Materials Science and Engineering A*, Vol. 214, No. (1-2), 1996, pp. 181-185.

[138] ASTM standard C20-00: Standard Test Methods for Apparent Porosity, Water Absorption, Apparent Specific Gravity, and Bulk Density of Burned Refractory Brick and Shapes by Boiling Water, West Conshohocken, PA, 2000.

[139] H. Putz, and K. Brandenburg: Pearson's Crystal Data, Crystal Structure Database for Inorganic Compounds, CD-ROM software version 1.3.

[140] R.J. Hill, and C.J. Howard: Quantitative phase analysis from neutron powder diffraction data using the Rietveld method, *Journal of* Applied *Crystallography,* Vol. 20, 1987, pp. 467-474.

[141] ASTM E9-89a: Standard Test Methods of Compression Testing of Metallic Materials at Room Temperature, American Society for Testing and Materials, 1989.

[142] P.B. Prangnell, T. Downes, W.M. Stobbs, and P.J. Withers: The deformation of discontinuously reinforced MMCs-I. The initial yielding behaviour, *Acta Metallurgica et Materialia*, Vol. 42, No. 10, 1994, pp. 3425-3436.

[143] ASTM C1161-02C: Standard test method for flexural strength of advanced ceramics at ambient temperature, American Society for Testing and Materials, Annual Book of Standards, West Conshohocken, PA, 2002.

[144] M. Bengisu: *Engineering Ceramics*, Springer, New York, USA, 2001.

[145] A.A. Nayeb-Hashemi, J.B. Clark: Phase Diagrams of binary magnesium alloys, ASM International, Metals Park, OH., 1998, pp.324-327.

[146] T. Hitoshi, A. Taroh, O. Tadashi, and K. Koji: Synthesis of TiB_2-TiC Composites by Solid-State Reaction between B_4C and Ti Powders, *Journal of the Ceramic Socity of Japan*, Vol. 107, No. 11, 1999, pp. 1041-1045.

[147] H. Zhao, and Y.B. Cheng: Formation of TiB_2-TiC composites by reactive sintering, *Ceramics International*, Vol. 25, No. 4, 1999, pp. 353-358.

[148] P. Shen, B. Zou, S. Jin, and Q. Jiang: Reaction mechanism in self-propagating high temperature synthesis of TiC-TiB_2/Al composites from an Al-Ti-B_4C system, *Materials Science and Engineering: A*, Vol. 454-455, 2007, pp. 300-309.

[149] D. Emin: Structure and single-phase regime of boron carbides, *Journal of Review Letters B*, Vol. 38, 1988, pp. 6041-6055.

[150] S.J. Palmer: The effect of temperature on surface tension, *Journal of Physics Education*, Vol. 11, No. 2, 1976, pp. 119-120.

[151] V. Kevorkijan, and S.D. Skapin: Mg-B$_4$C composites with a high volume fraction of fine ceramic reinforcement, *Journal of Materials and Manufacturing Processes*, Vol. 24, 2009, pp. 1337-1340.

[152] S. Brutti, G. Balducci, G. Gigli, A. Ciccioli, P. Manfrinetti, and A. Palenzona: Thermodynamic and kinetic aspects of decomposition of MgB$_2$ in vacuum: Implications for optimization of synthesis conditions, *Journal of Crystal Growth*, Vol. 289, No.2, 2006, pp. 578-586.

[153] ASM Handbook, *Nonferrous alloys castings: Magnesium and magnesium alloys,* ASM, Vol. 19, Casting, 1998, pp. 578.

[154] D. Askeland, and P. Phule: *The Science and Engineering of Materials*, Thomson, Inc., USA, 2006.

[155] P. Palcek, A. Námešný, M. Chalupová, B. Hadzima: Failure Mechanisms in Magnesium Alloys Matrix Composites, *22nd DANUBIA-ADRIA Symposium on Experimental Methods in Solid Mechanics*, Parma, Italy, 2005.